NASA Tech Briefs

National Aeronautics and Space Administration

Generating Liquid Hydrogen —

A spinoff of NASA's requirements for high-volume production, this commercial installation in New Orleans, Louisiana, produces up to 60 tons of liquid hydrogen each day for nonaerospace industries [*See the bottom of page A1.*]

Vol. 7, No. 3

Spring 1983

About the NASA Technology Utilization Program

The National Aeronautics and Space Act of 1958, which established NASA and the United States civilian space program, requires that "The Administration shall provide for the widest practicable and appropriate dissemination of information concerning its activities and the results thereof."

To help carry out this objective, NASA's Technology Utilization (TU) Program was established in 1962. Now, as an element of NASA's Technology Utilization and Industry Affairs Division, this program offers a variety of valuable services to help transfer aerospace technology to nonaerospace applications, thus assuring American taxpayers maximum return on their investment in space research; thousands of spinoffs of NASA research have already occurred in virtually every area of our economy.

The TU program has worked for engineers, scientists, technicians, and businessmen; and it can work for you.

NASA Tech Briefs

Tech Briefs is published quarterly and is free to engineers in U.S. industry and to other domestic technology transfer agents. It is both a current-awareness medium and a problem-solving tool. Potential products . . . industrial processes . .. basic and applied research . . . shop and lab techniques . . . computer software . . . new sources of technical data . . . concepts . . . can be found here. The short section on New Product Ideas highlights a few of the potential new products contained in this issue. The remainder of the volume is organized by technical category to help you quickly review new developments in your areas of interest. Finally, a subject index makes each issue a convenient reference file.

Further Information on Innovations

Although some new technology announcements are complete in themselves, most are backed up by Technical Support Packages (TSP's). TSP's are available without charge and may be ordered by simply completing a TSP Request Card found at the back of this volume. Further information on some innovations is available for a nominal fee from other sources, as indicated. In addition, Technology Utilization Officers at NASA Field Centers will often be able to lend necessary guidance and assistance.

Patent Licenses

Patents have been issued to NASA on some of the inventions described, and patent applications have been submitted on others. Each announcement indicates patent status and availability of patent licenses if applicable.

Other Technology Utilization Services

To assist engineers, industrial researchers, business executives, Government officials, and other potential users in applying space technology to their problems, NASA sponsors Industrial Applications Centers. Their services are described on page A7. In addition, an extensive library of computer programs is available through COSMIC, the Technology Utilization Program's outlet for NASA-developed software.

Applications Program

NASA conducts applications engineering projects to help solve public-sector problems in such areas as safety, health, transportation, and environmental protection. Two applications teams, staffed by professionals from a variety of disciplines, assist in this effort by working with Federal agencies and health organizations to identify critical problems amenable to solution by the application of existing NASA technology.

Reader Feedback

We hope you find the information in *NASA Tech Briefs* useful. A reader-feedback card has been included because we want your comments and suggestions on how we can further help you apply NASA innovations and technology to your needs. Please use it; or if you need more space, write to the Manager, Technology Transfer Division, P.O. Box 8757, Baltimore/Washington International Airport, Maryland 21240.

NASA Tech Briefs

National Aeronautics and Space Administration

Spring 1983
Volume 7, Number 3

COVERS: The photographs on the front and back covers illustrate developments by NASA and its contractors that have resulted in commercial and nonaerospace spinoffs. You can use the TSP Request Card at the back of this issue to learn more about the Liquid-Hydrogen Generating Plants [Circle 76] and the Portable Aerosol Analyzer [Circle 77].

About This NASA Publication

NASA Tech Briefs, a quarterly publication, is distributed free to qualified U.S. citizens to encourage commercial application of U.S. space technology. For information on publications and services available through the NASA Technology Utilization Program, write to the Manager, Technology Transfer Division, P.O. Box 8757, Baltimore/Washington International Airport, Maryland 21240.

"The Administrator of National Aeronautics and Space Administration has determined that the publication of this periodical is necessary in the transaction of the public business required by law of this Agency. Use of funds for printing this periodical has been approved by the Director of the Office of Management and Budget."

Change of Address

If you wish to have NASA Tech Briefs forwarded to your new address, use the Subscription Card enclosed at the back of this volume of NASA Tech Briefs. Be sure to check the appropriate box indicating change of address, and also fill in your identification number (T number) in the space indicated.

Communications Concerning Editorial Matter

For editorial comments or general communications about NASA Tech Briefs, you may use the Feedback card in the back of NASA Tech Briefs, or write to: The Publications Manager, Technology Utilization Office (LGT-1), NASA Headquarters, Washington, DC 20546. Technical questions concerning specific articles should be directed to the Technology Utilization Officer of the sponsoring NASA Center (addresses listed on page A4).

Acknowledgements

NASA Tech Briefs is published quarterly by the National Aeronautics and Space Administration, Technology Transfer Division, Washington, DC:
Administrator: **James M. Beggs;** Director, Technology Utilization and Industry Affairs Division: **Ronald J. Philips;** Publications Manager: **Leonard A. Ault.**
Prepared for the National Aeronautics and Space Administration by **Logical Technical Services Corp.:** Editor-in-Chief: **Jay Kirschenbaum;** Art Director: **Ernest Gillespie;** Managing Editor: **Jerome Rosen;** Chief Copy Editor: **Oden Browne;** Staff Editors: **Donald Blattner, Larry Grunberger, Jordan Randjelovich, Ted Selinsky, George Watson;** Graphics: **Luis Martinez, Janet McCrie, Huburn Profitt;** Editorial & Production: **Richard Johnson, Stephanie Godino, Leslie Iwaskow, Frank Ponce, Elizabeth Texeira, Vincent Susinno, Ernestine Walker.**

NASA TU SERVICES

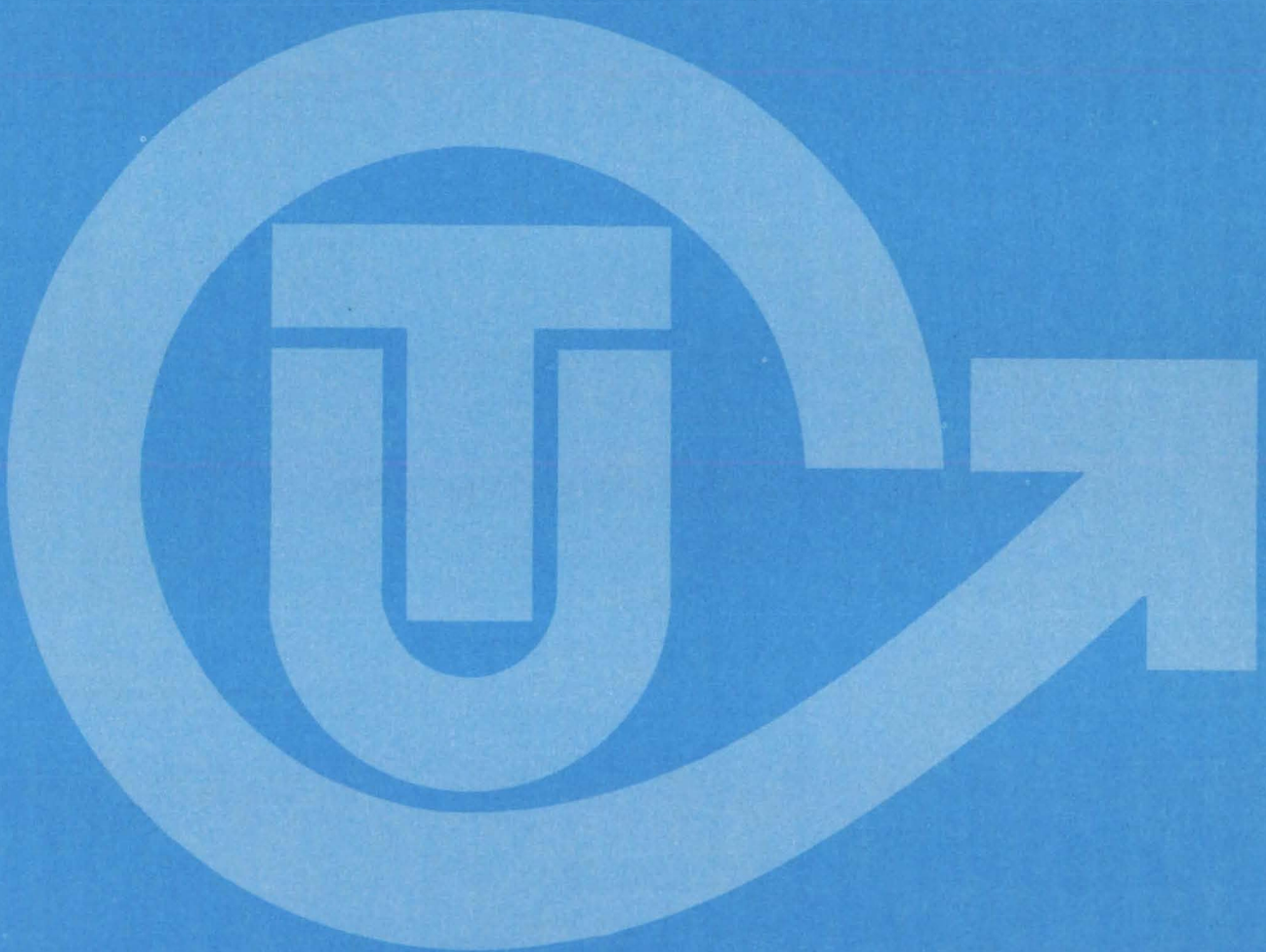

NASA TECHNOLOGY UTILIZATION NETWORK

★ TECHNOLOGY UTILIZATION OFFICERS

Stanley A. Miller
Ames Research Center
Code 240-10
Moffett Field, CA 94035
(415) 965-6471

Stanley A. Miller
Hugh L. Dryden Flight Research Center
Code 240-10
Moffett Field, CA 94035
(415) 965-6471

Donald S. Friedman
Goddard Space Flight Center
Code 702.1
Greenbelt, MD 20771
(301) 344-6242

John T. Wheeler
Lyndon B. Johnson Space Center
Code AT-3
Houston, TX 77058
(713) 483-3809

U. Reed Barnett
John F. Kennedy Space Center
Code PT-SPD
Kennedy Space Center, FL 32899
(305) 867-3017

John Samos
Langley Research Center
Mail Stop 139A
Hampton, VA 23665
(804) 865-3281

Harrison Allen, Jr.
Lewis Research Center
Mail Code 7-3
21000 Brookpark Road
Cleveland, OH 44135
(216) 433-4000, Ext. 6422

Ismail Akbay
George C. Marshall Space Flight Center
Code AT01
Marshall Space Flight Center, AL 35812
(205) 453-2224

Leonard A. Ault
NASA Headquarters
Code ETD-6
Washington, DC 20546
(202) 755-2244

Aubrey Smith
NASA Resident Office-JPL
4800 Oak Grove Drive
Pasadena, CA 91103
(213) 354-4849

Gilmore H. Trafford
Wallops Flight Center
Code OD
Wallops Island, VA 23337
(804) 824-3411, Ext. 201

● INDUSTRIAL APPLICATIONS CENTERS

Aerospace Research Applications Center
1201 East 38th Street
Indianapolis, IN 46205
John M. Ulrich, director
(317) 264-4644

Computer Software Management and Information Center (COSMIC)
Suite 112, Barrow Hall
University of Georgia
Athens, GA 30602
John A. Gibson, director
(404) 542-3265

Kerr Industrial Applications Center
Southeastern Oklahoma State University
Durant, OK 74701
James Harmon, director
(405) 924-0121, Ext. 413

NASA Industrial Applications Center
701 LIS Building
University of Pittsburgh
Pittsburgh, PA 15260
Paul A. McWilliams, executive director
(412) 624-5211

New England Research Applications Center
Mansfield Professional Park
Storrs, CT 06268
Daniel Wilde, director
(203) 486-4533

North Carolina Science and Technology Research Center
Post Office Box 12235
Research Triangle Park, NC 27709
James E. Vann, director
(919) 549-0671

Technology Applications Center
University of New Mexico
Albuquerque, NM 87131
Stanley Morain, director
(505) 277-3622

NASA Industrial Applications Center
University of Southern California
Denny Research Building
University Park
Los Angeles, CA 90007
Robert Mixer, acting director
(213) 743-6132

■ STATE TECHNOLOGY APPLICATIONS CENTERS

NASA/University of Florida
State Technology Applications Center
500 Weil Hall
University of Florida
Gainesville, FL 32611
J. Ronald Thornton, director

Gainesville:	(904) 392-6760
Boca Raton:	(305) 395-5100, Ext. 2292
Fort Lauderdale:	(305) 776-6645
Jacksonville:	(904) 646-2478
Orlando:	(305) 275-2706
Pensacola:	(904) 476-9500, Ext. 426
Tampa:	(813) 974-2499

NASA/University of Kentucky
State Technology Applications Program
109 Kinkead Hall
University of Kentucky
Lexington, KY 40508
William R. Strong, manager
(606) 258-4632

◆ PATENT COUNSELS

Robert F. Kempf
Asst. Gen. Counsel for patent matters
NASA Headquarters
Code GP-4
400 Maryland Avenue, SW.
Washington, DC 20546
(202) 755-3954

Darrell G. Brekke
Ames Research Center
Mail Code: 200-11A
Moffett Field, CA 94035
(415) 965-5104

Darrell G. Brekke
Hugh L. Dryden Flight Research Center
Mail Code: 201-11A
Moffett Field, CA 94035
(415) 965-5104

John O. Tresansky
Goddard Space Flight Center
Mail Code: 204
Greenbelt, MD 20771
(301) 344-7351

Marvin F. Matthews
Lyndon B. Johnson Space Center
Mail Code: AL-3
Houston, TX 77058
(713) 483-4871

James O. Harrell
John F. Kennedy Space Center
Mail Code: SA-PAT
Kennedy Space Center, FL 32899
(305) 867-2544

Howard J. Osborn
Langley Research Center
Mail Code: 279
Hampton, VA 23665
(804) 827-3725

Norman T. Musial
Lewis Research Center
Mail Code: 500-311
21000 Brookpark Road
Cleveland, OH 44135
(216) 433-4000, Ext. 346

Leon D. Wofford, Jr.
George C. Marshall Space Flight Center
Mail Code: CC01
Marshall Space Flight Center, AL 35812
(205) 453-0020

Paul F. McCaul
NASA Resident Office-JPL
Mail Code: 180-601
4800 Oak Grove Drive
Pasadena, CA 91103
(213) 354-2700

▲ APPLICATION TEAMS

Doris Rouse, director
Research Triangle Institute
Post Office Box 12194
Research Triangle Park, NC 27709
(919) 541-6980

James P. Wilhelm, director
SRI International
333 Ravenswood Avenue
Menlo Park, CA 94026
(415) 326-6200, Ext. 3520

TECHNOLOGY UTILIZATION OFFICERS

Technology transfer experts can help you apply the innovations in NASA Tech Briefs.

The Technology Utilization Officer at each NASA Field Center is an applications engineer who can help you make use of new technology developed at his center. He brings you NASA Tech Briefs and other special publications, sponsors conferences, and arranges for expert assistance in solving technical problems.

Technical assistance, in the form of further information about NASA innovations and technology, is one of the services available from the TUO. Together with NASA scientists and engineers, he can often help you find and implement NASA technology to meet your specific needs.

Technical Support Packages (TSP's) are prepared by the center TUO's. They provide further technical details for articles in NASA Tech Briefs. This additional material can help you evaluate and use NASA technology. You may receive most TSP's free of charge by using the TSP Request Card found at the back of this issue.

Technical questions about articles *in NASA Tech Briefs are answered in the TSP's. When no TSP is available, or you have further questions, contact the Technology Utilization Officer at the center that sponsored the research* [*see page A4*].

NASA INVENTIONS AVAILABLE FOR LICENSING

Over 3,500 NASA inventions are available for licensing in the United States — both exclusive and nonexclusive.

Nonexclusive licenses for commercial use of NASA inventions are encouraged to promote competition and to achieve the widest use of inventions. They must be used by a negotiated target date.

Exclusive licenses may be granted to encourage early commercial development of NASA inventions, especially when considerable private investment is required. These are generally for 5 to 10 years and usually require royalties based on sales or use.

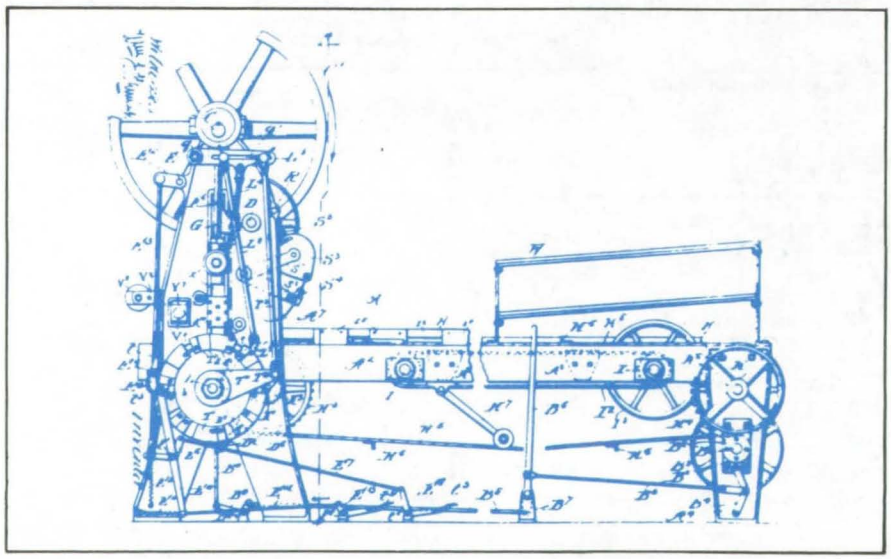

Additional licenses available include those of NASA-owned foreign patents. In addition to inventions described in NASA Tech Briefs, *"NASA Patent Abstract Bibliography"* (PAB), containing abstracts of all NASA inventions, can be purchased from National Technical Information Service, Springfield, VA 22161. The PAB is updated semiannually.

Patent licenses for Tech Briefs *are frequently available. Many of the inventions reported in NASA Tech Briefs are patented or are under consideration for a patent at the time they are published. The current patent status is described at the end of the article; otherwise, there is no statement about patents. If you want to know more about the patent program or are interested in licensing a particular invention, contact the Patent Counsel at the NASA Field Center that sponsored the research* [*see page A5*]. *Be sure to refer to the NASA reference number at the end of the Tech Brief.*

APPLICATION TEAMS

Technology-matching and problem-solving assistance to public-sector organizations

Application engineering projects are conducted by NASA to help solve public-sector problems in such areas as safety, health, transportation, and environmental protection. Some application teams specialize in biomedical disciplines; others, in engineering and scientific problems. Staffed by professionals from various disciplines, these teams work with other Federal agencies and health organizations to identify critical problems amenable to solution by the application of existing NASA technology.

Public-sector organization *representatives can learn more about application teams by contacting a nearby NASA Field Center Technology Utilization Office* [see page A4].

INDUSTRIAL APPLICATIONS CENTERS

Computerized access to over 10 million documents worldwide

Computerized information retrieval from one of the world's largest banks of technical data is available from NASA's network of industrial Applications Centers (IAC's). The IAC's give you access to 1,800,000 technical reports in the NASA data base and to more than 10 times that many reports and articles found in nearly 200 other computerized data bases.

The major sources include:

- *750,000 NASA Technical Reports*
- *Selected Water Resources Abstracts*
- *NASA Scientific and Technical Aerospace Reports*
- *Air Pollution Technical Information Center*
- *NASA International Aerospace Abstracts*
- *Chem Abstracts Condensates*
- *Engineering Index*
- *Energy Research Abstracts*
- *NASA Tech Briefs*
- *Government Reports*
- *Announcements*

and many other specialized files on food technology, textile technology, metallurgy, medicine, business, economics, social sciences, and physical science.

The IAC services range from tailored literature searches through expert technical assistance:

- *Retrospective Searches:* Published or unpublished literature is screened, and documents are identified according to your interest profile. IAC engineers tailor results to your specific needs and furnish abstracts considered the most pertinent. Complete reports are available upon request.
- *Current-Awareness Searches:* IAC engineers will help design a program to suit your needs. You will receive selected monthly or quarterly abstracts on new developments in your area of interest.
- *Technical Assistance:* IAC engineers will help you evaluate the results of your literature searches. They can help find answers to your technical problems and put you in touch with scientists and engineers at appropriate NASA Field Centers.

Prospective clients *can obtain more information about these services by contacting the nearest IAC* [see page A4]. *User fees are charged for IAC information services.*

STATE TECHNOLOGY APPLICATIONS CENTERS

Technical information services for industry and state and local government agencies.

Government and private industry in Florida and Kentucky can utilize the services of NASA's State Technology Applications Centers (STAC's). The STAC's differ from the Industrial Applications Centers described on page A7, primarily in that they are integrated into existing state technical assistance programs and serve only the host state, whereas the IAC's serve multistate regions.

Many data bases, including the NASA base and several commercial bases, are available for automatic data retrieval through the STAC's. Other services such as document retrieval and special searches are also provided. (Like the IAC's, the STAC's normally charge a fee for their services.)

To obtain information *about the services offered, write or call the STAC in your state [see page A4].*

COSMIC®

An economical source of computer programs developed by NASA and other government agencies

A vast software library is maintained by COSMIC — the Computer Software Management and Information Center. COSMIC gives you access to approximately 1,600 computer programs developed for NASA and the Department of Defense and selected programs for other government agencies. Programs and documentation are available at reasonable cost.

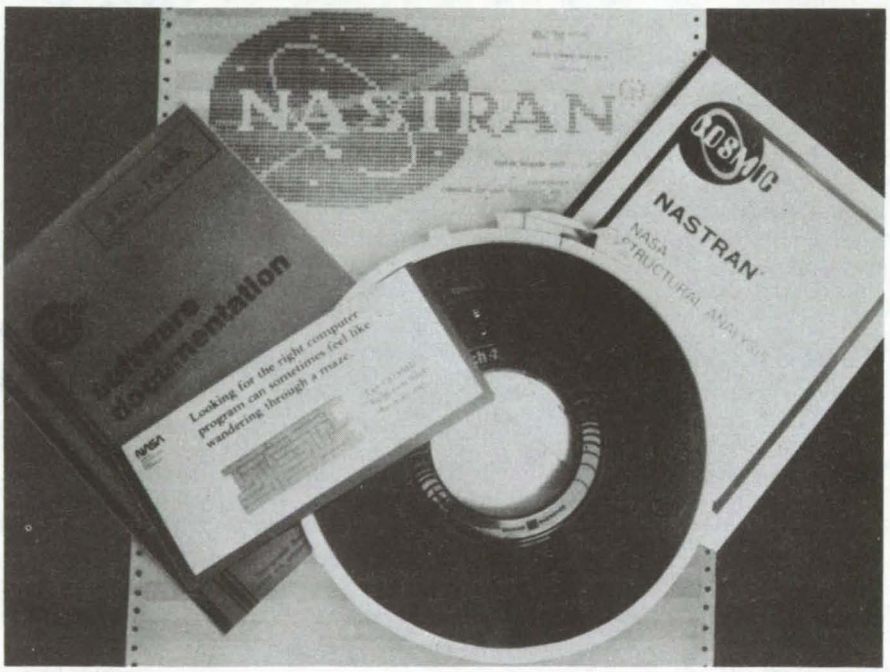

Available programs range from management (PERT scheduling) to information science (retrieval systems) and computer operations (hardware and software). Hundreds of engineering programs perform such tasks as structural analysis, electronic circuit design, chemical analysis, and the design of fluid systems. Others determine building energy requirements and optimize mineral exploration.

COSMIC services go beyond the collection and storage of software packages. Programs are checked for completeness; special announcements and an indexed software catalog are prepared; and programs are reproduced for distribution. Customers are helped to identify their software needs; and COSMIC follows up to determine the successes and problems and to provide updates and error corrections. In some cases, NASA engineers can offer guidance to users in installing or running a program.

Information about programs *described in NASA Tech Briefs articles can be obtained by completing the COSMIC Request Card at the back of this issue. Just circle the letters that correspond to the programs in which you are interested.*

NEW PRODUCT IDEAS

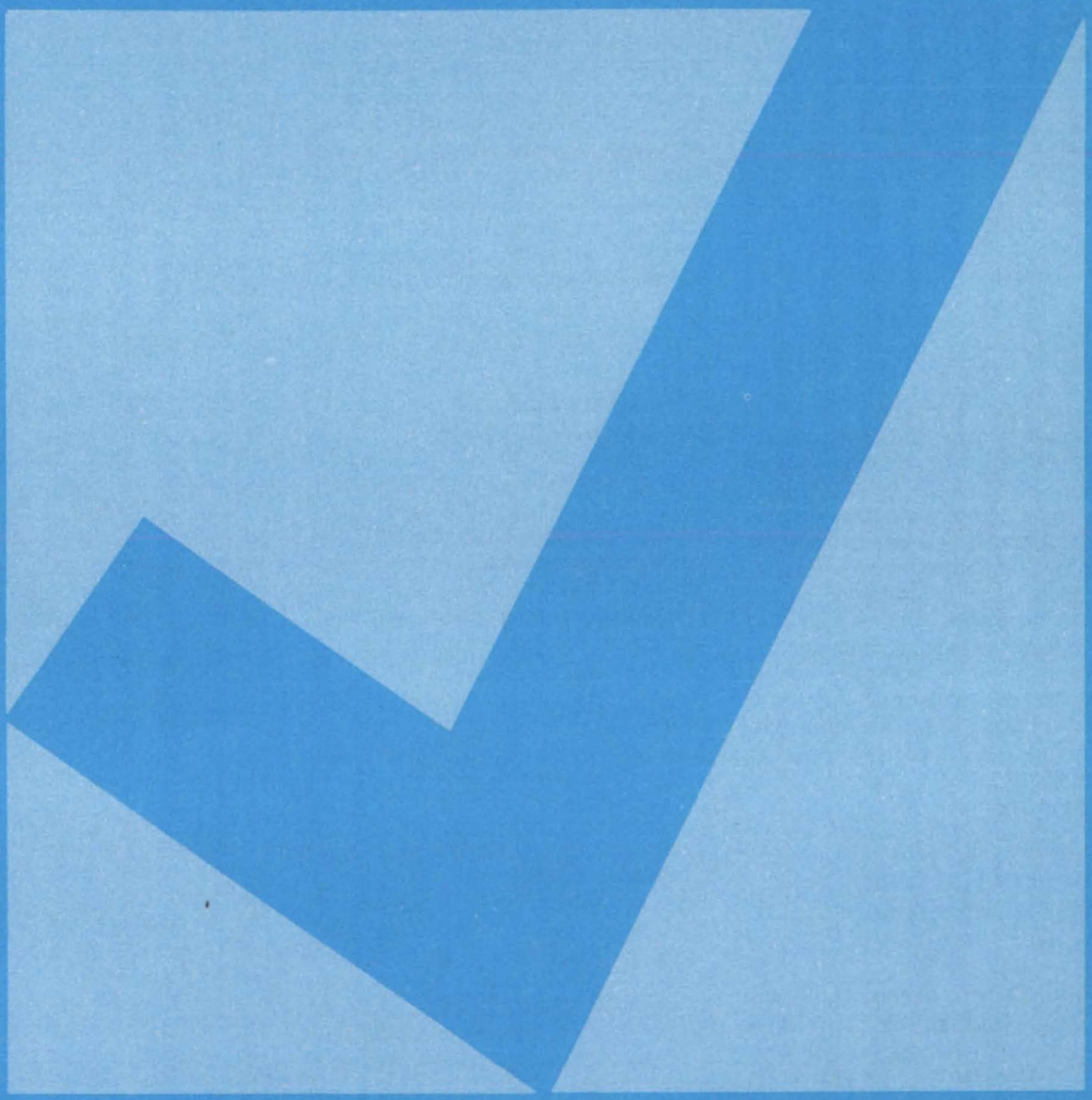

NEW PRODUCT IDEAS are just a few of the many innovations described in this issue of NASA Tech Briefs and having promising commercial applications. Each is discussed further on the referenced page in the appropriate section in this issue. If you are interested in developing a product from these or other NASA innovations, you can receive further technical information by requesting the TSP referenced at the end of the full-length article or by writing the Technology Utilization Office of the sponsoring NASA center (see page A4). NASA's patent-licensing program to encourage commercial development is described on page A6.

Robotic Water-Blast Cleaner

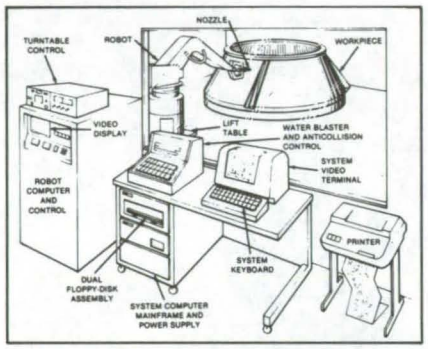

A water-blasting system under development will remove hard, dense, extraneous material from surfaces. A high-pressure pump forces water at supersonic speed through a nozzle manipulated by a robot. The impact of the water blasts away unwanted material from the workpiece, which is rotated on an air-bearing turntable. The automated system, which is adaptable to such industrial processes as cleaning iron or steel castings, removes the operator from the hazardous blast area and greatly improves the safety of personnel and equipment.
(See page 329.)

Reversible Hot-Melt Adhesive Attachment System

A reversible hot-melt adhesive attachment system works as well in vacuum as it does at atmospheric pressure. Electronic heaters warm a fiberglass cloth impregnated with a hot-melt adhesive.

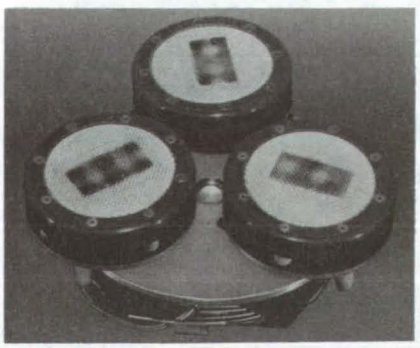

Once an attachment is made, the heaters are turned off and the adhesive is cooled rapidly for a "quick stick." To release the parts, current is applied to melt the adhesive. The system can be employed to tether tools or to attach temporary scaffoldings to walls, buildings, or beams. The fiberglass cloth is mounted in a head assembly that contains one foil heater, a fiberglass cloth, the hot-melt adhesive, a thermocouple, a heat sink, and a retainer ring.
(See page 344.)

Shell-Tile Thermal-Protection System

In a durable shell-tile thermal-protection system, upper and lower interlocking caps enclose stiffeners and flexible lightweight insulation. The material for these caps can be selected to match the expected temperature regimes.

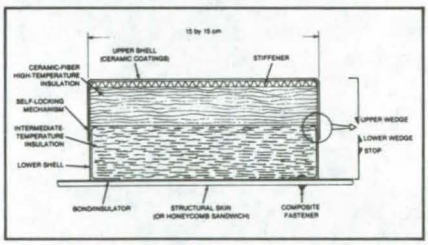

Candidates for upper caps are titanium, Rene, columbium, or reinforced carbon composites; and, for lower caps, titanium, graphite/polyimide, and other materials. The metallic-shell tiles can be fabricated in almost any shape, and can be constructed with dimpled sides for stiffness and to increase the conduction path.
(See page 296.)

Retaining-Ring Installation Tool

A new tool installs spiral retaining rings. The tool inserts rings in splined or irregularly shaped bores, bores at the bottoms of deep holes, and other limited-access installations. The tool consists of a piston in a tube. A user inserts a retaining ring into the tube through a slot and places the tube over the bore into which

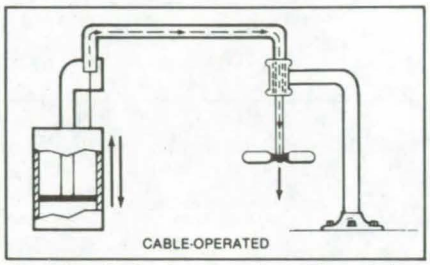

the ring is to be inserted. The piston squares the ring in the bore and pushes it along until it engages the ring groove.
(See page 334.)

Staked-Bearing Removal Tool

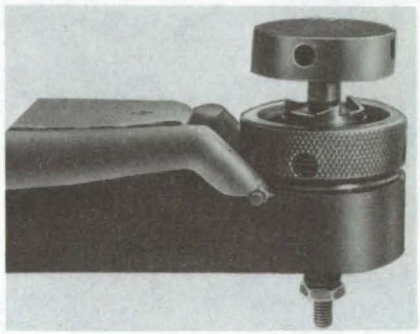

A portable air-powered tool can expedite bearing replacement in aircraft, ground vehicles, and other assembled structures. The tool cuts away retaining lips on one side of a bearing with minimal damage to the surrounding structure in preparation for removal of the bearing. It eliminates costly and time-consuming disassembly prior to conventional machining and pressing out of the spherical bearings.
(See page 330.)

Viewer Makes Radioactivity "Visible"

A battery-operated viewer generates three-dimensional visible-light simulations of objects that emit X-rays or gamma rays. The device could prove useful in applications ranging from radioactivity contamination surveys to monitoring radioisotope absorption in tumors.

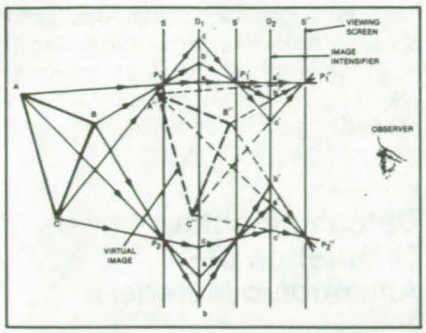

From any viewing angle, the field of view is approximately as wide as one would see looking through a small window of the same size as that of the detector in the instrument. There is no inherent limit to the detector size. A prototype of the viewer was tested with three small radioactive sources located at different distances from the viewer.
(See page 271.)

Coil-Welding Aid

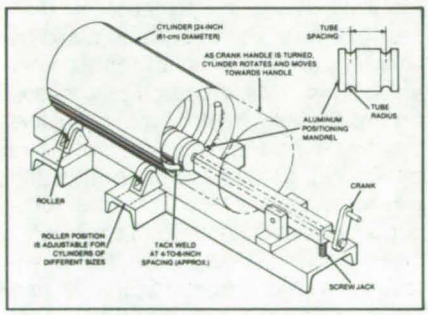

A new tool spaces the turns of a coil inside a cylinder and applies contact pressure while the coil is being tack-welded to the cylinder. It could speed the welding of heat-exchangers and other structures. The tool includes a shaft with an aluminum mandrel at one end and a crank at the other. Two grooves around the circumference of the mandrel are separated by the required coil pitch. Additional components include rollers, a shaft pivot point, and a screwjack. The device eliminates hand positioning and clamping of the individual coil turns.
(See page 325.)

Fire-Resistant Composites

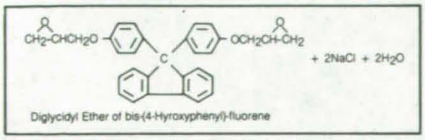

Diglycidyl ether of bis-(4-hydroxyphenyl)-fluorene (DGEBF), is thermally cured with diglycidyl ether of bisphenol A (DGEBA) to make strong, lightweight composites that have high char yield, low smoke density, and good temperature stability and fire resistance. The composites are used to manufacture printed-circuit boards and panels for buildings, ships, and aircraft. The new resin blend is prepared by reacting epichlorohydrin and sodium hydroxide with 9,9-bis-(hydroxyphenyl)-fluorene. The end point of the reaction is determined by gas or liquid chromatography, mass spectroscopy, or infrared techniques.
(See page 285.)

Printed Circuit Converts RF Energy to dc Power

An ultra-light-weight, large-area, antenna/rectifier system converts RF energy into dc electric power at an overall efficiency of 85 percent and a mass-to-dc-power-output ratio of 0.4 kg/kW. The flexible, low-cost, printed-circuit "rectenna" format is fabricated

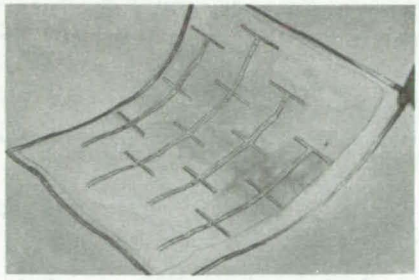

from laminated material consisting of a thin-film dielectric material bonded between two thin sheets of 1-oz copper. It includes a large number of repetitive circuits called "rectenna elements." Each element consists of a half-wave dipole, an input filter, and a Schottky barrier diode and produces 2 W of power.
(See page 242.)

Passive Magnetic Bearing

A new magnetic bearing for limited-rotation devices requires no feedback-control system to sense and correct the shaft position. A torsion wire assists permanent-magnet elements in maintaining shaft centering, eliminating the weight and bulk of position-control electromagnets, electronics, and power supply. The configuration easily lends itself to the incorporation of an integral torque motor, with only a modest increase in weight. Long life is expected for the bearing, even in vacuum and

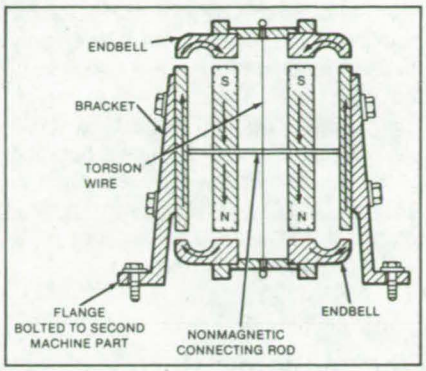

other environments in which debris accumulation, lubricant evaporation, or cold welding impair operation.
(See page 323.)

Self-Locking Connector

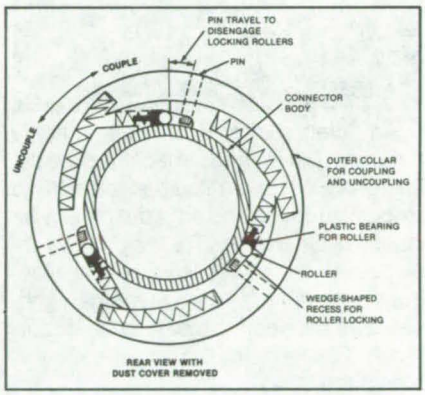

A connector lock resists vibration, automatically compensates for wear, and suffers no backlash when the parts are seated. The mechanism, which is spring-loaded into a normally locked position, is built into a coupling nut on the outer connector body. An outer collar is turned clockwise to tighten the nut, transmitting torque to the nut through six pins. The collar is rotated counterclockwise to unlock. Vibrations will tend to tighten the connector, even if the installer fails to tighten the nut, because the locking mechanism permits only tightening motions.
(See page 332.)

Reusable High-Pressure Connector

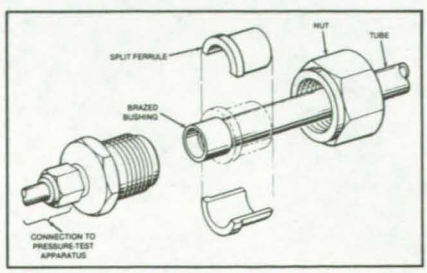

An improved fluid-line connector for high-pressure testing requires only minimal modification to the free end of the fluid line. The connector, which assures a strong joint for tests at 9,000 psi, consists of a split ferrule, a nut, and an O-ring seal. Following a test, the ferrule, nut, and O-ring fitting are removed, leaving the line unaltered except for a bushing brazed to its free end.
(See page 334.)

Electrochemical Deburring

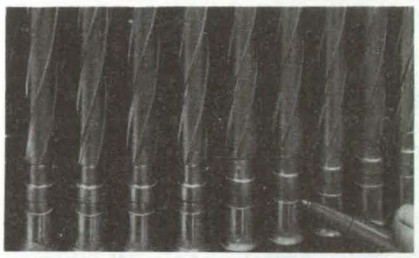

An electrochemical cell quickly removes burrs from machined parts. The process uses a liquid electrolyte to smooth surfaces and edges in otherwise inaccessible areas. The apparatus includes a dc power supply, an electrolyte, a sleeve, and electrical connections between the part to be deburred and one side of the power supply.
(See page 324.)

Solid-State Circuit Breaker

A circuit breaker with no moving parts protects direct-current (dc) loads. The current at which the circuit breaker opens (the trip current) is adjustable and

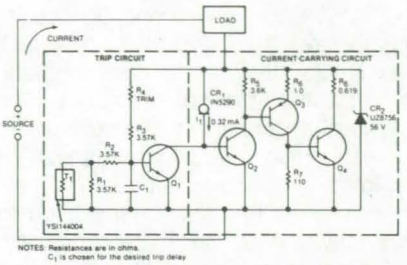

so is the time delay before the breaker trips. The two-terminal unit, which acts like a resettable delay fuse, can be placed on either the positive or negative side of the load. It is powered by the circuit it protects and is reset by either turning off the power source or disconnecting the load.
(See page 245.)

Instrumented Pick Detects Coal/Rock Interface

An instrument installed on the drum of a coal shearer for longwall mining measures the cutting force with a strain-gage-bridge load cell. The force is analyzed in

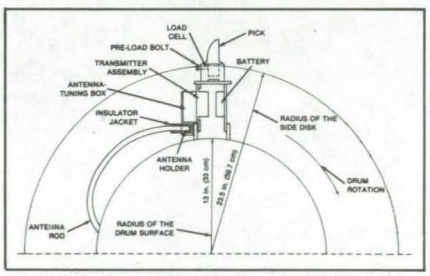

real time to determine whether coal or rock is being cut. The proposed system would automatically control the cutting drum so that it closely follows the coal/rock interface. A purer coal product (containing less rock) would result, and shearer downtime and maintenance would be reduced. Operators could be relocated away from the coal-dust concentration near the machine.
(See page 308.)

Determining the Orientation of Anisotropic Materials

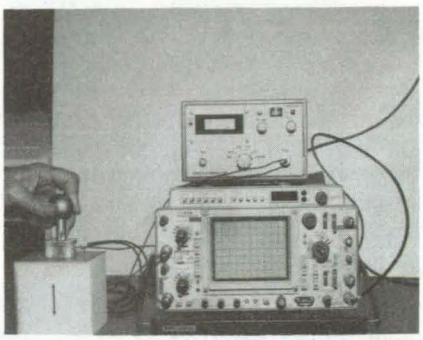

A hand-held acoustic transducer determines the fiber orientation in heat-resistant tiles. The transducer could be adapted for the inspection of other anisotropic materials, such as plywood and fiber/epoxy composites, or to find the direction of roll in sheet metal and other rolled products. A transmitter and two receivers are located on the transducer head so that they form a right isosceles triangle. To obtain the fiber orientation, the head is placed on the tile, and the signals from the receiving transducers are displayed on a two-channel oscilloscope. The difference in amplitudes of the two received signals indicates whether the fibers are oriented parallel or perpendicular to the tile surface.
(See page 299.)

Electronic Components and Circuits

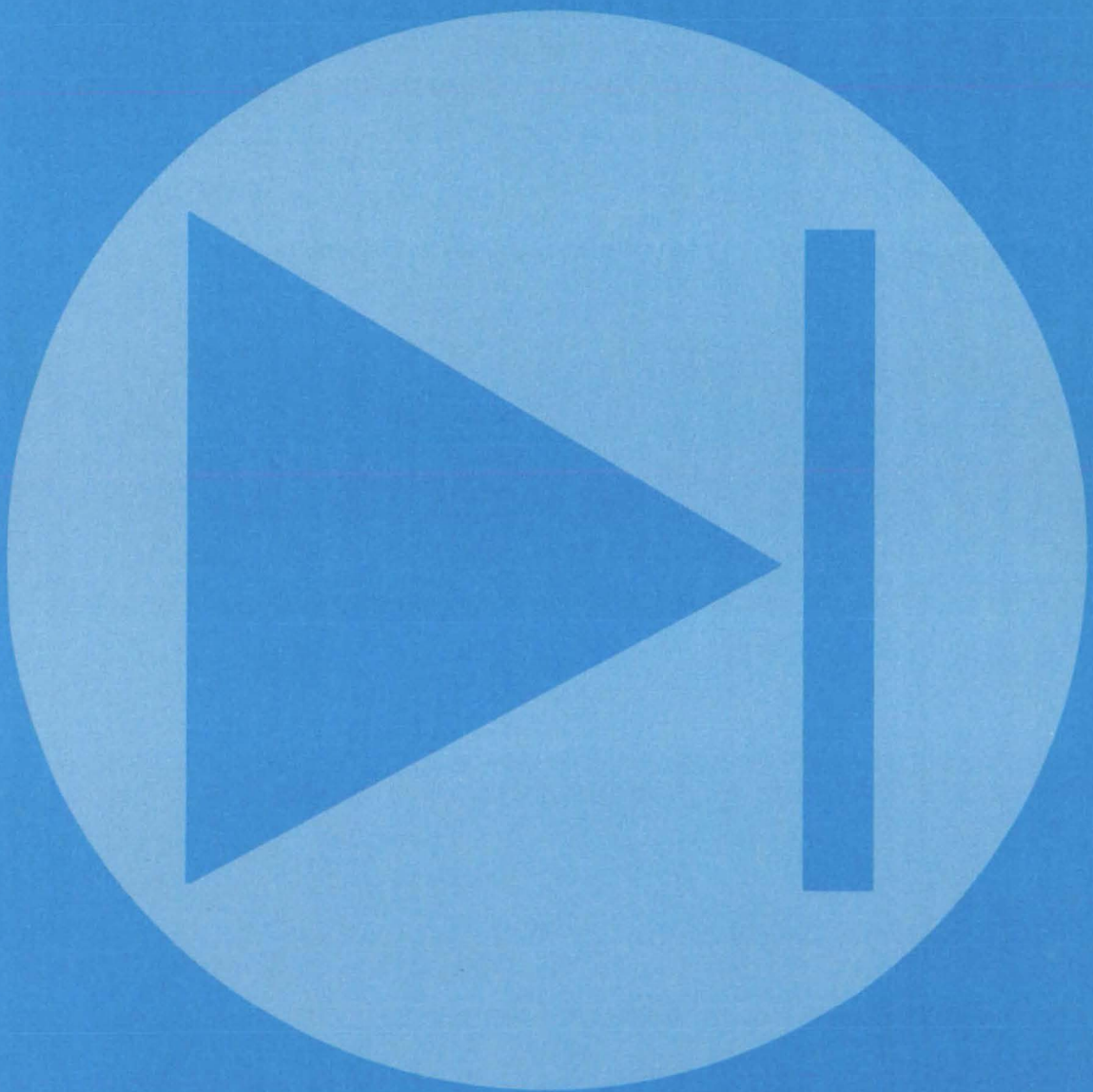

Hardware, Techniques, and Processes

Books and Reports

Digital Phase-Shift Standard

Circuit using just three IC's could be used to perform precise calibration.

John F. Kennedy Space Center, Florida

A digital phase-shift standard can be used in combination with an oscillator to calibrate other phase standards and phase-angle voltmeters. Previously, calibration of such phase shifters required several pieces of equipment and lengthy setup procedures.

The circuit can be used with input signals as low as 1 volt rms, in almost any waveform. It calibrates phase over a frequency range from dc to 2 kHz with an accuracy of $\pm 0.2°$. The output is two square waves, the phase difference of which is selectable in 30° increments by a 12-position switch. The frequency of the output square waves is one-twelfth the input-oscillator frequency.

The input from the oscillator is converted to a 9-volt level by an input transistor (see figure). Integrated circuit U_1 is a decade counter that counts the 9-volt pulses to six, then resets. Integrated circuit U_{2A} produces output A, the fixed-phase output, clocked by the first-decade (zero-output) pulse from U_1. U_{2B} produces output B, the variable-phase output, clocked by any one of the other five output pulses of U_1 selected by the rotary switch.

When the switch is in positions 1 through 5, the Q output of U_{2A} feeds the data (D) input of U_{2B}. When the switch is in positions 6 through 12, the inverted-Q ($\overline{Q}$) output of U_{2A} feeds the U_{2B} data input, causing output B to be inverted. This provision in effect adds 180° of shift to the shifts provided by positions 1 through 5 and thus gives a complete range of phase shifts.

In its present form, the circuit is constructed with complementary metal-oxide-semiconductor integrated circuits. Its frequency range could be extended to 100 MHz if emitter-coupled-logic was used.

This work was done by John A. Cramp of the Bionetics Corp. for **Kennedy Space Center.** *No further documentation is available.*

Inquiries concerning rights for the commercial use of this invention should be addressed to the Patent Counsel, Kennedy Space Center [see page A5]. Refer to KSC-11250.

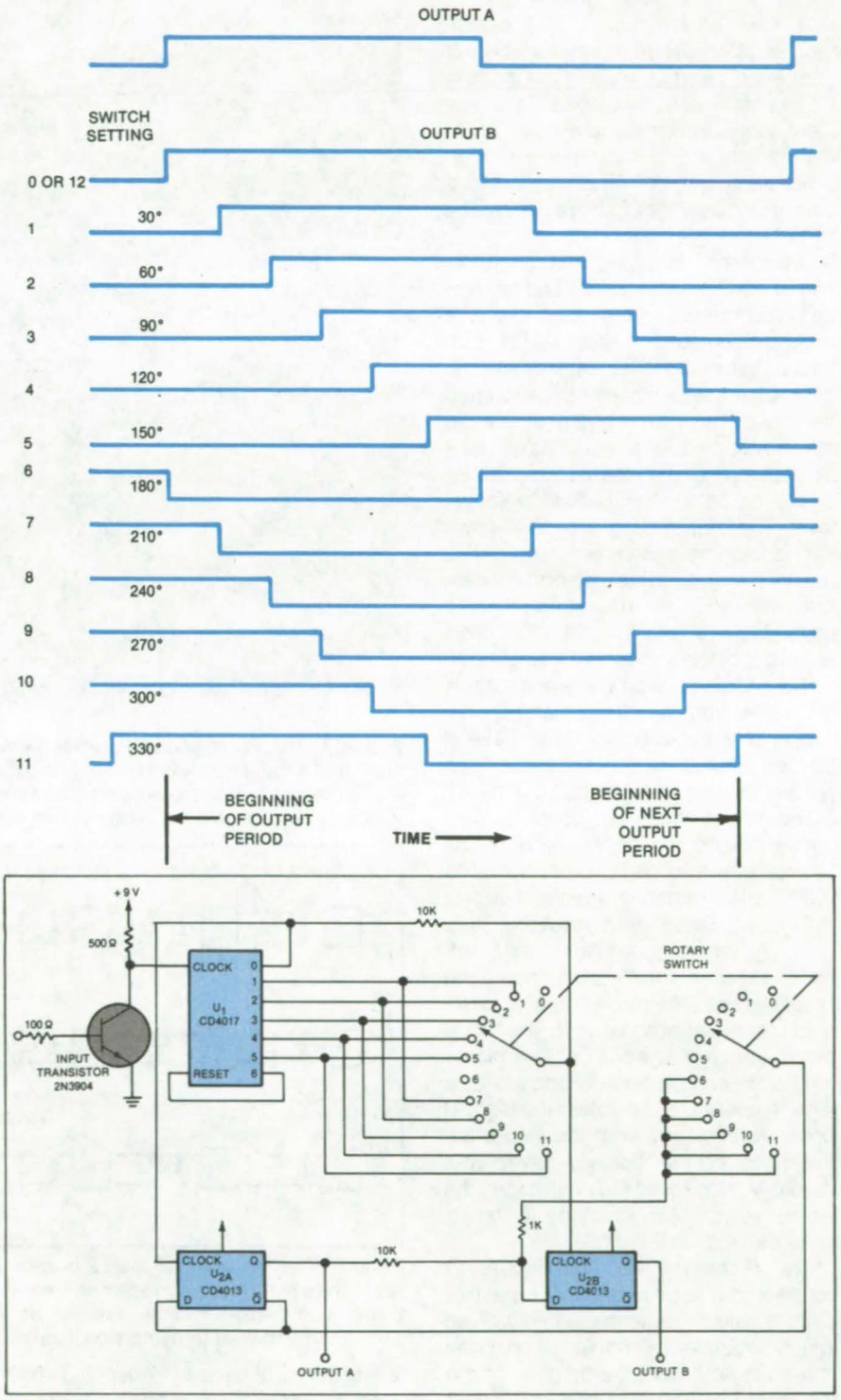

Phase-Shifter Circuit provides two square-wave outputs, A and B, with a phase difference between them that is selectable in 30° increments.

Printed Circuit Converts RF Energy to dc Power

An ultra-light-weight, large-area, antenna/rectifier has 85 percent conversion efficiency.

Lewis Research Center, Cleveland, Ohio

A new ultra-light-weight, low-cost, flexible 2.45-GHz-film, etched-circuit "rectenna" format, made from Kapton F-film, has been developed. This element allows the direct conversion of RF energy into dc electric power at an overall efficiency of 85 percent, and a mass-to-dc-power-output ratio of 0.4 kg/kW.

"Rectenna" is a functional abbreviation of the terms "rectifier" and "antenna" that denotes a special class of receiving antennas made up of continuous receiving cells, each smaller in dimension than a wavelength and each terminated with a rectifying device. At microwave frequencies it behaves as a dc restorer to shift the dc level either above or below the ground potential level. The output dc power then flows into a common load resistance. The resulting structure has a theoretical capture efficiency of 100 percent while maintaining a directivity that is characteristic of the aperture of a single cell.

The rectenna using the new format is fabricated from laminated material consisting of a thin-film dielectric material bonded between two thin sheets of 1-oz (28.3-g) copper [1.4 mils (3.6 μm) thick]. Standard photoetching processes, without the need to provide for interconnects between the two surfaces, are used to produce the rectenna foreplane shown in Figure 1. Specially-constructed GaAs Schottky barrier diodes were then bonded to the structure — one per each repetitive cell. The diode had special requirements imposed upon it. The diode has to be small, low-cost, have a plated heat sink, and be able to operate at a high temperature. To obtain the highest possible efficiency from the diode, the thickness of the epitaxial layer was carefully controlled to minimize the series resistance, which is a major source of loss in the diode.

The rectenna foreplane (Figure 2) consists of a large number of repetitive circuits called "rectenna elements," all joined together by transmission lines that serve to collect the dc power from the individual elements and to conduct the power to the edges of the array. There the circuit connections may be either series or parallel, depending upon load conditions. At certain locations along their length, those collecting buses also serve as short sections of microwave transmission line representing inductances in low-pass filter circuits and in the rectifier tank circuits. The transmission lines also serve to radiate

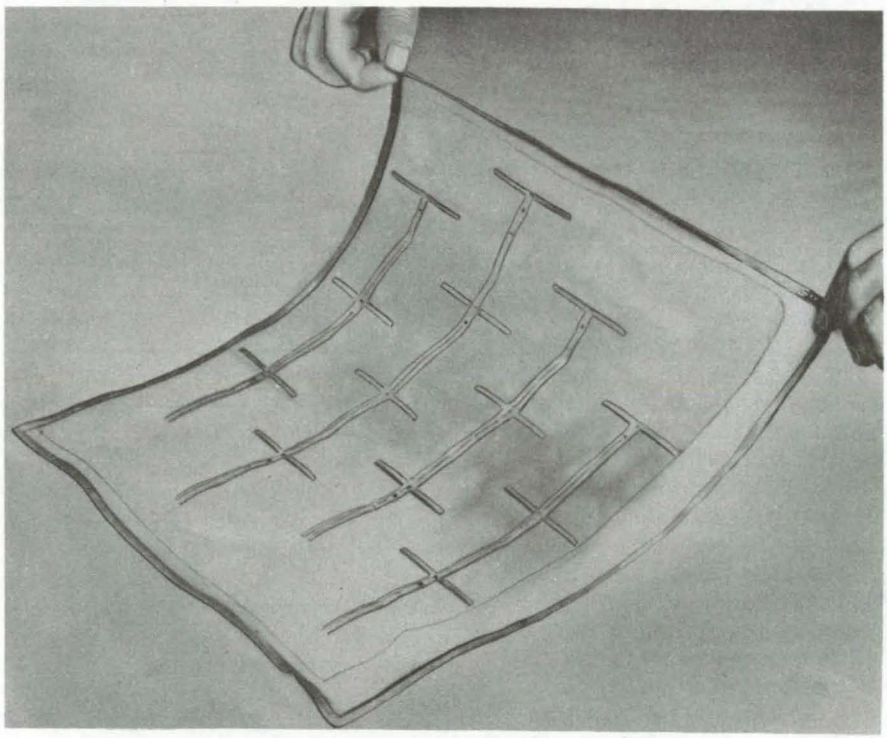

Figure 1. The **Printed-Circuit Rectenna** was fabricated from laminated material consisting of a thin-film dielectric bonded between two sheets of 1-oz copper. The rectenna foreplane was produced using standard photoetching processes without the need to provide for interconnects between the two surfaces.

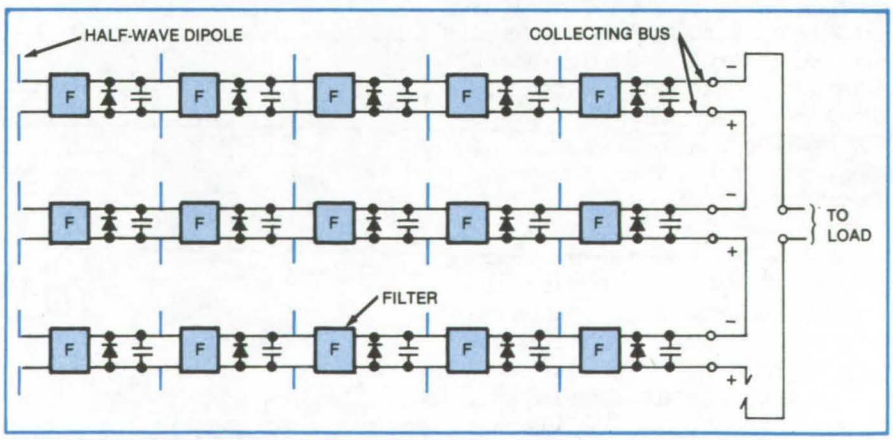

Figure 2. The **Rectenna RF to dc Power-Conversion System** consists of a large number of repetitive circuits called "rectenna elements." Each element, which can produce 2 W of power, comprises a half-wave dipole, an input filter, and a Schottky barrier diode. The two-wire microwave transmission lines also act as dc power-collecting buses.

and conduct away heat generated in the diodes during the rectification process.

Each rectenna element consists of a two-stage low-pass filter followed by a rectifier circuit. The rectifier circuit consists of a single diode, a section of microwave transmission line, and a large bypass capacitor, the physical location of which from the diode determines the length, and therefore the equivalent inductance, of the transmission line. The bypass capacitor also serves to filter out harmonic components from the dc power-collecting buses. Finally, it serves to short effectively a 1/4-wavelength section of transmission line to the left (in Figure 2) of each dipole antenna and thus prevents coupling of power from the antenna to the adjacent rectenna element.

The low-pass input filter serves a number of functions: It serves as a buffer between the half-wave rectifier circuit and the antenna, storing energy and making the rectenna appear as a constant impedance to the microwave beam. This buffering is essential to obtaining the high overall efficiency of 85 percent. The low-pass filter also serves to attenuate the flow of harmonic power from the rectifier circuit to the dipole antenna. The second section of the input filter is also frequently used as an impedance-matching device, particularly at low microwave input levels, where it is desireable to use a higher dc load resistance to reduce the impact on efficiency of the voltage drop across the Schottky barrier.

The necessity for the rectenna to radiate passively heat that is generated through an inefficiency of operation stresses the desirability of both highly efficient operation and operation at high temperature. The latter is desirable because of the fourth-power relationship between the quantity of heat radiated and the temperature. These considerations required the use of the GaAs Schottky barrier diode because of its established high efficiency and ability to operate at high temperatures. Computer studies on heat conduction and radiation along the etched circuits indicate that the rectenna can radiate the associated waste heat into a vacuum environment with a 30° C ambient temperature without exceeding a temperature of 160° C in the hottest part of the diodes.

Each rectenna element, in the most recent format of 2-mil (50-μm) Kapton F-film, weighs 0.8 g. Each element can conservatively produce 2 W of power to provide a weight-to-power-output ratio of 0.4 kg/kW. This should translate into, 1 kW/kg for the entire rectenna when the reflecting plane and spacers are added. Since each rectenna element occupies about 50 cm^2, the ratio of power output to area of the rectenna is 400 W/m^2.

If it were desired to operate the rectenna at lower power densities and still retain the ratio of 1 kW/kg, the present design could be changed in a number of ways to reduce weight of the foreplane per unit area; or, as might be the case in microwave-power high-altitude aircraft, the rectenna could be deployed to have some forced convective cooling and thereby greatly increase the amount of power that could be handled by each rectenna element. The present limitation of 2 W per element is based upon radiation cooling into a 30° C environment.

This rectenna offers higher conversion efficiency (85 vs. 15 percent) and lower specific weight (15:1 reduction) than conventional direct-energy-conversion devices. For space applications the 50-cm^2 element is able to convert 2 W of RF energy into usable dc power. The specific power density of this element is 0.4 kg/kW for an incident energy density of 400 W/m^2. This rectenna element allows a three-dimensional transfer of electrical power and permits the coupling of terrestrial or low-orbit power-transmission systems to power sources or sinks located in low Earth orbit or deep space.

This work was done by J. E. Triner of **Lewis Research Center** *and W. C. Brown of Raytheon Co. Further information may be found in NASA CR-156866 [N81-27401/NSP], "Design Definition of a Microwave Power Reception and Conversion System for Use on a High Altitude Powered Platform" [$11.50]. A copy may be purchased [prepayment required] from the National Technical Information Service, Springfield, Virginia 22161.*

Inquiries concerning rights for the commercial use of this invention should be addressed to the Patent Counsel, Lewis Research Center [see page A5]. *Refer to LEW-13913.*

Two-Wire to Four-Wire Audio Converter

A simple circuit provides an interface between normally incompatible voice-communication lines.

John F. Kennedy Space Center, Florida

A compact circuit enables the interconnection of two-wire and four-wire voice communication lines. The new converter employs standard circuitry and components. It is adaptable to many other two-to four-wire applications such as telephone answering devices and voice-controlled computers.

When a two-wire voice-communication line must connect with a four-wire line, the "hybrid" adapter furnished by the telephone company will not always do: The hybrid may not be suitable for the impedances of the lines. Such was the case at the Kennedy Space Center News Facility, where it was necessary to connect television cameras having two-wire equipment to a four-wire audio network that extends to remote locations. The converter replaces a large and cumbersome unit, a junction box that linked a television van to a long extension cable on the camera operator's headset.

The converter uses phase cancellation to isolate the two-wire receiving (input) half of the four-wire line from the two-wire transmitting (output) half of the four-wire line (see figure). The audio signal from the receiving half is split into two separate paths which provide equal gain. One of the paths provides an inversion, however, so that the signals cancel when they are recombined before insertion into the transmitting half.

The audio signal from the four-wire input (receiving) half is fed through input operational amplifier IC_1, which acts as

(continued on next page)

a buffer and a constant load. The output of IC_1 is fed through a 180-ohm series resistor to the ungrounded side of the television camera two-wire intercom: This connects the four-wire line with the two-wire line which carries both input and output audio to and from the camera operator. The combined audio is fed to a second operational amplifier, IC_2, the output of which is divided to the low level (less than 1 millivolt) required by the transmitter that feeds the two-wire transmitting half of the four-wire line.

A third operational amplifier, IC_3, amplifies the output of IC_1. After voltage division, the output of IC_3 is combined with the output of IC_2. Since IC_3 is noninverting, its output is out of phase with the output of IC_2, which is inverting. Balancing potentiometer R_9 is adjusted so that equal but opposite amplitudes appear at the junction of resistors R_{10}, R_{11}, and R_{12} and the audio signal from the four-wire input half is canceled.

The converter provides in excess of 40 dB of isolation between the input and output halves of the four-wire line. It is simple and inexpensive. It requires less than 20 milliamperes from an external power source. Its audio circuits are completely direct-coupled: There are no capacitors or transformers to cause unwanted phase shifts. The only adjustment is to a balance potentiometer which is set before use with a dummy-load resistor and should not be disturbed afterward.

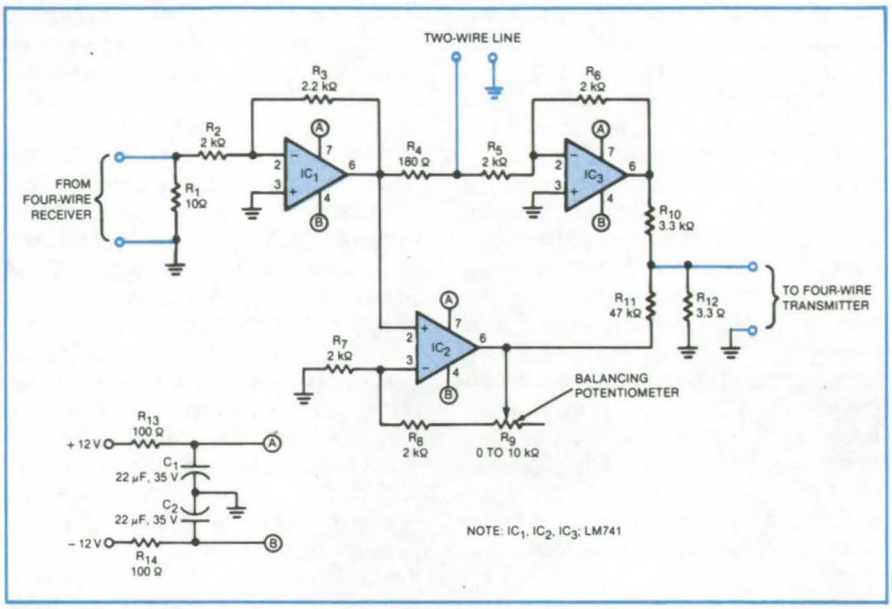

This Converter Circuit maintains 40 dB of isolation between the input and output halves of a four-wire line while permitting a two-wire line to be connected. A balancing potentiometer, R_9, adjusts the gain of IC_2 to null the feed-through from the input to the output. The adjustment is done on the workbench just after assembly by inserting a 1-kHz tone into the four-wire input and setting R_9 for minimum output signal. An 82-ohm dummy-load resistor is placed across the two wire terminals.

This work was done by Gerald L. Talley, Jr., and Brent L. Seale of **Kennedy Space Center.** *For further information, Circle 1 on the TSP Request Card.*

Inquiries concerning rights for the commercial use of this invention should be addressed to the Patent Counsel, Kennedy Space Center [see page A5]. Refer to KSC-11256.

Measuring Excess Noise in SDL's

A simple system measures noise deviation in semiconductor-diode lasers.

Langley Research Center, Hampton, Virginia

A new instrument gives quantitative information on the "excess noise" in semiconductor-diode lasers (SDL's). By proper selection of a detector, the instrument can test any SDL from the visible wavelengths through the thermal infrared.

Excess noise or amplitude instability is an important performance characteristic of SDL's that limits their usefulness. It can be orders of magnitude greater than the inherent quantum noise and can severely limit either baseband signal-to-noise ratios in optical communication systems or ultimate performance in optical heterodyne receivers. To evaluate the suitability of an SDL, it is necessary to be able to determine quantitatively the amount of excess noise in a given device.

The operation of the new instrument is based on the known relation between RF noise generated in a photodetector and the average photocurrent or photovoltage. For simplicity, a photodiode is assumed in the measurement system, although photoconductors can be used with only slight modification to the test instrument.

In the ideal case, a photodiode, when illuminated by a source of radiant energy, generates an average photocurrent that is proportional to the optical power. This photocurrent, I_{ph}, causes a shot-noise square current of

$$i_{sh}^2 = 2qI_{ph}\Delta f$$

where q is the electron charge (1.6×10^{-19} coulomb) and Δf is the bandwidth in which the observation is made. A stream of photons illuminating a photodiode causes the photodiode output noise power to follow the linear relation with respect to I_{ph}, but the presence of excess noise causes a deviation from that equation.

The system shown in the figure permits a quantitative determination of the amount that an SDL deviates from the

ideal. The system consists of a high-speed photodetector compatible in speed and wavelength to the application in which the SDL is to be used. The photodetector is an HgCdTe photodiode with a frequency response of approximately 200 MHz. The photodiode is connected to a high-gain (≥60-dB), low-noise (NF ≅ 2-dB), RF amplifier with a built-in bias port to allow reverse biasing of the photodetector.

The output of the RF amplifier is connected to a test set consisting of an RF power divider, an RF detector, and electronic components. The test set provides the following functions, without need for additional test instrumentation:

- Detection of noise power,
- Nulling of noise power due to the measurement system,
- Measurement of photocurrent,
- Photodetector biasing control,
- Output port for simultaneous RF spectrum analysis,
- Output ports for data recording,
- RF amplifier B+, and
- All internally-required B+ supplies.

The system is calibrated by using a near-ideal source such as a CO_2 laser to generate a reference curve of shot-noise power versus photocurrent. The total-noise power measured with the SDL under test for a given photocurrent provides the information needed to calculate excess noise.

Excess noise is defined as noise above the reference shot noise for a given photocurrent generated by an ideal source. Therefore, an excess-noise ratio (ENR) can be defined as the total-noise power divided by the shot-noise power. The nulling features of the test set allow automatic subtraction of both system noise and photocurrent caused by background sources, thereby greatly simplifying the excess-noise measurement. The test set also includes a digital panel meter and a function switch to allow self-sufficient measurements of photodetector bias, photocurrent, and noise power.

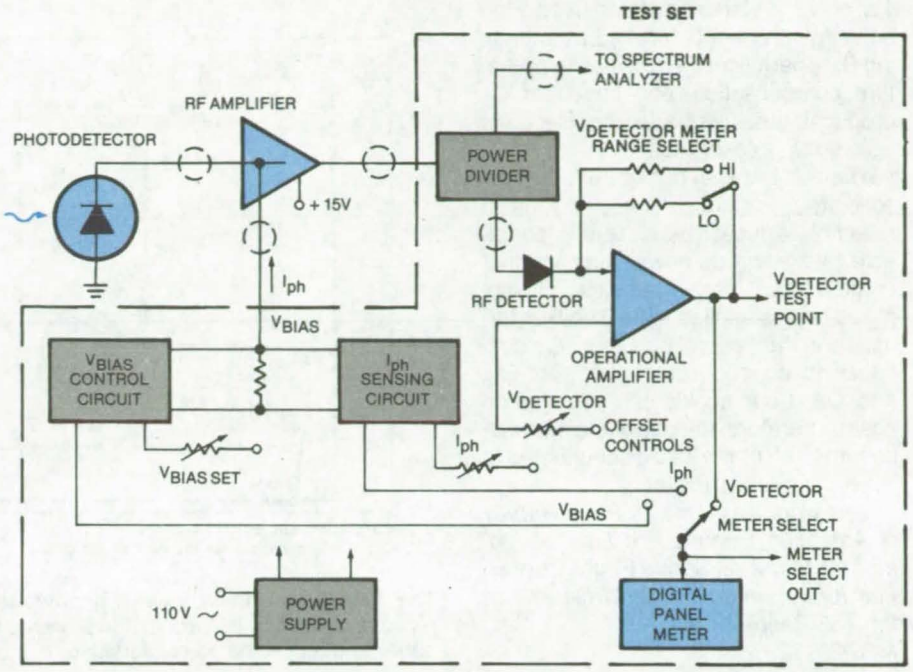

This **Test Circuit for Semiconductor-Diode Lasers** determines the excess noise in an SDL source by measuring the photocurrent generated in a photodetector exposed first to a reference laser and then to the SDL under test.

This work was done by Stephen J. Katzberg, Herbert R. Kowitz, Carroll W. Rowland, Thomas A. Shull, and Stephen L. Ruggles of **Langley Research Center** *and Leroy F. Matthews of Kentron International, Inc. For further information, Circle 2 on the TSP Request Card.*
LAR-12938

Solid-State dc Circuit Breaker

Two-terminal unit acts like a resettable delay fuse.

Marshall Space Flight Center, Alabama

A circuit breaker with no moving parts protects direct-current (dc) loads. The current at which the circuit breaker opens (the trip current) is adjustable and so is the time delay before the breaker trips. The forward voltage drop rises from 0.6 to 1.2 V as the current rises to the trip point. The breaker is reset by turning the source power off and then back on again.

The breaker uses solid-state electronic elements, as can be seen in the figure. It can be placed on either the positive or negative side of the load, but must be connected so that current flows through it in the direction shown.

The circuit inside the electronic breaker is divided into two parts: the current-carrying circuit and the trip circuit. At low voltage across the breaker, Q_1 conducts little current. Consequently, the 0.32-mA current through constant-current diode CR_1 saturates Q_2 and thereby turns on Q_3 and Q_4 to saturation. The total voltage drop across the breaker increases with increasing load current through the parallel resistance of R_6 and R_8. When the total drop across the breaker circuit reaches 1.2 V, Q_1 turns on to saturation, thus diverting the 0.32 mA, so that Q_2, Q_3, and Q_4 turn off. The breaker is thus open. The breaker then conducts only 0.32 mA plus $V_{supply}/(R_4 + R_3)$, which is only a few milliamperes.

Zener diode CR_2 protects the breaker electronics by limiting the forward voltage to 56 V and the reverse voltage to 0.6 V. Coarse adjustment of the trip level is obtained by changing R_6 and R_8; the values shown are for 2.2 A, but 0.73, 3.5,

(continued on next page)

1.6, and 3.0 A have also been used. Fine adjustment is accomplished by changing R_4. Thermistor T_1 provides temperature compensation, and capacitor C_1 produces a delay of a few milliseconds before the breaker trips.

The two-terminal configuration of the solid-state circuit breaker makes it resemble a fuse. Therefore it is adaptable to existing dc power supplies that contain fuses. Since nearly the full supply voltage is applied to the breaker terminals in the "open" condition, Q_1 continues to conduct, preventing Q_2, Q_3, and Q_4, from accidentally turning on again. Therefore, the power supply must be turned off or the load disconnected to reset the circuit breaker.

This work was done by Philip Harvey of American Science and Engineering, Inc., for **Marshall Space Flight Center.** *For further information, Circle 3 on the TSP Request Card.*
MFS-25172

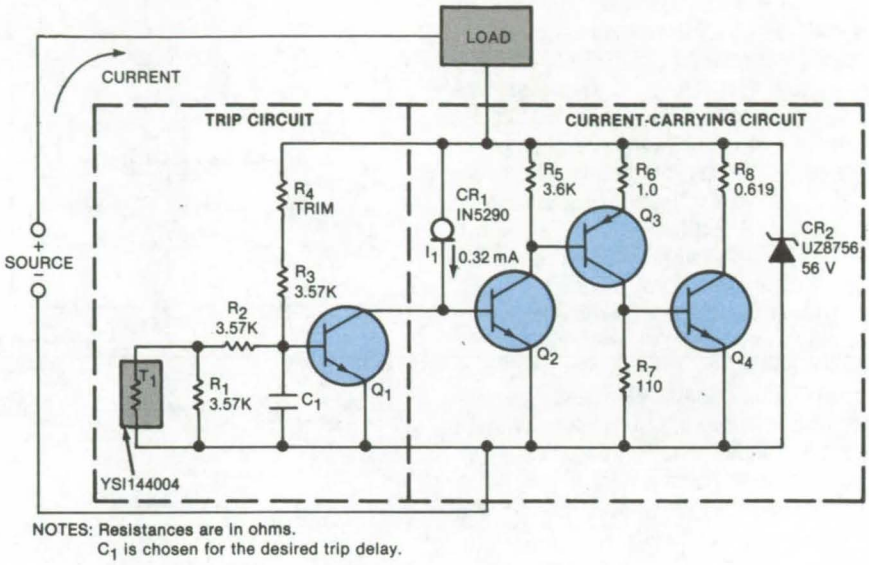

NOTES: Resistances are in ohms.
C_1 is chosen for the desired trip delay.

This **Solid-State Circuit Breaker** has two terminals, just like a fuse, and therefore can replace a fuse in a dc circuit. It is powered by the circuit that it protects and is reset by either turning off the power source or disconnecting the load.

Improved Connector Shell for Cable Shields

Braid is gripped around its entire circumference.

NASA's Jet Propulsion Laboratory, Pasadena, California

A new cable-connector shell improves electrostatic and electromagnetic shielding by electrically connecting the cable braid around its entire circumference. The extra protection afforded by this simple improvement is needed for metal-oxide-semiconductor integrated circuits and other delicate circuits that are susceptible to damage by electrostatic discharges.

Currently-available commercial connectors crimp or squeeze the cable braid but may leave gaps that can allow the entry of electrostatic and electromagnetic impulses.

The new connector shell completely shields the cable conductors. A crimpable sleeve and a ferrule clamp the braid to the shell metal over its full circumference (see figure). The inner conductors of the cable pass through the ferrule to the connector contacts within the shell. The braid surrounds the ferrule, and the sleeve surrounds the braid. When the sleeve is tightly crimped around the braid, the seal is complete.

The shell can be removed so that conductors can be connected to the connector contacts. The shell, and ferrule, can be made from a standard metal, such as aluminum, copper, or steel.

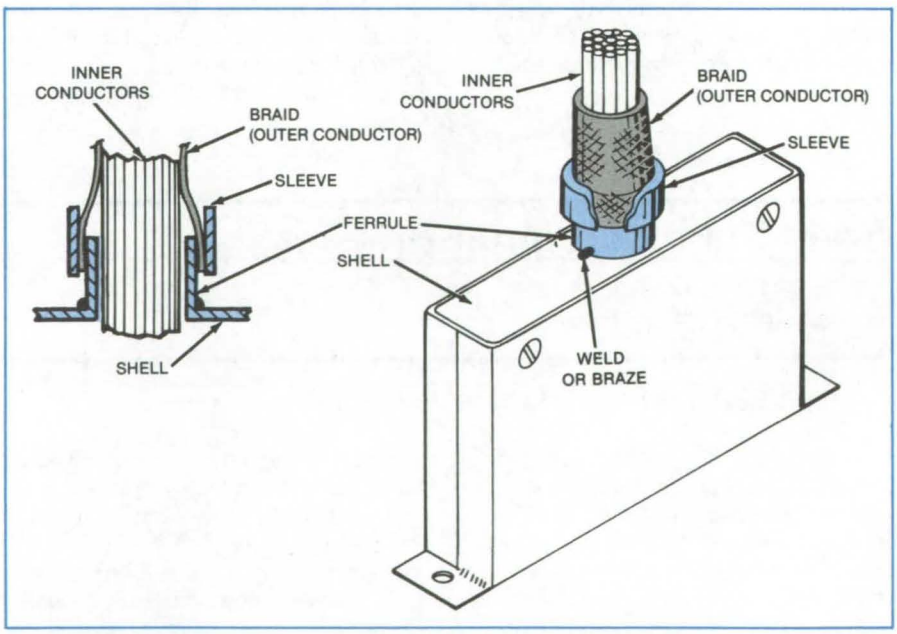

In a **New Connector,** cable braid is slipped over a ferrule, and a sleeve is slipped over the braid, clamping it tightly to the shell.

This work was done by Arthur L. Prisk and James W. Rotta, Jr., of Caltech for **NASA's Jet Propulsion Laboratory.** *For further information, Circle 4 on the TSP Request Card.*
NPO-15584

Add-On Shielding for Unshielded Wire

Prefabricated harness shields wires already soldered to connectors.

NASA's Jet Propulsion Laboratory, Pasadena, California

The fabrication sequence shown in the figure produces a compact braided shield that can be added to unshielded wire already soldered to a connector. The add-on shielding is assembled at a workbench and then slid onto the free end of the unshielded wire. The technique is especially useful for small-diameter wire attached to microminiature connectors.

In a typical application, the wire to be shielded is insulated (but unshielded) #28 AWG. A length of #26 AWG polytetrafluoroethylene (teflon) insulated unshielded wire is used as a mandrel. The difference in diameter between the mandrel wire and the wire to be shielded allows clearance to make it easier to thread the shield over the unshielded wire.

One and one-half to two turns of copper foil one-half in. (13 mm) wide, 1 mil (0.025 mm) thick are first wrapped tightly around the mandrel near one end. Braided shielding is then slipped over the copper, so that about one-sixteenth in. (1.6 mm) of the foil is exposed and the mandrel protrudes from the other end of the shield.

If a jumper is required, it is inserted through the braided shielding in contact with the copper foil, so that a bare portion of the jumper wire makes a minimum contact of three-sixteenths in. (4.8 mm) with the copper foil. The insulation of the jumper wire must not penetrate the shield. If two jumpers are required, they are inserted through the braid 180° apart.

The harness is dip-soldered approximately to the center of the wrapped foil or to the point of insertion of the jumper wire through the braid. The solder-dipped assembly is then trimmed to length, with about one-quarter in. (6.4 mm) to three-eights in. (9.5 mm) of the foil remaining flush with the shielding. About 0.020 in. (0.51 mm) is then filed to flatten and remove the deformed end section. Insulating shrink tubing can then be shrunk in place over the shielding if insulation is desired. Another piece of shrink tubing, one-half inch long, is slipped over the soldered end of the assembly to relieve stress on about one-fourth in. of the jumper wire.

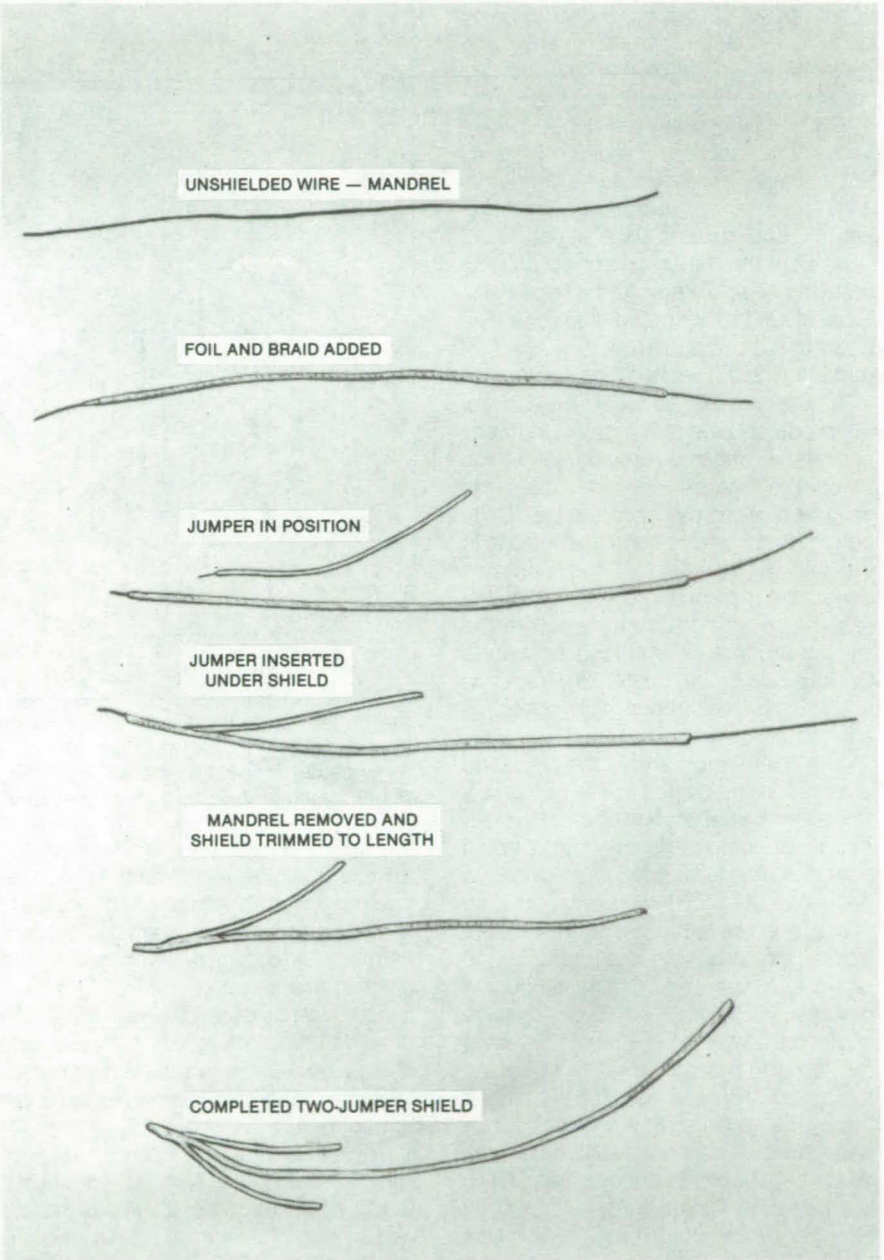

This **Fabrication Sequence** is used to produce compact shields that can be slipped into place from the free ends of wires already soldered into connectors at the other ends. A single-jumper shield is produced by the fabrication sequence shown here. For comparison, a two-jumper shield is also shown.

The tool wire is then removed, and the soldered end of the braid is reformed using a scriber. This also deburrs the entrance to the shield. The shield can then be fitted over the loose wire ends.

This work was done by John C. Koenig, Joseph W. Billitti, and John M. Tallon of Caltech for **NASA's Jet Propulsion Laboratory.** *For further information, Circle 5 on the TSP Request Card.*

NPO-15107

X-Ray Detector for 1 to 30 keV

Array of deep silicon cells can be used for imaging or spectroscopy.

Goddard Space Flight Center, Greenbelt, Maryland

An array of silicon X-ray-detecting diodes measures photon energy and provides an image of the X-ray pattern for photon energies in the range from 1 to 30 keV. Originally developed for use in X-ray telescopes, the detector array should also prove useful in industrial part inspection, pulsed-plasma research, and medical applications.

The spectrometer sensor consists of an array of adjoining silicon diode cells. Each diode has a central electrode (see figure). A rectangular vertical grid of metal forms the walls of the cells.

A bias voltage between the central electrode and the rectangular grid walls creates a depletion region (in which holes are scarce) that occupies the volume of each cell from the top to the bottom and from the central electrode to the wall. Thus, most of the electrons generated in the silicon by X-rays do not recombine with holes in the bulk of the silicon, but instead last long enough to be collected by the center electrode. As a result, the cells have high collection efficiency.

In the detector array, the depletion layer can be made as thick as necessary to assure the generation of enough electrons for detection at high photon energies: This is an advantage since the thickness of silicon necessary to convert the entire photon energy to electrons increases with the cube of the energy. In contrast, charge-coupled devices (CCD's) for X-ray detection have depletion layers only 5 μm thick along the top surface of the CCD array. Attempts to increase the depletion-layer thickness by increasing the diode voltage would cause the silicon to break down and become conductive. CCD's are therefore limited to detecting X-ray energies below about 1 keV. X-rays with greater energy simply pass through the depletion layer before they can generate a sufficient number of electrons, and the result is low electron-collection efficiency.

The high collection efficiency of the cellular detector results in a proportionality between the incident photon energy and the number of electrons collected: approximately 3.6 eV per electron. Since the electrons are collected in the cells in which they are formed, the signals from the separate cells can be used to form an image of the incident X-ray pattern — for example, by connecting the output of each cell to the corresponding element of a CCD or to individual on-chip amplifiers. Thus, the new detector offers good spatial and energy resolution, in contrast to earlier systems that had either one or the other but not both.

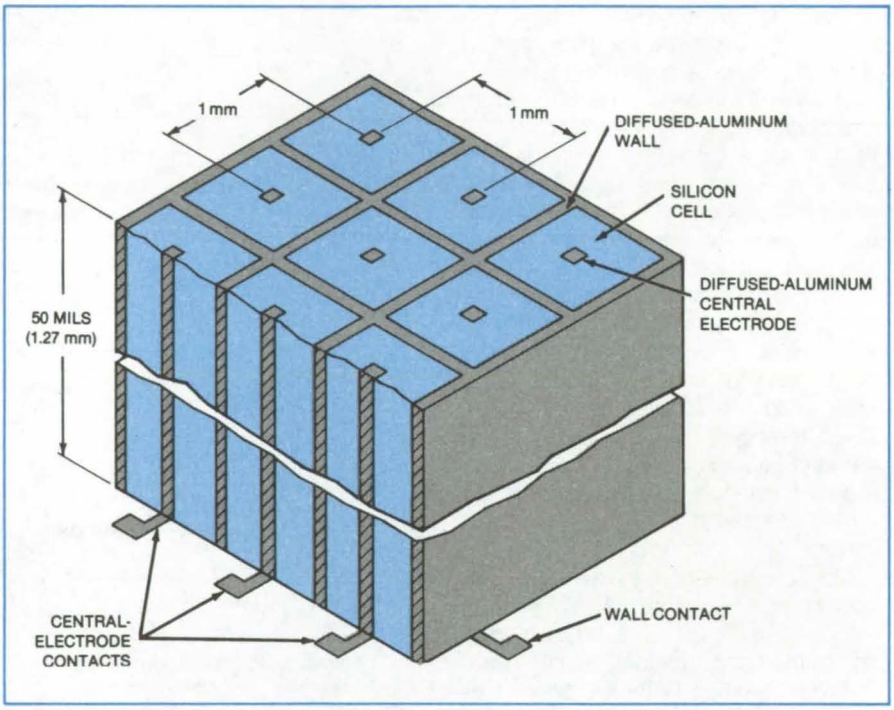

Regardless of How Thick the new X-ray detector is, a depletion region extends through it. Impinging X-rays generate electrons in quantities proportional to the X-ray energy. The X-ray detector could be mated to a charge-coupled-device array (or each collection terminal mated an on-chip amplifier system) for image generation and processing.

The array is made from a wafer of silicon having high resistivity (about 2,000 ohm-cm). The thickness of the wafer is slightly greater than the expected depth of penetration of X-rays. For X-rays in the 1-to-20-keV range, the wafer should be about 50 mils (1.27 mm) thick.

The vertical metal walls and central electrodes are formed by the diffusion of aluminum in silicon. Openings defining the horizontal sections of the walls and central electrodes are etched into a layer of photoresist to form a mask on one surface of the wafer. The opposite surface is heated to 1,200° C while the etched surface is held at the slightly lower temperature of 1,150° C. Aluminum deposited on the etched openings of the cooler surface quickly diffuses into the wafer because of the temperature gradient between the surfaces. The vertical movement of aluminum is so rapid that it has little time to diffuse horizontally. The cell walls and central electrodes are therefore essentially perpendicular to the wafer surfaces.

This work was done by George Alcorn, John Jackson, Jr., Patrick Grant, and Frank Marshall of **Goddard Space Flight Center.** *For further information, Circle 6 on the TSP Request Card.*

This invention is owned by NASA, and a patent application has been filed. Inquiries concerning nonexclusive or exclusive license for its commercial development should be addressed to the Patent Counsel, Goddard Space Flight Center [see page A5]. Refer to GSC-12682.

Level Sensor for Cryogenic Fluids

Comparator circuit is used with a hot-wire sensor.

Lyndon B. Johnson Space Center, Houston, Texas

A hot-wire sensor combined with the voltage-comparator circuit shown in the figure is used to monitor the liquid level in cryogenic-fluid storage tanks. The presence or absence of fluid is indicated by a lamp or other display device.

The fluid sensor is a platinum wire. When the wire is immersed, the fluid cools the wire, decreasing its electrical resistance. The presence or absence of liquid is indicated by comparing the probe resistance with a calibrated value.

In the circuit shown, a constant-current source sends current through the sensor. The voltage drop across the probe is compared with a calibrated voltage drop. When the probe voltage drop exceeds the calibrated value, the comparator turns on the lamp driver to give a visible warning that the probe is dry. The voltage comparator is calibrated for each liquid and probe by adjusting a potentiometer.

The voltage across a fixed resistor in series with the probe is monitored by another comparator to determine sensor continuity. As long as the current is flowing in the sensor, the comparator triggers the continuity-lamp driver. The circuit can easily be adapted for use with several different probes by adding switches and an extra calibration potentiometer for each probe.

This work was done by Norman E. Simmons and Richard A. Schroff of Rockwell International Corp. for **Johnson Space Center.** *For further information, Circle 7 on the TSP Request Card.*

MSC-20302

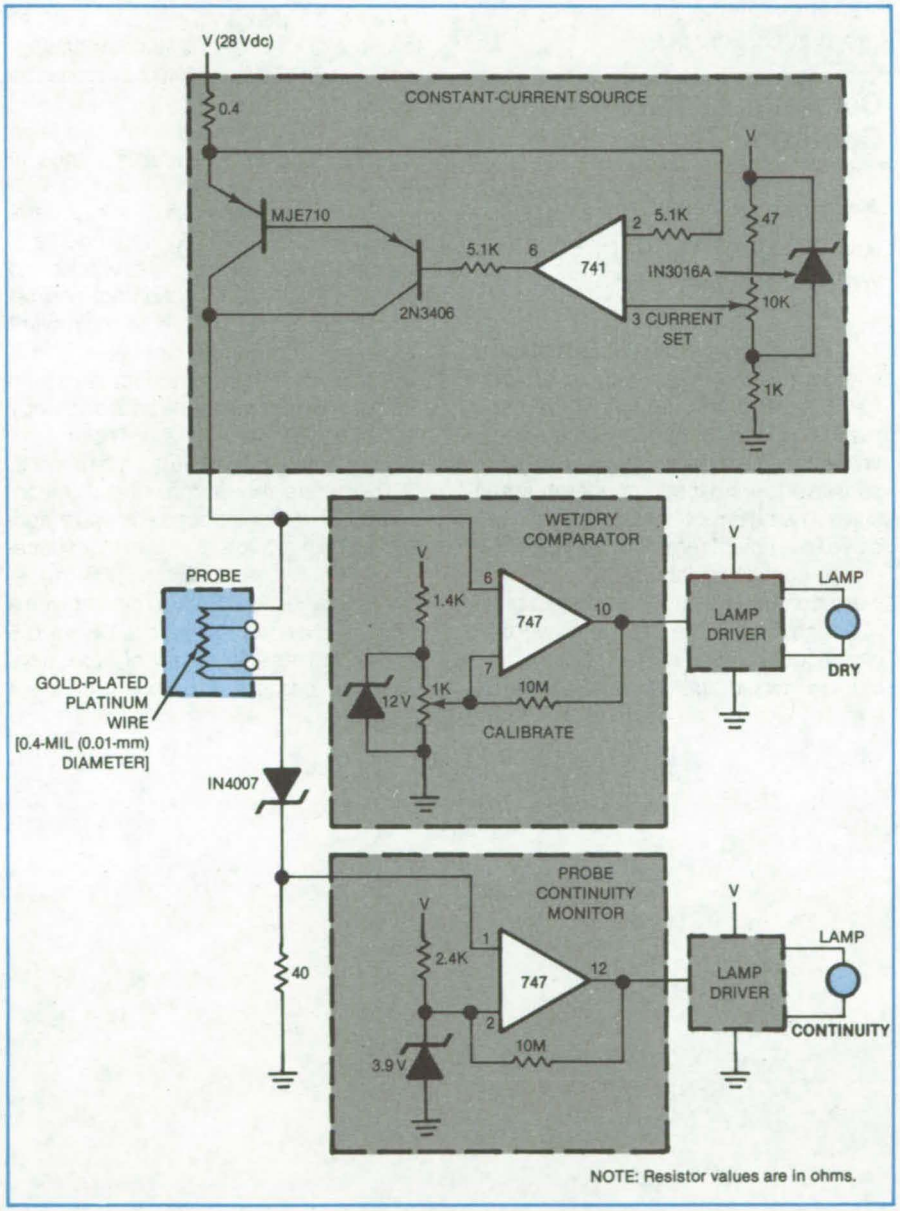

The **Sensor Circuit** is adaptable to different liquids and sensors. The constant-current source drives current through the sensing probe and a fixed resistor. The voltage-comparator circuits interpret the voltage drops to tell whether the probe is immersed in liquid and whether there is current in the probe.

Books and Reports

These reports, studies, and handbooks are available from NASA as Technical Support Packages (TSP's) when a Request Card number is cited; otherwise they are available from the National Technical Information Service.

Determining Solar-Cell Operating Temperature

A laboratory test measures the effect of windspeed and wind direction.

A recent report describes efforts to standardize the measurement of solar-cell operating temperature. A series of tests has shown that the solar-photovoltaic-cell temperature is extremely sensitive to windspeed, moderately sensitive to wind direction, and rather insensitive to ambient temperature. Tests run under controlled laboratory conditions were compared with outdoor field tests. Although most of the data taken were for one module type, it is likely that the conclusions would apply to other modules, particularly those having a glass front, a polymer back, and a metal frame.

The nominal operating cell temperature (NOCT) of cells in solar modules is an important characteristic: Typically, module power output decreases 0.5 percent per °C rise in cell temperature. Previous field measurements of NOCT appear to have been affected more strongly by fluctuations in windspeed (small gusts) than had been realized, leading to underestimates of NOCT.

NOCT is defined as the cell temperature of an open-circuited module irradiated at 80 mW/cm^2, with windspeed of 1 m/s and wind direction not parallel to the plane of the module, at an ambient temperature of 20° C. Until now, NOCT has been measured outdoors in natural Sunlight, where measurement accuracy is limited by variations in solar irradiance, ambient temperature, and wind.

To reduce the unknown and uncontrollable effects, indoor tests were conducted with artificial Sunlight in a space-simulator chamber 25 ft (7.6 m) in diameter. A 10-hp (7.5-kW) blower with a diffuser provided windspeeds from 0.5 to 3 m/s. The adjustment of laboratory room-air heaters controlled ambient temperatures from 19° to 38° C. The solar module under test was mounted on a pedestal that could be tilted and rotated to change panel orientation with respect to the wind. A turning mirror to one side provided makeup irradiance to keep module irradiance constant in spite of varying tilt angle. Module irradiance was monitored by measuring short-circuit currents in an array of calibrated solar cells temporarily placed on top of the module.

The module measured 1.2 by 0.7 m. It took about 30 minutes for cell temperatures to stabilize to ±0.1° C change per minute. The temperatures of two cells near the center of the module were monitored with thermocouples. From instrumentation considerations only, the accuracy of the NOCT determinations was probably better than ±4° C.

This work was done by John S. Griffith of State University of New York at Binghamton, Mulchand S. Rathod, and Joel S. Paslaski of Caltech and for **NASA's Jet Propulsion Laboratory.** *To obtain a copy of the report, Circle 8 on the TSP Request Card.*
NPO-15449

Electronic Systems

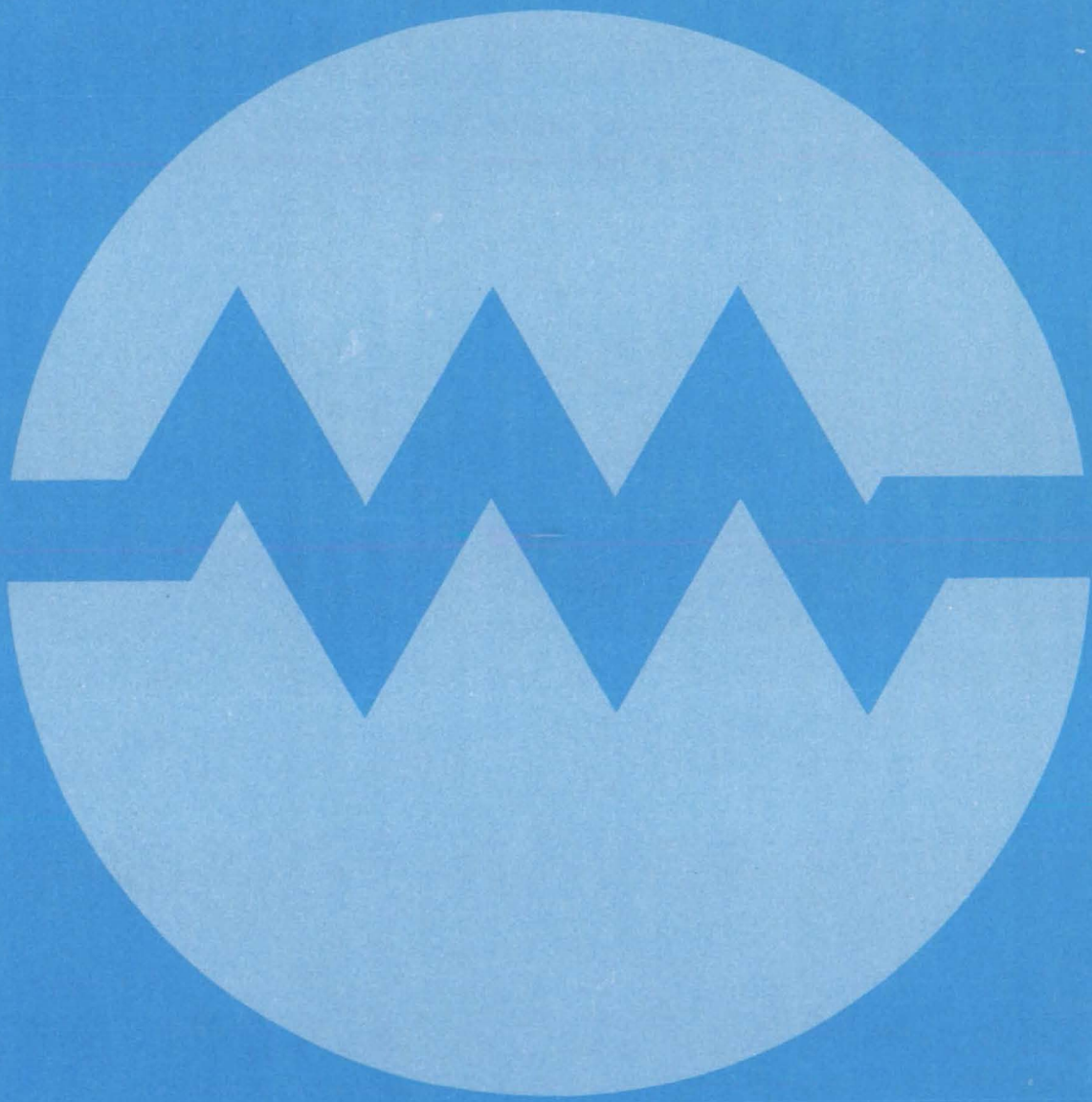

Hardware, Techniques, and Processes

Books and Reports

Fast Electronic Solar-Cell Tester

Microcomputer-controlled system gathers current and voltage data.

NASA's Jet Propulsion Laboratory, Pasadena, California

A microcomputer-controlled system measures solar-cell current/voltage (I/V) characteristics and determines key cell parameters, including short-circuit current; voltage, current, and power at the maximum-power point; and open-circuit voltage. A cell is automatically stepped through a sequence of electrical loads that increase from open-circuit to short-circuit, while the system measures the cell voltage and computes the power output. The data are displayed on a cathode-ray tube (CRT), recorded on an X-Y plotter, or stored on tape.

The system is illustrated in the figure. A shutter between the lamp and the cell reduces the exposure time and minimizes heating. Heating is further reduced by a dichroic reflector, which directs mostly visible light onto the cell while permitting much of the infrared light to escape. The cell is also cooled by forced air circulation.

Each load is applied to the cell by a programable dc power supply. Following the voltage measurement at each current setting, the microcomputer repeats and verifies the voltage measurement and computes the power output. The microcomputer steps the solar cell through approximately 200 test loads each second.

Data are obtained with three test sequences: In an initial sequence, dV/dI is determined at I = 0 followed by the measurement and verification of voltages at increasing currents in increments of 32 mA. Power is computed at each test point and compared with the previous value.

Upon detection of a decrease in power output, the program jumps to a sequence that decrements current by 1 mA until the maximum-power point has been passed again. The program then jumps to a third sequence that resumes the current stepping but with increments that are varied to maintain the voltage increments between 1.2 and 19.5 mV. The measurements continue until the plateau region of the I/V curve is completely mapped to the short-circuit (V = 0) point.

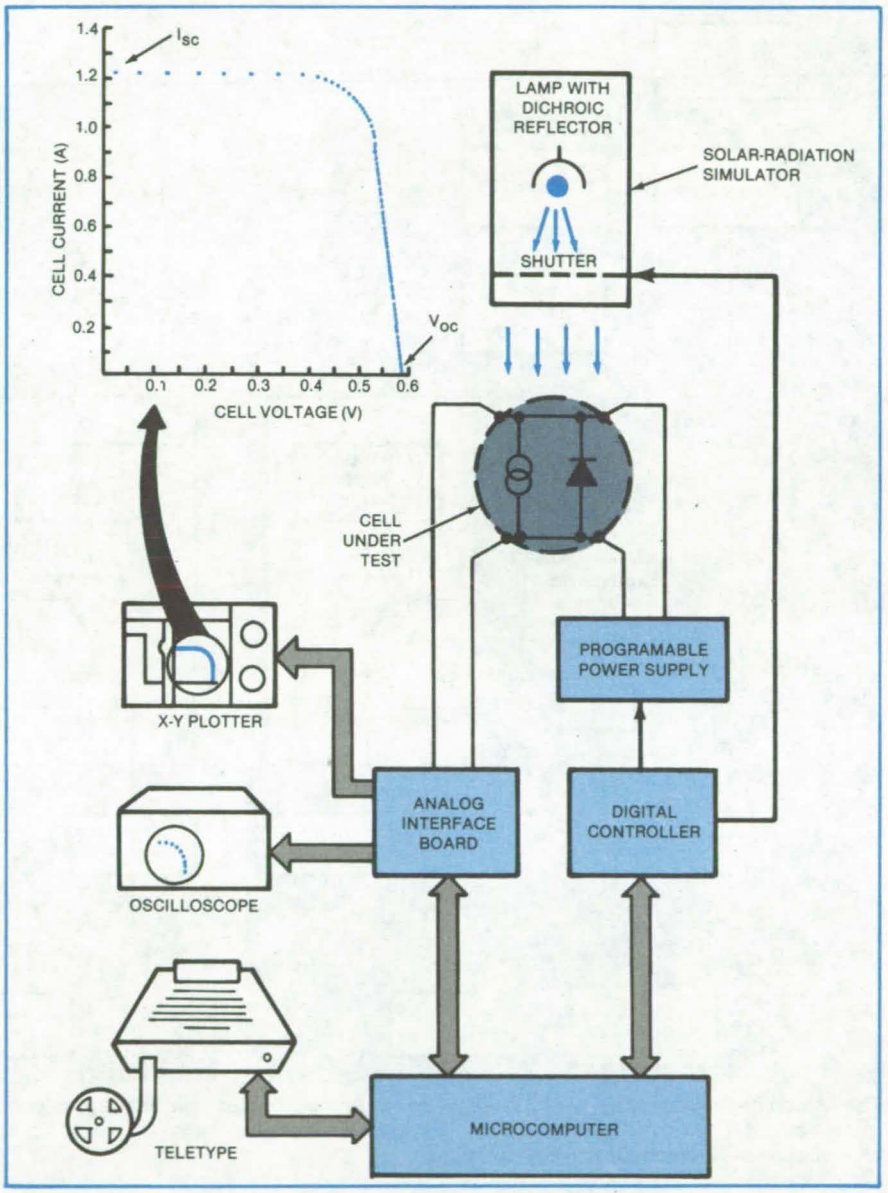

The **Programmable Photovoltaic-Cell Test System** consists of a light source, microcomputer, programable dc power supply, analog/digital interface, and data storage and display equipment. The system applies a series of test loads to the cell via the programable dc power supply to obtain the I/V characteristic curve and key cell-performance parameters.

The system tests a wide range of solar cells. The apparatus and programing technique are also applicable to other devices, such as other types of batteries and sensors.

This work was done by Jay W. Lathrop and Charles R. Saylor of Clemson University for **NASA's Jet Propulsion Laboratory.** *For further information, Circle 9 on the TSP Request Card.*
NPO-15676

Efficient Distribution of Frequency-Standard Signals

Path-length-corrected system can use microwaves or optical links with minimal hardware.

NASA's Jet Propulsion Laboratory, Pasadena, California

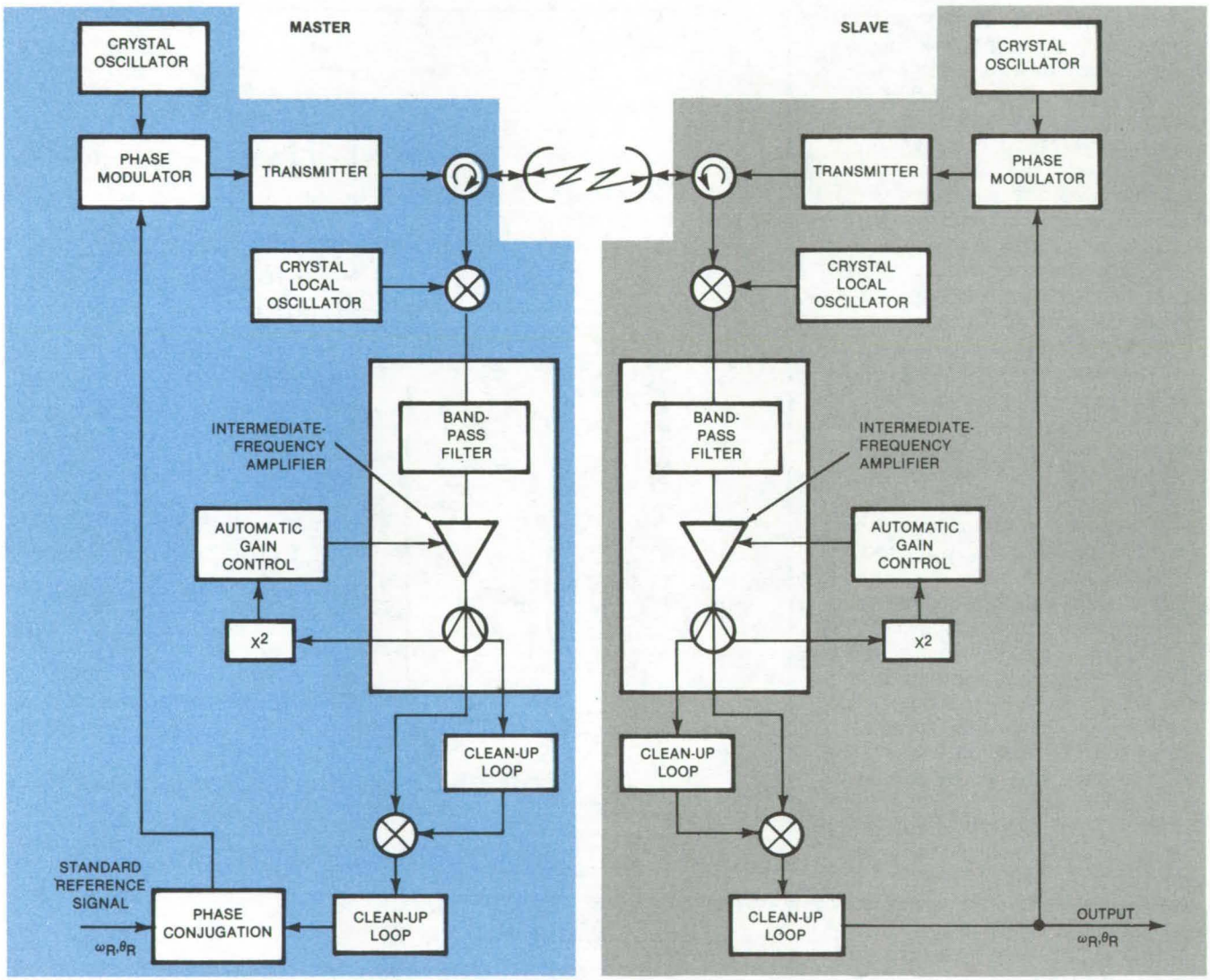

The Reference Frequency ω_R at phase angle θ_R modulates the transmitter at a master transmitter/receiver circuit and is recovered at a remote circuit. The two circuits continuously transmit to one another, on microwave or optical signals 100 MHz apart, to effect the synchronization of reference frequency and phase.

A low-power system distributes a precise frequency-standard signal to a network of remote stations. The system is "exact" (i.e., corrected for the transit time), yet is inexpensive because it transmits at only 20 milliwatts and requires no coding or synchronized switching circuits. Its correction capability is a few parts in 10^{15}.

The principal is to apply a compensating, advance phase shift to the master transmitter signal and then correct it by comparison with the phase of the delayed signal received from the slave transmitter. This operation is predicated on the path not exhibiting excessive dispersion over the 100-MHz frequency separation of the master and slave transmitters at the approximate 8-GHz carrier frequency.

The operation of the link is illustrated in the figure. The standard or reference frequency, ω_R, at phase angle θ_R modulates the master transmitter. The transmitters are crystal-controlled phase-modulated oscillators. The receivers at the opposite stations employ crystal-controlled local oscillators. The band-pass filters at the inputs to the intermediate-frequency (IF) amplifiers prevent transmitter leakage from disturbing the IF amplifiers.

At the output from each IF amplifier, a cleanup loop extracts the residual carrier, which is then used to demodulate the sidebands. Due to this method of demodulation, the phase and frequency of the demodulated reference are not functions of the transmitter frequency or

local-oscillator frequency; this feature greatly relaxes the design constraints on the circuit hardware. The detected signal then passes through a second cleanup loop that sets the ultimate bandwidth of the receiver and therefore its signal-to-noise ratio. As can be seen, the master and remote circuits are identical except for the addition of a phase conjugation circuit, where the standard is fed in, and a wider-bandwidth cleanup loop in the master circuit.

This work was done by Roger F. Meyer, Richard L. Sydnor, and John W. MacConnell of Caltech for **NASA's Jet Propulsion Laboratory.** *For further information, Circle 10 on the TSP Request Card.*
NPO-15392

Coding for Single-Line Transmission

Scheme for code generation and conversion has only modest equipment requirements.

John F. Kennedy Space Center, Florida

A new digital transmission code combines data and clock signals into a single waveform. Previously, Manchester-coded biphase waveforms were used in a NASA application. Manchester generators were needed for encoding, and bit synchronizers were needed for decoding. In contrast, MADCODE needs only four standard integrated circuits in both the generator and the converter plus five small discrete components.

In MADCODE, the beginning of each bit period (see Figure 1) is characterized by a low-to-high transition; since such a transition occurs only at the beginning of a bit period, the clock information is recovered from the code readily. There are three counts per bit period. The first count defines the clock signal. The third count marks the final portion of the bit period and ensures that a low-to-high transition can occur at the start of the succeeding bit period. Data are conveyed with the second count and are represented by a one (high) or a zero (low).

The clock signal is recovered from a MADCODE waveform by locking a phase-locked-loop circuit (clock detector) to an incoming signal (see Figure 2). The center frequency of the phase-locked loop is set at triple the bit rate of the triphase signal. A divide-by-3 counter (MC14017 or equivalent) provides feedback to the phase-locked loop.

The outputs of the counter are Q_0, Q_1, and Q_2, in sequence. Q_1 represents the second count time of the bit period. The trailing (high-to-low) transition of Q_1 marks the center of the data portion of the bit period. The incoming signal is sampled at that time, and the incoming data are recovered. The counter reset pulse, which returns the data counter to Q_0, indicates the beginning of a new bit period and establishes synchronization. The bit rate of the MADCODE converter can be varied over a wide range by adjustment of the components that control the operating frequency of the phase-locked loop.

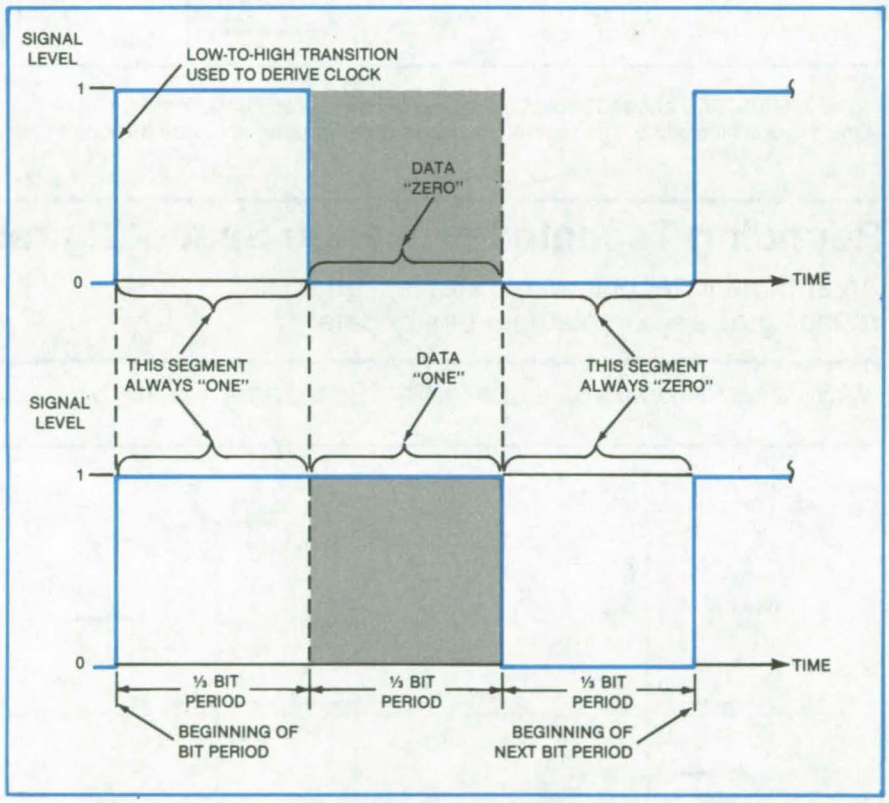

Figure 1. MADCODE Signals are characterized by a bit period divided into three equal segments, with a low-to-high transition at the beginning of every period.

The generation of MADCODE from data and clock signals is somewhat similar to data recovery as described above. The incoming clock frequency is tripled by a phase-locked loop. A 3-bit counter (with resetting controlled by the leading edge of the incoming clock signal or by Q_2, the counter output) is pulsed by the phase-locked loop and establishes the three counts per bit period. The incoming data signal is used to gate the counter outputs. This establishes the output waveforms:

Data	Code Output
"0"	100
"1"	110

(continued on next page)

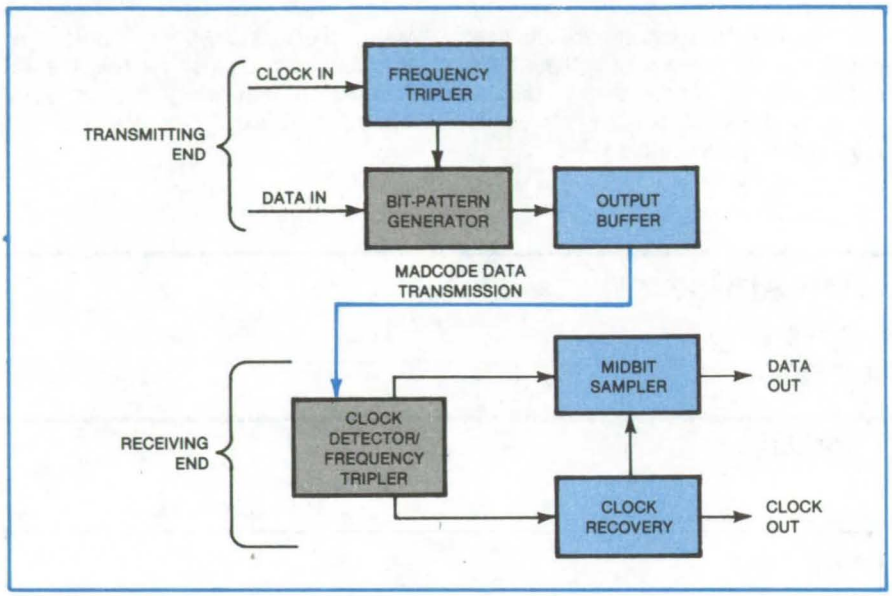

Figure 2. **MADCODE Allows Simple Coding and Decoding** for the transmission of digital signals over a single line. The scheme has been demonstrated in prototype equipment.

For greatest accuracy, the MADCODE generator uses an external clock. A clock signal can also be generated by using a crystal oscillator to control the phase-locked loop. Where less stability is required, the counter reset pulse can be used to gate incoming data, and no external clock is then required.

This work was done by Larry G. Madison of Martin Marietta Corp. for **Kennedy Space Center.** *No further documentation is available.*
KSC-11220

Rounding Technique for High-Speed Digital Signal Processing

An arithmetic technique facilitates high-speed rounding of 2's-complement binary data.

NASA's Jet Propulsion Laboratory, Pasadena, California

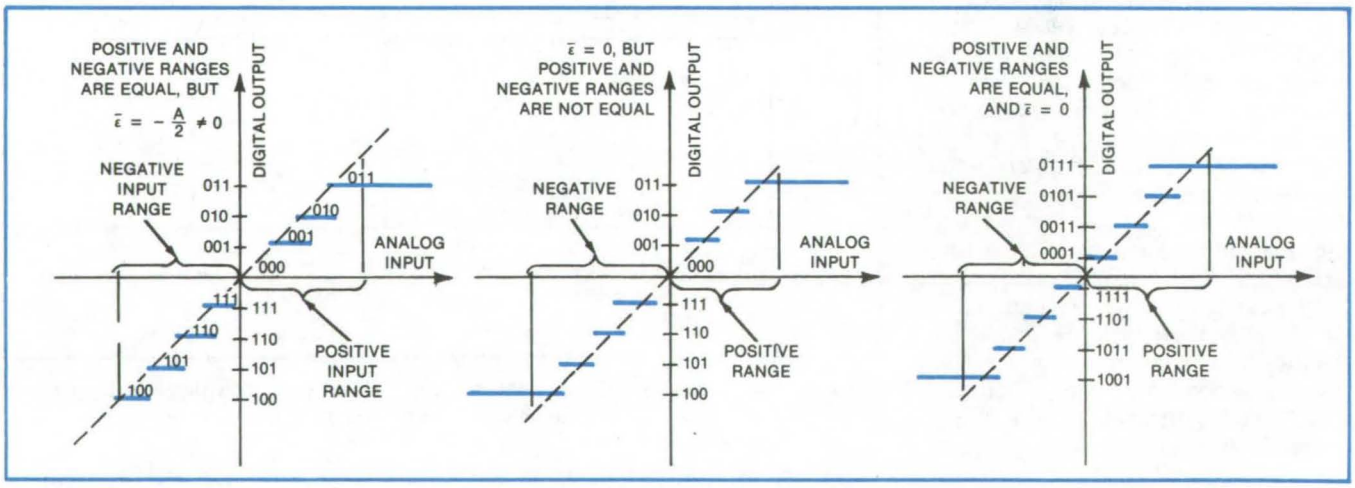

A/D Converter Output Versus Input is shown uncompensated (left), compensated by adding a voltage offset (center), and compensated by the new rounding technique (right). Although the mean error is zero with either compensation method, the positive and negative ranges are equal only with the new method.

Conventional rounding of 2's-complement numbers presents problems in high-speed digital circuits because it requires an adding operation. An alternate approach is truncation, which is not suitable when a large number of digital samples has to be accumulated because it produces a fairly-large mean error [minus one-half the least significant bit (LSB) for each digital sample]. The proposed technique consists of truncating k + 1 bits and then attaching a bit in the least significant position.

The attached bit is the result of an OR operation on the dropped bits. It can be shown that the mean error becomes zero. This method produces maximum errors as large as those due to truncation without compensation and an rms noise twice as large as that due to truncation or conventional rounding. Its advantages are that no adders are required to round and just one OR function is required, thus considerably reducing time delays.

An interesting application of the technique appears when the output of an analog-to-digital (A/D) converter is considered (see figure). If the analog input is considered as a digital number with an infinite number of bits, then its output is a truncation of the input. This produces the known mean error of minus one-half LSB, which is usually compensated for by introducing a voltage offset at the input. Although this approach does eliminate the average offset, it leaves the positive and negative ranges asymmetrical. An OR function on the dropped part will always produce a "1" since there is an infinity of bits in it.

Attaching a "1" at the end of a 2's-complement output from an A/D converter makes the mean output error zero, eliminating the need to introduce a voltage offset at the input. The technique also reduces the hardware needed to process the 2's-complement output in subsequent operations.

It is not necessary to supply the LSB actually, as long as its effect is accounted for in subsequent operations. For example, if two numbers have to be added, all that has to be done is to provide a "1" to the carry input of the adder.

Another advantage is that the 2's complement can be generated without using an adder. This is done by keeping the LSB a "1" and making the 1's complement of the rest of the word, a great advantage in high-speed circuits.

This work was done by Erwin R. Wechsler of Caltech for **NASA's Jet Propulsion Laboratory.** *For further information, Circle 11 on the TSP Request Card.*
NPO-15307

Receiver for Antenna Arrays

A scheme to obtain an amplified, demodulated output.

NASA's Jet Propulsion Laboratory, Pasadena, California

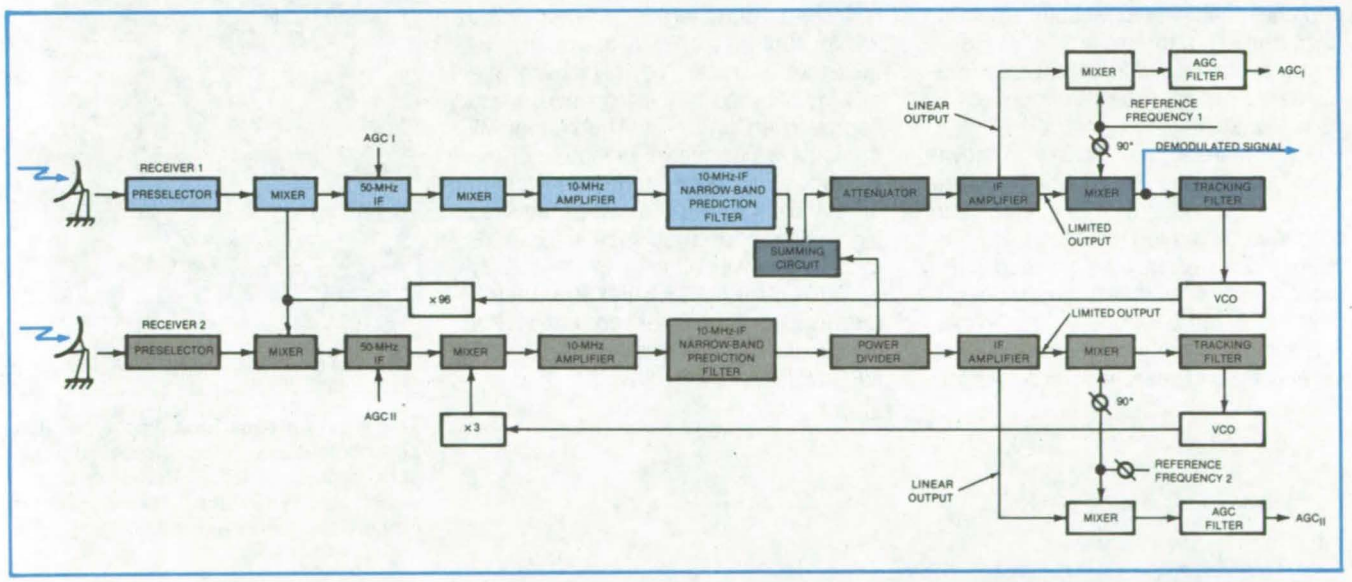

This **Diversity Reception** system can be used for narrow-band signals. The system can be extended to three or more receivers.

A diversity-reception system originally developed for use aboard spacecraft combines narrow-band signals from several antennas to yield an amplified demodulated signal. The net power gain for a two-receiver array is 3 dB.

The system, illustrated in the figure for a pair of receivers, has two IF stages in each receiver section. The phase-modulated signal outputs of the second IF sections of both receivers are combined, with proper adjustment for phase differences using a phase tracking loop, and are injected into the second IF section of one receiver, which is called the "master" section. The system output is taken from the output of the master section.

A phase-locked loop (PLL) in the master contains a voltage-controlled oscillator (VCO) that provides a first local oscillator frequency to mixers in the master and in the other receiving section. The second IF mixer of the master receives a reference frequency but the second IF mixer of the other section receives a signal from a PLL to track out any phase differences.

The second IF of both sections are filtered and combined into the second IF of the master through a summing circuit. Any fixed phase difference in the second system (for instance, due to differences in group delay through the antenna and low-noise amplifier) is canceled by an adjustment of the phase of a reference applied to a third mixer in the phase-tracking loop.

Each receiving section has its own automatic-gain-control (AGC) circuit to the first IF amplifier. With this system, an improved signal-to-noise ratio is achieved as a function of the number of receiving sections arrayed and of their power coupling into the master receiving section.

(continued on next page)

The system was originally developed for spacecraft command signals, which typically have bandwidths of a few hundred hertz. The phase modulation due to the signals is within the bandwidth of the narrow-band predetection filters but is high enough in frequency so as not to be tracked by the carrier-tracking loop that provides the first local oscillator for the array.

This work was done by Milton H. Brockman and Mahlon F. Easterling of Caltech for **NASA's Jet Propulsion Laboratory.** *For further information, Circle 12 on the TSP Request Card.*
NPO-15089

Searching for Clear-Air Turbulence

An airborne microwave system would locate the tropopause to assist in the avoidance of clear-air turbulence.

NASA's Jet Propulsion Laboratory, Pasadena, California

A system for determining the potential location and severity of clear-air turbulence is based on a passive microwave sensor. Mounted on the side of an airplane, for example, such a system could allow a pilot to evade clear-air turbulence. The sensor would permit safer, more comfortable flights for commercial airplanes and would enable safer in-flight refueling for military airplanes. Flight evaluation with prototype hardware (see figure) shows the concept to be workable.

An antenna scans the sky at elevations above and below the airplane horizon and measures thermal radiation produced by oxygen molecules at a frequency of 56 GHz. An onboard computer converts the measurements of sky brightness temperature versus elevation angle to a profile of air temperature vs. altitude and searches the profile for:

- Inversion layers — regions of the atmosphere in which temperature increases with altitude instead of decreasing as usual — and
- The tropopause — the interface between the troposphere and the stratosphere (sometimes the coldest altitude in the atmosphere).

Clear-air turbulence is often found within such regions. The system will therefore provide the pilot with the altitude location of the tropopause and nearby inversion layers. The system will compute a parameter indicative of the probability of moderately-severe clear-air turbulence and display an advised flight-change for turbulence avoidance.

This work was done by Bruce L. Gary of Caltech for **NASA's Jet Propulsion Laboratory.** *For further information, Circle 13 on the TSP Request Card.*
NPO-15351

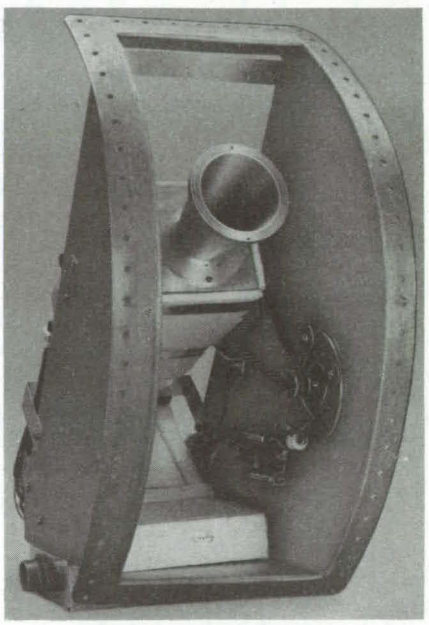

This **Horn Antenna** for a prototype clear-air-turbulence warning system is rotatable through ±45°. Installation is in a wheel well in NASA's C-141 Kuiper Airborne Observatory aircraft.

Printed Circuit Converts RF Energy to dc Power

A new ultra-light-weight, low-cost, flexible 2.45-GHz-film, etched-circuit "rectenna" format, made from Kapton F-film, converts RF energy directly to dc power at an overall efficiency of 85 percent and a mass-to-dc-power-output ratio of 0.4 kg/kW. The element is fabricated from laminated material consisting of a thin-film dielectric bonded between two thin sheets of copper.
(See page 242.)

Heart-Rate and Breath-Rate Monitor

A circuit requiring only four IC's measures heart rate and breath rate to an accuracy of ± 1 pulse/minute. An inexpensive phase-locked loop generates a linear output signal proportional to the input. The circuit measures heart rates between 20 and 255 beats/minute and respiration rates between 4 and 6 breaths/minute.
(See page 289.)

X-Ray Detector for 1 to 30 keV

An array of silicon diodes measures photon energy and provides an image of the X-ray pattern for photon energies in the range of 1 to 30 keV. The detector array should provide useful for imaging and spectroscopy in industrial part inspection, pulsed-plasma research, and medical applications.
(See page 248.)

Focal-Plane-Array Optical Proximity Sensors

Objects are detected at beam-axis intersections.

NASA's Jet Propulsion Laboratory, Pasadena, California

A proximity-sensing system originally developed to trigger the braking system of an automatically controlled car should be useful in industrial situations requiring three-dimensional location or detection of objects. The system includes an array of light sources and receivers that respond when a reflecting object intercepts one or more light beams at a specified range.

As shown in Figure 1, the system consists of several illuminator boxes and detector boxes. For the automatically controlled car, the boxes are mounted along the front bumper. Proximity to an object is sensed when one or more beams from the illuminator boxes strike the object and reflect into one or more detector boxes.

The elements within an illuminator box or a receiver box are grouped at the focal plane of a compound lens (Figure 2). A focal-plane stop restricts the fields of view to the required regions in front of the lens: for example, high or low, left or right. The use of one lens for several elements reduces the number of required optical adjustments.

The compound lens, although resembling a fine camera lens, need not have all the attributes of a camera lens, such as full color correction and the ability to focus to extremes. The basic requirements are that its image quality, field of view, and depth of focus should be adequate.

In each illuminator box, the lens forms a bundle of nearly-parallel light beams: one beam for each light source. Each detector in a detector box lies at a position in the focal plane at which a light beam coming in from a designated viewing direction would be focused. The outgoing-beam (illuminator) axis of a source and the viewing axis of a corresponding detector are chosen so that the two axes intersect where an object is to be sensed.

The multiplicity of detectors in an array enables each detector box to view more than one region and also enables two detector boxes to view one or more regions in common. Similarly, each illuminator box could illuminate more than one region. For example, in the automatically controlled vehicle, each detector box has two incoming-beam axes that intercept the illuminating beam at 16.5 ft (5 m) and 5 ft (1.5 m), respectively.

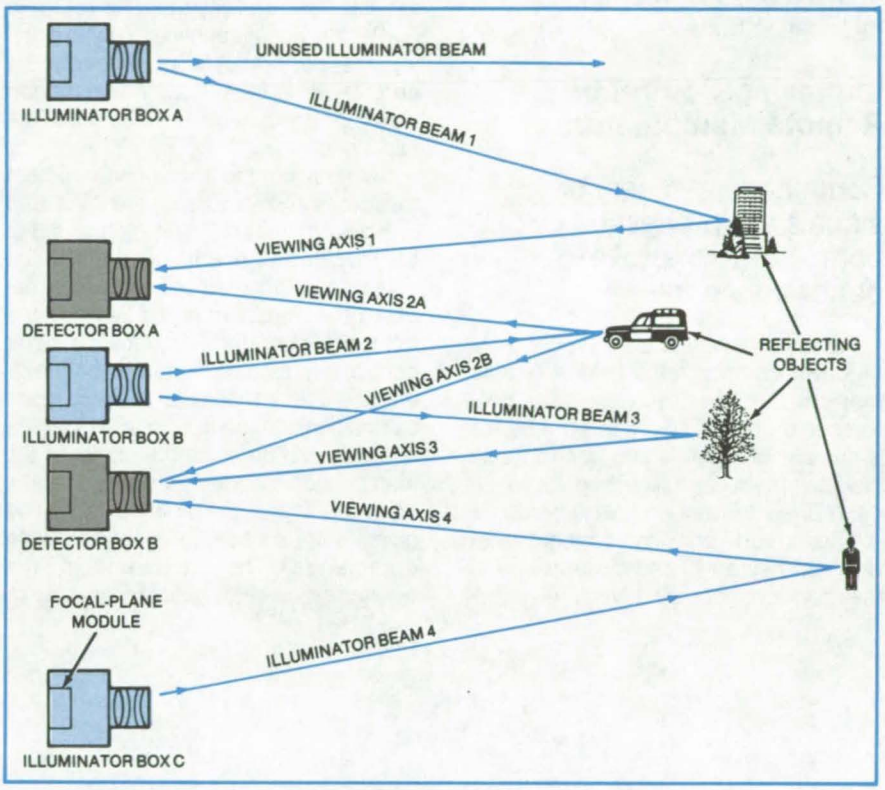

Figure 1. The **Illumination and Detection Axes** in a set of proximity sensors are chosen to intersect at prescribed distances. An object that enters any of the fields of view defined by the intersections will reflect light to one or more of the detectors. This system has some redundancy: Both detector boxes A and B view the same object at an intersection with illuminator beam 2.

This work was done by Alan R. Johnston of Caltech for **NASA's Jet Propulsion Laboratory.** *For further information, Circle 14 on the TSP Request Card.*
NPO-15155

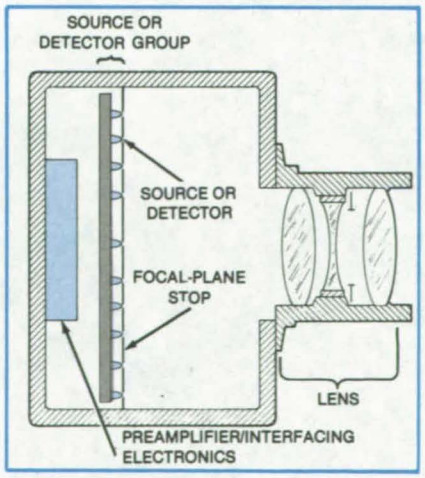

Figure 2. **A Group of Light Sources or Detectors** is mounted in a box at the focal plane of a lens. Each box can therefore illuminate or view several axes, each corresponding to a source or detector of the group.

Books and Reports

These reports, studies, and handbooks are available from NASA as Technical Support Packages (TSP's) when a Request Card number is cited; otherwise they are available from the National Technical Information Service.

Improving Control of Remote Manipulators

Commands and sensor signals are processed by computer to improve performance feel.

Advanced theoretical and experimental developments in the field of remote manipulators are discussed in a conference preprint. The report synthesizes a number of sensing and control techniques previously discussed in *NASA Tech Briefs* articles and elsewhere.

The broad unifying concept that distinguishes advanced systems is that the performance of a remotely controlled manipulator can be improved by having the manipulator itself affect the control signals. This concept was developed for manipulators to be used in Space Shuttle missions (such as unloading cargo in space and retrieving satellites and stowing them for return to Earth): It is equally applicable for improving the performance of manipulators and robots in hazardous areas, underwater, or in many other commercial applications.

Sensors on the manipulator detect the forces and torques on the joints and grasping members ("end effectors") of the manipulator and its proximity to the object to be grasped. A computer processes the signals from the sensors and from the operator's joystick or other control interface, commands the movements of the manipulator, and feeds back signals to the interface so that the operator can perceive the action of the manipulator. Mode switches let the operator adjust the relative weighting given to the sensor signals and position commands. The feedback to the operator may be by graphics display or by voice, as well as by the feel of the controls.

A typical example of the manipulator technology is the force-reflecting position hand controller described in "Remote Manipulator Has Realistic 'Feel' " (NPO-15065), on page 321 of this issue. In another example, a lifting mechanism is required to place a beam with each end on a support stand. During the beam handling, immediate control of the manipulator passes back and forth between operator and computer. The operator transmits to the computer and manipulator via an analog control console and voice input. The computer network transmits to the operator via a video screen, graphics display, and voice output. The portions of the task that do not require operator intervention or decision are controlled automatically by the computer alone.

This work was done by Antal K. Bejczy of Caltech for **NASA's Jet Propulsion Laboratory.** *To obtain a copy of the report, Circle 15 on the TSP Request Card.*
NPO-15049

Physical Sciences

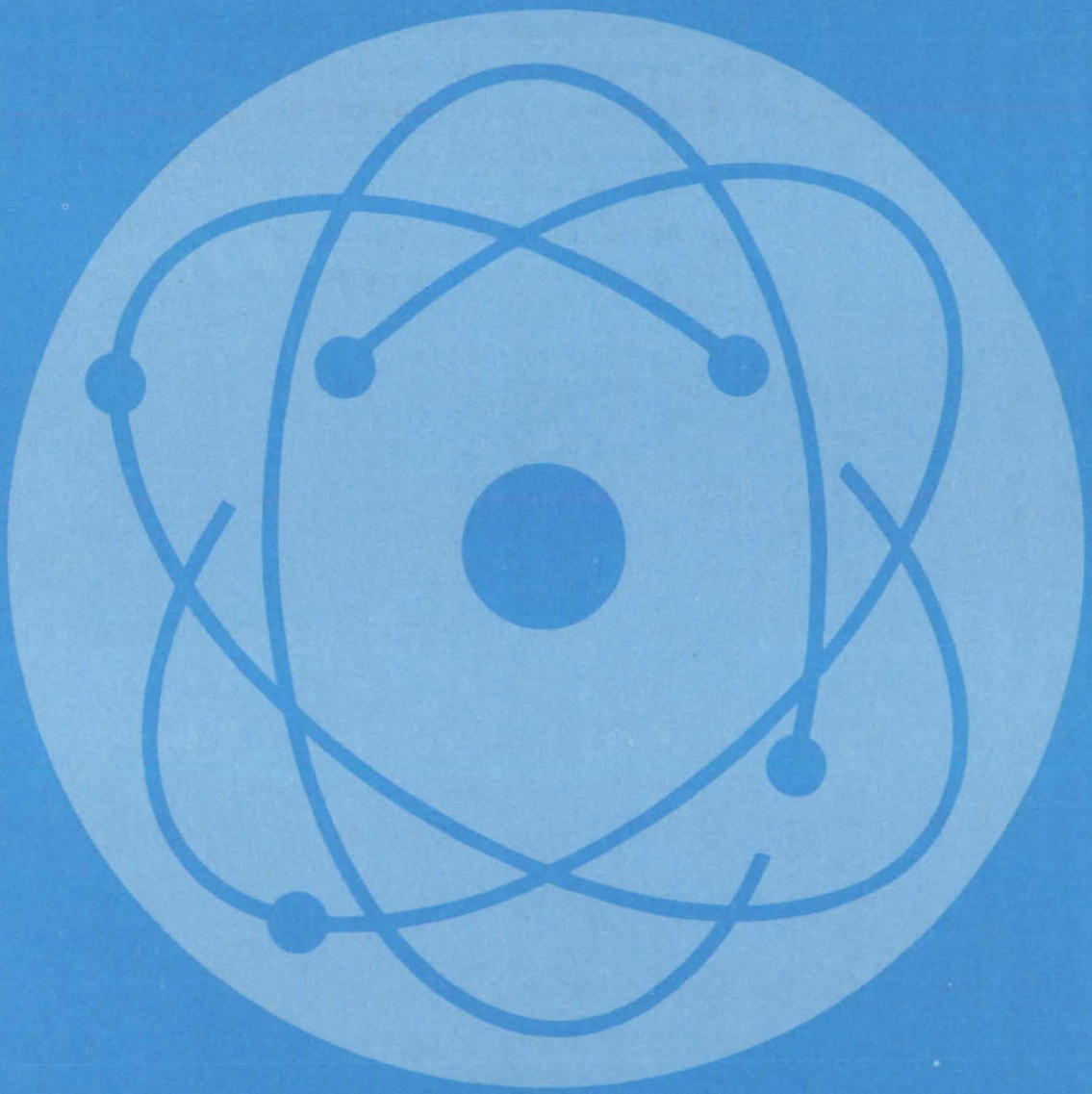

Hardware, Techniques, and Processes

Books and Reports

Fabricating Grating Couplers on Optical Fibers

Microscopic corrugations are formed on fiber surfaces.

Lyndon B. Johnson Space Center, Houston, Texas

Recent experiments show the feasibility of incorporating diffraction gratings into the surfaces of thinly-clad optical fibers. Grating couplers would couple signals into and out of single-mode optical waveguides without requiring precise alinement of the components, although their in-service efficiency has yet to be verified.

Coupling is most efficient when the grating is close to the fiber core (which typically has a diameter of 2 to 6 μm). Therefore, before forming the surface grating, a portion of the fiber cladding must be removed. This can be done by mechanical polishing to form a flat grating substrate or by chemical etching to form a thin cladding as a substrate for a grating that extends all the way around the fiber (see Figure 1).

The grating is scribed holographically. After photoresist is applied to the substrate, the pattern of lines is exposed onto the resist by setting up an interference pattern using two laser beams. The grooves are then produced in the developed photoresist by ion milling (see Figure 2).

Various grating patterns could be used. The simplest would be a series of uniformly-spaced parallel lines. With such a grating, different wavelengths would enter (and leave) the fiber at different angles. This characteristic would be convenient for multiplexing and demultiplexing signals of different wavelengths. A series of gratings of various spacings could be used to pick off or insert signals of different wavelengths (one wavelength for each location).

Light leaving the fiber through the grating could be brought to a focus without a separate lens if the grating spacing varied with distance along the fiber. Such a grating is said to be "chirped." The uses for the grating include optically multiplexing and demultiplexing fiber-optic communications channels; measuring a wavelength spectrum; and sensing temperature by an optical wavelength shift (such as the emission wavelength of an injection laser diode, which is temperature-sensitive).

This work was done by Charles R. Chubb, John K. Powers, and David A. Bryan of McDonnell Douglas Corp. for

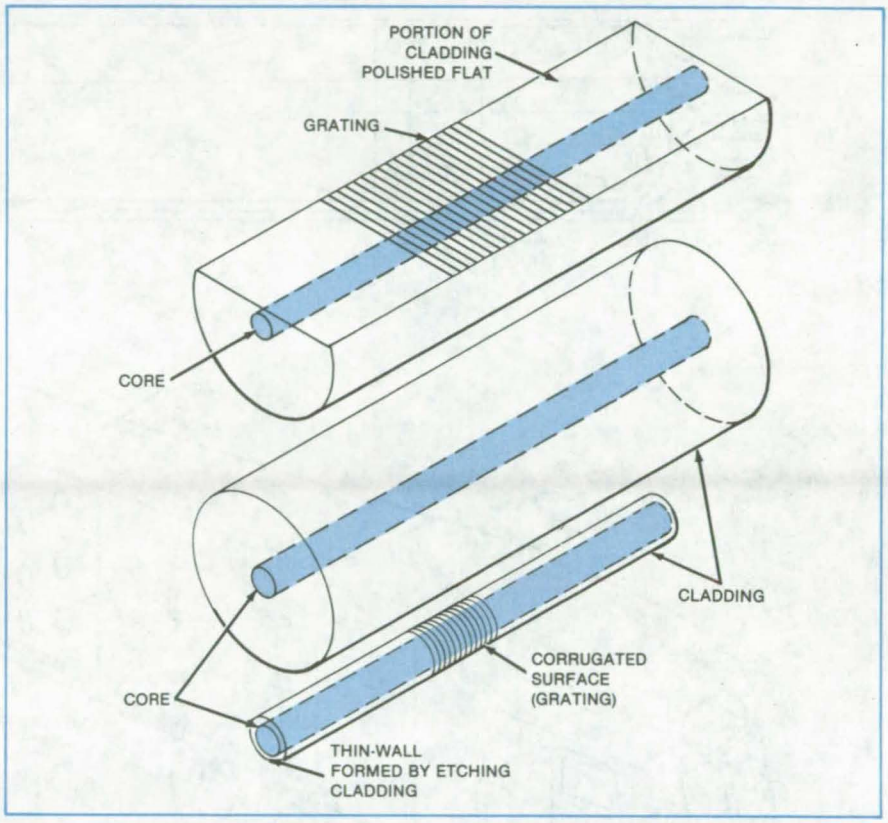

Figure 1. The **Thick Fiber Cladding Is Partly Stripped Away** so that the grating will be formed near the core. To form a flat substrate for the grating (above), the fiber is encased in epoxy, then polished flat. To form a round substrate for the grating (below), the cladding is chemically etched through most of its thickness.

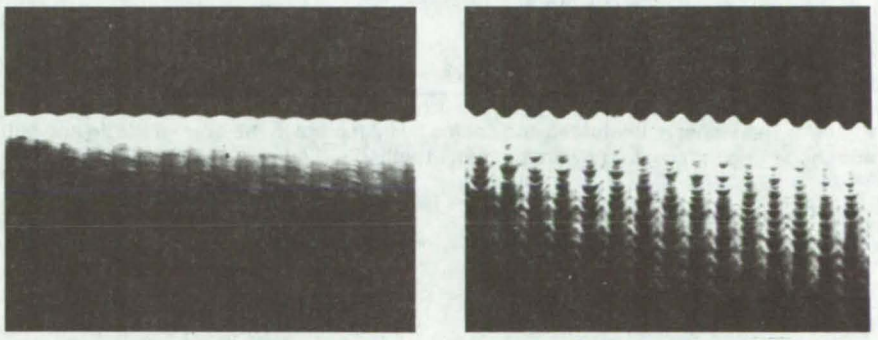

PHOTORESIST GRATING ON A GLASS FIBER BEFORE ION MILLING

GRATING ON AN OPTICAL FIBER AFTER ION MILLING

Figure 2. A **Photoresist Is Holographically Exposed,** developed, and ion-milled to produce the corrugations of the grating surface. This is a round grating of the type shown in Figure 1, except that it is on a thick-wall cladding.

Johnson Space Center. *For further information, Circle 16 on the TSP Request Card.*
MSC-20286

Improved Cattle Hauler

Better aerodynamics and ventilation would increase fuel efficiency and decrease shipping losses.

Dryden Flight Research Center, Edwards, California

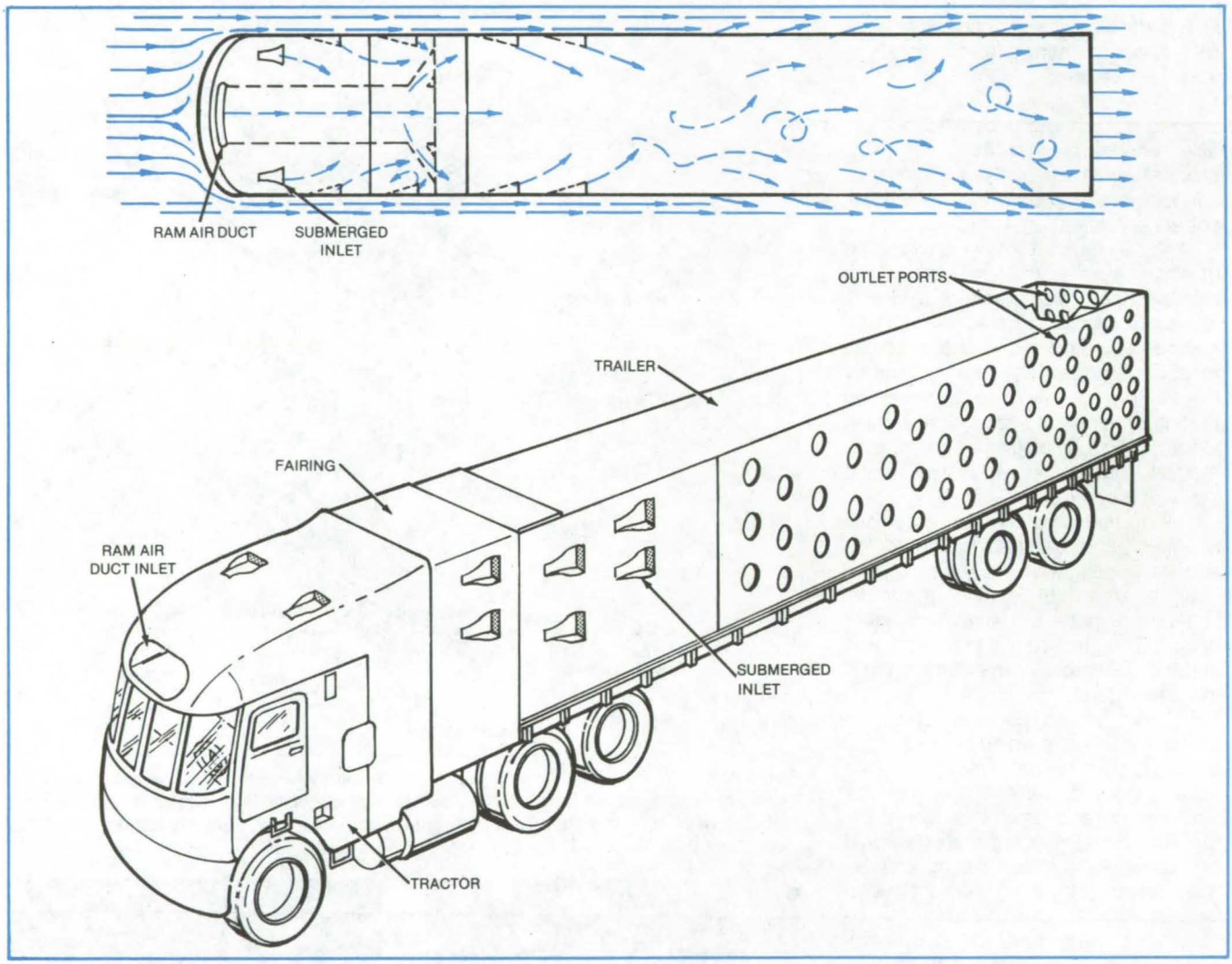

Figure 1. The **Trailer Is Ventilated** and cooled by inlet ports in the front of the rig and outlet ports in its middle and rear. The rounded cab and the fairing reduce drag by creating an attached airflow.

Ventilation and temperature control in livestock hauling rigs is improved by a proposed design that incorporates aerodynamic concepts. The aerodynamic refinements would also improve fuel efficiency.

In the new design (see Figure 1), the front of the cab is rounded, and a fairing covers the space between the cab and trailer. The combination establishes an airstream that is aerodynamically attached to the exterior of the rig.

While the rig moves at highway speeds, a ram inlet in the front of the cab supplemented, as required, by submerged inlets in the cab, fairing, and trailer, along with outflow ports in the trailer, continuously flush the livestock area. The ingested airflow sweeps toxic fumes, and gases generated in the trailer, and discharges them from the trailer to prevent stagnant pooling. The airflow also continuously flushes the space between the cab and trailer, preventing the buildup of heat, which can be tragic to cattle riding in the front of the trailer. The number and distribution of the inlet and outlet ports, which would be established empirically, ensure a continuous pressurization of the

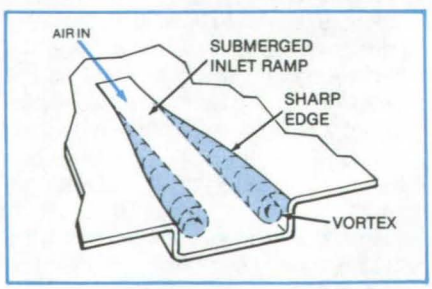

Figure 2. The **Submerged Inlet** consists of a ramp and a pair of curved divergent walls that intersect the exterior surface in sharp edges to produce vortexes that improve the airflow into the rig.

trailer. The same design concepts may be applied to "straight" (that is, nonarticulating) livestock trucks.

The submerged inlet (see Figure 2), which was originally developed to ingest air from the surface of an aircraft fuselage and deliver it to the engine and other components, has a pair of curved divergent walls that minimize the disturbance to the downstream attached airflow caused by ingesting air. Also to minimize turbulence, the ram air inlet has smooth nicely rounded edges. By restricting the flow through the inlet and outflow ports, temperature can be controlled in colder climates.

This work was done by Edwin J. Saltzman of **Dryden Flight Research Center.** *For further information, Circle 17 on the TSP Request Card.*

Inquiries concerning rights for the commercial use of this invention should be addressed to the Patent Counsel, Dryden Flight Research Center [see page A5]. *Refer to FRC-11058.*

Charged-Particle Flux Sensor

Improved design has greater collection efficiency.

Marshall Space Flight Center, Alabama

An improved version of the Faraday cup is expected to increase the accuracy of measurements of the flux density of charged particles (usually electrons or protons). Earlier current collectors of this type were constructed without specific attention to current losses from secondary emission or reflection of the incident particles. Consequently, measurement errors reached as high as 20 to 30 percent. The new sensor traps most of the secondary and reflected primary charged particles, thus assuring nearly complete current collection and accuracy over a wide range of incident flux densities.

The charged-particle beam enters the sensor (see figure) through an aperture in the grounded, conductive outer case. The particles strike the cone and are either absorbed by the cone or reflected to the inner wall of the sensing cup (which is electrically connected to the cone). The apex angle of the cone should be as acute as possible (preferably less than 45 °), so that reflected and secondary particles are eventually trapped even though they might undergo multiple reflections. The particles or their charges are thus absorbed by the cone and cup, and their combined charges travel to ground through the current meter.

Proper shielding is essential to the operation of the sensor. The outer case serves as a shield to prevent incident particles from reaching the sensing cup by any route other than the designated collection aperture. A protective cup surrounds the electrical terminal at the rear of the cone assembly to prevent the particle beam from reaching that terminal and giving a false current reading. The cable that carries the sensed current to the current meter is shielded, either by multiple layers of metallic braid or by flexible metal tubing, with all exposed parts grounded to prevent charge buildup.

The new sensor can be used to measure electron or proton flux density in the range from 10^7 to 10^{20} $cm^{-2}s^{-1}$. The lower current limit can be extended by enlarging the aperture. The upper limit can be extended by adding thicker insulation and water cooling.

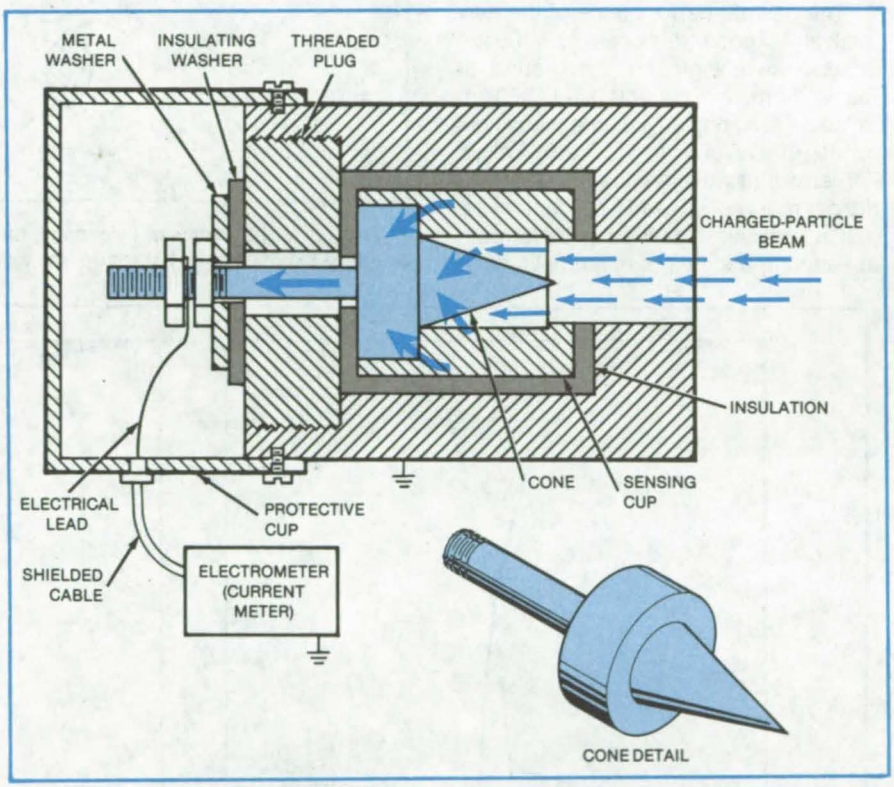

The **Charged-Particle Flux Sensor** traps charged particles incident along the axis through the collection aperture. The geometry of the cone-and-sensing-cup combination assures that most of the particles are trapped, even those that undergo multiple reflections.

This work was done by Don A. Gregory and Charles D. Stocks of **Marshall Space Flight Center.** *For further information, Circle 18 on the TSP Request Card.*

This invention is owned by NASA, and a patent application has been filed. Inquiries concerning nonexclusive or exclusive license for its commercial development should be addressed to the Patent Counsel, Marshall Space Flight Center [see page A5]. *Refer to MFS-25641.*

Lensless Scanning Telescope

Proposed dual-aperture device minimizes aliasing.

Langley Research Center, Hampton, Virginia

A new lensless scanning telescope concept was originally developed at Langley Research Center for possible application in a scanning radiometer for a spacecraft. In the spacecraft application, the radiometer would scan at right angles to the line of flight, giving complete coverage from horizon to horizon. Designers of terrestrial optical systems should also be interested in the concept.

The desired performance of the new design is good response for 100-km spatial wavelength on the ground at nadir from a spacecraft at 500-km altitude, requiring an instantaneous field of view (IFOV) of 4° to 6°. Possible aliasing errors at wavelengths of 100 km or longer must not exceed 2 percent. Aliasing in this case is defined as the error in measuring a signal of unit amplitude in

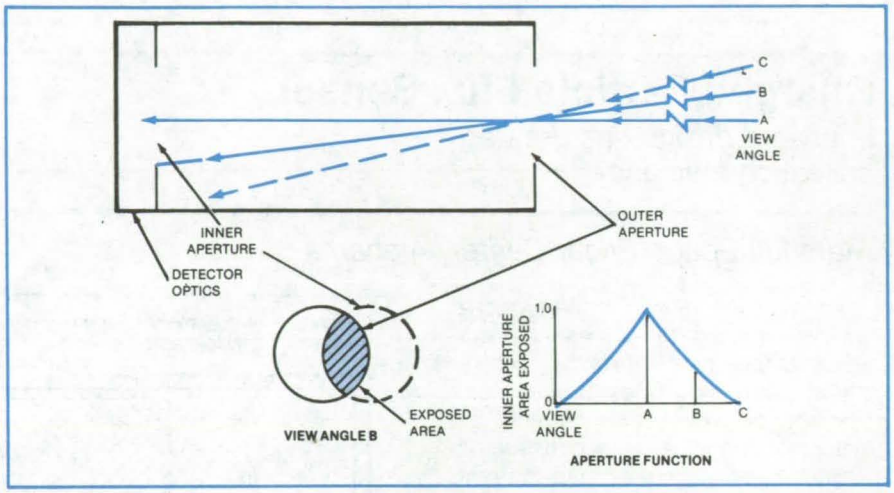

Figure 1. For the **Lensless Telescope,** the aperture function shows the area of the inner aperture exposed to a distant source as a function of the viewing angle.

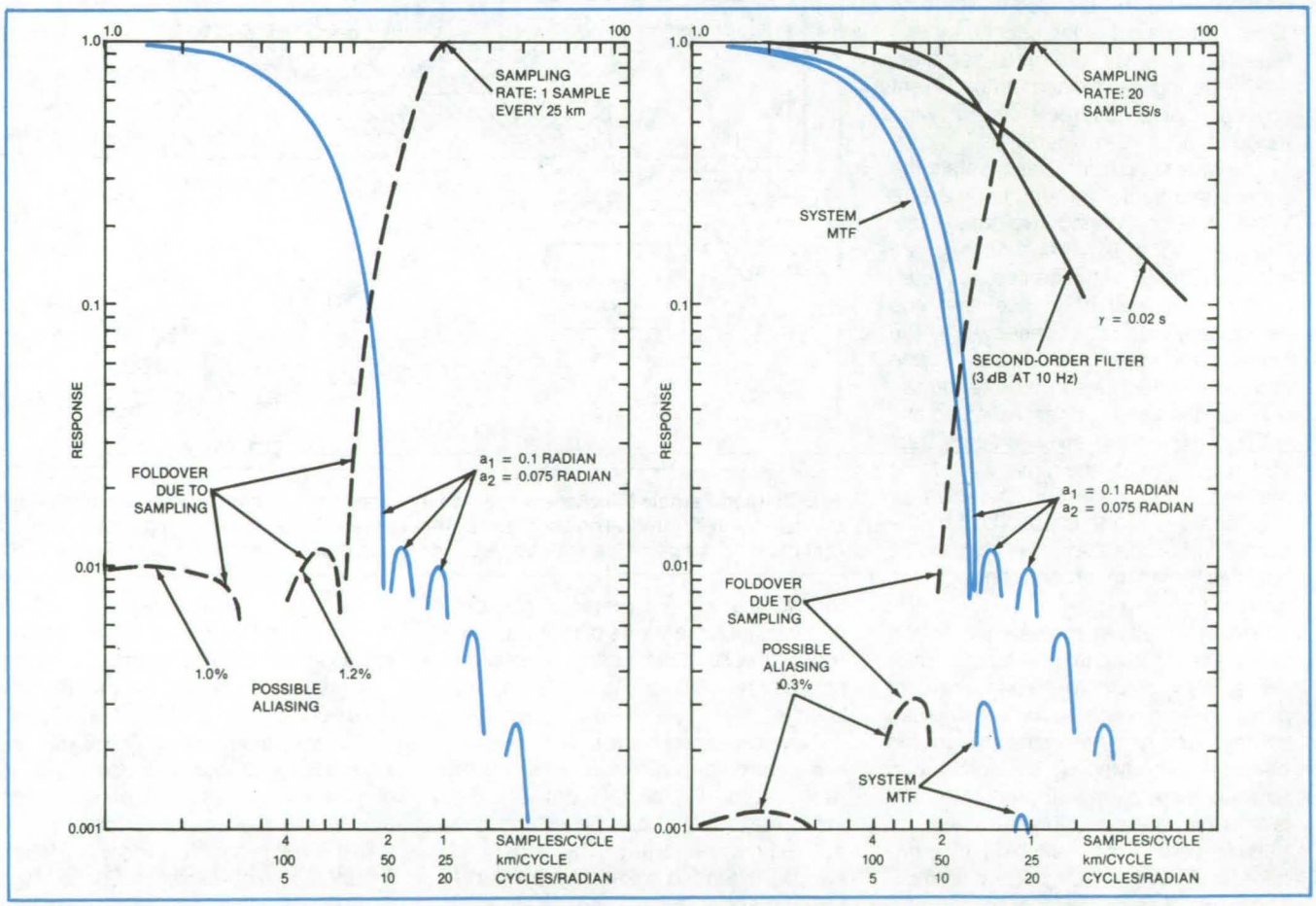

Figure 2. The **Scanner TF** is shown at the left across the scan and, at the right, along the scan. Telescope parameters are: inner aperture diameter = 7.5 mm, outer aperture diameter = 10 mm, and distance between apertures = 100 mm.

the spatial frequency range of interest, caused by unit signals at spatial frequencies above 12 cycles per radian.

An investigation of the aperture function (equivalent to the point-spread function) of two circular apertures, one behind the other, shows that in the geometrical-optics limit with a point source at infinity, the aperture function (AF) is identical to the modulation transfer function (MTF) of a diffraction-limited circular lens when plotted against spatial frequency. Figure 1 shows the combination of two apertures with a point source of light A at a distance located on the centerline of the apertures. With the source at B, only part of the light going through the first aperture goes through the second. From C, none of the light goes through the second aperture. The transfer function (TF) of this lensless telescope is equal to the square of the TF of a circular field stop in the image plane of a lens (see Figure 2).

With apertures on the order of 10 mm-diameter and nominal IFOV (defined as the angle of view through the outer aperture from the center of the inner aperture) greater than 3°, diffraction can be neglected. Outer aperture diameter is 10 mm, inner aperture diameter is 7.5 mm, and the distance between apertures is 100 mm. The F/number is F/10.

A reasonable time constant is assumed for the detector, and a second-order electronic noise filter compatible with other elements is utilized. Scan speed of 1 radian per second is set according to the groundspeed of the satellite and the available data rate so as to provide four samples per 100 km in both directions. With a nominal IFOV of 0.1 radian, or 5.7°, a response of about 48 percent is achieved at 100-km spatial wavelength along scan and 60 percent across scan with possible aliasing of less than 0.3 percent along scan and 1.25 percent across scan.

If equal response in both directions is desired, it would be necessary to decrease the time constant of the detector to 0.008 second or less. Another approach would be to make the apertures elliptical, retaining the 10- and 7.5-mm dimensions in the cross-scan direction and reducing the dimensions along scan to 8 and 6 mm, respectively. Possible configurations include use of the detector itself as the inner aperture or use of a concentrating lens in or behind the inner aperture to image the outer aperture on a smaller detector.

This work was done by Howard B. Edwards of **Langley Research Center.** *For further information, Circle 19 on the TSP Request Card.*
LAR-12648

Precise Measurement of Effective Focal Length

Computerized instrument measures effective focal lengths to 0.01 percent accuracy.

Goddard Space Flight Center, Greenbelt, Maryland

A computer-controlled instrument measures the effective focal length (EFL) of optical systems to 0.01 percent accuracy. The instrument also determines the shape of the focal surface and measures the modulation transfer function at points on and near the focal surface.

The EFL of even high-performance lenses, such as those used in surveillance satellites, varies slightly with field angle and if there are refracting elements, with wavelength as well. For small off-axis field angles ϕ, EFL is defined as the ratio y/ϕ, where y is the distance from the optical axis to the off-axis image point.

The variation of EFL with y is a measure of image distortion in the lens. Such residual image aberrations must be accurately measured, so that they can be corrected for during image processing and analysis. Even if no aberrations are detectable, the precise determination of EFL that results is equally valuable.

A laser source with a spatial filter (a precise pinhole) and a relay lens is initially placed on axis at the focal point of the lens (see figure). The conical light beam from this source passes through a beam splitter and illuminates the full aperture of the lens under test. Wavelengths are selected either by retuning the laser, by substituting lasers operating at different wavelengths, or by selecting among different discrete lines of one laser with filters.

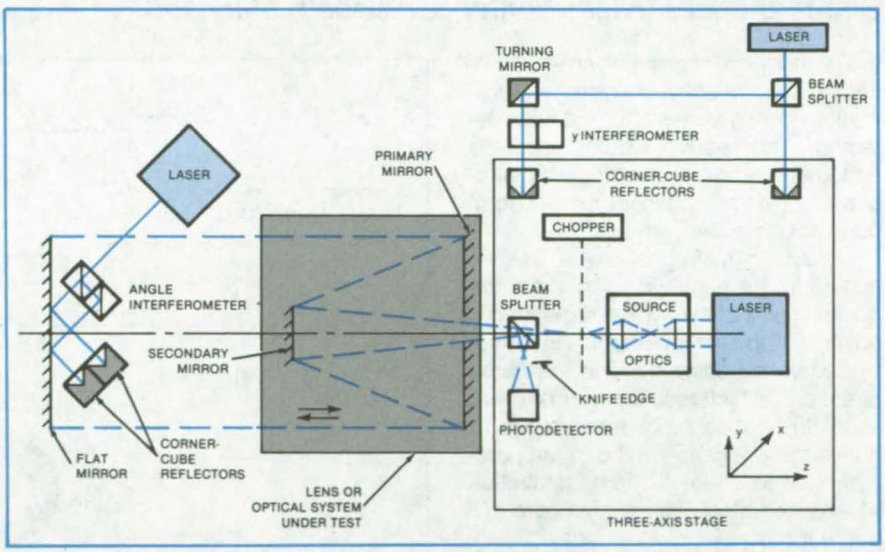

Laser Interferometers (color) are used to measure mirror angle ϕ and stage coordinate y in this instrument for accurate measurement of focal properties of optical systems. The instrument operates under computer control to measure effective focal length, focal-surface shape, modulation transfer function, and astigmatism.

The point-source system, beam splitter, knife edge, and detector are all rigid-

(continued on next page)

ly attached to a three-axis stage. The x and y coordinates of the stage motion are perpendicular to the optical axis, and the z coordinate is along it.

After passing through the lens, the beam is reflected from a flat mirror and passes back through the lens a second time. As it converges back toward the focal point, the beam splitter diverts part of the beam toward a knife edge and a silicon photodetector. The plane of the knife edge is located the same distance from the beam splitter as the point source. Thus the diverted beam comes to a focus in the plane of the knife edge if the point source is located at the focal point of the lens. The photodetector signal is proportional to the fraction of the beam not intercepted by the knife edge.

When the point source is moved off axis in the y direction, the mirror must be rotated through an angle ϕ about an axis parallel to the x-axis to keep the image of the point source at the knife edge. If either y or ϕ is varied independently, the image spot can be swept across the knife edge, producing a knife-edge response function signal in the detector. The distance between the ½-power points of successive knife-edge scans is input to the computer with the respective values of ϕ to determine EFL. The computer numerically differentiates the knife-edge response function to obtain the line-spread function. The computer then calculates the modulation transfer function, which is the Fourier transform of the line-spread function.

The instrument achieves its high accuracy by using laser interferometers to measure the critical coordinates ϕ and y. The alinement of these interferometers and that of the three-axis stage to the flat mirror are critical to the accuracy of the EFL measurement. The values of all four coordinates x, y, z, and ϕ are under the control of the computer via motorized stages.

The instrument can also evaluate astigmatism in the lens. The knife edge is repositioned parallel to the x-axis, and a second determination of the focal surface is made in the same manner as before except that the stage is moved in the x direction to sweep the image spot across the knife edge when taking knife-edge response functions. If the lens is astigmatic, the two focal surfaces will not coincide except at the optical axis.

This work was done by Timothy D. Wise and James B. Young of Hughes Aircraft Co. for **Goddard Space Flight Center.** *For further information, Circle 20 on the TSP Request Card.*

This invention is owned by NASA, and a patent application has been filed. Inquiries concerning nonexclusive or exclusive license for its commercial development should be addressed to the Patent Counsel, Goddard Space Flight Center [see page A5]. *Refer to GSC-12745.*

Cooling by Para-to-Ortho-Hydrogen Conversion

A catalyst speeds the conversion, increasing the capacity of a solid-hydrogen cooling system.

Goddard Space Flight Center, Greenbelt, Maryland

The addition of a catalyst would increase the capacity of hydrogen-sublimation cooling systems for radiation detectors. The catalyst would speed the endothermic conversion of para-hydrogen to ortho-hydrogen at heat-absorption stations in the vent line.

Molecular hydrogen exists in two states: In the para-hydrogen state, the nuclear spins of the two hydrogen nuclei point in opposite directions; in ortho-hydrogen the spins point in the same direction. As hydrogen warms from near absolute zero to room temperature, it converts from nearly 100 percent para-hydrogen to an equilibrium distribution of approximately 25 percent para, 75 percent ortho.

Conversion from para-hydrogen to ortho-hydrogen is an endothermic (energy-absorbing) process and thus can be used to absorb heat. However, the conversion rate is too slow (hours) to be exploited unless a catalyst accelerates the conversion. Metal films, such as nickel, copper, or iron supported by alumina in silica are suitable catalysts: In the presence of one of these, conversion takes place in a fraction of a second.

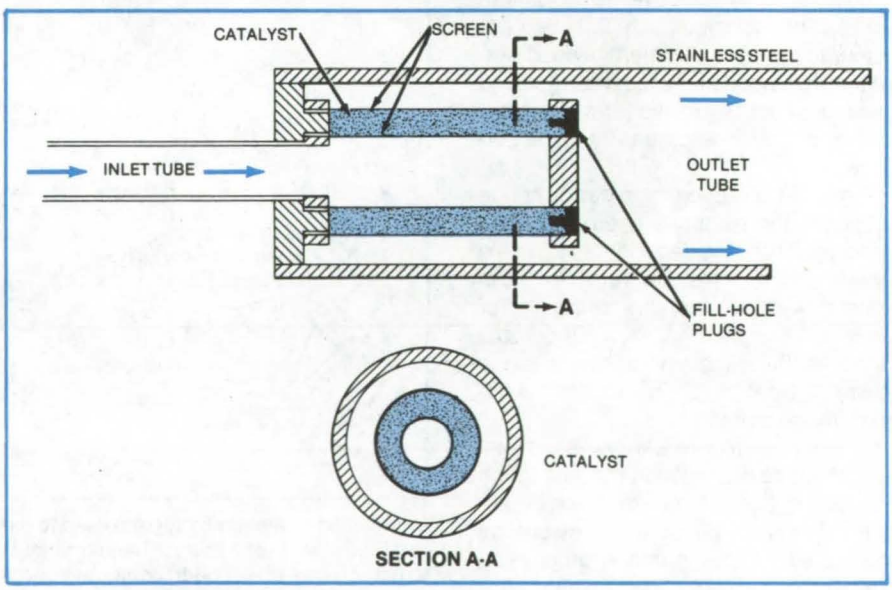

In a **Radial-Flow Catalytic Converter** para-hydrogen is converted to an equilibrium mixture of para-hydrogen and ortho-hydrogen as it passes through a porous cylinder of catalyst.

One possible configuration for the catalytic converter is shown in the figure. The porous catalyst is held between two cylindrical screens. At typical hydrogen-cooler flow rates (a few milligrams per second), the ortho/para-hydrogen distribution after conversion should closely approach the equilibrium distribution for the operating temperature of the converter.

Due to the particular shapes of the enthalpy curves of the para-hydrogen and equilibrium-mixture states, the converter provides maximum cooling capacity when operated near an exhaust-vapor temperature of 100 K. At a hydrogen flow rate of 10 milligrams per second, a vent line employing a catalytic converter operating in that temperature range would provide a total of 11.8 watts of cooling. A similar noncatalytic system using only the sublimation and warming of the hydrogen to 100 K would provide only 7.9 watts of cooling.

This work was done by Allan Sherman of **Goddard Space Flight Center** *and Ted Nast of Lockheed Corp. For further information, Circle 21 on the TSP Request Card.*

This invention is owned by NASA, and a patent application has been filed. Inquiries concerning nonexclusive or exclusive license for its commercial development should be addressed to the Patent Counsel, Goddard Space Flight Center [see page A5]. Refer to GSC-12770.

Submillisecond Optical Knife-Edge Testing

Data are sampled much faster than the optical system drift rate.

Goddard Space Flight Center, Greenbelt, Maryland

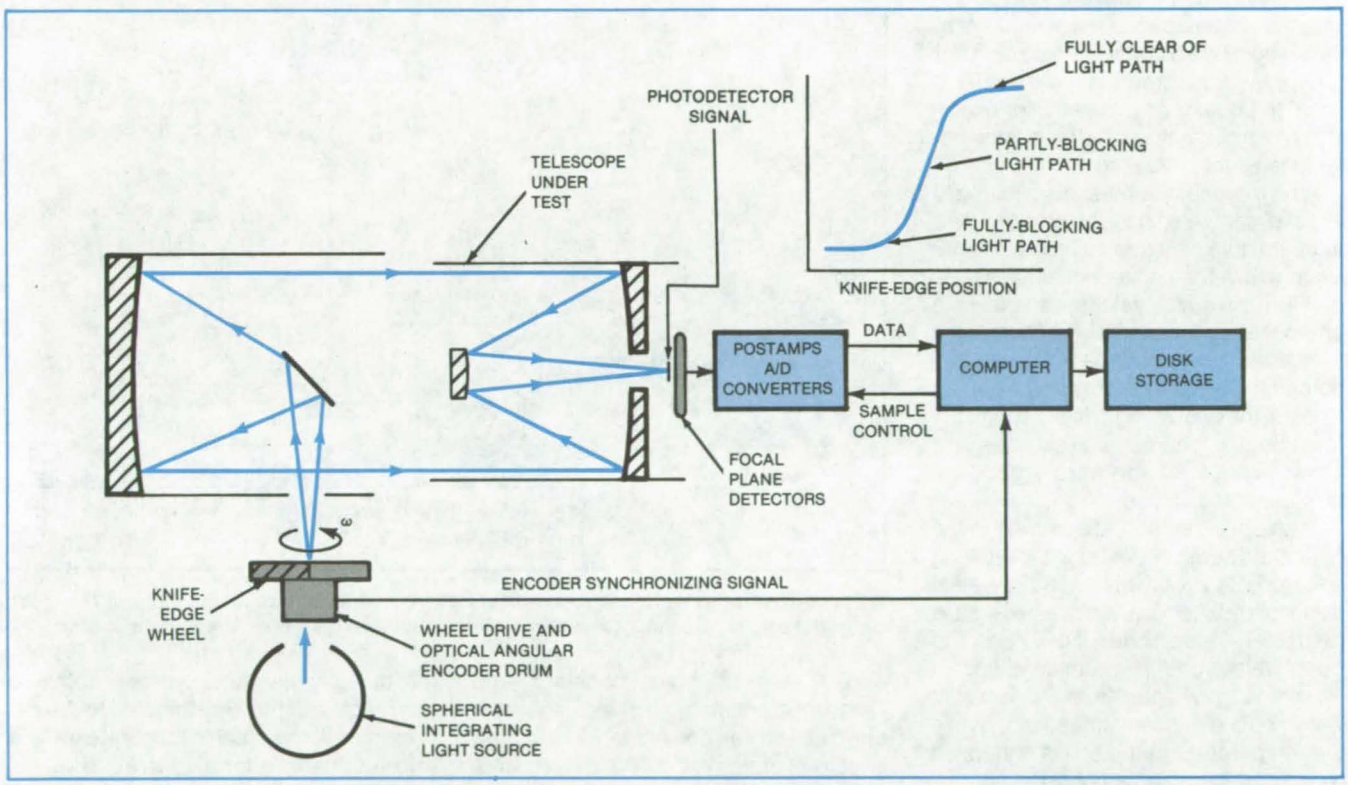

Fast Computer-Controlled Sampling of an optical knife-edge response (KER) signal increases the accuracy of optical-system aberration measurement. The inset shows a typical KER signal plotted against the position of one rotating bar on a knife-edge wheel.

A computer-aided measurement technique obtains the knife-edge response (KER) of an optical system within intervals as small as 10^{-4} second. Submicrosecond-response detectors in the optical focal plane convert optical signals to electrical signals that are converted to digital data, sampled, and fed to a computer for storage and subsequent analysis.

Because the KER sampling intervals are much shorter than the drift time of the optical system under test, sampled optical data are virtually free of the effects of index-of-refraction gradients that could interfere with measurement reliability. Thus, measurements are only negligibly distorted by thermal, vibrational, or flexural effects or by electronic drift.

The fast KER test apparatus is shown in the figure. It includes the optical system under test, an optical KER signal-generator wheel (multiple-knife-edge wheel and light source), and an optical angular-position encoder for the wheel. A set of photodetectors is located at the focal plane, followed by an analog-to-digital converter/sampler, a digital computer, and a data-storage unit.

The KER wheel consists of alternating clear and opaque bars that rotate through the light path to produce a chopped optical signal. The image of the moving knife edge is formed at the focal plane of the system under test. A photodetector array in the focal plane converts the instantaneous knife-edge image into an electrical signal.

The detector outputs are sampled by the analog-to-digital converter, which is

(continued on next page)

synchronized to the knife-edge wheel by an optical encoder. The sampling rate (typically, 450 kHz) is chosen to give a sufficient number of data points (about 45) across the intensity ramp in the knife-edge image. The KER, line-spread function, modulation transfer function, and square-wave response for the system under test are subsequently obtained by computer analysis of the stored data.

This work was done by P. E. Thurlow of Hughes Aircraft Co. for **Goddard Space Flight Center.** *For further information, Circle 22 on the TSP Request Card.*

This invention is owned by NASA, and a patent application has been filed. Inquiries concerning nonexclusive or exclusive license for its commercial development should be addressed to the Patent Counsel, Goddard Space Flight Center [see page A5]. Refer to GSC-12740.

Determining the Point of Zero Zeta Potential in Solid Samples

In a new technique, the sample does not have to be in powder form.

Langley Research Center, Hampton, Virginia

Although current techniques for measuring the point of zero zeta potential (pzzp) in semiconductors require that the sample be in powder form, that is not always the form in which the material is used. In photochemical cells, for example, a solid semiconductor photoelectrode is usually required.

A new technique measures the pzzp in solid samples, possibly making it a more reliable indicator for some materials than are the conventional tests. The method incorporates the sample in a photochemical cell and measures the temperature dependence of the flatband potential. The pzzp is obtained from the slope of the best straight line through the measured points. Tests on samples with known values for the pzzp agree well with expected values.

In the new method, diagramed in the figure, the semiconductor is the working electrode in a conventional three-electrode photochemical cell. A reversible hydrogen electrode (RHE) is the counterelectrode. The semiconductor is illuminated by light from a 100-watt xenon bulb or similar light source, while the temperature of the cell is controlled by a water bath and a heater.

For each temperature in the range of interest, the onset potential — the potential with respect to the RHE at which the photocurrent is zero — is measured by using a high-impedance voltmeter and a recorder. The pzzp for a cell with this configuration can be obtained from the slope of a plot of the flatband potential (related to the onset potential) as a function of temperature according to the equation:

$$\frac{\Delta V_{FB}}{\Delta T} = \frac{2.3R}{F}\left(pH_{pzzp} - \log_{10}\frac{n}{N_C}\right)$$

where ΔV_{FB} is the flatband potential, R and F are the gas constant and Faraday's constant, respectively, n is the free carrier density, and N_C is the density of states in the conduction band. The quantity pH_{pzzp} is the pH of a solution that corresponds to the point of zero zeta potential. This is the way the point of zero zeta potential is usually represented.

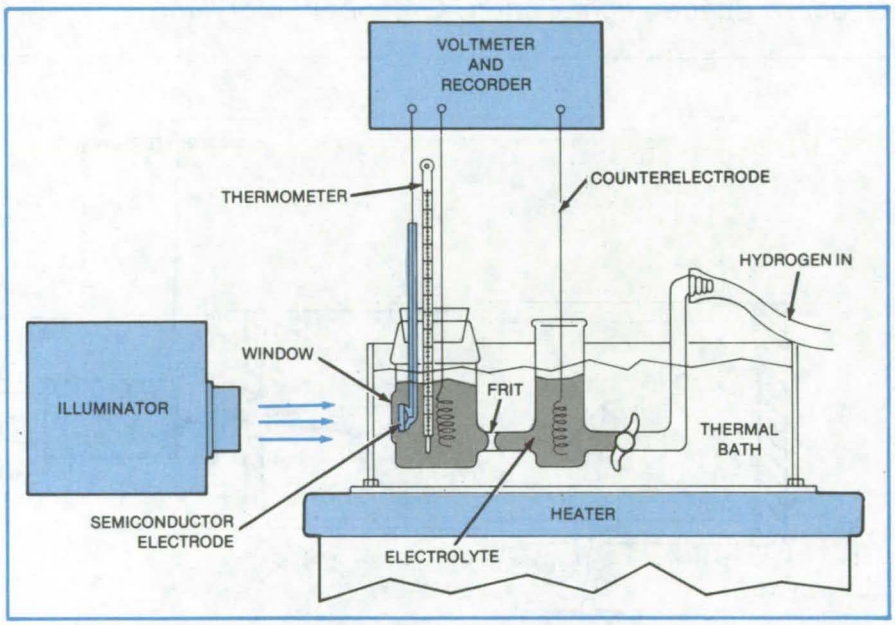

A **Three-Electrode Photoelectrochemical Cell** is used to determine the point of zero zeta potential of a semiconductor material. The illuminator can be a xenon light source.

Four different n-type metal-oxide semiconductors were analyzed by this technique. The temperature dependence of the onset potential for WO_3, α-Fe_2O_3, TiO_2, and $SrTiO_3$ between 20° and 60° C was measured, and pH_{pzzp} was determined for each material. The results were compared with values given in the literature for these semiconductors. The differences between literature values and the measured values obtained were typically about 10 percent and may be attributed to the difference in physical configuration — a powder sample for the literature values versus a large surface for the measurements.

This work was done by Charles E. Byvik of **Langley Research Center** *and Benjamin Reichman of Christopher Newport College. For further information, Circle 23 on the TSP Request Card.*

This invention is owned by NASA, and a patent application has been filed. Inquiries concerning nonexclusive or exclusive license for its commercial development should be addressed to the Patent Counsel, Langley Research Center [see page A5]. Refer to LAR-12893.

Viewer Makes Radioactivity "Visible"

A battery-operated viewer could aid in contamination surveys and medical diagnoses.

Goddard Space Flight Center, Greenbelt, Maryland

A prototype battery-operated viewer has demonstrated the feasibility of generating three-dimensional visible-light simulations of objects that emit X-rays or gamma rays. The device could prove useful in applications ranging from radioactivity contamination surveys to monitoring radioisotope absorption in tumors.

From any viewing angle, the field of view is approximately as wide as one would see looking through a small window of the same size as that of the detector in the instrument. In a prototype, the detector was round, with a diameter of 2.5 cm, but there is no inherent limit to detector size.

The geometrical relationship between the viewer components and images is indicated in the figure. The radioactive object ABC on the left emits X-rays or gamma rays that pass through an array of pinholes in the lead plate S, forming inverted images of the object at the input plane of detector D_1. (The pinhole array covers the entire plate S. The figure shows ray paths for two of the pinholes, P_1 and P_2.)

The images formed by the pinholes are converted to intensified visible-light images by the X-ray imaging detector D_1. Light from these images passes through a second pinhole array S' with hole spacing identical to that in plate S. These ray tracings show that a real, visible-light image $A'B'C'$ of the original object ABC is formed in space the same distance to the right of plate S' as the original object was to the left of S.

Due to the symmetry of the system, the depth coordinate of the visible image is reversed from that of the original object: The object point A furthest from the observer becomes the image point A' closest to the observer. As shown in the lower part of the figure, the depth-coordinate reversal can be eliminated by the addition of an image intensifier D_2 and a third pinhole array S'' to form a virtual image $A''B''C''$.

(continued on next page)

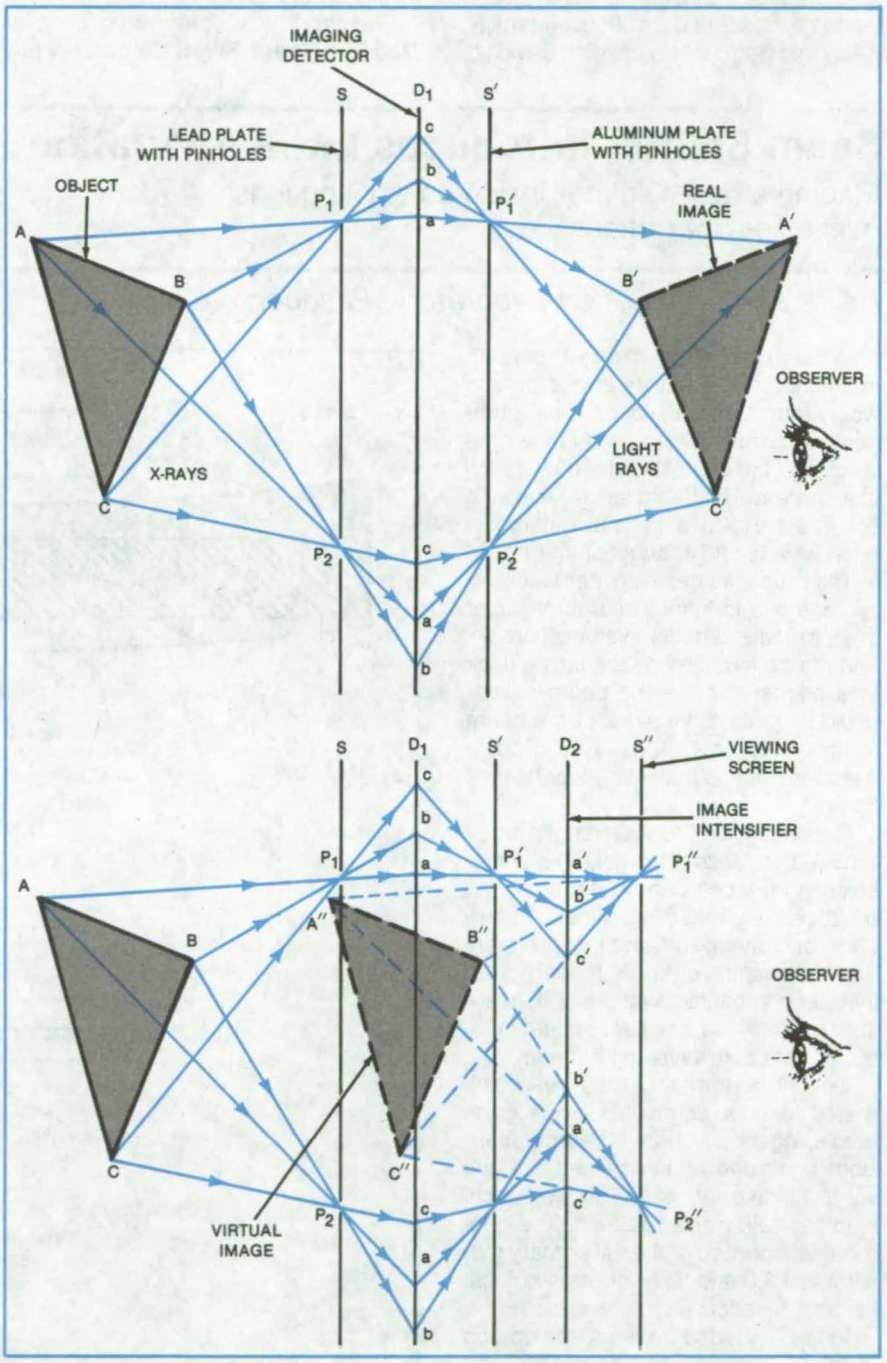

The **Operating Principle** of the viewer is illustrated in simplified form with a triangular object ABC. Ray paths are traced for two pinhole positions, P_1 and P_2, to show the location of the reconstructed image. In a second version of the viewer (below), the addition of an image intensifier D_2 and a third pinhole plate S'' eliminate the depth-coordinate inversion inherent in the simpler viewer.

The reconstructed images $A''B''C''$ are three-dimensional because there are many pinholes like P_1 and P_2, each with a slightly different viewing direction of the object. Therefore the reconstructed image can also be viewed from many different directions, giving full parallax both horizontally and vertically.

The imaging detector D_1 is the "Lixiscope" described in "Low-Intensity X-Ray and Gamma-Ray Imaging Device," on page 67 of *NASA Tech Briefs*, Vol. 3, No. 1 and in "Improved Lixiscope," on page 269 of Vol. 6, No. 3.

A prototype of the viewer was tested with three small radioactive sources located at different distances form the viewer. The viewer showed these as small globules of light with a realistic sensation of depth.

This work was done by Lo I Yin of **Goddard Space Flight Center.** *For further information, Circle 24 on the TSP Request Card.*

This invention is owned by NASA, and a patent application has been filed. Inquiries concerning nonexclusive or exclusive license for its commercial development should be addressed to the Patent Counsel, Goddard Space Flight Center [see page A5]. Refer to GSC-12640.

Beam Splitter Introduces Little Aberration

Placing a beam splitter inside an existing lens minimizes aberrations.

NASA's Jet Propulsion Laboratory, Pasadena, California

A beam-splitter prism array "buried" in a concentric Bouwers corrector lens would introduce only longitudinal chromatic aberration when used in the converging beam of a Schmidt/Bouwers optical system. The beam splitter makes it possible to form a separate image in each wavelength channel of interest.

The proposed beam-splitter takes advantage of a fortuitous characteristic of this particular optical system; namely, that the system already requires a thick lens element where the beam splitter could be placed. Versions of the beam splitter have been devised for dividing the beam into as many as six parts (see figure).

Depending on the wavelength range required in each channel, the beam-splitting surfaces can be either broadband partially-reflecting metalized surfaces or dichroic surfaces that preferentially transmit or reflect particular wavelength bands. Without the beam splitter, a separate optical system is required for each wavelength range.

Optical performance has been estimated for four Schmidt/Bouwers cameras using the six-channel beam splitter. Both one-sided and two-sided designs were studied at each of two focal lengths: 1.800 and 2.625 m. The geometrical aperture of the full primary mirror was f/3.0 and f/3.5 for the two focal lengths, respectively.

In the two-sided systems, the portion of the instrument aperture not blocked by the corrector/beam-splitter assembly consists of two D-shaped regions that are used separately, forming two independent optical systems. Based on calculations of diffraction and geometric

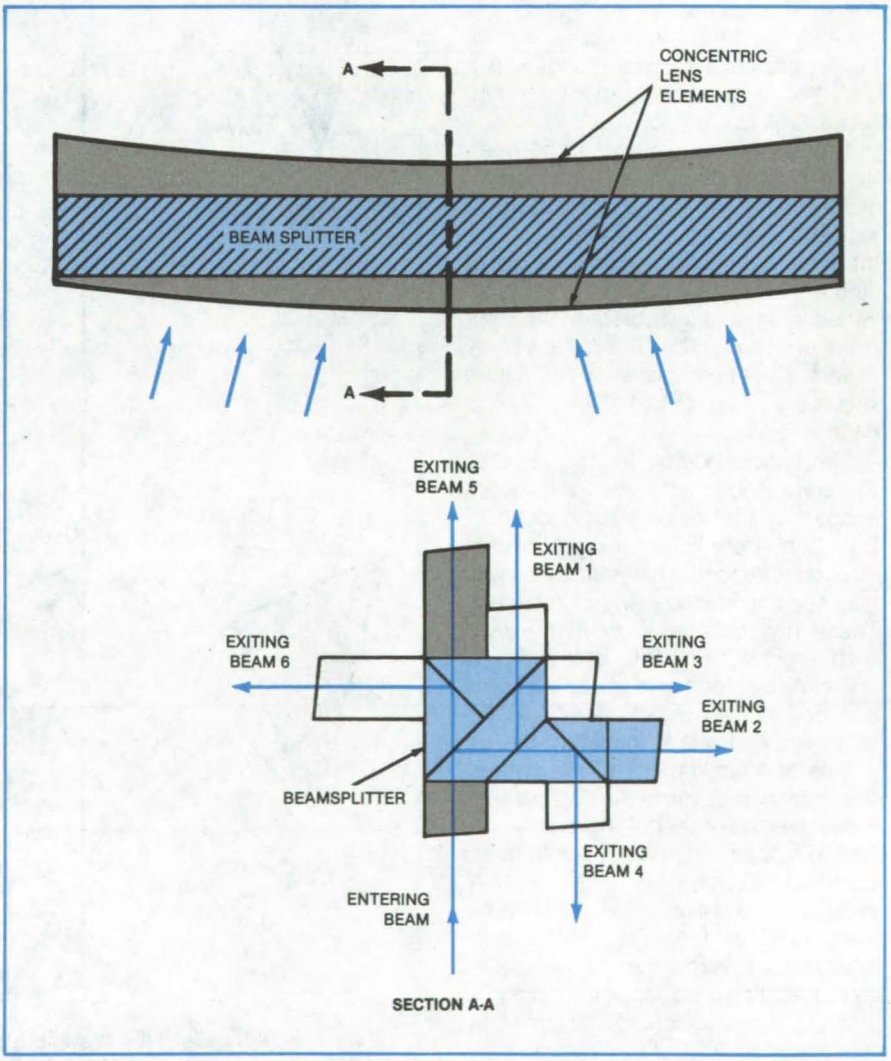

The **Six-Channel Beam Splitter** has optical paths of lengths equal to the distances traveled by the rays within the colored section shown in the lens. The lens element cemented to each of the exit faces of the beam splitter is optically concentric with the element cemented to the entrance face and with the center of curvature of the monocentric optical system. The precise dimensions of each exit element are chosen to optimize performance in the wavelength band exiting in each channel.

modulation transfer functions, it is estimated that the 1.800- and 2.625-m cameras may have resolutions of as small as 15 or even 10 m on the ground, when used at a satellite altitude of 700 km.

This work was done by Nathan L. Evans, Jr., of Caltech for **NASA's Jet Propulsion Laboratory.** *For further information, Circle 25 on the TSP Request Card.*
NPO-15580

Optical-Fiber-to-Channel-Waveguide Coupler

A holding device is made by etching V-shaped grooves in silicon.

NASA's Jet Propulsion Laboratory, Pasadena, California

An accurate fixture (see figure) couples single-mode optical fibers to $LiNbO_3$:Ti diffused-channel waveguides. The fibers, with a core diameter of about 5 μm, are held at 110-μm center-to-center separation and alined with similarly-spaced channel waveguides of about 2- by 5-μm rectangular cross section.

To fabricate the fiber holder, V-grooves are formed in (100)-oriented Si wafers by etching with KOH according to standard etching methods. The fibers are self-centering in the V-grooves.

Two Si chips are used on each end of the $LiNbO_3$:Ti chip. After the fibers have been positioned in the grooves, the fiber ends and the Si edge are polished so that the fiber faces and the Si edge are alined. The two input fibers on the first Si chip can be alined and fixed into place prior to alinement of the second. An adjustment normal to the Si surface is made possible by flexing the Si wafer with a setscrew.

This work was done by O. Glenn Ramer of Hughes Aircraft Co. for **NASA's Jet Propulsion Laboratory.** *For further information, Circle 26 on the TSP Request Card.*
NPO-15555

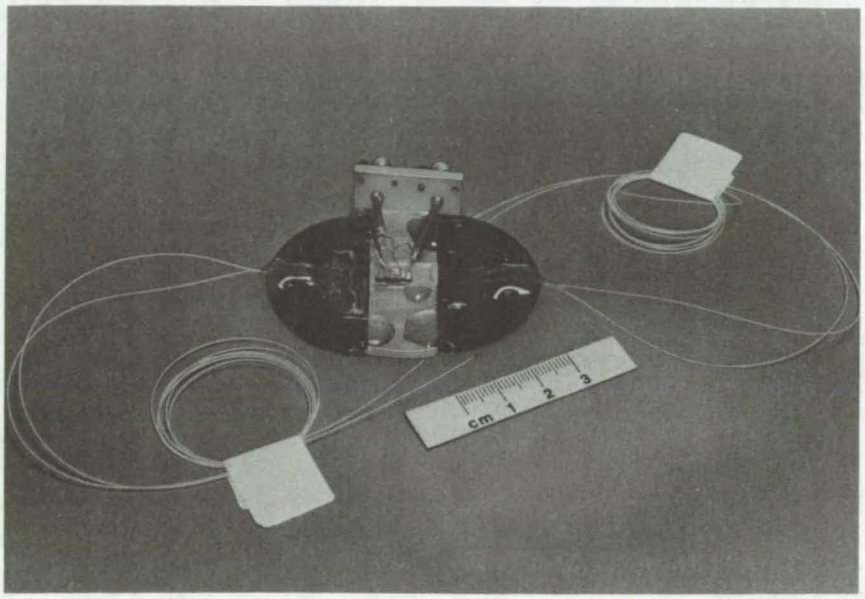

In this **Waveguide Coupler** close tolerances are achieved for high-efficiency coupling between optical fibers with a core diameter of 5 μm and a 110-μm center-to-center separation (multiple fibers) and channel waveguides measuring 2 by 5 μm in the cross section. The fibers are held in V-shaped grooves on silicon chips.

Books and Reports

These reports, studies, and handbooks are available from NASA as Technical Support Packages (TSP's) when a Request Card number is cited; otherwise they are available from the National Technical Information Service.

Controlling Industrial Noise

A handbook gives theoretical background and practical advice.

A handbook gives basic, comprehensive information on noise in industrial environments. It is intended to aid engineers in understanding, measuring, and controlling noise, whether or not they have experience in acoustics.

The basic physics of sound is covered. Such topics as longitudinal propagation, frequency, speed, physical quantities and units, diffraction, and resonance are reviewed.

Measurement techniques are described. Included are loudness evaluation, the weighting of measurements to correlate them with human response, frequency analysis, filtering, source identification, source directivity, sound power-level estimation, and conducting a noise survey.

(continued on next page)

Instrumentation for sound and vibration measurements is discussed. Microphones, accelerometers, sound-level meters, noise dosimeters, frequency analyzers, amplitude and statistical analyzers, and calibration methods are treated.

Noise- and vibration-control materials are described; and some relevant physical properties, including absorption coefficients, are tabulated. Techniques of vibration control are surveyed with examples of typical applications of absorbing and insulating materials and structures. Environmental and legislative considerations are summarized with special attention to the engineering compromises often imposed by such considerations.

Three general types of noise-control procedures are discussed: those implemented at the source, along the transmission path, and at the receiver. The most satisfactory solution usually results from noise reduction at or near the source. Unfortunately, control at the source is not always practical for machinery already installed, and in such cases retrofit techniques must be applied at some stage along the path of propagation. These techniques may involve enclosure of the source, absorption at room boundaries to control reverberation, or vibration isolation if there is significant transmission through the structure.

The alleviation of noise at the receiver is normally a last resort or a temporary expedient. The provision of personal hearing protection, the control of exposure duration, and complete enclosure of personnel in a well-insulated booth are the alternative methods of noise reduction at the receiver.

Specific noise sources and solutions are covered in detail. Among the topics treated are jet and turbulence noise, fan and compressor noise, duct-borne noise, and transmission and gear noise.

An appendix summarizes Occupational Safety and Health Administration regulations and assessment of hearing impairment. A glossary and a bibliography are provided.

This work was done by The Bionetics Corp. for **Langley Research Center.** *Further information may be found in NASA SP-5108 [N82-11858/NSP], "Handbook for Industrial Noise Control" [$7.50]. A copy may be purchased [prepayment required] from the National Technical Information Service, Springfield, Virginia 22161.*
LAR-13001

Materials

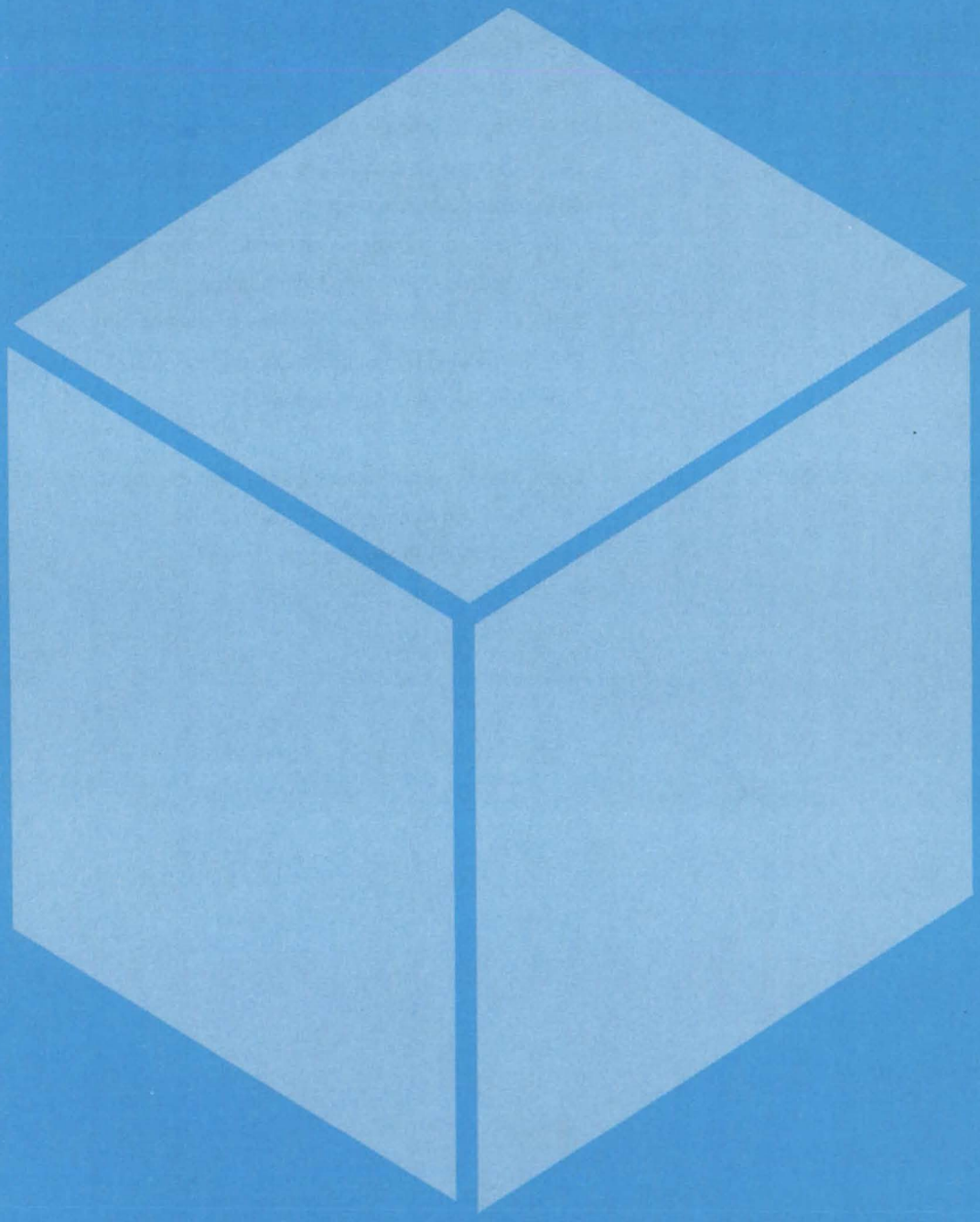

Hardware, Techniques, and Processes

Books and Reports

Aromatic Polyimides With Group VI Linkages

Thermally-stable, solvent-resistant polyimides are readily processable by hot-melt techniques.

Langley Research Center, Hampton, Virginia

A new polymer system combines the thermal- and solvent-resistant properties of aromatic polyimides with the processability of PPX polymers. PPX polymers include the polyphenylene oxide, polyphenylene sulfide, and polyphenylene sulfone classes. They are generally more processable by the hot-melt or thermoplastic techniques than are the aromatic polyimides (PI polyimides). However, the PPX systems are also more susceptible to attack by solvents and have lower glass-transition temperatures than does the PI group.

A process for preparing an aromatic polyimide that can be fabricated by conventional hot-melt extrusion has resulted in polymer systems with imide ring structures and oxygen or sulfur linking groups. The incorporation of oxygen and/or sulfur and/or sulfone linking units between benzene or other aromatic ring systems in the backbone of aromatic linear polyimides yields aromatic linear polyimides with the general formula of PPX-PI. This synthetic modification results in a class of polymers with better thermoplastic and/or hot-melt flow properties than the base polyimide.

Conversely, the incorporation of imide groups into the PPX system results in solvent-resistant polymers that were previously soluble or that swelled in common solvents. These polymers of the PPX-PI type can be thermoplastically and/or hot-melt processed in the 250°-to-390° C range to yield tough, high-quality moldings; strong, solvent-resistant adhesive bonds; and well-formed films and laminates. Thermoplastic consolidation can be done below 250° C in all cases.

PPX-PI structures are shown in the figure. The structures 1, 2, and 3 have good hot-melt flow characteristics. Polymers 1A and 2A, similar to 1 and 2, exhibit some thermoplastic characteristics but only limited hot-melt flow. Polymer 3A has no thermoplastic or hot-melt characteristics.

When the polymer powders were subjected to molding conditions of 300° C and 500 psi (3.45 MPa), polymers 1, 2

(continued on next page)

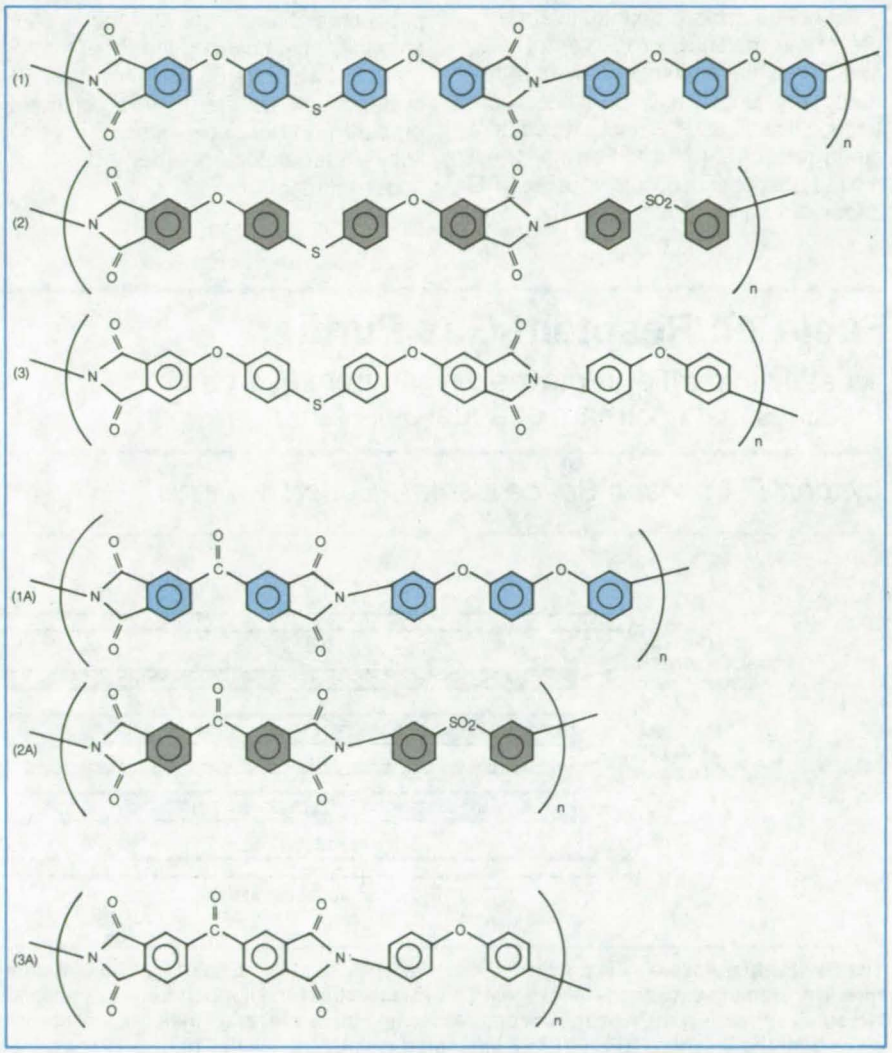

The six **Polymers** shown here were prepared as powders and tested. Polymers 1, 2, and 3 have the best hot-melt flow characteristics of the group.

Solvent	Polymer 1	Polyer 2
Methylethyl Ketone	Insoluble	Insoluble
Cyclohexanone	Insoluble	Insoluble
Xylene	Insoluble	Insoluble
Tricresylphosphate	Insoluble	Insoluble
Cresol	Swelling	Swelling
Methylenechloride	Swelling	Slight Swelling

The **Solvent Resistance** of polymers 1 and 2 in the figure is shown here.

and 3 exhibited a high degree of melt flow. For these three, all of the resin flowed out of the mold. With 1A and 2A, the polymer powder softened just enough to fuse and yield transparent moldings. Polymer powder 3A did not soften enough to fuse completely, and the resulting part was opaque and easily broken.

To obtain a more quantitative measure of the melt-flow properties of 1, 2, and 3, they were examined by capillary rheometry. Both 1 and 2 exhibited continuous flow at 350° C under a constant strain rate of 0.404 s^{-1}. Polymer 3 exhibited discontinuous flow at 390° C under the same strain rate. The other three systems, as expected, would not flow.

The solvent resistance for polymers 1 and 2 is excellent, as shown in the table. Both 1 and 2 PPX-PI polymers are unaffected by the first four solvents listed in the table, whereas the PPX polymers are generally all dissolved by these solvents, especially cyclohexanone and tricresylphosphate. The cresol and methylenechloride, which caused the PPX-PI polymers to swell, are solvents for the PPX systems. All of the PPX-PI polymers prepared do not show signs of crystallinity either before or after solvent or heat treatments.

This work was done by Terry L. St. Clair, Harold D. Burks, and Robert M. Ely of **Langley Research Center.** *Further information, may be found in NASA TR-84494 [N82-27493/NSP], "Synthesis and Characterization of a Melt Processable Poly-Imide" [$7.50]. A copy may be purchased [prepayment required] from the National Technical Information Service, Springfield, Virginia 22161.*

This invention is owned by NASA, and a patent application has been filed. Inquiries concerning nonexclusive or exclusive license for its commercial development should be addressed to the Patent Counsel, Langley Research Center [see page A5]. Refer to LAR-12980.

Fuel-Cell Reactant-Gas Purifier

A catalytic purifier removes oxygen from hydrogen feedlines just upstream of a fuel-cell stack.

Lyndon B. Johnson Space Center, Houston, Texas

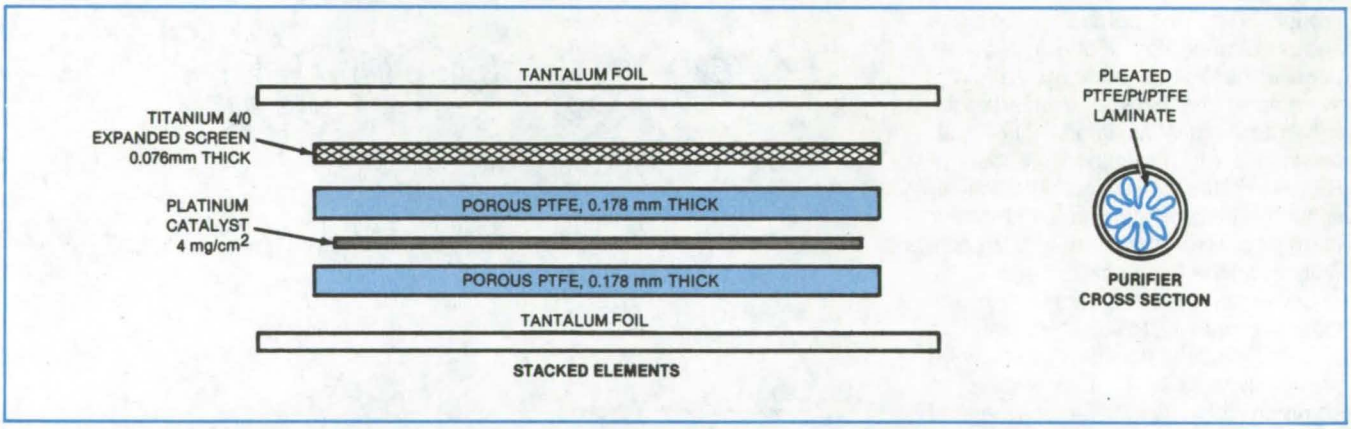

The Gas Purifier Assembly is pressed at 690 kPa (100 psi) at 94° C (200° F). The tantalum foils constitute endplates for the pressing fixture. The titanium-expanded metal screen provides a structural support during pressing. With the screen in place, areas of the PTFE between wire strands remain nearly uncompressed and therefore retain their original porosity. After pressing, the titanium screen is peeled away from the finished PTFE/Pt/PTFE laminated sheet. The finished purifier is shown in cross section at the right. Pleating maximizes the exposure of catalyst surfaces to the gas stream, while minimizing flow restrictions.

A purifier catalytically removes small quantities of oxygen from a hydrogen stream before the gas enters a fuel cell. The purifier is needed because contaminant gases in the fuel-cell feedlines may affect cell performance and possibly cause a failure. A plumbing leak can admit air, for example, and if the leak is on the hydrogen side, the combination of hydrogen and oxygen could burn the electrolyte and damage the cell.

The purifier consists of a layer of platinum sandwiched between two sheets of porous polytetrafluoroethylene (PTFE). The figure shows the platinum and PTFE elements stacked and ready for pressing. Following this step, the purifier is cut to size, pleated, and inserted into a convenient length of metal tubing.

The porous PTFE serves three purposes:

1. it physically contains platinum particles,
2. it provides a diffusion path for the passage of reactant gases to the catalyst and a pathway for product water back to the gas stream, and
3. it creates a hydrophobic surface at the gas/PTFE interface to prevent the formation of a water film on the platinum.

The purifier is inserted into the hydrogen line slightly upstream of the inlet to the fuel cell. In one test, a 7.5 cm × 7.5 cm PTFE/Pt/PTFE sheet was fabricated and inserted into a section of 3/8-in. (0.95-cm) tubing. The purifier was 90 percent efficient in removing oxygen from a gas stream containing 2 percent oxygen in hydrogen.

This work was performed by Hoyt McBryar of **Johnson Space Center** *and Thomas A. Ollila of General Electric Co. No further documentation is available. MSC-20103*

Recycling Lithium Carbonate/Lithium Hydroxide Waste

A hazardous-waste disposal problem is eliminated by regeneration.

John F. Kennedy Space Center, Florida

A proposed chemical process would recycle the Li_2CO_3/LiOH waste mixture produced when LiOH absorbs CO_2 from the air (as in systems that maintain breathable atmospheres). The regeneration process would eliminate the need to dispose of the caustic waste and would use less energy than simple calcination of the entire waste mass.

The decomposition temperature of Li_2CO_3 (about 640 ° C) is higher than the 450 ° C melting point of LiOH. Consequently, during the incineration of a Li_2CO_3/LiOH mixture, the LiOH fuses into a solid mass, which is not the desired form for reuse. In addition, both LiOH and Li_2CO_3 decompose to Li_2O at or below the incineration temperature: This is undesirable because the Li_2O absorbs CO_2 at only one-fifth the rate of LiOH.

In the proposed recycling process (see figure), the Li_2CO_3/LiOH mixture is dissolved in hot water. The water solubility of Li_2CO_3 is significantly reduced by the presence of LiOH and is further reduced by the elevated water temperature. The Li_2CO_3 therefore precipitates out of the solution, after which it is removed and incinerated to Li_2O. Since Li_2CO_3 is expected to be the smaller component of the waste mixture, this separation before the incineration step saves considerable energy that would otherwise be wasted by incinerating the LiOH.

The Li_2O that results from incineration of the Li_2CO_3, is returned to the hot-water tank to be rehydrated to LiOH. The mostly LiOH solution is drawn off and dried in CO_2-free air. If necessary, the dried LiOH is ground to the fineness required for reuse.

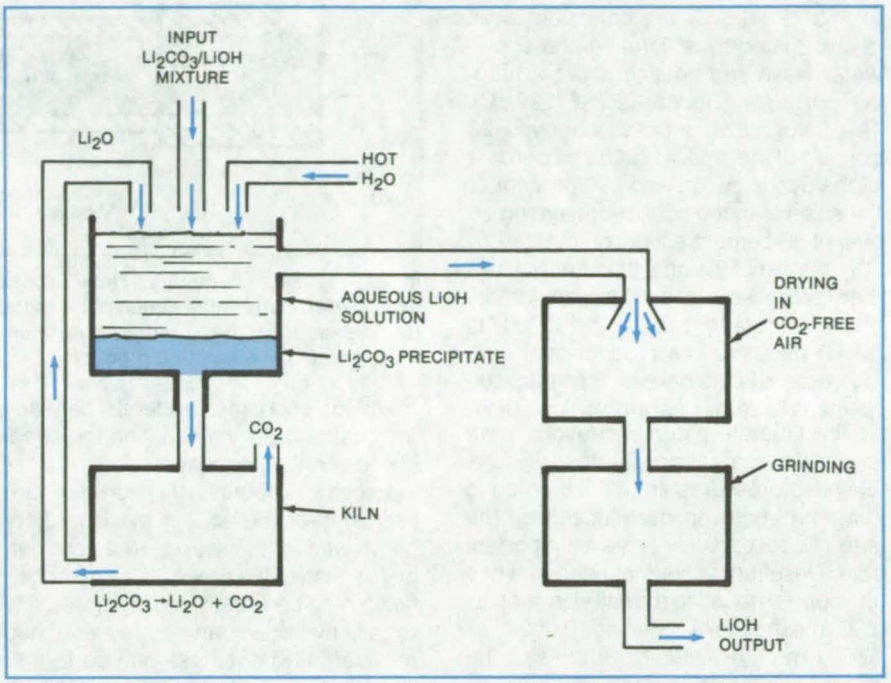

The **Proposed Li_2CO_3/LiOH Recycling Process** relies on the low solubility of alkali carbonates in the corresponding hydroxides. The Li_2CO_3 precipitate is calcined to Li_2O, then rehydrated to LiOH.

The process has been partly verified on a laboratory scale. It may be generally applicable in that the relative insolubility of carbonates in saturated aqueous solutions of the corresponding hydroxides is a general property of the alkali metals.

This work was done by J. S. Flowers and J. L. Flowers of Flowers Chemical Laboratories for **Kennedy Space Center.** *No further documentation is available.*

Inquiries concerning rights for the commercial use of this invention should be addressed to the Patent Counsel, Kennedy Space Center [see page A5]. *Refer to KSC-11261.*

Desulfurizing Coal by Chlorinolysis and Hydrogenation

A two-process combination removes more sulfur than either process alone.

NASA's Jet Propulsion Laboratory, Pasadena, California

More than 85 percent of the organic and pyritic sulfur in coal is removed by a combination of chlorinolysis and hydrogenation, according to experiments. Chlorinolysis removes about 30 percent of the organic sulfur but becomes ineffective when a higher removal percentage is attempted. Hydrogenation removes more than 60 percent of the organic sulfur remaining after chlorinolysis but is otherwise generally ineffective unless the coal has first been chlorinated. Thus the two steps are complementary. The reducing (hydrogenation) process takes place at 600 ° to 700 °C, a

(continued on next page)

temperature range that is high enough to promote the desired reactions but low enough to prevent excessive loss of coal due to oxidation or charring.

In one of several laboratory demonstrations, PSOC 282 coal ground to 325 mesh was agitated in water through which chlorine gas was bubbled at atmospheric pressure. After 45 minutes at 158° F (70° C), the coal slurry was dechlorinated by a filtration and spray-water wash and heating under a nitrogen purge for 1 hour at 750° F (399° C). This chlorination process removed 28 percent of the organic sulfur, 84 percent of the pyritic sulfur, and 100 percent of the sulfates in the coal, representing an overall 60-percent sulfur removal.

A sample of the coal thus treated was then processed in a hydrogen atmosphere in a rotating quartz tube at 700° C for 60 minutes. The product coal contained about 62.5 percent less total sulfur than the same coal after chlorination.

The laboratory demonstrations were carried out at atmospheric pressure. Elevated pressures are not expected to promote improved desulfurization. The size of coal particles plays an important role. Desulfurization is enhanced when the coal is ground to a small size such as 200 mesh [sieve opening 0.0029 in. (0.074 mm)] or finer. Nevertheless, the process works on coarse particles — as large as 0.125 in. (3 mm). There is ample room for economic tradeoffs between the cost of crushing coal and the effectiveness of hydrogenation.

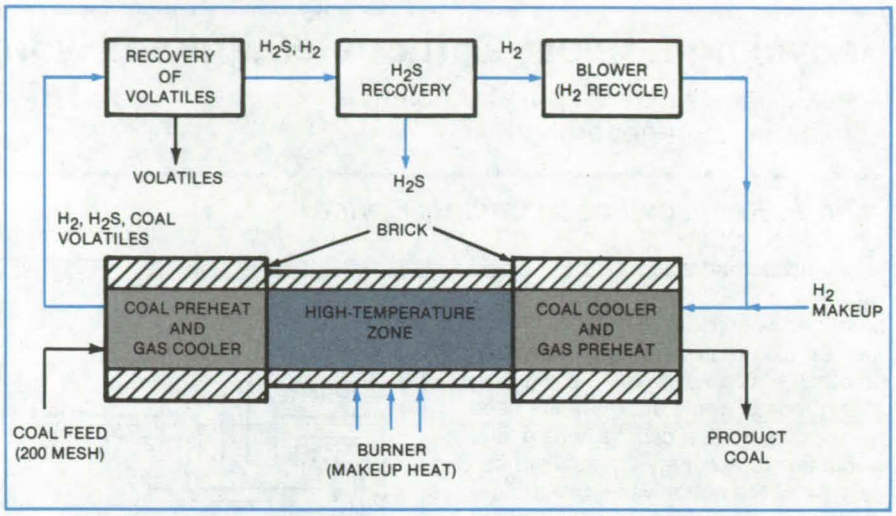

In a **Proposed Continuous-Flow Process** for desulfurizing coal, coal is fed to a hydrogenator after it has been chlorinated. The coal flows against the hydrogen current to increase mixing and reduce hydrogen consumption. Excess hydrogen is recovered from the gaseous reaction products.

Excess amounts of hydrogen are passed over the coal in the laboratory demonstration. However, in a commercial version of the process, the hydrogen flow could be greatly reduced, and any excess hydrogen can be recovered and recycled. Hydrogen use can be further limited if hydrogen is added in a countercurrent to the flow of coal. Toward this end, hydrogenation can be carried on in a fluidized bed or moving bed of coal (see figure). Although the hydrogenation time was 60 minutes in the laboratory, shorter retention times will be necessary in a viable commercial process.

This work was done by John J. Kalvinskas and Naresh K. Rohatgi of Caltech for **NASA's Jet Propulsion Laboratory.** *For further information, Circle 27 on the TSP Request Card.*
NPO-15304

Stronger Carbon Fibers for Reinforced Plastics

New process makes fibers 70 percent stronger at lower carbonization temperatures.

Ames Research Center, Moffett Field, California

Carbon fibers produced at low carbonization temperatures for carbon-reinforced plastics are stronger when produced by a new technique. Novel features of the new method are a pretreatment in a gaseous or liquid conditioning material, such as benzoic acid, and the addition of a small amount of acetylene to the usual nitrogen atmosphere in the final carbonization step. The starting material, as in the standard process, is polyacrylonitrile filaments.

In one version of the process, a tow of filaments is passed through a molten benzoic acid bath at 175° C under slight tension for about 3 hours. The result is fibers having less than 10 percent shrinkage or extension. The tow is then oxidized under tension at 260° C over a contact time of about 3 hours in a tubular reactor, producing a fiber with less than 5 percent shrinkage or extension. The oxidized tow is then heated under tension at a rate of 20° C/min to a temperature of 700° C in an atmosphere of 5.34 percent acetylene, 94.66 percent nitrogen.

The new process increases the elastic modulus and tensile strength of the fibers (see table). Tensile strength is increased by more than 70 percent.

Alternative pretreatment agents to benzoic acid are other aromatic carboxylic acids, such as phthalic acid, terephthalic acid, or naphthoic acid. They may be used as liquids or gases. Hydroquinone may also be used.

Alternatives to acetylene as carbonizing agents are methane, ethylene, fuel gas, and aliphatic hydrocarbons generally; benzene and other aromatic hydrocarbons and nonhydrocarbon organic materials, such as carbon disulfide, can also be used. In general, any carbonaceous material that is gaseous at the carbonization temperature and decomposes within a few minutes is suitable.

The new process can also be varied to make carbon fibers of higher electrical resistance — an important safety consideration in some situations. The process variations that increase strength do not necessarily increase resistance.

This work was done by Domenick E. Cagliostro and Narcinda R. Lerner of **Ames Research Center.** *For further information, Circle 28 on the TSP Request Card.*

Inquiries concerning rights for the commercial use of this invention should be addressed to the Patent Counsel, Ames Research Center [see page A5]. Refer to ARC-11261.

SAMPLE TREATMENT	MODULUS OF ELASTICITY	TENSILE STRENGTH	PERCENT CHANGE IN TENSILE STRENGTH
OLD METHOD	11.9×10^6 psi (82.0×10^9 N/m^2)	0.090596×10^6 psi (0.6246×10^9 N/m^2)	NONE (REFERENCE)
NEW METHOD	12.6×10^6 psi (86.9×10^9 N/m^2)	0.15417×10^6 psi (1.0630×10^9 N/m^2)	+70.20

Stronger Carbon Fibers result from a benzoic acid pretreatment and the addition of acetylene to the nitrogen carbonizing atmosphere.

Gelled Anti-icing Agents

A gelling agent such as pectin is added to an antifreeze/water mixture.

Lyndon B. Johnson Space Center, Houston, Texas

Gelled anti-icing agents have been proposed to prevent ice formation on vertical or horizontal surfaces. The formulations include water with dimethyl sulfoxide (DMSO) as the deicer and pectin as the gel former.

Previously recommended for use as an antifreeze in closed radiators, DMSO reacts with water to form solutions with freezing points as low as −69° C (see figure). Mixtures of DMSO and pectin form soft, gelatinous materials that are easily spread onto surfaces. A hydrated silica (Hi-SIL T-600, or equivalent) can also be included to increase the viscosity, environmental resistance, and atmospheric stability of the mixture. Ranges of compositions recommended are: 1 to 5 parts water, 95 to 99 parts DMSO, 1 to 10 parts pectin, and 0 to 10 parts hydrated silica.

Without the gelling agent, a deicer runs off vertical surfaces. Gelled deicers are also much less volatile than plain deicers. A 0.25-inch (6-mm) DMSO gel layer (50 DMSO:50 H_2O:2 pectin) lost 75 percent of its volume in a 106-day outdoor exposure, but remained functional. Without the pectin, the solution would have completely evaporated in far less time.

These anti-icing agents were developed for use on the Space Shuttle external tanks. They have wide market potential for ice prevention on runways, highways, bridges, and sidewalks.

[See the related article "Modified Antifreeze Liquids for Use on Surfaces" (MFS-25741) on page 286 of this issue.].

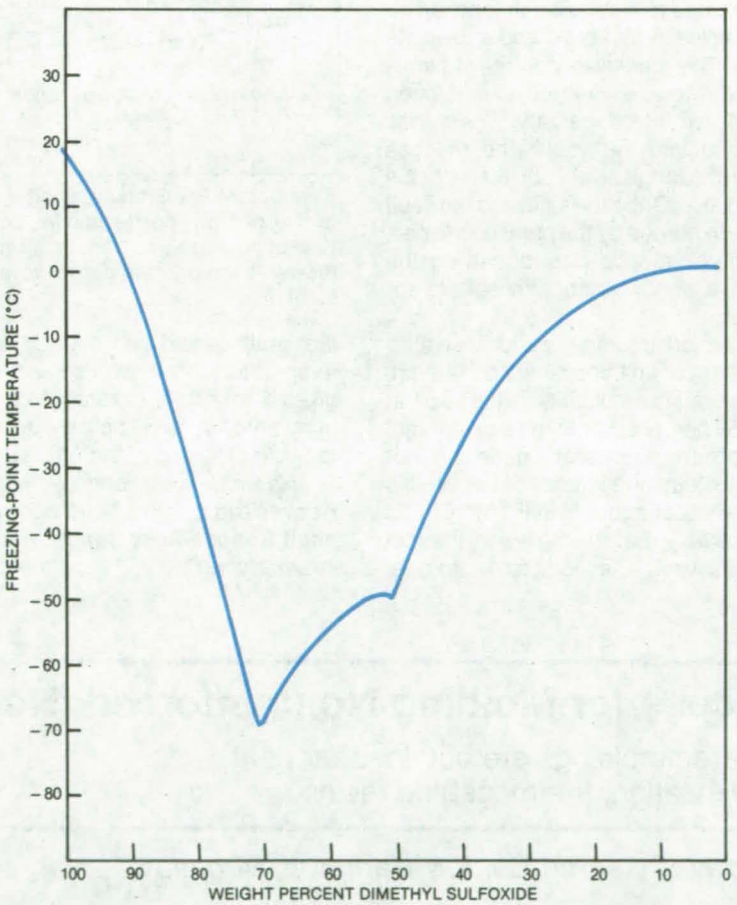

An **Antifreeze Solution** of DMSO and water is an ingredient of anti-icing gels.

This work was done by Orville F. Markles and Harold H. Sperber of Rockwell International Corp. for **Johnson Space Center.** *No further documentation is available.*
MSC-20088

Preserving Color in Developed Photographic Film

Sealed storage container has moist nonoxidizing atmosphere to retard fading.

Marshall Space Flight Center, Alabama

A controlled-atmosphere vault (see figure) retards the fading and deterioration of developed high-speed film. Although refrigerators and other cool, dry areas are satisfactory for the storage of relatively stable film, the color dyes fade in some high-speed films, even in such facilities. Fading is accompanied by color-balance shift and density changes that often result in the loss of scientific information.

The vault contains an externally controlled tank of gas (usually nitrogen) with a perforated gas-distribution tube, an air purge valve, a film rack, and a sealable cover. The gas-tank control valve is opened after the vault cover has been sealed to introduce dry, inert gas (nitrogen) into the vault. The dry gas forces the original air out through the purge valve. Once the air inside the vault has been purged by the pressurized gas, the purge valve is closed, sealing the film in a nonoxidizing atmosphere for storage.

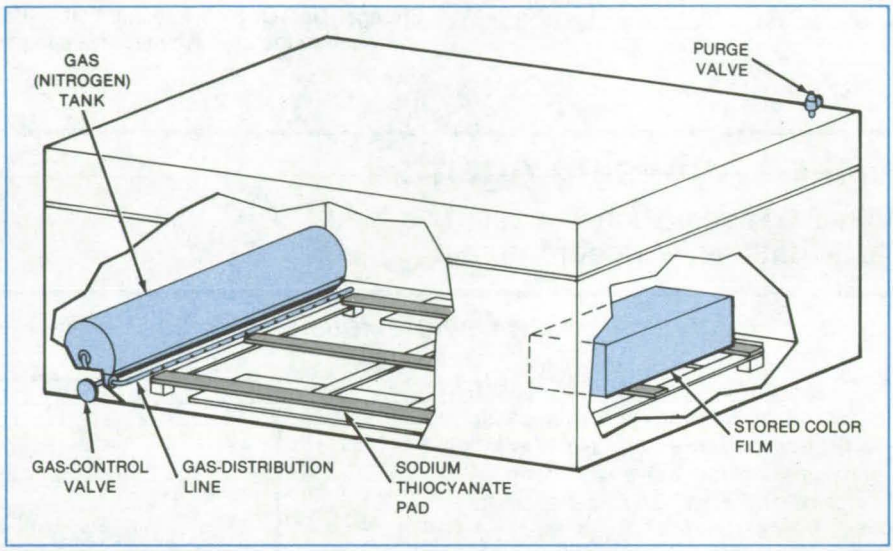

This **Color-Film Storage Vault** contains a nonoxidizing atmosphere that retards the fading of high-speed-emulsion color dyes. An externally controlled valve regulates the flow of nitrogen gas from an internally mounted tank. The gas purges ambient air from the vault through the purge valve and maintains the vault pressure slightly above ambient.

For short storage periods, water-charged sodium thiocyanate pads maintain the relative humidity in the vault at 40 to 50 percent. For long-term storage, the sodium thiocyanate pads are not used: Instead, the interior of the vault is maintained at about 50° F (10° C) and low humidity. Before retrieving the film from the vault after long-term storage, the vault should be returned to room temperature. The film should also be given 1 to 2 days to return to a relative humidity of 40 to 50 percent before use, to avoid cracking of the emulsion.

This work was done by Richard B. Hoover and Charles M. Rhodes of **Marshall Space Flight Center.** *For further information, Circle 29 on the TSP Request Card.*

This invention has been patented by NASA (U.S. Patent No. 4,287,152). Inquiries concerning nonexclusive or exclusive license for its commercial development should be addressed to the Patent Counsel, Marshall Space Flight Center [see page A5]. Refer to MFS-23250.

Process for Molding Nonreinforced (Neat) Resins

Void-free moldings are obtained for neat, condensation, thermosetting resins.

Langley Research Center, Hampton, Virginia

A problem associated with the molding of nonreinforced, condensation, thermosetting resins such as phenolics and polyimides is the control and removal of volatiles. While the removal of volatiles is facilitated by fibrous reinforcement in a composite material, this is not the case in a neat resin molding. The source of the volatiles is the resin solvent and/or the by-products, typically water or alcohol, of the condensation reaction. While volatiles aid in resin flow, they also cause the formation of voids and/or cracks in the molded part and contribute to shrinkage. The application of molding pressure in addition to temperature will aid resin flow, but will also tend to trap the volatiles in the molded part.

A process was developed for producing solid, void-free, neat resin parts from condensation, thermosetting resins. It consists essentially of thermally and mechanically treating the resin prior to molding to reduce the amount of volatiles. With the volatiles reduced, the molding temperature and pressure are applied in such a way as to drive out the remaining volatiles during molding.

Specifically, liquid Larc-160 resin was measured out in open-top containers in a 1:16 volumetric ratio (resin:container space) to allow for expansion and then placed in a positively-vented air-circulating oven. The oven temperature was raised from ambient to 200° F (93° C) and held for 1 hour, then raised to 420° F (215° C) and held for 2 hours. The containers were then removed from the oven and cooled to ambient temperature.

Some of the containers (60 percent) were mechanically processed. That is, the foamed contents were crushed and passed through a 20-mesh screen. The remaining containers (40 percent) were placed in a preheated [600° F (315° C)] oven. After 1 hour at 600° F, these contents of Larc-160 were removed, cooled, crushed and passed through a 20-mesh screen. The two processed Larc-160 powders were then recombined and blended into a homogeneous mixture.

Once recombined, the processed Larc-160 resin was loaded into a 200° C preheated mold through a 300° C preheated press transfer pot. A series of pressing and releasing, or breathing, cycles was continued on the resin with the transfer ram while the mold temperature rose from 200° to 260° C in a period of about 1 hour. The breathing cycles allowed for further outgassing of the volatiles. The heat on the bottom of the mold was raised to 335° C, and 4,000-psi (28×10^6-N/m^2) pressure was applied to the resin.

By curing from the bottom up, the generated volatiles tended to traverse upward and out of the molded part. At 270° C mold temperature, the mold sides were insulated, and the top platen temperature was raised to 335° C. The 4,000-psi pressure and 335° C curing temperature were held on the resin for 1 hour after the mold temperature reached 300° C. The part was demolded hot.

The ratio of the differing processed stages of other resin systems as well as processing temperatures, pressures, and the number of levels to which the resin systems are processed prior to molding will probably vary from those used with the Larc-160. Experience and knowledge of the chemical, thermal, and flow characteristics of other resin systems will guide the processor in determining processing temperatures, pressures, number of levels, and mixing ratios required to obtain void-free neat resin moldings.

This work was done by George E. Dickerson of **Langley Research Center.** *No further documentation is available.*
LAR-12981

Measuring Diffusion and Recombination in Polycrystalline Silicon

Light-beam-induced currents yield information about solar-cell material.

NASA's Jet Propulsion Laboratory, Pasadena, California

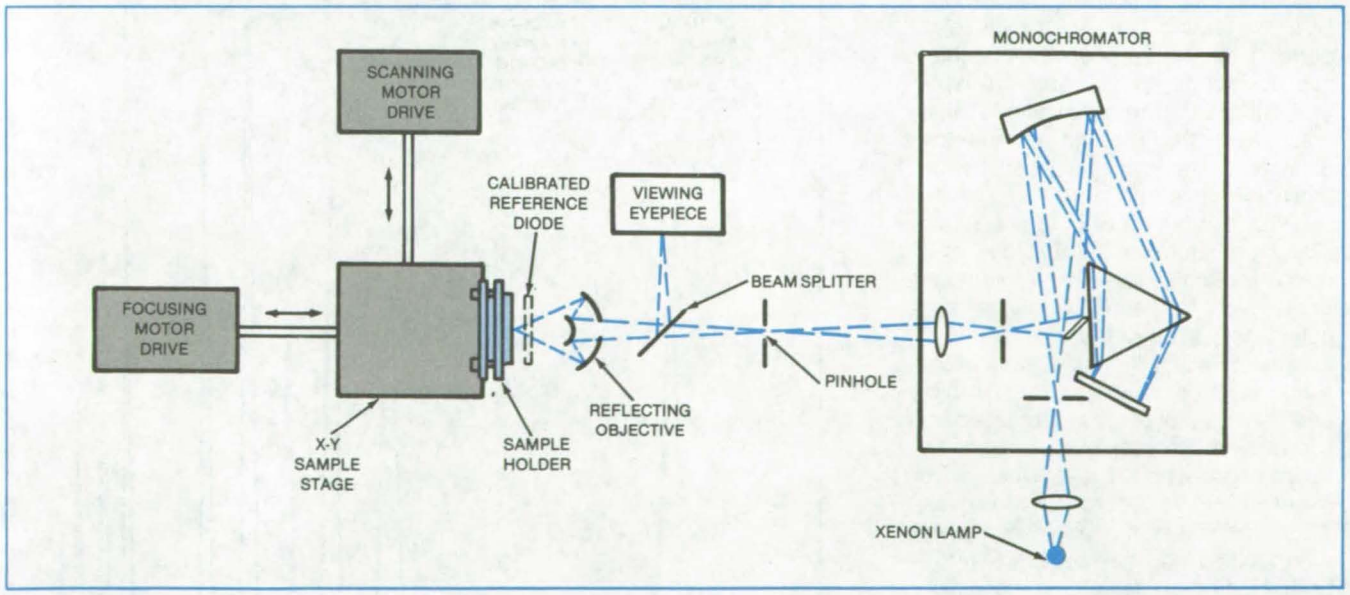

Setup for Measuring Light-Beam-Induced Currents closely simulates the solar wavelengths and intensity. The apparatus measures the short-circuit current generated when a 5-by-12-μm spot of the concentrated light is scanned across grains and grain boundaries in the material under test.

Minority-carrier diffusion length and surface recombination velocity in polycrystalline silicon are determined from measurements of light-beam-induced short-circuit currents. The technique is an updated version of the light-spot-scanning technique. It was developed for evaluation of the effects of processing changes on the properties of polycrystalline silicon on ceramic (SOC) for use in solar cells.

A high-pressure short-arc xenon lamp is the light source. The xenon spectrum has several readily identified peaks with known wavelengths that have intensities of about 1 Sun (that is, they generate a

(continued on next page)

current density of the order of 30 mA/cm^2). The peaks are in a convenient range for determining the diffusion length in silicon.

The xenon lamp is focused on the entrance slit of a monochromator (see figure) which isolates a particular narrow band of wavelengths for refocusing. The light from the exit slit of the monochromator is focused on one pinhole of a wheel containing pinholes in a variety of sizes. The light from the pinhole is focused by a reflecting objective, for which focusing is independent of wavelength. Thus, light can be focused on a solar-cell specimen in the visible and scanned over the specimen in the infrared.

A dc motor with a variable speed control moves the cell in the scanning directions. A small motor moves the cell for focusing. The instrument, except for the xenon lamp and monochromator, is mounted in a light-tight box. Absolute spectral response measurements are made by inserting a calibrated reference diode in front of the sample and comparing the direct currents generated by the lamp.

A layer of liquid electrolyte is interposed between the light source and the solar cell. Held in place by a fused-quartz window and an O-ring, the electrolyte provides an optically transparent electrical contact. The electrolyte is a solution of europium chloride in hydrochloric acid.

The technique was used to evaluate SOC samples for the diffusion and recombination effects of cell processing and of chemical and structural defects. Scans of several cells showed that there is a characteristic "good-grain" diffusion length, L_{max}, that is dependent on doping and cell processing and is assumed to indicate intragrain chemical defect density. There is also a grain-boundary diffusion length, L_{min}, that is less than L_{max}, by a factor of 10 to 20.

This work was done by J. David Zook of Honeywell, Inc., for **NASA's Jet Propulsion Laboratory.** *For further information, Circle 30 on the TSP Request Card.*
NPO-15601

Improving Hydrocarbon Separation in Gas Chromatography

Modified silica spheres enhance chromatographic separation.

Ames Research Center, Moffett Field, California

Gas chromatographic separations of low-molecular-weight hydrocarbons are enhanced if modified silica spheres are used as the stationary phase. Commercially-available silica spheres are modified by reacting them with molecules containing isocyanate and isothiocyanate groups. Possible applications of the surface-derivatized spheres that result from the reaction include the analysis of samples produced by atmospheric or soil probes.

Silica in the form of porous spheres (Porasil, or equivalent) is able to resolve many low-molecular-weight hydrocarbons, such as paraffins, olefins, and acetylenes, at elevated temperatures. Chemically modifying the surface of the silica with isocyanates or isothiocyanates improves the separation of some hydrocarbons, even though the total amount of bound organic derivative is not high (1 to 3 percent). Moreover, the support-bonded phase, when properly conditioned, may be used with a helium-ionization detector at very high sensitivity.

The figure shows the separation of a mixture of hydrocarbons by the modified spheres as measured with a helium-ionization detector. Lower-hydrocarbon

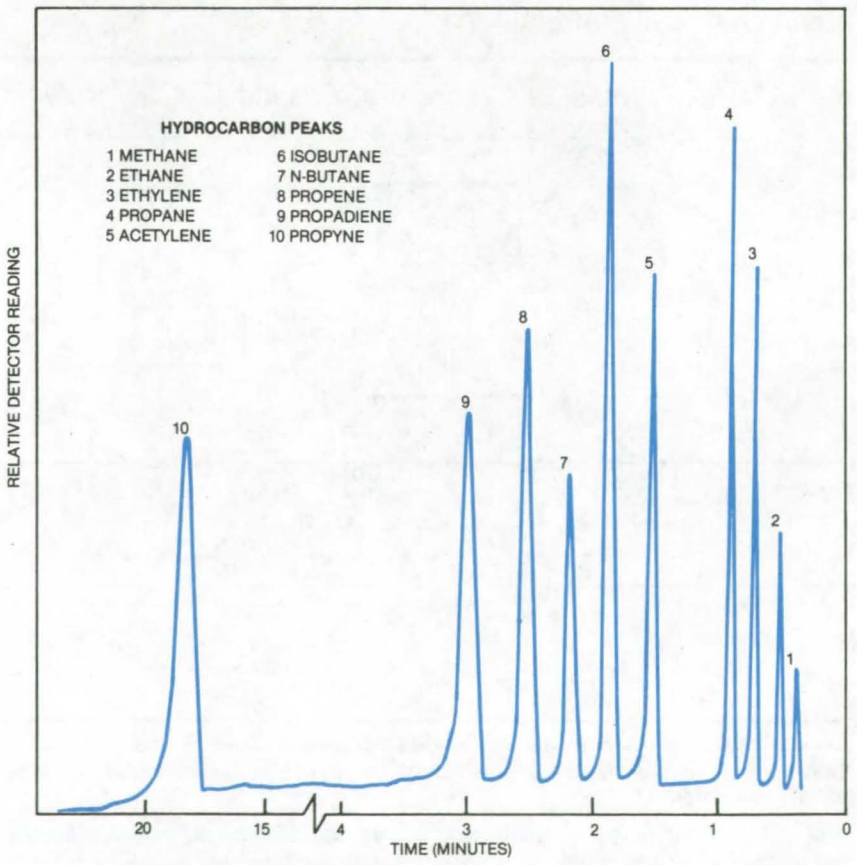

Gas-Chromatographic Separation of a Hydrocarbon Mixture is shown for a column packed with 3,4-dichlorophenylisocyanate-modified Porasil. A helium-ionization detector was used.

separations can be carried out swiftly at ambient temperatures (~25° C) at the parts-per-billion-to-sub-ppb level. Reproducible results are obtained as long as the carrier gas is dry.

This work was done by Glenn E. Pollock, Dan R. Kojiro, and F. H. Woeller of **Ames Research Center.** *For further information, Circle 31 on the TSP Request Card.*

Inquiries concerning rights for the commercial use of this invention should be addressed to the Patent Counsel, Ames Research Center [see page A5]. *Refer to ARC-11431.*

Fire-Resistant Composites

A resin blend produces high-char-yield, low-smoke composites.

Ames Research Center, Moffett Field, California

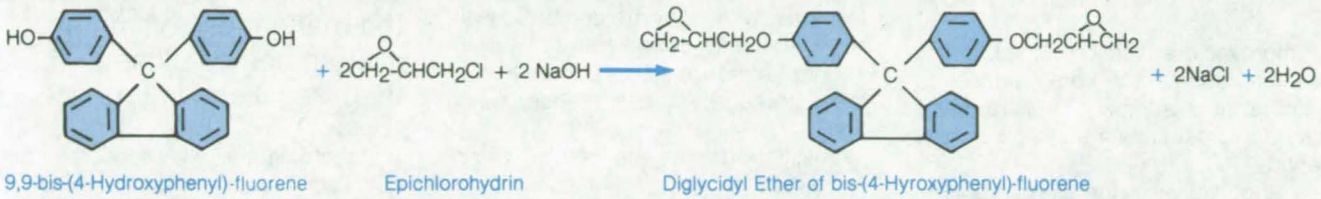

Diglycidyl Ether of Bis-(4-Hydroxyphenyl)-Fluorene is prepared by reacting epichlorohydrin and sodium hydroxide with 9,9-bis-(hydroxyphenyl)-fluorene. The end of the reaction is determined by gas or liquid chromatography, mass spectroscopy, or infrared techniques.

A new compound, diglycidyl ether of bis-(4-hydroxyphenyl)-fluorene (DGEBF), is thermally cured with diglycidyl ether of bisphenol A (DGEBA) to make strong lightweight composites that have good temperature stability and fire resistance. The composites are used to manufacture printed-circuit boards and panels for buildings, ships, and aircraft.

DGEBF is prepared by reacting epichlorohydrin, which is commercially available, with 9,9-bis-(4-hydroxyphenyl)-fluorene in the molar ratio of between 7:1 and 10:1; that is, a large excess of epichlorohydrin. The 9,9-bis-(4-hydroxyphenyl)-fluorene starting material is prepared by reacting fluorenone and phenol with a catalyst, anhydrous hydrogen chloride, and a cocatalyst, β-mercaptoproprionic acid. After preparing the starting material, the reactants are heated at 100° to 116° C for between 4 to 6 hours. The DGEBF is crystalline.

Depending on the end use, the resins are blended in proportions that vary in weight ratios of about 1:5 to 1:1 of DGEBF to DGEBA. To accelerate thermal curing, a catalyst, trimethoxyboroxine (TMB) or ethyltriphenyl phosphonium iodide, is added to the resins. A typical formulation might be 10 gm DGEBA, 4.1 gm DGEBF, and 1.35 gm TMB. The blend of resins is prepared by melting or by combining the ground solid particles of each of the components, adding the catalyst, mixing the particles, and heating to cure the composition.

A thickness of greater than one-eighth inch (0.3 cm) is desirable for structural integrity if the resin blend is used to prepare molded products. The blend can be mixed with reinforcing material such as glass or graphite, which can be in the form of fibers, chopped fibers, or tape. To prepare the reinforced resin composites, the reinforcing fibers or cloth are coated or impregnated with the resin blend and cured by heating at a temperature of about 149° to 216° C for a time ranging from about 10 to 180 minutes. Alternately, the composites can be cured under pressure.

In tests on composites made with the resins, the char yield was very high, 81 percent, and the smoke density low. The limiting oxygen indices were typically greater than 49 percent.

This work was done by Demetrius A. Kourtides and John A. Parker of **Ames Research Center.** *For further information, Circle 32 on the TSP Request Card.*

Inquiries concerning rights for the commercial use of this invention should be addressed to the Patent Counsel, Ames Research Center [see page A5]. *Refer to ARC-11331.*

Books and Reports

These reports, studies, and handbooks are available from NASA as Technical Support Packages (TSP's) when a Request Card number is cited; otherwise they are available from the National Technical Information Service.

Standards for Epoxies Used in Microelectronics

Report has significant commercial applications.

Improved qualification standards and test procedures for epoxy adhesives used in the assembly of high-reliability hybrid microcircuits are listed in a new report.

The objective of the standards is to resolve problems in the areas of outgassing, bond shear strength, corrosivity, volume resistivity, ionic impurities, electrical stability, and the frequency of qualification testing. Eight epoxy adhesives — four conductive and four insulative — were tested to develop data for specification requirements. The test findings are included in the report.

The specification requires both qualification of the material by the supplier and qualification of the processes to be used in assembly of the hybrid microcircuit by the user. This dual qualification is believed to be essential to insure that the microcircuits have the reliability required for space applications. The report includes estimates of the cost and the time required to perform the user and supplier qualification tests.

This work was done by S. V. Caruso, J. J. Licari, B. L. Weigand, and C. A. Soykin of Rockwell International Corp. for **Marshall Space Flight Center.** *To obtain a copy of the report, Circle 33 on the TSP Request Card.*
MFS-25810

Modified Antifreeze Liquids for Use on Surfaces

Viscosity agents and antifreeze liquids are evaluated.

Viscosity modifiers can substantially improve the effectiveness of antifreeze compounds in preventing frost formation on cold surfaces, according to a NASA report. Unmodified antifreeze liquids tend to drain away too rapidly. However, when they are combined with such viscosity modifiers as gelling agents, antifreeze liquids adhere to surfaces and perform their intended function.

The report presents results of an evaluation of two antifreeze liquids, dimethyl sulfoxide and ethylene glycol, and five viscosity modifiers: gelatin, gum tragacanth, starch, agarose powder, and citrus pectin. The purpose of the evaluation was to find the best way of dealing with frost formation on the Space Shuttle. The Shuttle external tank has several areas where frost tends to accumulate, including protrusions not covered by insulation and louvers on oxygen vents. Although the frost is relatively harmless, thick accumulations can break off and damage the Shuttle thermal-protection tiles.

Microgels, having a pastelike consistency, can be applied to vertical surfaces more effectively than can conventional gels. Microgels can be formed readily with agarose but not with pectin. Ethylene glycol is preferred to dimethyl sulfoxide as an antifreeze because of its lower flammability, reduced health hazard, lower evaporation rate, and broader eutectic range.

Gelled antifreeze is effective for surface temperatures of about -18° C but ineffective at -184° C. It seems likely that the insulating properties of the gels contribute more to their effectiveness than does the formation of a eutectic with added water.

Pectin gels are dissolved readily by liquid water. At cryogenic surface temperatures, however, the gel is so cold that it frosts before any of it can dissolve.

[See the related article "Gelled Anti-Icing Agents" (MSC-20088) on page 281 of this issue.]

This work was done by Robert O. L. Lynn of **Marshall Space Flight Center.** *To obtain a copy of the report, Circle 34 on the TSP Request Card.*

Inquiries concerning rights for the commercial use of the technology described in the report should be addressed to the Patent Counsel, Marshall Space Flight Center [see page A5]. Refer to MFS-25741.

Solidifying Bi/MnBi at Low Gravity

The intrinsic coercivity of the manganese/bismuth system comes close to the theoretical maximum.

According to a new report, the directional solidification of Bi/MnBi magnetic alloy under low gravity enhances its magnetic properties. The magnetic properties of low-gravity Bi/MnBi alloy make it an attractive material for use in motors and other small electrical and electronic components. Samarium/cobalt alloys have filled this need to some extent, but the high cost of samarium prohibits widespread use. If Bi/MnBi can be made economically under near-zero-gravity conditions — in an orbiting space factory, for example — the cost of compact, lightweight magnetic parts may decrease.

In sounding-rocket experiments, a eutectic alloy of MnBi in Bi was allowed to solidify at about one ten-thousandth of normal Earth gravity. Heat was removed from the alloy in one direction only during solidification so that a rod structure was created. The resulting MnBi rods in a Bi matrix were smaller in diameter and more closely spaced (by about half) than those solidified under normal gravity. The rods were more highly magnetic than those formed at normal gravity, exhibiting an intrinsic coercivity of 97 percent of the theoretical maximum of 35,000 oersteds: This is the largest ever reported for any permanent magnet alloy except for certain samarium/cobalt alloys.

This work was done by Joe Drauch, Ralph Lange, Ron A. Pirich, and William Poit, Jr. of Grumman Aerospace Corp. for **Marshall Space Flight Center.** *To obtain a copy of the report, Circle 35 on the TSP Request Card.*
MFS-25736

Life Sciences

Hardware, Techniques, and Processes

Heart-Rate and Breath-Rate Monitor

Off-the-shelf components measure physiological rates to an accuracy of ±1 pulse/minute.

Lyndon B. Johnson Space Center, Houston, Texas

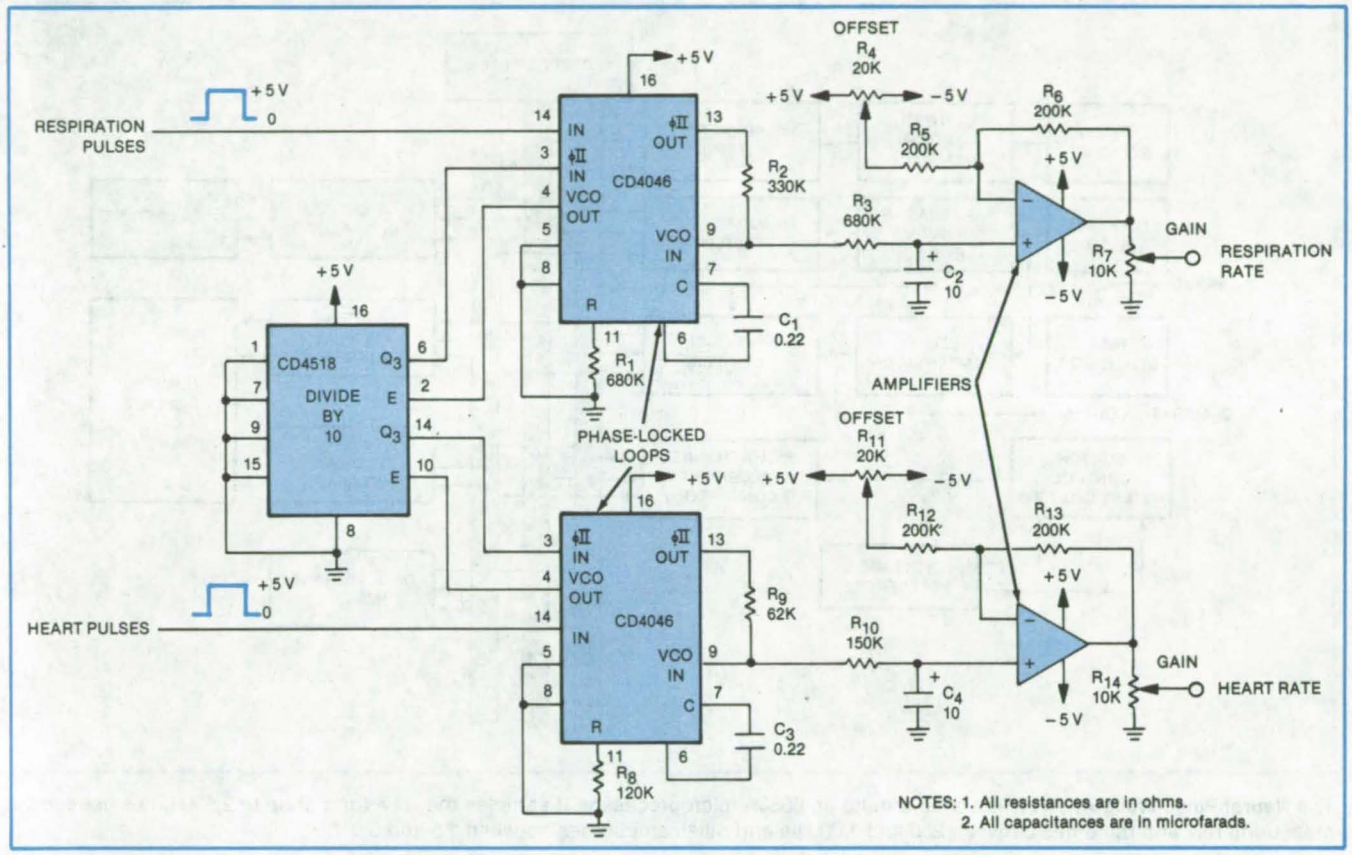

Phase-Locked Loops lock on heart-rate and respiration-rate input signals. Each loop IC contains two phase comparators. The positive-edge-triggered circuit is used in this application.

A circuit requiring only four integrated circuits (IC's) measures both heart rate and breath rate. The dual-rate-measurement circuit has performed satisfactorily in practical clinical situations. The basic element — an inexpensive phase-locked-loop IC (4046) — is used to generate a linear output signal proportional to the input rate. This component is commercially available and is particularly suitable for making biomedical measurements. The simplicity of the circuitry, fast response time, good linearity, and good stability are desirable features achieved with this technique.

The accompanying figure is a circuit schematic. In the phase-locked loop, a phase comparator detects the phase and frequency difference between the input signal and the voltage-controlled oscillator output. The comparator output is proportional to the phase and frequency difference.

After low-pass filtering, the comparator output is fed back to the voltage-controlled oscillator to reduce the frequency difference between the oscillator signal and the input signal. When the oscillator frequency comes close to the input signal frequency, the phase-locked loop forces the oscillator to lock in frequency with the signal input. The external components for the low-pass filters (R_2, R_3, and C_2 for respiration rate; R_9, R_{10}, and C_4 for heart rate) give the required time constants.

With the divide-by-10 circuit in the feedback path from the voltage-controlled oscillator output to the phase comparator input, the oscillator locks at 10 times the input frequency. At this higher frequency, the timing components — particularly the capacitor — can be lower in value. They therefore cost less and operate more stably.

The circuit measures heart rates between 20 and 255 beats per minute. For respiration, the range is 4 to 63 breaths per minute. The allowable rise time for heart-rate monitoring is 3 seconds. For respiration, it is up to 15 seconds. Linearity in both branches is ±1 pulse per minute.

This work was done by Tommy G. Cooper of Narco Scientific for **Johnson Space Center.** *For further information, including circuit design theory and performance specifications, Circle 36 on the TSP Request Card.*

This invention is owned by NASA, and a patent application has been filed. Inquiries concerning nonexclusive or exclusive license for its commercial development should be addressed to the Patent Counsel, Johnson Space Center [see page A5]. Refer to MSC-20078.

Microprocessor-Based Neural-Pulse-Wave Analyzer

Contributions from several nerve units are identified and separated.

Ames Research Center, Moffett Field, California

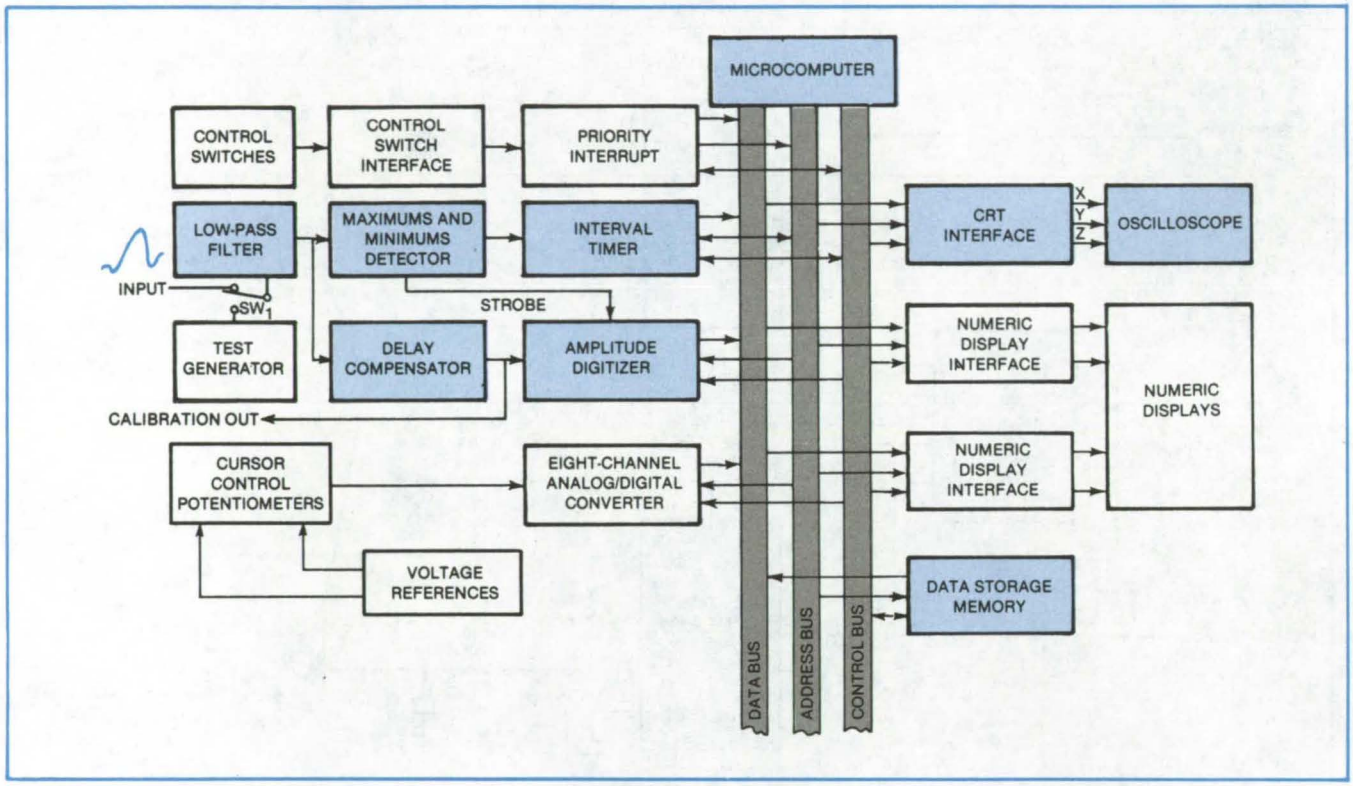

The **Neural-Pulse-Wave Analyzer** is based around an 8080A microprocessor. It samples the waveform at up to 2,500 times per second, measuring rise and fall times between 200 and 1,000 μs and pulse amplitudes between 1.5 and 8.0 V.

A microprocessor-based system analyzes the amplitudes and rise times of neural waveforms. By displaying histograms of the measured parameters, it helps researchers determine how many nerves are contributing to a signal and to specify the waveform characteristics of each. Tests using simulated nerve signals and real signals from the otolith nerve of a frog show the system to be effective in analyzing the noisy, multiple-source neural pulse signals.

The new system, illustrated in the block diagram, analyzes waveforms that consist of a maximum flanked by minimums on each side. The minimums may be of different heights. The waveshape is characterized by rise amplitude, rise time, fall amplitude, and fall time. The parameters are measured relative to the maximum and the minimums.

A typical signal consists of a mixture of such pulses from several nerve units. Since there is always some parameter drift, background noise, and pulse overlap, a distribution of values is measured for each parameter. These distributions are analyzed statistically by the microcomputer software to separate the contributions of the individual nerve units.

As the neural waveform is scanned, pulse maximums and minimums are continuously identified and measured for amplitudes and rise times. These parameters are stored in a "raw data" file. A search of the raw data locates measurements that fall within the noise limits and places them in "noise-sorted" files. Finally, histograms are created for each of the noise-sorted files (rise amplitude, rise time, fall amplitude, and fall time) and displayed on an oscilloscope in the x-y-z mode.

An operator looking at the histograms can locate peaks that represent single pulse sources and can determine the number of sources making up the signal. If the signal contains multiple sources or if further noise reduction is required before source characterization can be accomplished, the "D-histogram" mode must be used. Before entering this mode, the operator moves two cursors on each histogram to create discrimination windows around interesting peaks. Then, upon entering this mode, the noise-sorted files are resorted according to the cursor boundaries set previously. The results are improved noise rejection, full or partial separation of overlapping peaks, and isolation and identification of related peaks in different histograms.

This work was done by Gilbert K. Kojima of **Ames Research Center** *and Francesco Bracchi of the Universita di Milano, Milan. For further information, Circle 37 on the TSP Request Card.*
ARC-11388

Mechanics

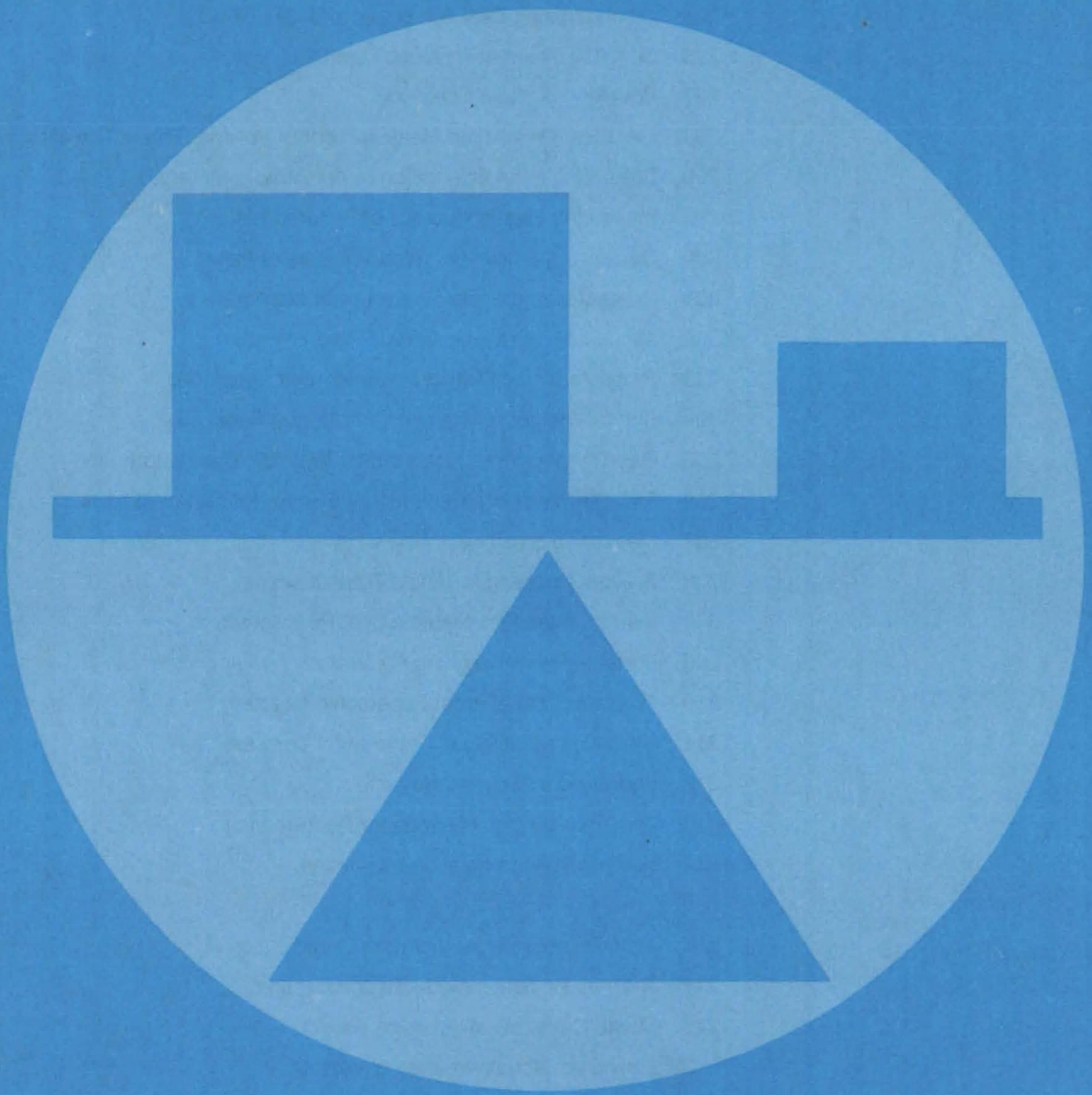

Hardware, Techniques, and Processes

Computer Programs

Instrument Measures Airflow Friction Without Contact

A laser interferometer monitors the thickness of a shearing oil film.

Ames Research Center, Moffett Field, California

A new dual-beam laser interferometer determines the airflow friction against a body by measuring the time-varying thickness of a wind-sheared oil film. The measurements yield the skin friction between the film and an airstream. The kinematic viscosity of the oil can also be determined.

The interferometer uses two laser beams of known separation. It is therefore more accurate than single-beam interferometers, which require that the distance from the beam to the leading edge of the oil film be determined. Since it is not placed in the wind tunnel, the new interferometer does not affect airflow.

A droplet of oil is applied to the surface of a model in the wind tunnel. As air flows over the surface, the film formed by the droplet changes in thickness. Two light beams — formed by a single laser aimed at an angled interferometer flat — are focused on the film (Figure 1). One beam is upstream from the other and passes through a half-wave retardation plate, which rotates the beam polarization 90° before it reaches the film.

After they have been reflected from the oil film and the model surface, the two beams are separated by a polarization beam splitter and focused on photodetectors. The light-intensity signals from the photodetectors are recorded.

As the airflow in the wind tunnel spreads the oil film and changes its thickness, alternate constructive and destructive interferences within each beam are produced by the beam reflections from the body and film surfaces. These interferences modulate the light intensity reaching each photodetector.

Each crest (or trough) on a recorded light-intensity trace (Figure 2) represents an oil thickness corresponding to maximum constructive (or destructive) interference between the reflection from the film surface and that from the model surface. The change in oil thickness can therefore be determined precisely in terms of the known laser wavelength by counting the number of fringes over a given timespan. With this information and other known parameters, the skin friction can be calculated. On the basis

(continued on next page)

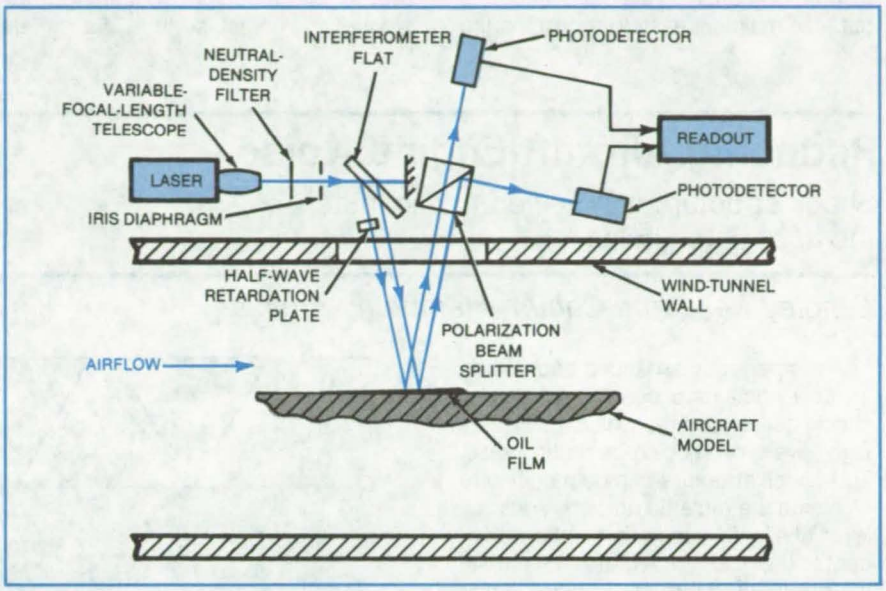

Figure 1. **The Beam From a Helium/Neon Laser** is split into two beams by an angled interferometer flat after a neutral-density filter has reduced the original beam intensity to a level that will not heat the oil film. The reflected upstream and downstream beams are directed to separate photodetectors.

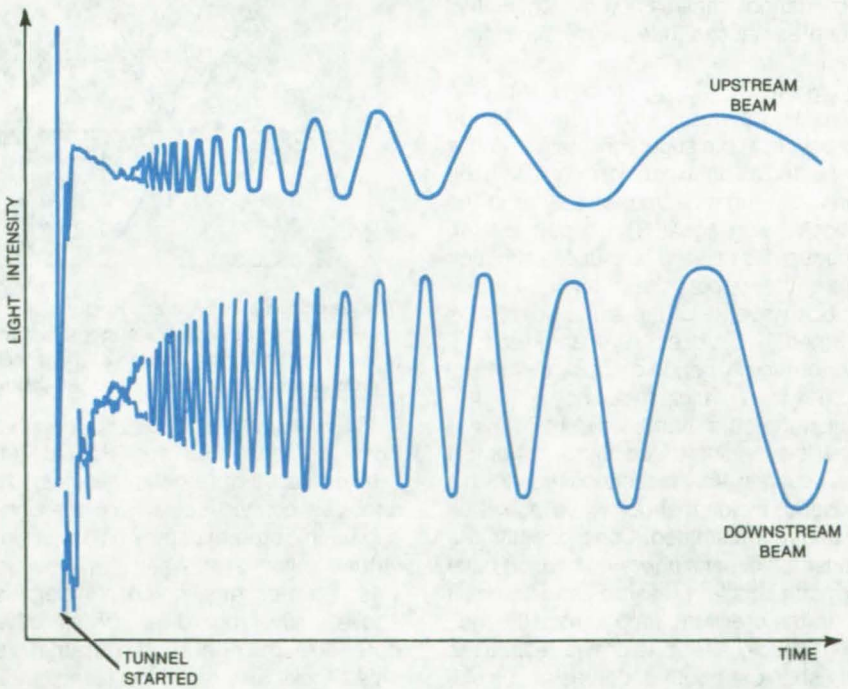

Figure 2. **Recorded Light-Intensity Traces** contain peaks that, over a given timespan such as 1 minute, represent the change in thickness of the oil film. The skin friction is calculated from the number of peaks in the timespan, and such factors as airflow pressure gradient, angles of incidence of the laser beams, indices of refraction of the oil and optical components, beam spacing, and laser wavelength.

of similar measurements made with the body surface tilted and without wind, one can also determine the kinematic viscosity of the oil.

The laser transmitter and receiver are mounted on platforms outside the wind tunnel. This independent mounting not only eliminates the detrimental effects of tunnel vibration on the measurements but also makes it easy to reposition the interferometer quickly to any location in the tunnel where a window for the light beams is available.

Any time period can be selected for recording interference signals — it is not necessary to record during the total time that the oil flows under the influence of the airstream. Errors from prerun oil flow, tunnel starting transients, and initial surface waves are therefore eliminated.

This work was done by Daryl J. Monson of **Ames Research Center.** *For further information, Circle 38 on the TSP Request Card.*

Inquiries concerning rights for the commercial use of this invention should be addressed to the Patent Counsel, Ames Research Center [see page A5]. *Refer to ARC-11354.*

Reducing Aircraft-Engine Noise

Shock structure is modified to eliminate the associated noise.

Langley Research Center, Hampton, Virginia

An imperfectly-expanded supersonic jet flow contains a periodic or regular shock cell structure, which generates high levels of shock-associated noise. This shock structure can be modified to eliminate the radiated noise by adding a layer of slightly supersonic airflow adjacent to the noisy jet. A drastic change in the shock structure takes place when this added layer increases in velocity from subsonic to supersonic. This abrupt change in the shock cell system arises principally because a subsonic flow cannot transmit flow discontinuities such as shocks, but a supersonic flow can.

When the "layer" flow is subsonic (see figure, top), an incident oblique shock, s, in the supersonic jet stream is reflected as an expansion fan, f, with the pressure jumps across the fan and the shock being equal. The expansion fan propagates upward, and upon reflection from the upper shear layer, another shock wave, s, of the same strength is formed. This process is repeated spatially, forming a periodic shock cell structure with very high shock noise.

On the other hand, when the "layer" flow is supersonic (see figure, bottom), it can sustain flow discontinuities. In this case an incident shock wave, s, will be partially transmitted. Consequently, the reflected expansion wave, f, would have a much smaller pressure jump across it than the pressure jump across the incident shock. After one or two reflections the shock strength becomes negligible, and a shock cell pattern of longer than one or two periods cannot be maintained, resulting in the almost total elimination of shock-associated noise.

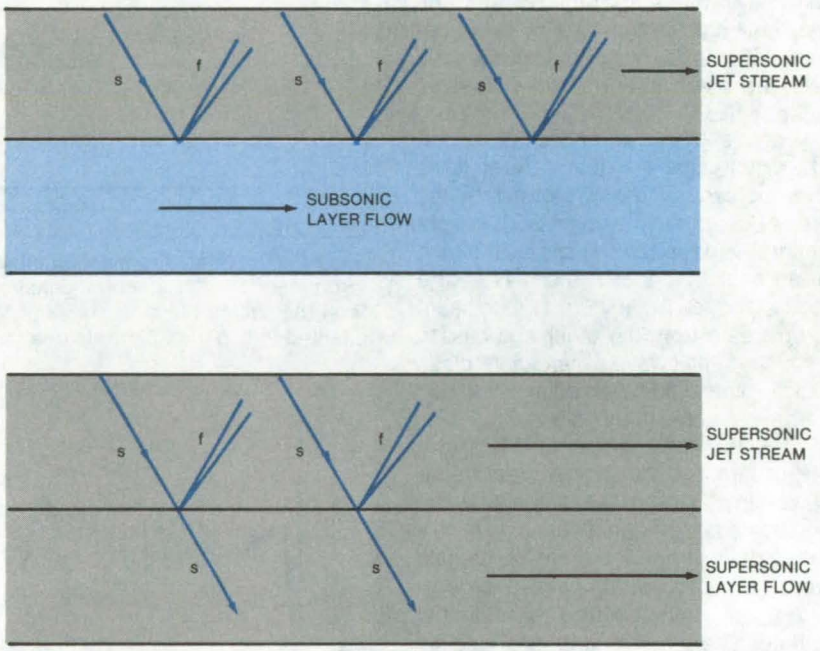

The **Shock Wave Repeats** in the supersonic flow adjoining a subsonic flow layer, as shown at the top. When a supersonic layer is added, as shown at the bottom, the shock wave is partially transmitted at the interface. The result is almost total elimination of the shock pattern after one or two reflections.

The effectiveness of this concept has been demonstrated for coaxial jets representative of turbofan engines. The shock-associated noise from the outer supersonic stream of the coaxial jet was virtually eliminated when the inner jet was operated at a mach number just above unity, regardless of all other outer-stream operating parameters. This shock-noise-reduction technique is applicable to inverted as well as to normal-velocity-profile coannular jets. The technique can also be used to eliminate or reduce the shock noise of turbojet engines.

This work was done by Himatlal K. Tanna, William H. Brown, and Christopher K. W. Tam of Lockheed Corp. for **Langley Research Center.** *Further information may be found in NASA CR-3454 [N81-30908/NSP], "Shock Associated Noise Reduction from Inverted-Velocity-Profile Coannular Jets" [$15]. A copy may be purchased [prepayment required] from the National Technical Information Service, Springfield, Virginia 22161.*
LAR-12890

Noise Control in Propeller-Driven Aircraft

Double-wall sidewalls minimize interior noise and weight.

Langley Research Center, Hampton, Virginia

An analytical model predicts the noise levels inside propeller-driven aircraft during cruise at mach 0.8. The model has been applied to three aircraft with fuselages of different size (wide-body, narrow-body, and small-diameter) to determine the noise reductions required to achieve an A-weighted sound level that does not exceed 80 dB. The model was then used to determine noise-control methods that could achieve the required noise reductions.

Two classes of noise-control treatments were investigated: treatments that can be added to existing structures and advanced concepts that would require changes to the fuselage primary structure. Only one treatment, a double wall with a limp panel, provided the required noise reduction. Weight penalties associated with the treatment were estimated for the three aircraft.

Conventional skin/stringer/frame fuselage construction is the baseline for the two general noise-control methods, add-on and advanced. Add-on concepts included increased structural damping, increased acoustic absorption in the cabin, and the use of double-wall sidewalls. Advanced concepts included increased skin thickness, increased frame stiffness, increased number of frames, and the use of honeycomb structure.

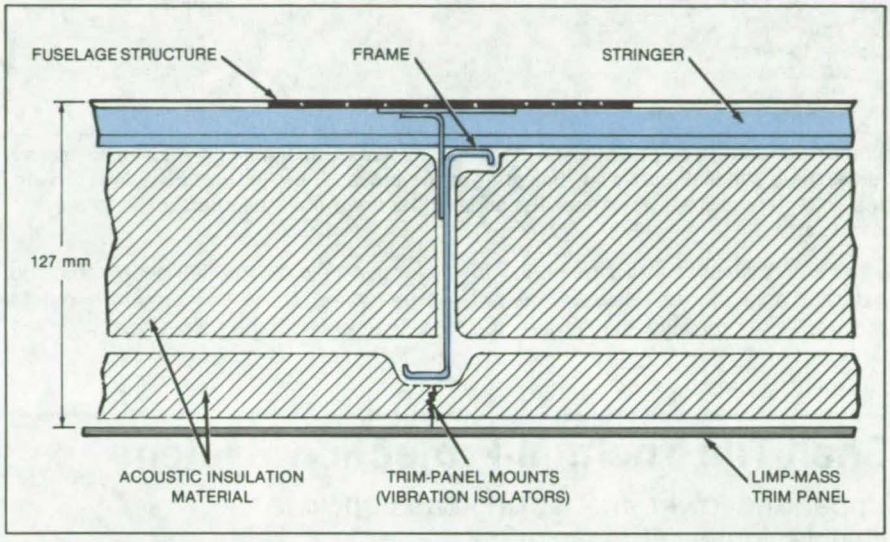

A **Double Wall With a Limp Panel** gives the required noise reduction inside propeller-driven aircraft

Only one concept, that of a double-wall sidewall, provides the high noise reductions required at low frequencies to achieve the 80-dB(A) goal. The outer panel of the double wall was formed by the fuselage skin, the inner panel was a limp-mass trim panel, and the region between was filled with porous material. A diagram of the effective double-wall sidewall treatment is shown.

This work was done by David C. Rennison and John F. Wilby of Bolt Beranek and Newman Inc. for **Langley Research Center.** *Further information may be found in NASA CR-159200 [N80-25102/NSP], "Interior Noise Control Prediction Study for High-Speed Propeller-Driven Aircraft" [$24]. A copy may be purchased [prepayment required] from the National Technical Information Service, Springfield, Virginia 22161.*

LAR-12954

Discriminating Between Liquid and Gas Flows

Variations in momentum density would change the position of a sensor.

NASA's Jet Propulsion Laboratory, Pasadena, California

A proposed flow sensor would distinguish flowing gases from liquids. The sensor would allow liquids to pass, but would signal a valve to turn off the flow of gases. The concept was developed for propulsion systems in which liquid fuel is forced out of a storage tank by a high-pressure gas. A controller based on such a device would stop the flow of gas from the fuel tank after the liquid has been depleted.

The device is contained in a cylindrical housing (see figure) on the fuel-outlet pipe. In the housing a rodlike obstruction is mounted on a shaft. The shaft can slide axially on bearings in the housing. The housing is enlarged around the obstruction so that flow is not significantly reduced. The obstruction is urged to a reference position by a coil spring around the shaft.

Operation of the sensor is based on the fact that the mass density and therefore the momentum density of the gas are substantially less than the mass and momentum densities of the liquid. When liquid flows through the device and pushes against the obstruction, it forces the obstruction to slide in the downstream direction against the spring pressure, moving an armature at the

(continued on next page)

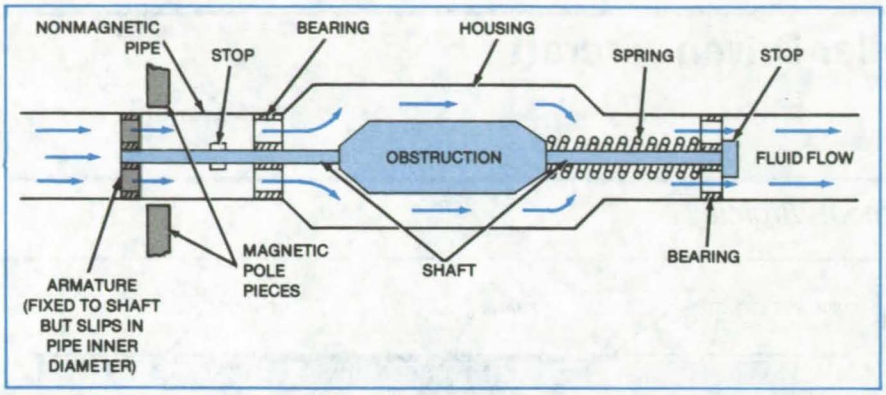

When Gas Flows, the spring moves the armature away from the magnetic pole pieces, as shown here. When liquid flows, the spring is compressed, and the armature lines up with the pole pieces. Stops at or near the ends of the shaft limit the shaft travel to prevent damage.

other end of the shaft into alinement with external pole pieces. However, when the gas flows through the device, the force on the obstruction decreases, and the spring shifts the armature out of alinement with the pole pieces.

The pole pieces are the sensing portion of a reluctance-type magnetic pickup and are mounted outside the nonmagnetic pipe used to carry the liquid. The circular armature on the end of the internal shaft is made of magnetic material and is perforated to minimize its obstruction to the fluid flow. When the armature lines up with the pole pieces, the magnetic path is complete; but when gas starts to replace the liquid flow, the armature shifts and breaks the magnetic path. The magnetic pickup then generates a signal that activates a shutoff valve.

This work was done by C. Martin Berdahl of Caltech for **NASA's Jet Propulsion Laboratory.** *For further information, Circle 39 on the TSP Request Card.*
NPO-15531

Shell-Tile Thermal-Protection System

Upper and lower interlocking caps enclose flexible lightweight insulation.

Langley Research Center, Hampton, Virginia

A durable shell-tile thermal-protection system, originally developed for the outer surface of reusable Earth-to-orbit transports, consists of interlocking upper and lower hard caps, incorporating appropriate stiffeners and enclosing lightweight fibrous insulation. It is anticipated that the new shell tile will be more durable than the reusable surface insulation (RSI) currently used on the Space Shuttle orbiter.

Previous thermal-protection systems include ablators, corrugated metallic panels, and sintered silica fibrous tiles. Unlike the shell tile, however, ablators are not reusable, while corrugated metallic panels are not aerodynamically smooth and have a relatively-high parts count. Reusable and surface insulation, a lightweight and very insulative sintered silica-fiber tile, is relatively new, and the full implications of this system are not yet known. However, the tiles are adhesively bonded to the vehicle through a strain isolation system and are known to be relatively fragile.

The shell tile consists of two interlocking hard caps, an upper and a lower. The material for these caps can be selected to match the appropriate temperature regimes. Candidates for upper caps are titanium, Rene, columbium, and even reinforced carbon composites. Candidates for lower caps are titanium (because of its low weight and low conductivity), graphite/polyimide, and other materials — the exact material selection depends on the thermal and structural requirements of the particular application.

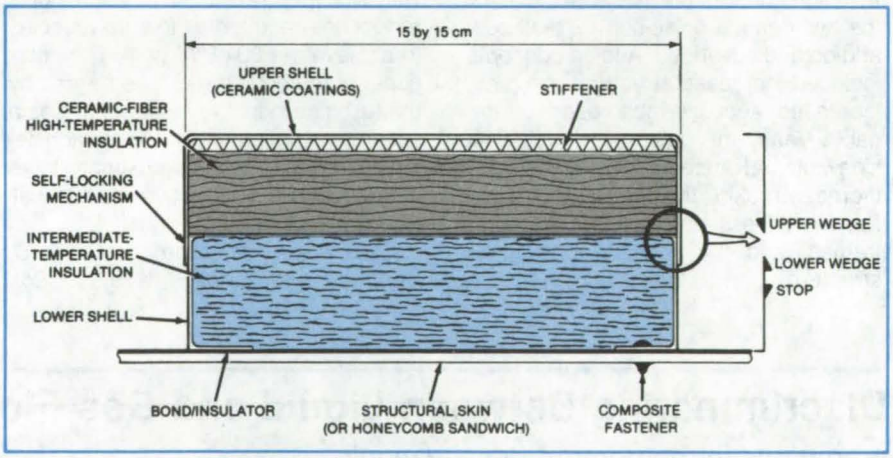

In the **Metallic-Shell Tile,** upper and lower caps lock together, enclosing stiffeners and insulation.

As shown in the figure, the tile consists of a structural upper cap having a dimpled lightweight sheet to add stiffness and strength. A high-temperature package of lightweight insulation is inserted into the upper cap. In the lower cap, an even lighter insulation, of somewhat lower temperature capability, is used. The self-locking mechanism which positions and holds the upper and lower caps together, consists of tapered wedges attached to each cap.

The tiles can be fabricated in almost any shape, such as square or hexagonal, and can be constructed with

dimpled sides to add stiffness and increase the conduction path. Further, the upper cap could be fabricated from a dimpled sheet with a flat offset outer panel to overlap adjacent tiles.

Because the tile has a strong structural outer shell, very weak insulation having a much lower density than RSI can be used internally. Also, insulation and other materials within the upper and lower caps can be changed to match temperature profiles.

Since the shell tile has adequate shear and tensile strengths, a strain isolation system is not needed between aluminum structure and tile, thus contributing to lower overall weight and less complexity. Also, the bottom shell can be mechanically fastened to the structure, the insulation inserted, and the upper cap assembly attached by downward pressure until the self-locking mechanism engages.

This work was done by Ian O. MacConochie, Ashby G. Lawson, and H. Neale Kelly of **Langley Research Center.** *For further information, Circle 40 on the TSP Request Card.*

This invention is owned by NASA, and a patent application has been filed. Inquiries concerning nonexclusive or exclusive license for its commercial development should be addressed to the Patent Counsel, Langley Research Center [see page A5]. Refer to LAR-12862.

Checking Surface Contours

Rubber impressions are viewed with an optical comparator

Lyndon B. Johnson Space Center, Houston, Texas

Surface features that cannot be viewed directly or measured easily can be observed as impressions in a removable silicone-rubber casting of the critical area. The method has been used to check the weld quality of the seam between the two hemispheres of a spherical pressure vessel.

A simple mold (see figure) is constructed from aluminum sheet or any other easily shaped material compatible with the silicone-rubber ingredients. The mold is placed over the surface to be measured. A newly-mixed silicone-rubber compound is poured in the mold and allowed to cure.

Once hardened, the silicone-rubber casting is removed and cut into thin sections. The sections are placed on an optical comparator and magnified 10 to 50 times so that their projected profiles can be measured. When the projection shows an unusual contour, the comparator operator traces the image on paper and affixes the dimensions.

The General Electric Co. RTV-21 (or equivalent) silicone rubber used in the pressure-vessel tests is stable within 0.002 inch over 4 inches (0.05 mm over 10 cm). It provides excellent resolution of contours and will even pick up fingerprints on a polished surface. Moreover, it does not require mold-release agents.

The rubber compound cures quickly, and the mold can usually be removed within 30 minutes. If tin octoate is used as the catalyst (instead of the usually-supplied tin dilaurate), the setting time can be as short as 1 minute. The rubber is hard enough to permit accurate measurements when cured and is nonflammable and nontoxic.

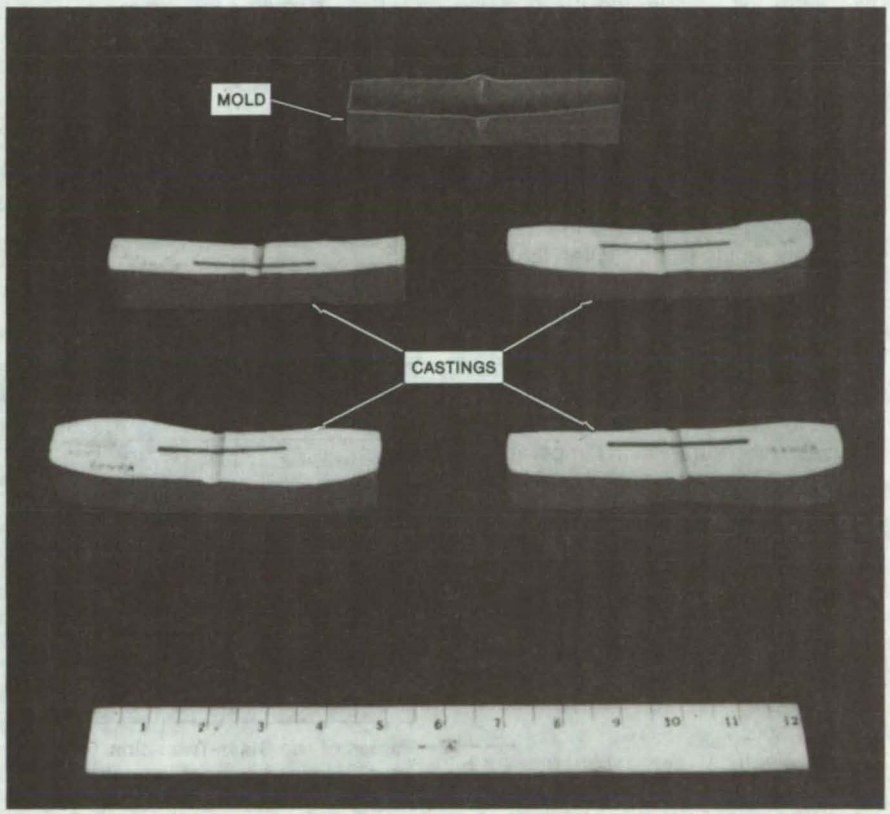

A **Simple Mold** was used to make external castings of the circumferential weld bead around a pressure vessel.

This work was done by Daniel Velega of Beech Aircraft Corp. for **Johnson Space Center.** *No further documentation is available.*
MSC-20318

Electrical Dissipation Measurement of Polymer Phase Transitions

The change in dipole packing occurring with each transition is sensed by its effect on the dissipation factor.

Langley Research Center, Hampton, Virginia

A simple technique measures the solid/solid, glass/rubber, and liquid/liquid transition temperatures in polymers having dipole moments. The technique is based on a change in dipole packing that occurs with each transition and is measured as a change in the electrical dissipation factor. The apparatus for determining phase transitions from electrical dissipation is shown in the figure.

The polymer sample, in the form of a thin film, is tested as the dielectric of a capacitor. The capacitor electrodes and their leads are fabricated from 0.02-mm aluminum foil — thin enough to eliminate the need for guard rings. The electrodes are backed by optically flat disks for uniform contact of electrode and sample. The upper disk is twice as thick as the lower.

Thermocouple beads are located at midthickness of the upper disk. These beads experience the same thermal environment as the sample when the muffle furnace temperature is increased. The capacitor dissipation factor is monitored and recorded at equal temperature intervals, and the data are analyzed and plotted.

The technique was used to measure the glass/rubber transition temperatures of four generic classes of high-molecular-weight polymers. The values of the transition temperatures, shown in the table, are in good agreement with the values obtained by other methods. The agreement demonstrates that measurement of the dissipation factor, a dielectric property, is a reliable method for determining phase transitions in polymer solids.

The electrical dissipation measurement technique has potential applications for such polymer systems as polysulfones, polyimides, epoxies, and polyethylene. Some possibilities are continuous quality control in the manufacture of thin films; moisture content monitoring of potting materials used in the manufacture of solid-state devices; the detection of environmental aging of polymeric structural components in automobiles, aircraft, and boats; and monitoring of the condition of polymeric storage containers for chemical waste.

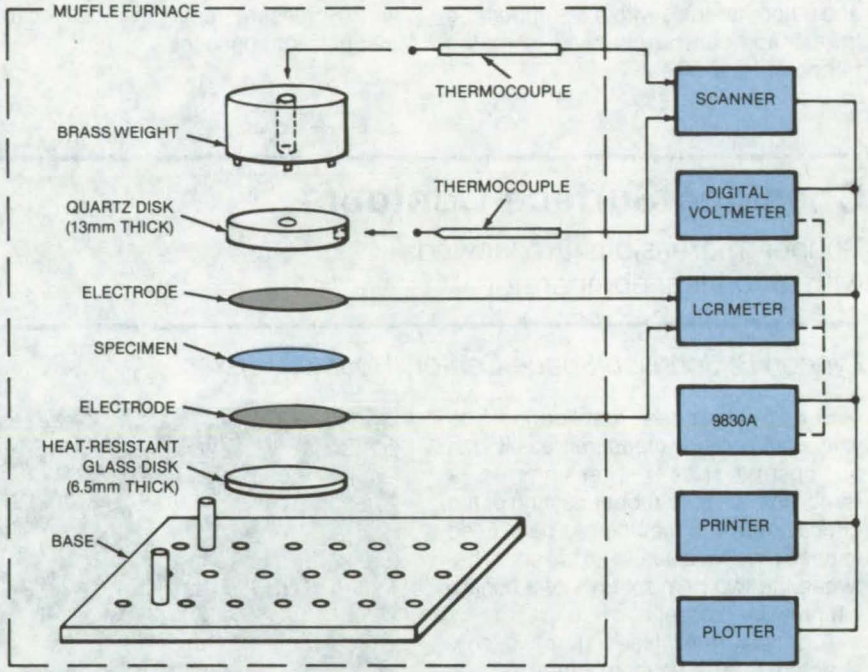

Electrical Dissipation Measurement yields transition temperatures of polymers with permanent dipole moments.

Polymer Material	Thickness (mm)	Dielectric Constant (Ambient)	Measured T_g (K)	Reference T_g (K)
•Polycarbonate of Bisphenol A	0.051	7.7×10^{-4}	424	422
•Polysulfone	0.130	1.4×10^{-3}	458	463
•Poly(ethylene Terephthalate)				
Dielectric Type	0.003	1.3×10^{-3}	355	353
Dielectric Type	0.008	2.0×10^{-3}	362	–
Nondielectric Type	0.019	3.3×10^{-3}	356	–
•Polyimide (Unoriented)				
PMDA – p,p′ – ODA	0.006	3.9×10^{-3}	657	672
PMDA – p,p′ – ODA	0.025	1.6×10^{-3}	661	–
PMDA – p,p′ – ODA	0.076	1.7×10^{-3}	628	–
BTDA – p,p′ – ODA	0.003	1.3×10^{-3}	591	553
BTDA – DAPI	0.025	1.0×10^{-3}	593	593

Values of the **Glass-Transition Temperature** of several high-molecular-weight polymers were measured using the variation with temperature of the electrical dissipation factors.

This work was done by Edward R. Long, Jr., and Anton Schuszler II of **Langley Research Center.** *For further information, Circle 41 on the TSP Request Card.*
LAR-12861

Determining the Orientation of Anisotropic Materials

Ultrasonics probe the direction of tile fibers.

Lyndon B. Johnson Space Center, Houston, Texas

A hand-held acoustic transducer is used to determine the fiber orientation of heat-resistant tiles installed on the outer surface of the Space Shuttle. The success in this application suggests extending the technique to the inspection of other anisotropic materials. Plywood and fiber/epoxy composites could be examined to determine fiber direction; and ultrasonics could be used to find the direction of roll in sheet metal and other rolled products.

The tiles are constructed in the form of planar laminates, with the fibers randomly oriented within each plane. Sound traveling along a fiber is attenuated differently from sound traveling across the fiber. Since the longitudinal component of attenuation is present in waves traveling along the fiber layers but not in waves traveling perpendicular to them, the difference in attenuation can be used to determine the orientation of the fiber layers.

The transducer used in the Space Shuttle application has one transmitter and two receivers located on the transmitter head so that they form a right isosceles triangle, with the transmitter at the right angle. The transducer head is placed on the outer surface of a painted tile (fiber orientation cannot be observed), and the signals from the receiving transducers are displayed on the two-channel oscilloscope.

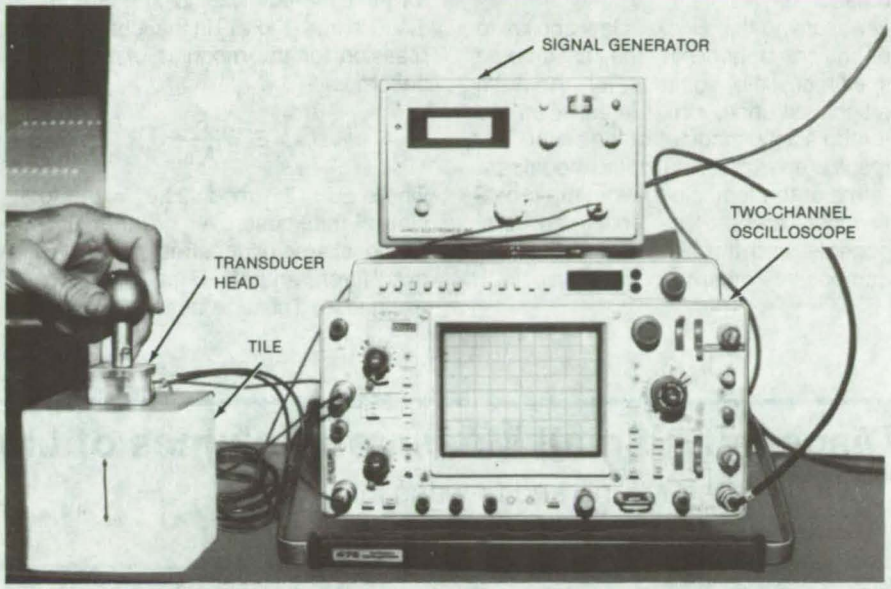

In this **Tile-Testing Assembly,** the signal generator charges a broadband acoustic transducer. The acoustic emissions are picked up by two receiving transducers, the output signals of which are coupled to the two-channel oscilloscope. The transmitting and receiving transducers are located in the transducer head.

If the signals transmitted along the two orthogonal directions are approximately equal regardless of angular orientation of the transducer head on the tile surface, then the fibers are lying parallel to the skin surface. If the signals are radically different, then the fiber plane in the tile is misoriented.

This work was done by Frank E. Sugg and Philip J. Hodgetts of Rockwell International Corp. for **Johnson Space Center.** *For further information, Circle 42 on the TSP Request Card.*
MSC-20229

Measuring Elastic Modulus of Sintered Metal

Technique minimizes the effect of the substrate on a thin sintered coating.

NASA's Jet Propulsion Laboratory, Pasadena, California

A uniaxial tension test yields an approximate value for the elastic modulus of a sintered material on a thin substrate. The test method is more useful than the bending tests previously used.

The test measures the stress/strain characteristic of positive nickel electrodes in nickel/cadmium batteries. An electrode is composed of a central perforated nickel-plated steel sheet about 4 mils (0.1 mm) thick, coated on each face by porous sintered nickel about 8 mils (0.2 mm) thick.

In the past, three-point or four-point bending tests have been used. It was assumed that the substrate affects the bending stress only negligibly because it is located in the center of the sintered layer at the neutral bending axis and that the major part of the load is carried by the outer layers. However, these assumptions are not realistic because the steel sheet is fairly thick.

The new test uses uniaxial tension instead of bending. A small sample of material about 1 inch (2.5 cm) square is cut from the electrode material. Two aluminum rods 0.5 inch (1.27 cm) in diameter and 3 inches (7.62 cm) long are

(continued on next page)

bonded on the opposite faces of the specimen by a thin coating of a viscous epoxy cement. The high viscosity prevents the cement from entering the pores of the sintered layers. The specimen is placed in a testing machine and subjected to tension and the applied load and specimen elongation are measured.

Assuming that Hooke's law applies to each component in the assembled specimen, the equation for the total elongation under stress is easily solved for the elastic modulus of the sinter. The result is an expression for the modulus in terms of the total elongation, the cross-sectional areas of the specimen components, and the elastic moduli of the components other than the sinter.

A convenient simplification occurs if it is assumed that the sinter is much less stiff than the other components. [The moduli of elasticity for the aluminum, epoxy, and steel in the specimen are approximately 10^7, 10^6, and 3×10^7 lb/in.^{2} (7×10^7, 7×10^6, and 21×10^7 kPa) respectively. The anticipated modulus for the sintered nickel is on the order of 1,000 lb/in.^{2} (7 kPa).] In that case, the expression for the modulus of the sinter becomes

$$E = \frac{F l}{A \Delta l}$$

where E = the modulus, l = the total sinter thickness, A = the cross-sectional area under stress, F = the applied force, and Δl = the total sample elongation. These quantities are easily measured, and it is no longer necessary to determine the moduli of the other components.

Strictly speaking, the stress experienced by the specimen is not simply a uniaxial tension but is more closely related to a triaxial tension. The departure of the state of stress from uniaxial to triaxial increases as the ratio of thickness to stressed cross-sectional area decreases. However, if the ratio is kept constant, accurate comparative data can be obtained on a variety of specimens.

This work was done by Robert F. Fedors and Albert F. Eastman of Caltech for **NASA's Jet Propulsion Laboratory.** *For further information, Circle 43 on the TSP Request Card.*
NPO-15589

Dispensing Small Measured Volumes of Liquid

Unit measures, filters, and unloads oil into a container.

Marshall Space Flight Center, Alabama

A pressurized dispenser loads a precise quantity of liquid into a vessel. It can be used, for example, in automobile manufacturing to dispense antifreeze solution into radiators or oil into engines, transmissions, or differentials.

The dispenser was developed for loading oil into a gearbox on the Space Shuttle solid-rocket booster. It uses gaseous nitrogen to control pressure, flow rate, and quantity precisely, with minimal contamination from the atmosphere.

In the new unit, 5 quarts (4.7 liters) of lubricating oil are placed in a 10-liter pressure-dispensing vessel that is then pressurized to 50 psig (345 kPa). The oil is forced through a 10-μm disk filter to a 5-liter pressure-dispensing vessel in a portable console (see figure). The console incorporates a gaseous-nitrogen reservoir that has been precharged to a pressure of 500 psig (3,450 kPa). From the 5-liter vessel, the oil is forced into a graduated sight glass at 10 psig (68.9 kPa) to a level of 170 cm^3. The oil is then forced out of the sight glass under 2 psig (13.8 kPa) pressure into the gearbox.

This work was done by G. Larson and J. Smith of United Space Boosters Inc. for **Marshall Space Flight Center.** *No further documentation is available.*
MFS-25690

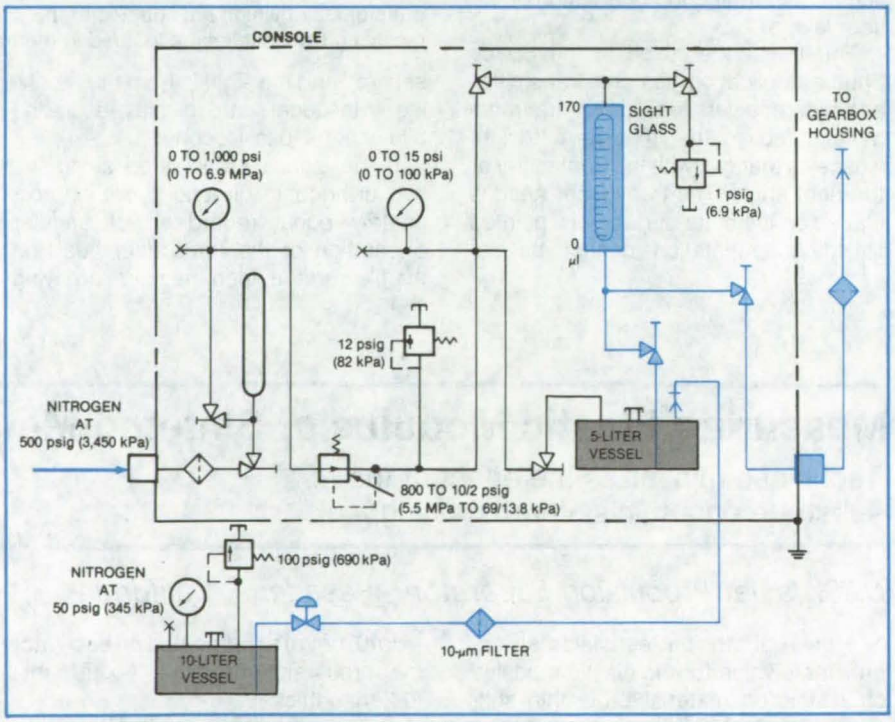

A Portable Console contains hardware and instruments for measuring and dispensing 5 quarts (4.7 liters) of lubricating oil.

Characterizing Shear Properties of Membranes

Shear stiffness is determined for use in vibration analysis.

Marshall Space Flight Center, Alabama

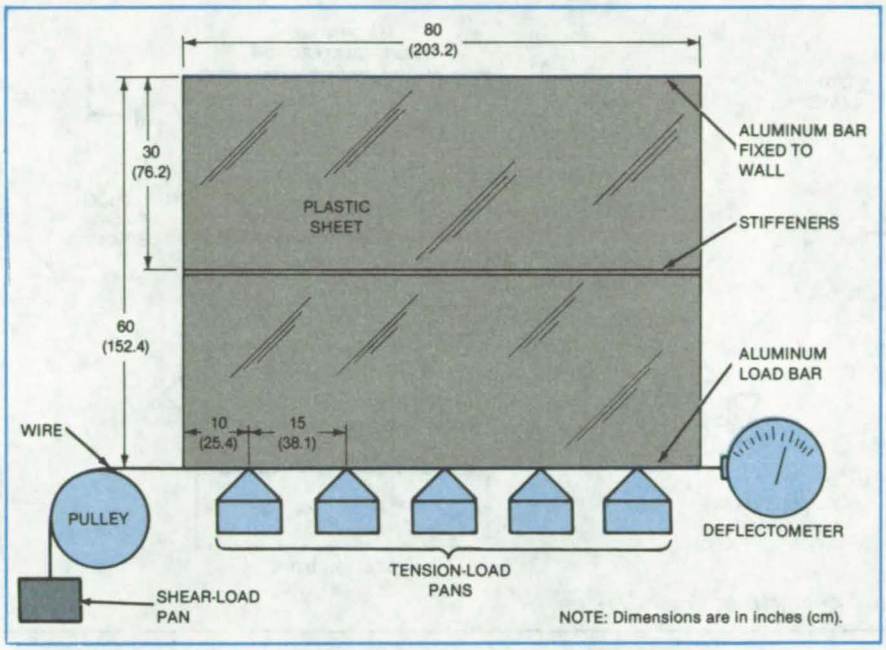

Figure 1. A **Plastic Sheet Is Statically Deflected in Shear** while under a tension loading. The shear and tension loads and lateral deflections are measured to obtain the static shear-stiffness parameter of the sheet.

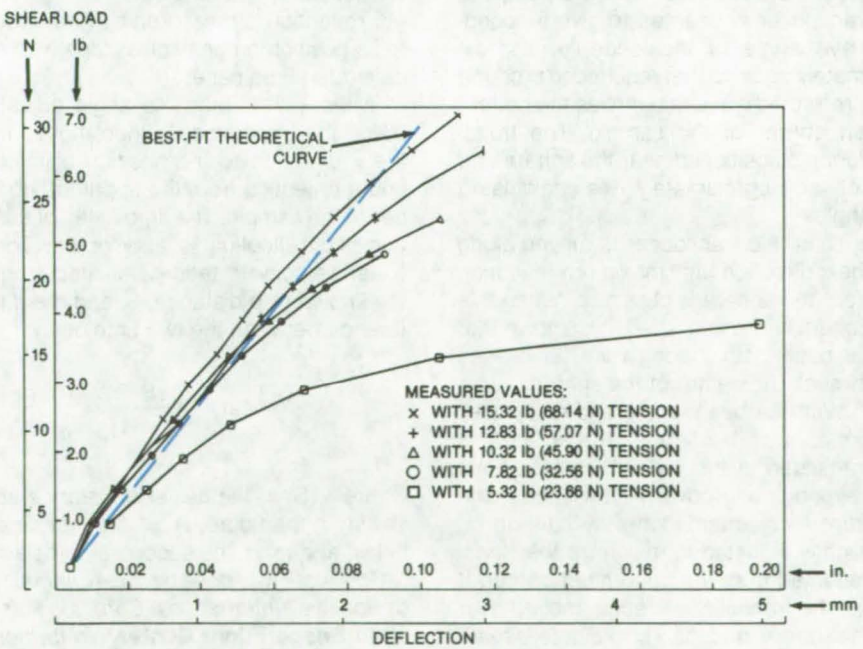

Figure 2. **Load Versus Deflection** is plotted for the experiment shown in Figure 1. The marked deviation of the 5.32-lb-tension load curve from the other curves is believed due to the formation of wrinkles.

Values of shear stiffness for flexible sheet materials are needed for finite-element dynamic analysis of in-plane vibrations. It is often assumed that the static shear stiffness closely approximates the dynamic shear stiffness.

A method has been devised to obtain static shear-stiffness data for membranes. The shear deflection of the membrane is measured under various applied static shear loads, and the measurements are plotted. A match is attempted between the experimental plot and predicted load-vs.-deflection curves until the best-fitting theoretical curve is found. The stiffness of the membrane is then taken as that used to calculate the best-fitting theoretical curve.

The simple experiment illustrated in Figure 1 gave the results shown in Figure 2. The portion of the shear stiffness induced by the blanket tension is small compared to the inherent shear stiffness of the sheet, as can be seen by comparison of the lower portions of the experimental curves. The experimental curve for the lowest tension loading is somewhat inconsistent with this conclusion, but the deviation is believed to be due to the formation of wrinkles (a result one would expect with insufficient tension).

This work was done by B. A. Simpson of Lockheed Missiles & Space Co., Inc., for **Marshall Space Flight Center.** *No further documentation is available.*
MFS-25745

Measuring Ultrasonic Shear-Wave Velocity

A technique using a reference sphere increases accuracy.

Marshall Space Flight Center, Alabama

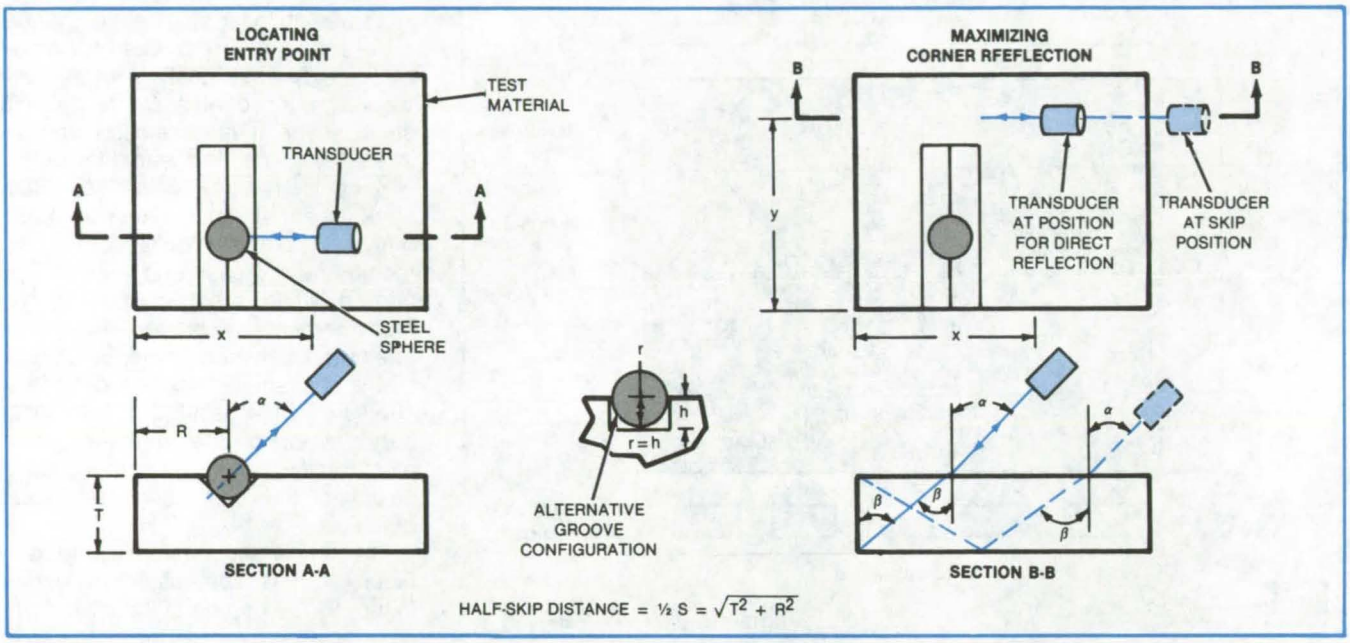

A New Method for Measuring Ultrasonic-Shear-Wave Velocity can yield results with less than 1 percent error. The sample contains a groove in which a steel sphere is placed. The sphere acts as a reference point for measuring path lengths and propagation times.

A new technique improves the accuracy of measurements of ultrasonic-shear-wave velocity. The technique eliminates the need to measure the incident sound angle, which was previously a source of error. In tests of the method, velocity measurements were within 1 percent of published data.

Previous measurements had been hampered by difficulties in locating the point where the beam enters the test material. This was because of unavoidable uncertainties in the beam-width and transducer orientation.

In the new method, a steel sphere placed in a groove on the sample surface establishes the point of entry with certainty. Once the entry point is known, the velocity measurement proceeds in the conventional way — by measuring the time it takes for the beam to traverse a known path length.

As shown in the figure, an ultrasonic transducer coupled to a sonic pulser/receiver transfers energy to and from the test sample immersed in a water tank. A small steel sphere is placed in a groove that is machined into the sample. The center of the sphere is coplanar with the sample surface.

At the start of a measurement, the transducer is oriented to give a sound-wave angle of incidence, α, approximately equal to that required to produce a refracted wave that strikes the bottom left corner of the sample. The transducer is positioned near the sphere and set at approximately the calculated angle.

Next, the transducer is moved along the x direction until maximum reflection from the sphere is observed. When this condition is established, it is known that the beam path is along a line that passes through the center of the sphere.

With the beam angle and entry position thus fixed, the transducer is translated in the y direction to a point beyond the groove. At this point, the transducer orientation may have to be slightly adjusted to maximize the signal reflected from the bottom left corner. If so, the transducer is again moved over the sphere, and the x coordinate is readjusted to again maximize the reflected signal.

These steps are repeated until maximum reflection is obtained from both the sphere and the corner, indicative of a refracted wave of the desired angle of refraction, β. The time delay of the corner reflection is measured by reference to its position on an oscilloscope with a calibrated time base.

Without disturbing the angle adjustment, the transducer is then moved in the x direction to the position of maximum reflection from the upper left corner of the sample. The time delay of this one-skip reflection is also noted. The shear velocity is then calculated from the known skip distance, S, and the difference between the two time delays:

$$V_{shear} = \frac{\frac{1}{2}S}{t_2 - t_1}$$

where $\frac{1}{2}S$ = the half-skip distance as shown in the figure, t_1 = the first time delay, and t_2 = the second time delay.

This work was done by J. L. Nummelin of Rockwell International Corp. for **Marshall Space Flight Center.** *No further documentation is available.*

Inquiries concerning rights for the commercial use of this invention should be addressed to the Patent Counsel, Marshall Space Flight Center [see page A5]. *Refer to MFS-19680.*

Probe Array for Testing Printed-Circuit Substrates

Spurious conduction paths are found by an array of miniature test probes.

Goddard Space Flight Center, Greenbelt, Maryland

An array of tiny probes tests complex printed-circuit boards prior to the mounting of microcircuit chips and other active and passive components. A complete testing cycle — the insertion and alinement of a board, performance of the entire computer-controlled test, printing of the results (e.g., "pin 206 shorted to pins 048, 116, 195"), and removal of the board — requires about a minute. Performed manually, the same tests sometimes require as much as 30 hours.

The method has been demonstrated by checking for spurious conduction paths on 20 production specimens of a substrate containing 135 electrical nodes. The probe array for the tests consists of 142 miniature plungers mounted on centers as close as 1.0 mm in an area of 20 by 46 mm. Controlled by a program written specifically for this purpose, the system scans each of the probes for electrical connection with any of the others in just a few seconds.

The probes are mounted in a support plate (see figure). The pattern for the probes is determined from the pattern of the substrate to be tested.

The lead wires from the probes to the connector pins are immobilized, either by potting with a reworkable silicone elastomer or by strapping to a bar. The substrate to be tested is mounted on a platen and adjustable stage for precise positioning. Fine adjustments are made in the platen orientation to compensate for deficiencies in probe-imprint patterns on the substrate.

This work was done by A. G. Robison, C. C. Bianchi, C. B. Albert, and J. Ehland of General Electric Co. for **Goddard Space Flight Center.** *For further information, Circle 44 on the TSP Request Card.*

This invention is owned by NASA, and a patent application has been filed. Inquiries concerning nonexclusive or exclusive license for its commercial development should be addressed to the Patent Counsel, Goddard Space Flight Center [see page A5]. Refer to GSC-12759.

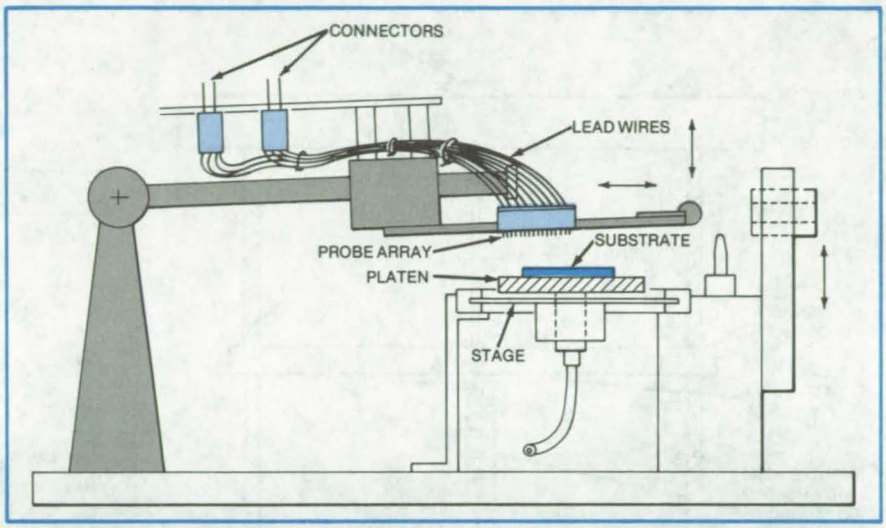

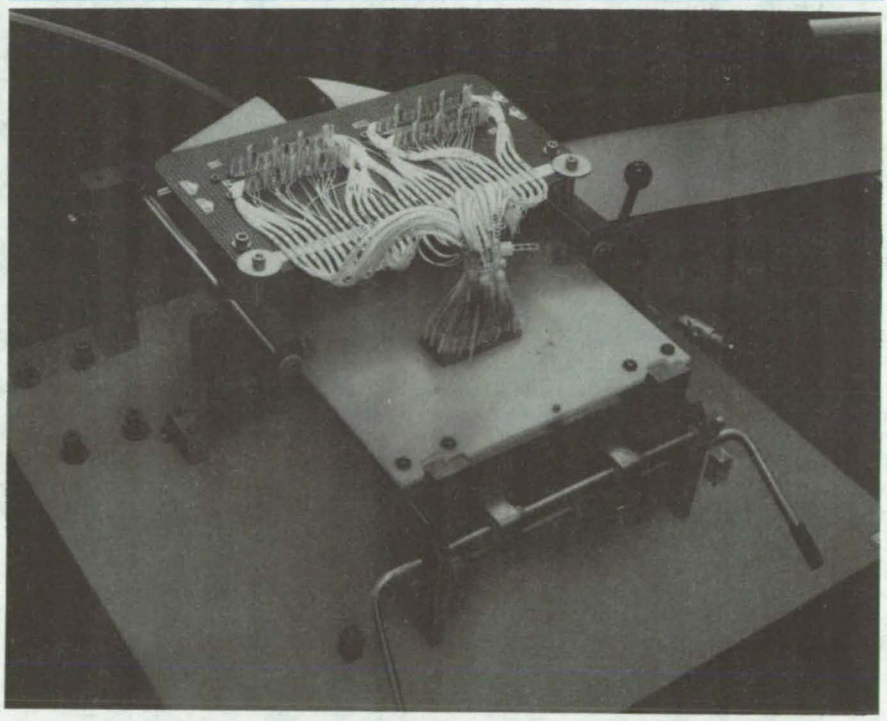

The **Probe Array,** the printed-circuit substrate to be tested, and the alinement mechanism are sketched (above). The photograph (below) shows the test apparatus as seen from above the probe.

Sample Holder for Cryogenic Adhesive Shear Test

Five samples would be tested in one cooldown.

Marshall Space Flight Center, Alabama

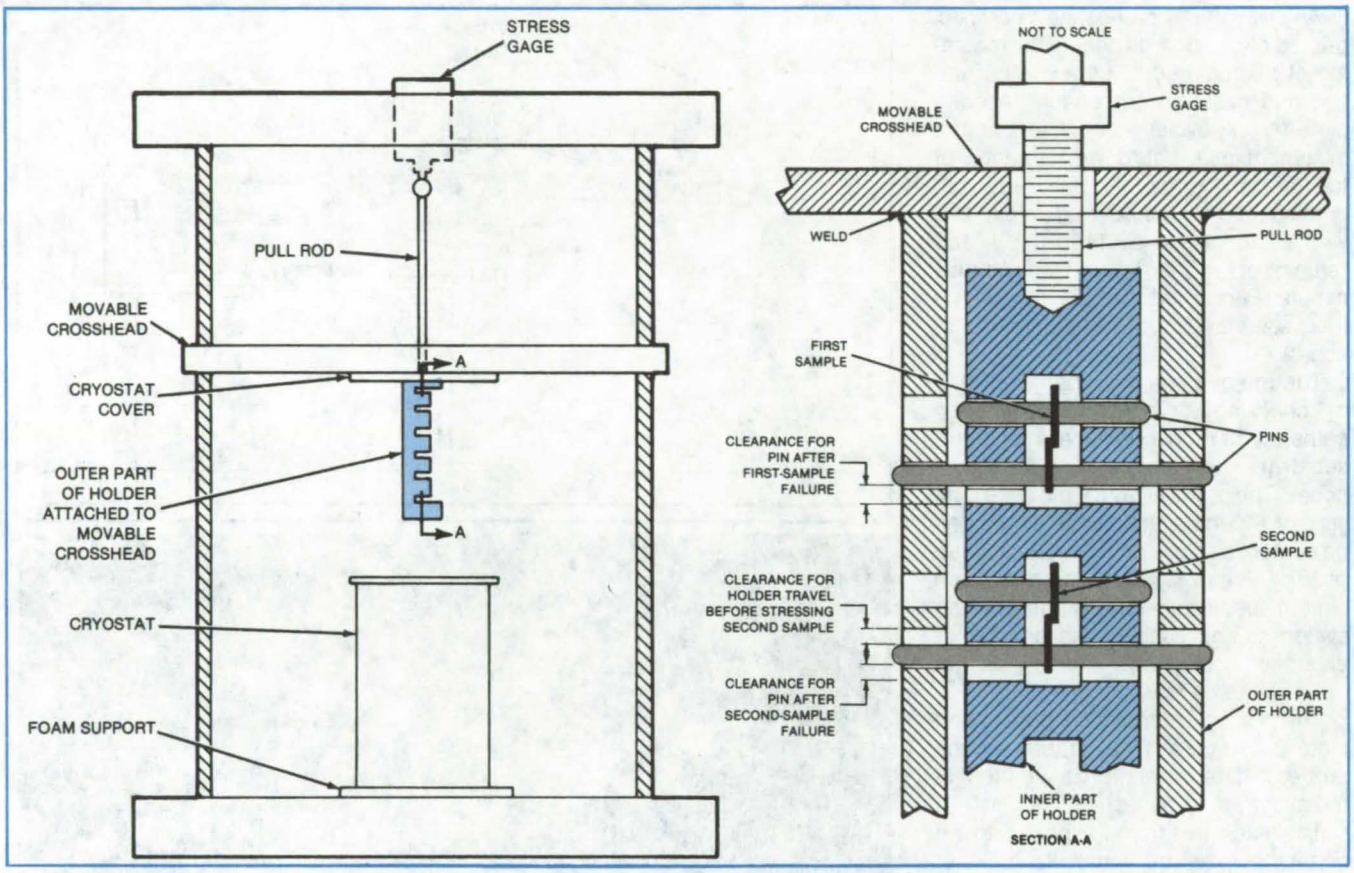

The **Five-Sample Holder** is shown mounted in a testing machine. During use it is submerged in the cryogenic liquid held in the cryostat. As the movable crosshead of the testing machine moves gradually downward, the samples are placed under tension, one after another, starting with the top one; each sample fails in turn before the next is stressed.

A five-sample holder has been proposed to speed up testing lap-shear strength of adhesives at cryogenic temperatures. This is an improvement over the single-sample technique described in ASTM Method D 2557-72, "Strength Properties of Adhesives in Shear by Tension Loading in the Temperature Range From -267.8 to -55° C (-450 to -67° F)."

The concentric mounting of the components of the new holder would also simplify the alinement of the test fixture. Moreover, the new holder permits use of a simpler cryostat vessel: The holder is immersed in the liquid in the cryostat from above, so a conventional dewar flask can be used to hold the cryogen. The holder used in the ASTM method requires a cryostat with a hole through the bottom for attaching the bottom part of the sample holder to the testing machine.

The samples (lap-shear specimens prepared as described in the ASTM method) are mounted in a line, one above the other in the proposed holder (see figure). The outer part of the holder applies tension to the pins through the lower ends of the samples. The holes in the outer part are arranged with graduated free travel so that as that part moves down, tension is applied first to the lower pin of the topmost sample and then to the next, with each sample stressed to failure before the next sample comes under tension. A recording of tension versus holder travel would show five ramps, one for each sample.

The two parts of the sample holder are cylindrical. The outer part is cut from stainless-steel tubular stock, the inner from solid rod stock. One side of the outer cylinder is machined away to provide access to the interior to insert the samples into the inner part of the holder. Clearance slots are also provided in the outer cylinder so that the pins through the upper holes in the samples may be inserted without having to disassemble the holder.

The overall length of the portion of the holder containing the samples is 1.12 meters (44 inches) each sample is 190.5 millimeters (7.5 inches) long, as described in the ASTM method.

This work was done by Frank E. Ledbetter, Johnny M. Clemons, William T. White, Benjamin Penn, and Marie L. Semmel of **Marshall Space Flight Center.** *For further information, Circle 45 on the TSP Request Card.*
MFS-25729

Gas-Temperature Measurement With Minimal Perturbation

Heat-flux transducers determine the temperature of hot, high-velocity, turbulent gases.

Lyndon B. Johnson Space Center, Houston, Texas

A proposed method for measuring the temperature of hot, turbulent gases uses three heat-flux calorimeters. One calorimeter measures only the radiative heat flux, while the other two measure the total heat flux (convective and radiative) but at two different temperatures.

The three calorimeters (see figure) are positioned such that they all have the same view of the flow and heating conditions. One total-heat calorimeter is mounted in a heat sink (thus externally cooled), and the other total-heat calorimeter is mounted so that it is thermally isolated to produce different gage surface temperatures and, thereby, different convention heat-transfer rates. The gages are all mounted flush with the wall to minimize flow disturbances.

Using the three instruments, the gas temperature is determined by the following algebraic relation:

$$T_G = \frac{(q_1 - q_R)T_{W2} - (q_2 - q_R)T_{W1}}{(q_1 - q_R) - (q_2 - q_R)}$$

where q_1 and q_2 are the heat fluxes from the two total-heat calorimeters, q_R is the radiative-heat flux, T_{W1} and T_{W2} are the wall temperatures measured by thermocouples on the total-calorimeter surfaces, and T_G is the temperature to be determined.

The capacities of the thermal isolator and the heat-sink conductor are a function of the materials used and the predicted heating rate and load expected. They are chosen to minimize the heat loss of gage 1 due to conduction to the wall and to minimize the increase in the wall temperature near gage 2.

A prototype using this concept is to be installed on the Space Shuttle to measure the temperature of the rocket-engine plumes in the base heat-shield region. The method could be adapted for commercial uses in such operations as monitoring the temperatures of flue gases, piped liquid or gaseous products, or internal-combustion or jet-engine exhausts.

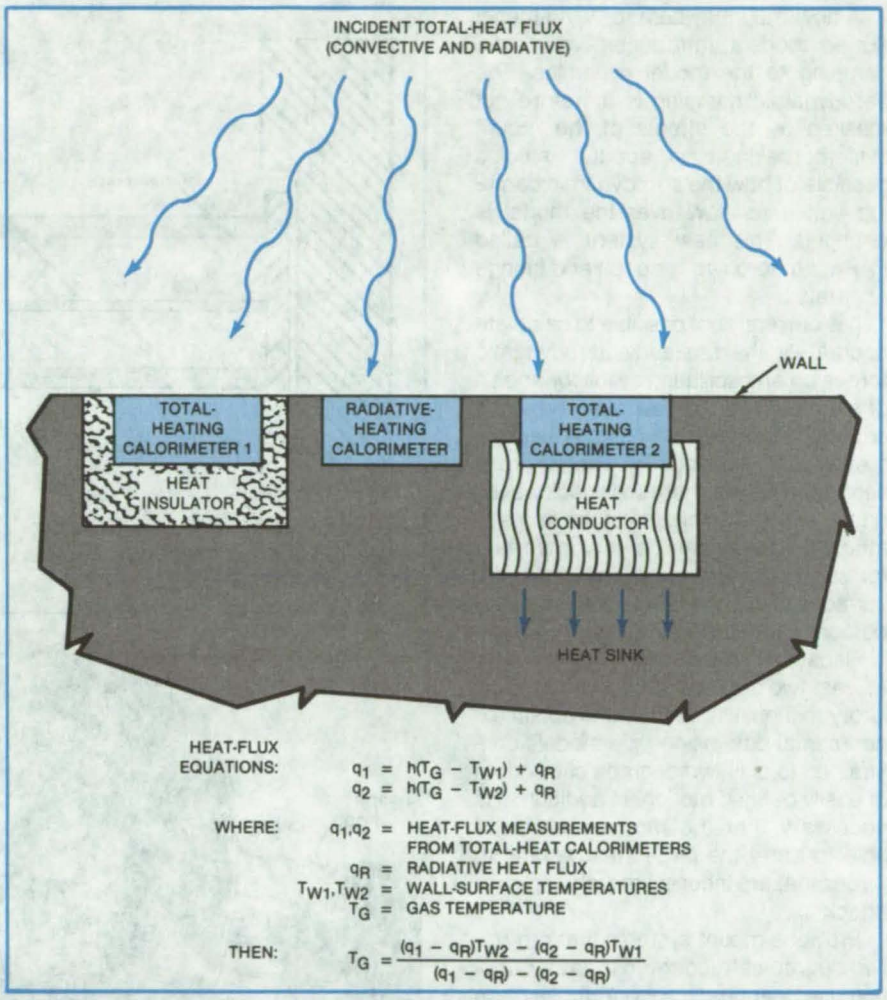

The **Proposed Temperature-Measurement Concept** uses a radiative-heat calorimeter and two total-heat calorimeters grouped so that the instruments experience the same view of the flow and heating conditions. The profile of the instruments permits flush mounting thus minimizing any disturbances to the flow by the instruments. The output of the radiative-heat calorimeter is subtracted from the outputs of each of the total-heat calorimeters to obtain convective heat flux.

This work was done by Tsun-sen Fu and Michael Quan of Rockwell International Corp. for **Johnson Space Center.** *No further documentation is available.*
MSC-20338

Two-Degree-of-Freedom Mount System for Flutter Models

Flexible rods replace conventional bearing supports to minimize structural damping.

Langley Research Center, Hampton, Virginia

A new mount system for wind-tunnel flutter models introduces very little damping to the model dynamics. The aerodynamic damping is therefore not masked by the effects of the mount system, making more accurate studies possible of how the aerodynamic damping varies as flow over the model is changed. This new system is called PAPA, an acronym for pitch and plunge apparatus.

It is currently not possible to calculate accurately the unsteady aerodynamic forces on an oscillating airfoil for angles of attack where the flow over the airfoil cannot be calculated with potential-flow theory. Such flow occurs when there is separated flow or there are shock waves on the airfoil. The effects of the angle of attack on flutter can be very important for supercritical and other airfoils, the surfaces of which are nearly flat for long portions of their cord.

Because conventional flutter involves at least two degrees of freedom of oscillatory motion, it is desirable to obtain experimental data using rigid models constrained to only two degrees of freedom of easily defined motion. In addition, it is necessary that the mount system be able to carry the large steady-state lift forces that are inherent at high angles of attack.

Previous mount systems that provide two-degree-of-freedom oscillatory motion use bearings to support those parts of the devices that move. However, these bearings introduce inherent damping, which may change as the loads on the model change. This damping in the mount system is often on the same order of magnitude as the aerodynamic damping.

For the new mount system, shown in the figure, the model is rigidly attached to a splitter plate. Both the model and the splitter plate are considered to be one rigid body. Another plate, which is the face of a turntable, is flush with the sidewall of the wind tunnel. The turntable can be rotated to change the model angle of attack.

The splitter plate is attached to the turntable by four circular rods, which have fixed/fixed end conditions. This means that when the splitter plate moves relative to the turntable, the deflection curves of the rods have zero slopes at both ends. The splitter plate is constrained so that it cannot roll or yaw. One of the purposes of the brace shown in-line with the model axis is to make the translational stiffness of the splitter plate greater in the drag direction. This brace also has fixed/fixed end conditions. It is partially surrounded by a windscreen that prevents flow over its surface. An additional function of the brace and its

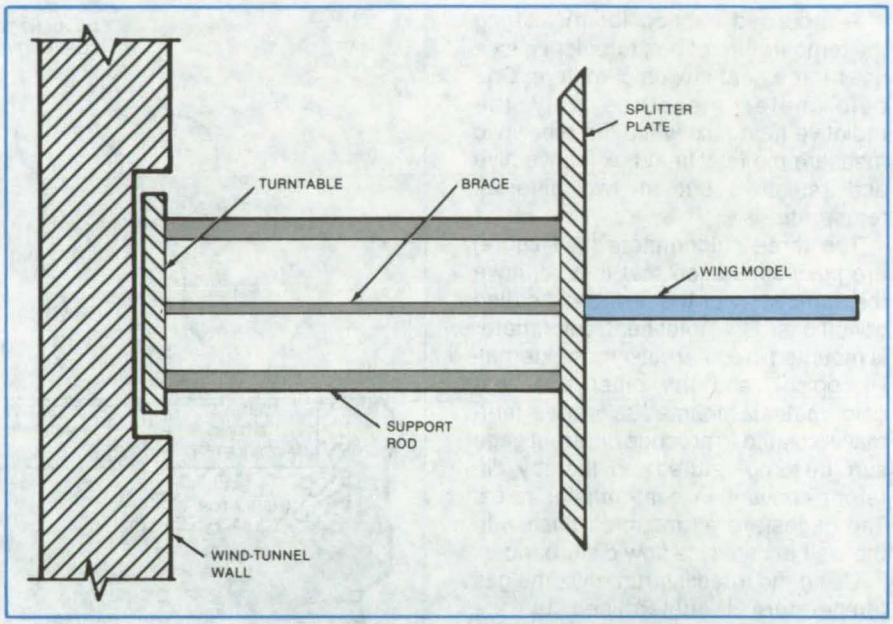

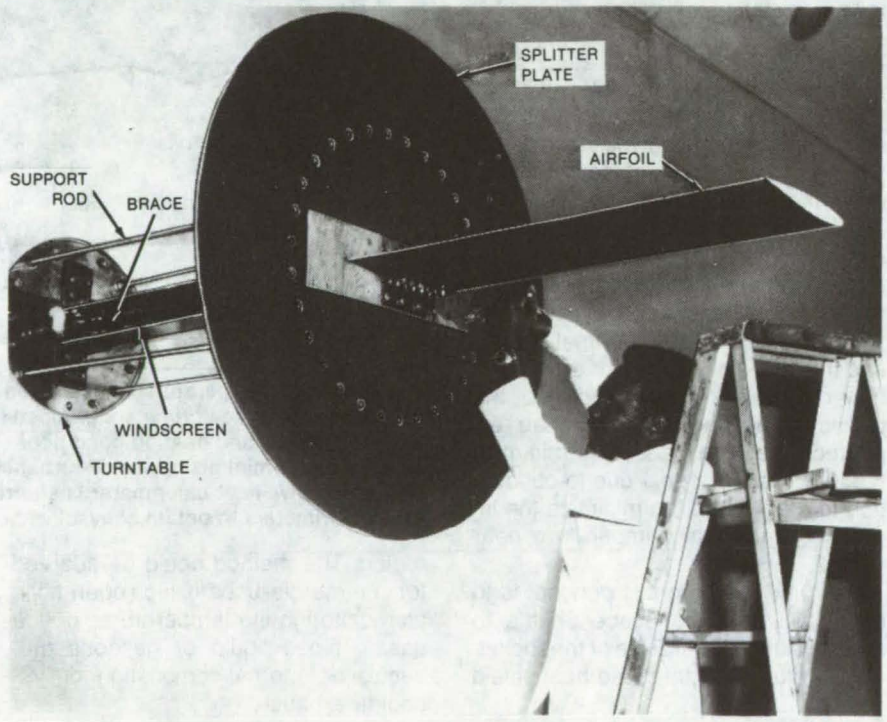

This **Flexure Mount System** replaces conventional bearing supports.

windscreen is that if vertical oscillation of the splitter plate becomes excessive, the brace hits its windscreen, thereby limiting the amplitude of oscillation.

An important concept in the use of the new mount system is the procedure by which lift forces on the model are managed. When there is no lift, the weight of the airfoil and splitter plate is carried by the brace and rods. As the turntable is rotated to give the model positive angles of attack, the resulting lift first relieves the weight. Only for values of lift greater than the weight are net up forces carried by the brace and rods.

With the new mount system, the steady-state and oscillatory pressures on a model can be measured using existing techniques. It is possible to use currently-available force-input techniques to drive the mount system so that unsteady pressures can be measured on the model as it oscillates.

There are no constraints on the shapes of models for which this mount system can be used. For example, data can be obtained for swept wings. The quantity, size, and spacing of the circular rods can be varied. It is also possible to obtain data using flexible models where both the structural vibration modes of the model and the mount system are involved in the flutter motion. Shielding of the moving parts of the mount system from the flow may be required in some applications to ensure that oscillations are caused only by aerodynamic forces on the model.

This work was done by Moses G. Farmer of **Langley Reserch Center.** *Further information may be found in NASA TM-83302 [N82-23549/NSP], "A Two-Degree-of-Freedom Flutter Mount System With Low Damping for Testing Rigid Wings at Different Angles of Attack" [$7]. A copy may be purchased [prepayment required] from the National Technical Information Service, Springfield, Virginia 22161.*

This invention is owned by NASA, and a patent application has been filed. Inquiries concerning nonexclusive or exclusive license for its commercial development should be addressed to the Patent Counsel, Langley Research Center [see page A5]. Refer to LAR-12950.

Measuring Small Leak Holes

Hole sizes are deduced from pressure measurements.

Lyndon B. Johnson Space Center, Houston, Texas

A novel extension of existing pressure-measuring techniques determines the sizes of small gas leaks. The technique is simple and could be useful in many situations in which small leaks are tolerable but large leaks are not.

The measuring apparatus consists of a pitot tube attached to a water-filled manometer (see figure). The compartment to be tested is pressurized with air. The pitot probe is placed at a known distance from the leak, facing along the centerline of the jet of leaking air. The dynamic pressure of the jet is measured at that point, and the static pressure is measured in the compartment. The leak size can then be calculated from the following approximate expression

$$D_O = 0.3X\sqrt{\frac{q_X}{P_O}}$$

where D_O = leak diameter, X = distance from leak initiation point, q_X = dynamic pressure at position X, and P_O = compartment pressure. (This equation may not apply under sonic flow conditions.)

When the leak origin is concealed from direct observation, its area can still be deduced with a more complex equation by using data from two different dynamic-pressure readings and the jet centerline distance between them. A correction must be applied to the equations for long gaps or distributed leaks (that is, "line" leaks rather than "point" leaks).

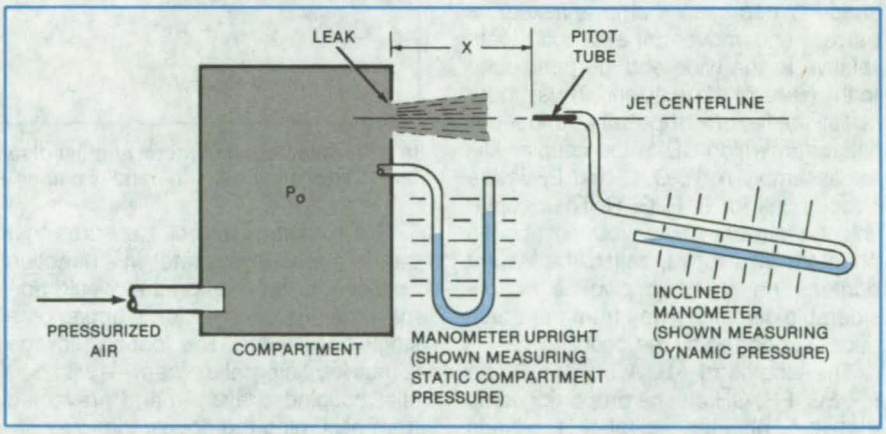

A **Pitot-Tube-and-Manometer Combination** measures the dynamic pressure at the centerline of a jet of leaking air. For extra sensitivity the manometer is filled with water (rather than mercury). For even more sensitivity, the manometer column can be tilted to stretch the distance along the column between marks corresponding to a given vertical-distance or pressure interval.

The new technique has several advantages: It permits each leak to be determined individually in multileak situations, whereas previous methods measured total leakage only. Measurements can be made without touching the surface and without being able to see the leak hole. The inaccuracy inherent in subjectively judging leak size by the feel of the flow is eliminated.

The method can be used to measure leakage from compartments of any size. Possible fields of use include aircraft, spacecraft, nuclear reactors, furnace testing, clean rooms, and ventilation systems.

This work was done by Donald E. Koch and James G. Stephenson of Rockwell International Corp. for **Johnson Space Center.** *For further information, including the theory of the technique and representative test data, Circle 46 on the TSP Request Card.*
MSC-20113

Flexible Coupling for Angle Transducer

Flexure strips ensure parallelism between input and output shafts.

NASA's Jet Propulsion Laboratory, Pasadena, California

A precise flexible coupling for an angular-displacement transducer compensates for misalinement and prevents the pivot reaction force from twisting its members into the undesired one of two stable configurations. The coupling is essentially a gimbal mounting that behaves as a four-bar linkage. It creates a remote phantom pivot point that remains stationary for small displacements of the coupling.

The transducer is mounted on two flexure strips (at points C and D in the figure). The opposite ends of the flexure strips are mounted to a ring (at points A and B). Two additional flexure strips are mounted to the ring at 90° separations from the first two (at points E and F), and their opposite ends are mounted to the frame (at points G and H).

The flexure strips have a trapezoidal shape. When such a strip is flexed, its narrow end moves in a circular path relative to the wide end, perpendicular to the plane of the wide end. Thus, under stress the flexure strips act as a four-bar linkage in which $\overline{CD}$ is the coupler link for assembly A, B, C, D and $\overline{EF}$ is the coupler link for E, F, G, H. The coupler link of a four-bar linkage rotates about a phantom pivot point, called the instant center. The phantom pivot is a considerable distance away from the transducer supported by the coupling.

The lengths of $\overline{AB}$, $\overline{AC}$, $\overline{BD}$, $\overline{DC}$ and $\overline{EF}$, $\overline{EG}$, $\overline{FH}$, $\overline{GH}$ can be proportioned so that the phantom pivot will remain momentarily stationary. Thus, for small displacements, the phantom pivot behaves as if it is fixed.

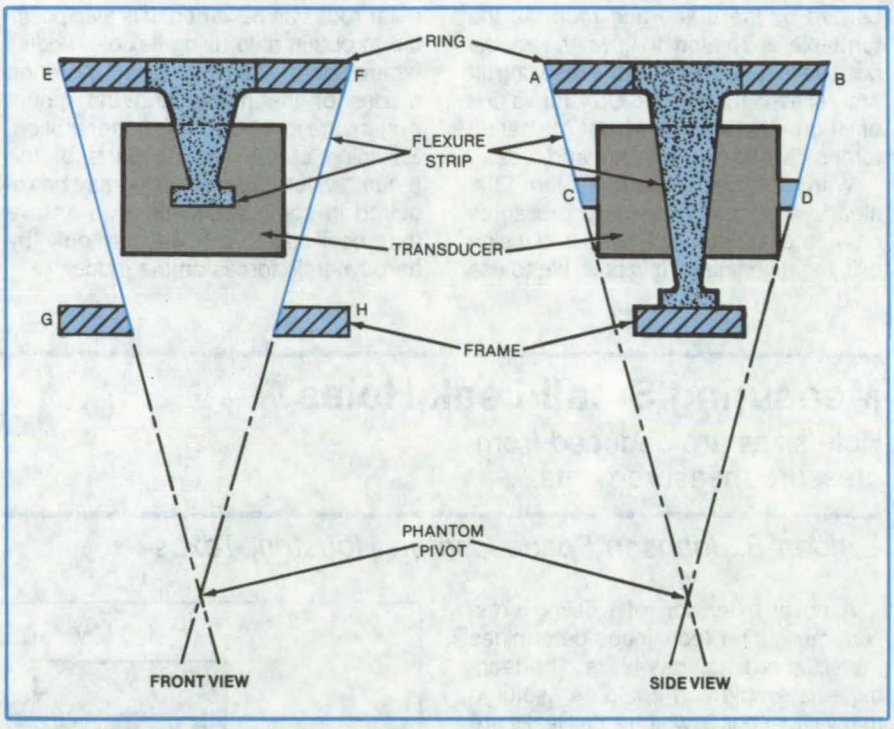

In a **Flexible Coupling** for an angular-displacement transducer, input link $\overline{GH}$ and output link $\overline{CD}$ remain always in parallel planes.

The remote pivot point ensures that the linkage always rotates in a direction opposite to the rotation that would normally be produced by force acting on a single-bar linkage. The four-bar linkage is thus kept a parallelogram — with parallel coupled shafts — and prevented from assuming the double-triangle configuration (the other stable configuration).

Sometimes it is preferable to position the pivot above rather than below the transducer. In such case, the size of $\overline{EF}$ relative to that of $\overline{GH}$ and of $\overline{AB}$ relative to that of $\overline{CD}$ should be interchanged.

This work was done by Robert A. Mayo of Caltech for **NASA's Jet Propulsion Laboratory.** *For further information, Circle 47 on the TSP Request Card.*
NPO-15412

Instrumented Pick Detects Coal/Rock Interface

Strain-gage signals indicate whether coal or rock is being cut.

Marshall Space Flight Center, Alabama

A cutting-force measuring system will provide more-efficient automatic guidance of coal shearers in longwall mining. A signal from a sensitized pick on the cutting drum of a coal shearer is analyzed in real time to permit automatic control of the cutting drum. The objective of the system is to move the cutting drum so that it closely follows the coal/rock interface.

Drum positioning is presently done by operators who follow the shearer and adjust the drum based on visual observation, cutting-noise characteristics, and the feel of the shearer vibrations. If

these decisions could be automated or performed remotely, the operators could be relocated away from the coal-dust concentration near the machine. If the accuracy of the decisions could be improved, a purer coal product (containing less rock) would result and shearer downtime and maintenance would be reduced.

The sensitized pick — one of the picks on the cutting drum of a coal shearer — is constructed in an assembly that includes a strain gage and load cell to measure the cutting force applied to the pick, (see figure). The signal from a 350-Ω strain-gage bridge in the load cell is fed to an FM strain transmitter operating in the 88 to 108-MHz FM broadcast band. A broadband amplifier with an output power of 8 dBm is used to increase output power and to isolate the strain transmitter from the effects of varying antenna loading. A quarter-wave shunt-fed antenna constructed from a curved 76-cm (30-in.) length of solid steel rod, 1 inch (2.5 centimeters) in diameter, is welded to the cutting drum at the grounded end and connected to the amplifier (through a matching transformer) through an insulator mounted on the trailing side of the base of the pick assembly. The FM force signal is received by a remote recorder.

Sample pick-force signals were obtained in tests at the Simulated Longwall Facility, Bruceton, PA, and in actual mining cuts at the York Canyon Mine, Raton, NM. By visual observation of recorded waveforms, the differing character of the signals is more obvious in the test-facility signals than in the mine signals. The principal signal differences are that in the test facility, the leading portion of the rock signal has a sharper rise time, a higher amplitude, and fewer large-scale fluctuations than the coal signal: This is to be expected, since the rock is harder and the coal tends to fracture in large chunks.

The coal/rock detection algorithm used in the tests employs a ratio technique: A low-pass-filtered value of the peak signal occurring during an interval at the leading edge of the signal is compared to the average amplitude of the entire signal. If the peak/average ratio exceeds a certain value, rock cutting is indicated. While this system works reasonably well, it can be confounded by temporary variations due to such things as prefracturing in the rock and variations in signal amplitude due to changes in the cutting rate. In order to attain the reliability necessary for automatic drum positioning under real mining conditions, a more sophisticated algorithm will have to be devised.

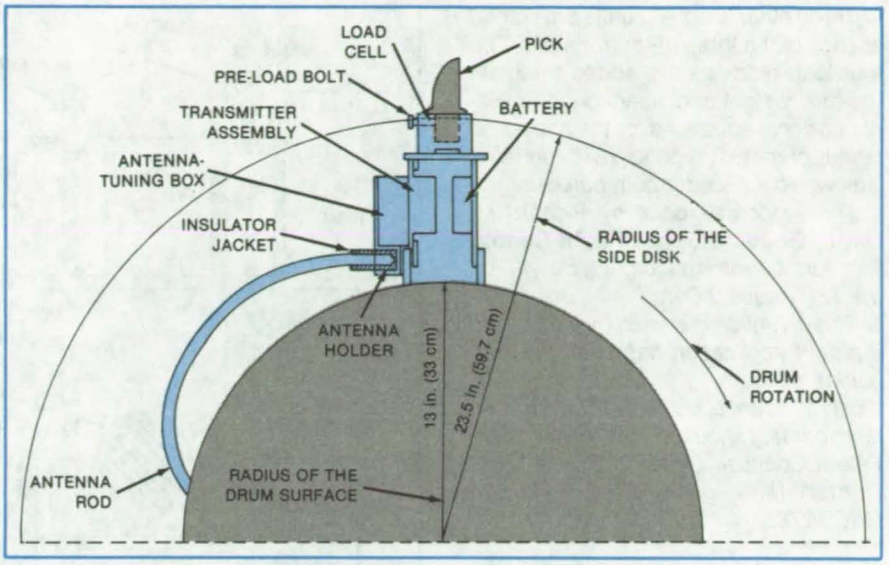

An **Instrumented Pick** installed on the cutting drum of a coal shearer for longwall mining measures cutting force with a strain-gage-bridge load cell. The force signal is transmitted to a remote recorder. To protect it from damage, the transmitter is located in the base of the pick assembly. The antenna is located in the "shadow" of the rotating pick. Changes in the characteristics of the force signals from the pick are used to determine whether the pick is cutting coal or rock.

This work was done by T. K. Wu and Joseph W. Erkes of General Electric Co. for **Marshall Space Flight Center.** *For further information, Circle 48 on the TSP Request Card.*
MFS-25753

Portable Pallet-Weighing Apparatus

Weighing is safer and more convenient.

Goddard Space Flight Center, Greenbelt, Maryland

Electrical load cells are used in a device that determines the total mass and horizontal-plane center of mass of a fully-integrated Spacelab pallet. The portable apparatus is intended for standard four-trunnion pallets but is readily adaptable to any large Space Shuttle payload or other loads where shifting of cargo is to be avoided.

The apparatus (see figure) is slipped into position on the integration or transportation fixture, with the cradle below the trunnion. For safety, the weighing-device frame is temporarily bolted to the transportation frame. The lifting bolts are then turned in their respective nuts until the cradle lifts the trunnion about 0.020 to 0.030 in. (0.51 to 0.76 mm) above its resting position in the cradle lock (not shown) of the transportation frame. This lifting applies the weight at the trunnion through the lifting bolts to the upper load plate. The upper load plate therefore pushes against the electrical load cell, which puts out a signal proportional to the applied load.

(continued on next page)

Three other weighing units are placed at each of the three other trunnions. The four load readings are added to obtain the total weight and inserted in the two-dimensional equations for the horizontal center of mass. (In principle, three readings would suffice for both purposes.)

This work was done by Richard M. Day of **Goddard Space Flight Center.** *For further information, Circle 49 on the TSP Request Card.*

This invention is owned by NASA, and a patent application has been filed. Inquiries concerning nonexclusive or exclusive license for its commercial development should be addressed to the Patent Counsel, Goddard Space Flight Center [see page A5]. Refer to GSC-12789.

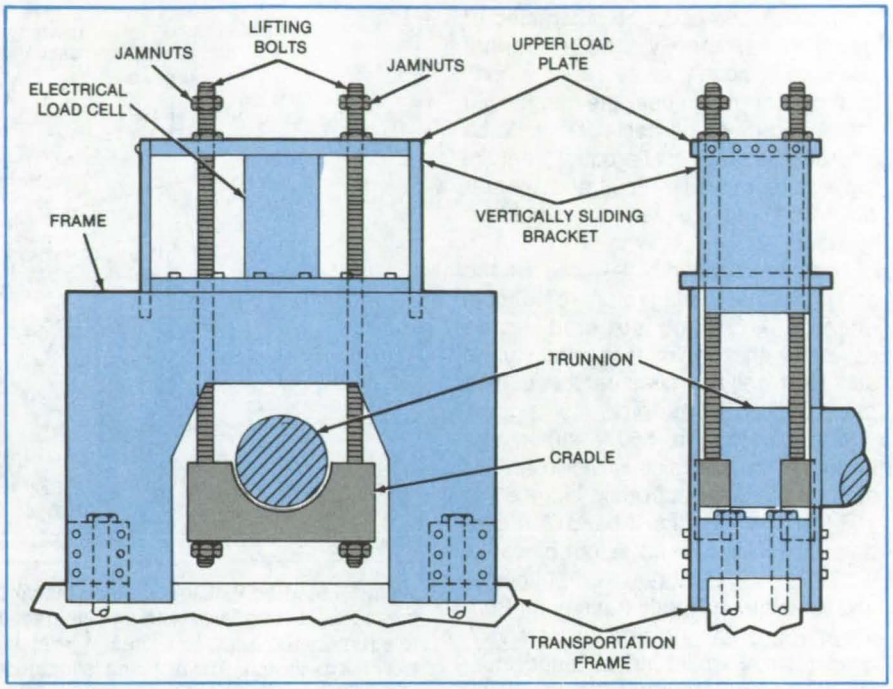

The **Portable Pallet-Weighing Device** lifts the trunnion of the pallet a short distance above its resting place. The weight at the trunnion is applied to the load cell. Similar units are placed at all four trunnions.

Proposed Short-Throat Supersonic Nozzles

Enlarged, fractional-radius-ratio transonic-nozzle throats promise negligible performance losses.

Marshall Space Flight Center, Alabama

Progress in the numerical analysis of supersonic flow fields has yielded promising results for nozzles having radius ratios less than 1.0. Evaluation of numerical solutions down to radius ratios of 0.5 indicates a negligible performance loss in the nozzle throat, provided that the throat area is enlarged to compensate for the decrease in discharge coefficient caused by the sonic-line warpage. The numerical procedure analyzes mach numbers along the wall and in the flow field (see figure), wall pressures, gas temperatures, and nozzle-throat discharge coefficients.

Advantages of the proposed nozzle contours are lower wall drag, lower wall heat input, and shorter nozzle length. The use of these nozzles has been suggested in turbines, jet engines, magnetohydrodynamic systems, laser systems, and in other supersonic-flow devices.

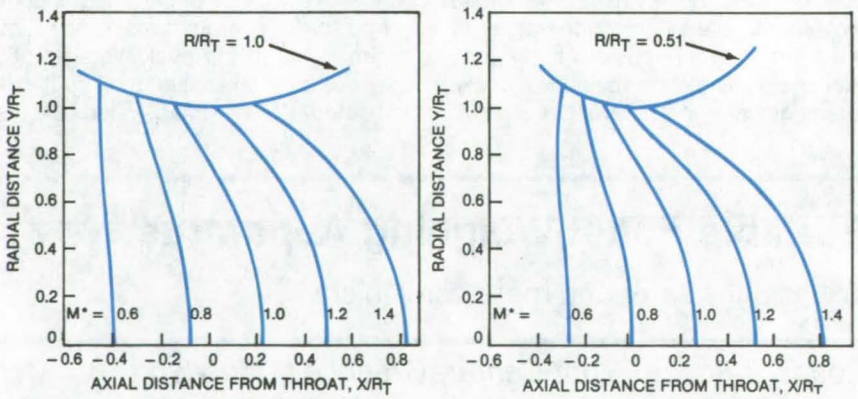

Flow-Field-Calculation Results are shown here for nozzles having two different R/R_T ratios (where R = radius of curvature of the nozzle wall in a plane that includes the axis, and R_T = the throat radius in a plane perpendicular to the axis). The colored lines represent constant-mach-number (M*) surfaces in the flow field.

This work was done by William R. Wagner and Gary H. Ratekin of Rockwell International Corp. for **Marshall Space Flight Center.** *No further documentation is available.*

MFS-19759

Simplified Modeling of Tetrahedral Trusses

Models reduce the time and cost of structural analyses.

Langley Research Center, Hampton, Virginia

Two models reduce the complexity of calculations of the static and dynamic behavior of tetrahedral-truss structures. The models are used for structures with repeating tetrahedral units (see Figure 1): Examples include large antennas to be deployed in space, long plate or box configurations, or radio towers.

In one model, a structure with many lattice units (bays) is replaced by an analogous structure with a smaller number of bays. The increase in the coarseness of the grid is somewhat arbitrary: It is limited only by the requirement to maintain enough degrees of freedom for subsequent vibration analysis, prediction of thermal distortion, or other calculations. For example, a 1,000-km-long plate structure with 10,000 bays of 100-m length might be anayzed as a 10-bay structure with 100-km-long elements.

In the transformation to the simpler analogous structure, one of the two basic scaling parameters is R, the ratio of the length of a surface element in the analogous model to that in the real structure. (In most cases, this is also the coarseness-increase factor.) The properties of the surface and diagonal struts in the model are related to those of the structure through simple scaling relations that impart the average stiffness properties and overall dimensions of the structure to the model.

The second transformation parameter, T, is the ratio of the length of a diagonal element in the model to the length of the corresponding element in the structure. (This ratio is not the same as R because the angle θ between the diagonal element and the surface plane is changed by the transformation to the model.) The ratios T and R are sufficient to prescribe the transformation of the entire system of loads, strains, structural parameters, and material elastic and thermal properties to and from the model (see Figure 2).

The second model approximates many repeating structural units as a continuum. The great advantage of continuum models is that analytic solutions can often be obtained, either in closed form or in relatively-tractable Taylor series.

(continued on next page)

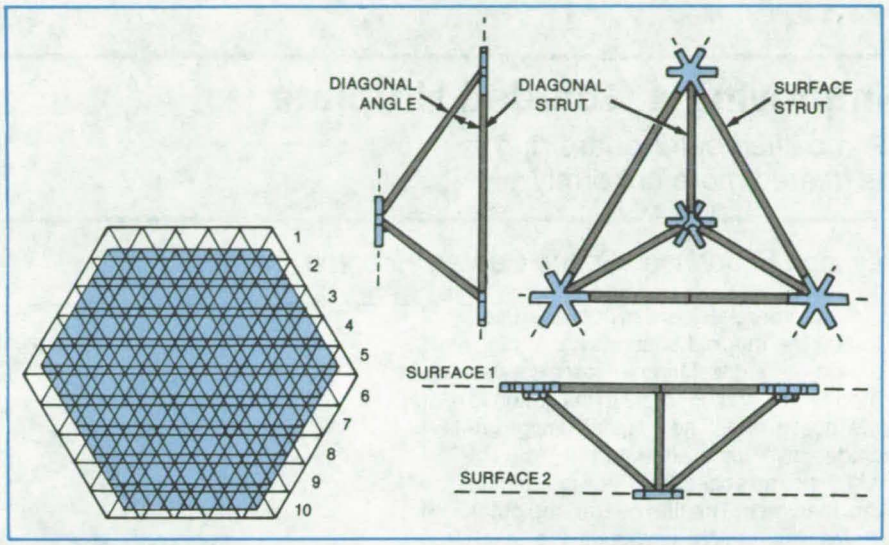

Figure 1. A **Hexagonal Antenna Support** or other tetrahedral-lattice structure exhibits great complexity in mathematical analysis, and the complexity quickly increases with the number of elements. Approximate solutions for the static and dynamic behavior of the structure can be obtained with a model consisting of an analogous structure with fewer repeating elements.

Element Parameter	Symbol	Surface Elements Ratio	Diagonal Elements Ratio
Length	ℓ, d	R	T
Area	A	R	T
Young's Modulus	E	1	T^2
Axial Stiffness	K	1	T^2
Axial Force	P	R	TR
Strain	ε	1	R/T^2
Stress	σ	1	R
Axial Shortening	Δ	R	R/T
Tube Thickness	t	1	$T\sqrt{R}$
Tube Radius	r	R	$\sqrt{R}$
Tube Diameter	D	R	$\sqrt{R}$
Euler Load	Pcr	R	TR
Slenderness	$\sqrt{2}\ell/r_c$	1	$T\sqrt{R}$
Density	ϱ	R_c/R^2	R_d/T^2
Element Weight	W	R_c	R_d
Shear Modulus	G	Not Used	Depends on Details of Strut Construction and Fastening
EI	EI	R^3	T^3R
Thermal Coefficient	α	1	R/T^2

Definitions:
K = 2AE/d
R_c = Ratio of Number of Real Cover Elements to Analogous Number
R_d = Ratio of Number of Real Diagonals to Analogous Number

Definitions:
$\ell'/\ell = R$
$\sin\theta/\sin\theta' = T$
Real Parameter × Transformation Ratio = Analogous Parameter
Depth of Structure (H) Is Constant
Diagonal Angle θ' = arctan [(1/R) tan θ]

Figure 2. **Transformation Ratios for a Tetrahedral Truss** specify the relationships between corresponding quantities that describe the real structure and the analogous model. All transformations are scaled by means of the ratios T and R.

The continuum models for tetrahedral trusses are flexible beams and plates. Their behavior is mathematically characterized by the continuum expressions for thermoelastic strain and kinetic energies, from which the equations of motion are derived. As with the coarser grid model, the transformation to the continuum involves the calculation of model properties that preserve the overall dimensions and the average material and stiffness properties of the structure. The resulting transformation equations relate the stiffness coefficients (extension, bending, transverse-shear, and torsional) of the continuum beam model to the structural geometry, structural dimensions, and structural-material stiffness properties.

This work was done by Alex Leondis of General Dynamics Corp. for **Langley Research Center.** *For further information, Circle 50 on the TSP Request Card.*
LAR-12815

Improving a Guarded Hotplate

A modified outer guard ring is heated more uniformly.

Lyndon B. Johnson Space Center, Houston, Texas

A commercial guarded hotplate, used to test the thermal conductivity of high-temperature insulating materials, was modified by adding layers of insulation to the guard ring. The original design includes five separate heaters, four of which are arranged in a stack containing the specimen. The fifth heater, the outer guard ring, which surrounds the stack assembly and maintains an environmental test temperature, has no built-in thermal barrier. To prevent excessive heat loss in the outward direction, the operator must increase the power supply to hold the desired temperature.

The modified outer guard ring, shown in the figure, includes six compressible sheets of thin fibrous-ceramic paper that form a thermal barrier to outward heat flow. The ceramic paper presses the heating coils against the ring, thus allowing the ring to be more uniformly heated. Tests on rigid silica insulating material showed temperature variations around the outer guard ring to be less than 15° F (8° C), while 80° F (44° C) variations were typical with the previous design.

This work was done by Donald Chafey and Gilbert C. Hennessee of Lockheed Missiles & Space Co., Inc., for **Johnson Space Center.** *No further documentation is available.*
MSC-20447

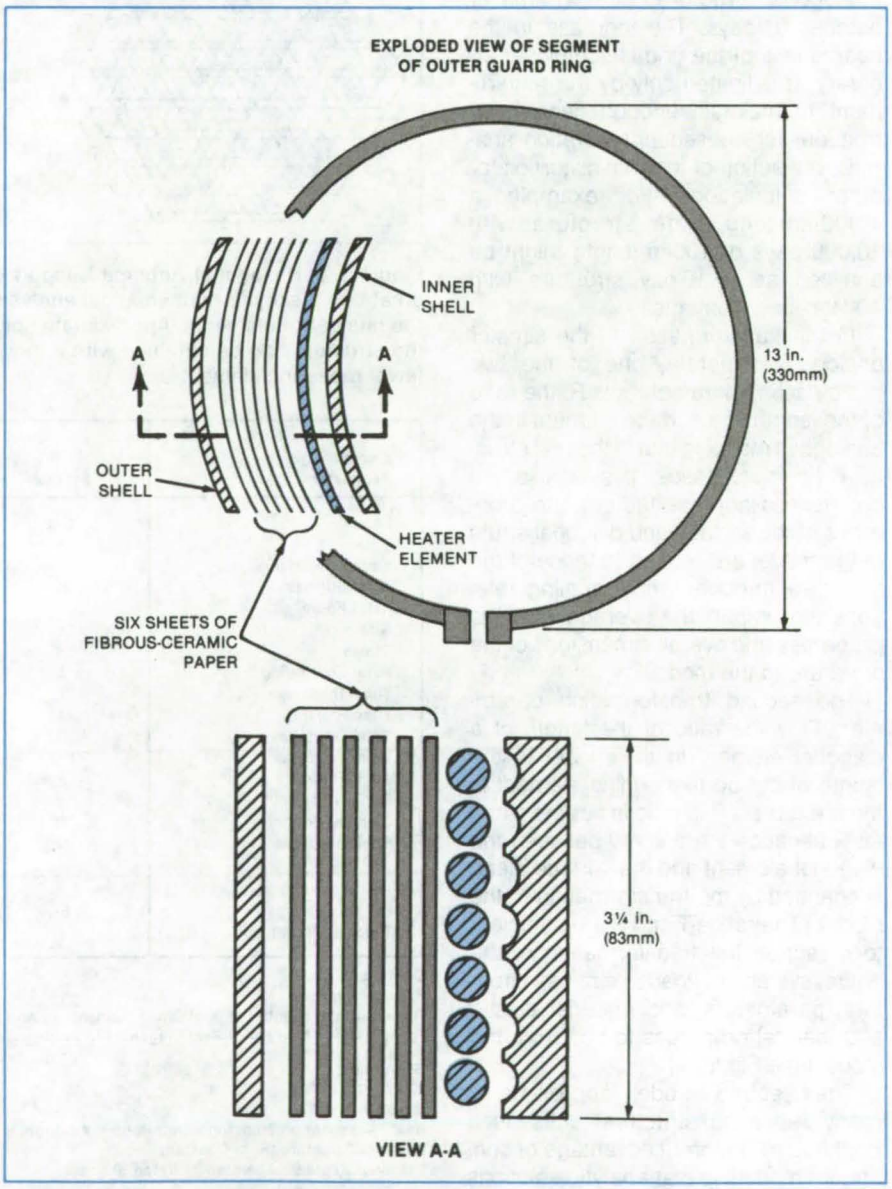

A **Modified Guarded Hotplate** includes additional insulation consisting of six sheets of thin fibrous-ceramic paper. The ceramic paper forms a barrier to outward heat flow. With this modification, the heater consumes about 30 percent less power than it did before.

Task Board Tests Manipulator Performance

Robotics systems can be quantitatively evaluated.

NASA's Jet Propulsion Laboratory, Pasadena, California

A "task board" has been constructed to facilitate time-and-motion studies for remote manipulators (see figure). The apparatus is equipped with holes, objects of various shapes to be grasped, and sensors with switches to indicate contact.

Some sensors detect the raising of a manipulator-held tool, others detect the touching of a contact point by the tool, and still others measure conformity to tolerance and movement distances. A spring-loaded plunger in a receptacle on the board measures tool penetration. Openings and closings of the switches trigger external circuitry that measures and records the time required for a remote manipulator to perform basic tasks. The task board is expected to be useful in the evaluation of industrial robots programed to assemble parts.

The board enables the measurement of the time a robot takes to perform each of the following elementary manipulations:

- *Move* — transporting the end effector a given distance;
- *Turn* — rotating the end effector about the long axis of the robot forearm through a given angle;
- *Apply Pressure* — applying force to overcome object resistance (accomplished with little or no motion);
- *Grasp* — closing the end effector to gain control of an object;
- *Release* — opening the end effector to relinquish control of an object;
- *Pre-position* — operating the basic hand element to aline and orient one object with another within a given tolerance;
- *Insert* — operating the basic hand element to engage objects along a trajectory within a given tolerance;
- *Disengage* — operating the basic hand element to separate objects along a trajectory within a given tolerance;
- *Crank* — moving the hand element through a constrained circular path to rotate an object, with the forearm pivoting at the elbow and the upper arm essentially fixed; and
- *Contact* — moving the hand to hold down an object.

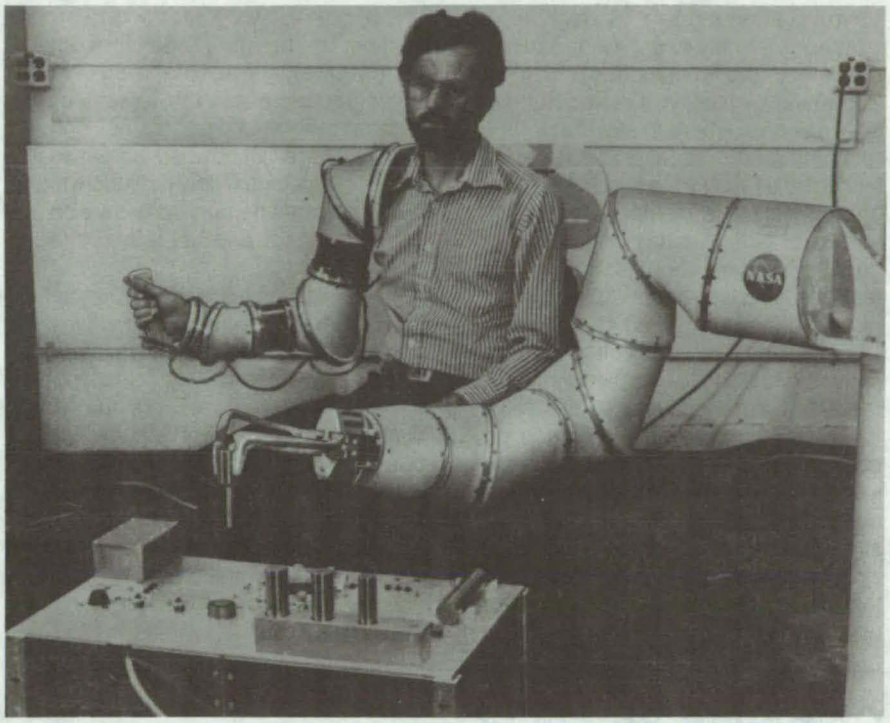

An **Operator Uses the Task Board** to perform a time-and-motion study of a manipulator system that employs force feedback. Outputs of sensors on the board are recorded for analysis.

This work was done by John W. Hill of SRI International for **NASA's Jet Propulsion Laboratory.** *For further information, Circle 51 on the TSP Request Card.*

NPO-15150

Curved Caps Raise Corrugated Strength

Flat caps are replaced by curved caps for a wider cap/web attachment in a new concept for constructing corrugated panels. The wider joint restrains the cap, enabling it to carry its design load without edge rotation or premature buckling.

(See page 341.)

High-Absorptance Radiative Heat Sink

The absorptance of black-painted open-cell aluminum honeycomb is improved relatively inexpensively by cutting the honeycomb at an angle or bias rather than straight across. This ensures that at least two specular reflections occur before the incident radiation escapes.

(see page 345.)

Self-Alining Quick-Connect Joint

A quick-connect tapered joint requires a minimum of manipulation and force. The joint is simple, compact, strong, lightweight, self-alining, and has no loose parts. It consists of matching male and female thin-walled metallic or molded plastic cones and split metallic locking rings.

(See page 331.)

Vortex Lift Augmentation by Suction

Lift performance is improved on a 60° swept Gothic wing.

Langley Research Center, Hampton, Virginia

Vortex lift at moderate to high angles of attack on highly swept wings has been used to improve takeoff performance and maneuverability of advanced high-speed aircraft where the favorable lift effects induced by a leading-edge vortex system are required to achieve performance goals. One of the concerns with vortex lift is that vortex breakdown occurs suddenly at about 30° angle of attack, causing an abrupt loss in lift coupled with increased drag and pitchup.

To increase the vortex lift at all angles of attack, to delay to a higher angle of attack, and to reduce the abruptness of the vortex burst, a new design is proposed in which the suction of the propulsion system augments the vortex. In this concept, a turbofan placed at the downstream end of a leading-edge vortex system induces the vortex to flow into the inlet, which delays the onset of vortex breakdown. The downstream ingestion of the core and surrounding vortex flow by the turbofan also concentrates and increases the velocity of the upstream vortex flow. This not only increases vortex lift but also increases the velocity of potential flow over the wing to provide a more negative pressure on the upper surface and thereby increase potential-flow lift.

In order to evaluate this lift augmentation, an experimental investigation was conducted in the Langley Research Center high-speed 7- by 10-foot (2- by 3-meter) wind tunnel on the aerodynamic performance of suction applied near the wing tips above the trailing edge of a 60° swept Gothic wing. Moveable suction inlets were symmetrically mounted in the proximity of the trailing edge, and the amount of suction was varied to maximize wing lift. Tests were conducted at mach 0.15, 0.30, and 0.45, and the angle of attack was varied from −4° to +50°.

The suction augmentation increases the lift coefficient over the entire range of angle of attack. The lift improvement exceeds the unaugmented wing lift by over 20 percent. Moreover, the augmented lift exceeds the lift predicted by vortex lattice theory to 30° angle of attack. Suction augmentation is postulated to strengthen the vortex system by increasing its velocity and making it more concentrated. This causes the vortex breakdown to be delayed to a higher angle of attack.

This work was done by Allan H. Taylor, L. Robert Jackson, and Jarrett K. Huffman of **Langley Research Center.** *For further information, Circle 52 on the TSP Request Card.*
LAR-12969

Computer Programs

These programs may be obtained at very reasonable cost from COSMIC, a facility sponsored by NASA to make new programs available to the public. For information on program price, size, and availability, circle the reference letter on the COSMIC Request Card in this issue.

Time-Domain Modal Vibration Identification

Natural frequencies, damping factors, and damped mode shapes are identified.

The Ibrahim Time-Domain modal vibration identification program (ITD) uses multple free-decay responses of a test structure directly in the time domain to identify the modal parameters of the structure: the natural frequencies, the damping factors, and the damped mode shapes. When only random response data are available, the program first estimates the required free-decay response functions using the multiple-channel random-decrement technique.

An oversized analysis model and least-squares solution approach are used to reduce the effects of noise on the identification accuracy. A unique concept, the "Modal Confidence Factor," effectively differentiates the valid structural modes from extraneous "noise modes" that are also calculated when an oversized model is used.

ITD is written in FORTRAN IV for batch execution and has been implemented on a CDC 6000-series computer with a central-memory requirement of approximately 63K words. The ITD program was developed in 1979.

This program was written by Samir R. Ibrahim of Old Dominion University Research Foundation for **Langley Research Center.** *For further information, Circle A on the COSMIC Request Card.*
LAR-12924

Thermal Radiation Model Renodalization

Simplified radiation models reduce programing cost.

The Thermal Radiation Model Renodalization program redefines a thermal model nodal geometry subsequent to generation of radiation interchange data. Previously, the geometry of a radiation model had to be identical to, or possibly more complex than, the thermal analyzer model.

This renodalization program allows a radiation model to be much different from, even less detailed, than the thermal analyzer model. Thus, radiation models may be greatly simplified in many applications to reduce computer cost. This also adds flexibility to the usual thermal analysis procedure since model nodalization may be changed at any time, even late in the analysis cycle. The Thermal Radiation Model Renodalization program is readily used with the TRASYS thermal radiation program and SINDA thermal analyzer program.

This program is written in FORTRAN V for batch execution and has been implemented on a UNIVAC 1100 series computer with a central memory requirement of approximately 50K of 36-bit words. This program was developed in 1981.

This program was written by David. J. Russell of Rockwell International Corp. for **Johnson Space Center.** *For further information, Circle B on the COSMIC Request Card.*
MSC-20348

Monte Carlo Investigation of Trajectories

Orbital sequences are modeled, simulation statistics generated, and user-requested variables scanned.

The Monte Carlo Investigation of Trajectory Operations and Requirements (MONITOR) program performs spacecraft mission maneuver simulations for geosynchronous, single-maneuver, and comet-encounter trajectories. The MONITOR program is multifaceted. It models various orbital sequences and missions, generates Monte Carlo simulation statistics, and parametrically scans user-requested variables over specified intervals. The program has been used primarily to study geosynchronous missions and can model the trajectories of satellites deployed by the Space Shuttle. The performance of a Monte Carlo error analysis of user-specified orbital parameters using predicted maneuver-execution errors can make MONITOR a significant part of any mission planning and analysis system.

The MONITOR program can be executed in four operational modes. In the first mode, analytic state covariance matrix propagation is performed using state transition matrices for the coasting and powered burn phases of the trajectory. A two-body central-force field is assumed throughout the analysis. Histograms of the final orbital elements and other state-dependent variables may be evaluated by a Monte Carlo analysis. In the second mode, geosynchronous missions, from parking orbit injection through station acquisition, can be simulated. A two-body central-force field is assumed throughout the simulation. Nominal mission studies can be conducted; however, the main use of this mode lies in evaluating the behavior of pertinent orbital trajectory parameters by making use of a Monte Carlo analysis.

In the third mode, the MONITOR program performs parametric scans of user-requested variables for a nominal mission. Various orbital sequences may be specified; however, primary use is devoted to geosynchronous missions. A maximum of five variables may be scanned at a time. The fourth mode simulates a mission from orbit injection through comet encounter with optional Monte Carlo analysis. Midcourse maneuvers may be made to correct for burn errors and comet movements.

The MONITOR program is written in FORTRAN IV for batch execution and has been implemented on an IBM 360-series computer with a central memory requirement of approximately 255K of 8-bit bytes. The MONITOR program is an evolutionary development of the Two-Body Error Analysis (TBERR) Program. Final modifications to MONITOR were completed in 1980.

This program was submitted by Alan B. Glass of Computer Sciences Corp. for **Goddard Space Flight Center.** *For further information, Circle C on the COSMIC request Card.*
GSC-12705

Flow Over Nonaxisymmetric Nozzles

Code solves three-dimensional Navier-Stokes equations.

A set of computer codes solves the three-dimensional Navier-Stokes equations for the flow over nonaxisymmetric nozzles. These codes compute the internal and external viscous flowfield about an isolated nozzle, so that the flow characteristics and performance of three-dimensional jet engine exhaust nozzles can be predicted. The approach is based on using an efficient implicit numerical method to solve the unsteady Navier-Stokes equations in a boundary-conforming curvilinear coordinate system to obtain the desired time-asymptotic steady-state solution. Flow turbulence effects are simulated by algebraic turbulence models for the effective turbulent eddy viscosity and Prandtl number.

This set of codes consists of three programs:

- The RGRIDD program constructs a boundary-conforming curvilinear coordinate system and computational grid for complicated three-dimensional nozzle configurations.
- The NOZLIC program generates the initial conditions for the NOZL3D code and can construct simple coordinate systems and grids for two-dimensional or axisymmetric converging-diverging nozzles.
- The NOZL3D program performs an implicit numerical solution to the spatially parabolized form of the three-dimensional unsteady Navier-Stokes equations in general curvilinear coordinates.

The NOZL3D program obtains a solution in the following manner. The three-dimensional flow region is represented by a computational space that consists of a rectangular parallelepiped. This computational space is covered with a rectangular grid of nodal points that are equally spaced in each of the three coordinate directions in the space. Finite-difference analogs of the unsteady Navier-Stokes equations are solved on this grid by an implicit numerical method that advances the solution over a sequence of time steps using a "sweeping" procedure to obtain the final steady-state solution.

These programs are written in FORTRAN IV and ASSEMBLER. There are both batch and interactive versions of the RGRIDD program, each having a central memory requirement of approximately 60K (octal) of 60-bit words. The NOZLIC and NOZL3D are intended for batch execution. Both "disk" and "core" versions of NOZLIC and NOZL3D are supplied. The disk versions have been implemented on a CDC CYBER 170 series computer with central memory requirements of approximately 140K (octal) and 175 (octal) of 60-bit words respectively. The core versions are for implementation on CDC 7600 or CDC 203 computers and have problem-dependent central memory requirements. These programs were developed in 1980.

This program was written by P. D. Thomas of Lockheed Missiles and Space Co., Inc., for **Langley Research Center.** *For further information, Circle D on the COSMIC Request Card.*
LAR-12962

Shock-Free Airfoil Cascades

Fast design and analysis uses fictitious gas concept.

The CAS22 computer program was developed to provide for the fast design and analysis of shock-free airfoil cascades. CAS22 is applicable to the aerodynamic analysis and transonic shock-free redesign of existing two-dimensional cascades of airfoils. CAS22 can be used in three separate modes of operation:

1. As an analysis code for full-potential, transonic, shocked or shock-free cascade flows;
2. As a design code for shock-free cascades that uses Sobieczky's fictitious gas concept; and
3. As a shock-free design code followed automatically by an analysis to confirm that the newly obtained cascade shape provides for an entirely shock-free transonic flow field.

In all modes CAS22 generates its own four-level, boundary-conforming O-type computational grid.

The mathematical model of the flow is a full-potential equation. Its artificially time-dependent form is solved in a fully conservative form by using a finite area technique, rotated type-dependent upstream differencing, and successive line over relaxation. Isentropic shocks are captured by using a first-order artificial viscosity in fully conservative form.

The shock-free design is performed by implementing Sobieczky's fictitious gas concept of elliptic continuation from subsonic into supersonic flow domains. Recomputation inside each supersonic zone is performed by the method of characteristics in the rheograph plane by using isentropic gas relations. The new shock-free contour is determined from the condition that the stream function is equal to zero on the airfoil surface. Besides being capable of converting existing cascade shapes with multiple shocked supersonic regions into shock-free cascades, CAS22 can also unchoke previously choked cascades and make them shock-free.

The CAS22 program is written in FORTRAN IV for batch execution and has been implemented on an IBM 370 series computer with a central memory requirement of approximately 315K of 8-bit bytes. The CAS22 program was developed in 1982.

This program was written by Djordje S. Dulikravich of Universities Space Research Association for **Lewis Research Center.** *For further information, Circle E on the COSMIC Request Card.*
LEW-13842

Predicting Aircraft Noise Levels

Program predicts noise levels from data on fan, combustor, turbine, and airframe sources.

A computer program has been developed for predicting aircraft noise levels either in flight or in ground tests. The noise sources include fan inlet and exhaust jet flap (for powered lift), core (combustor), turbine, and airframe.

The Lewis Research Center had previously developed prediction methods for various noise sources. During the development of these predicting methods, it became obvious that computer-programed versions were required for adequate checkout. By adding to these computer programs the capacity to solve the geometrical relationships between an aircraft in flight and an observer on the ground, these programed predictions were made useful in evaluating noise estimates and footprints for various proposed engine installations being studied.

There are two main program versions for using these prediction routines: The first (FOOTPR) is a procedure to calculate at various observer stations the time history of the noise (as spectra, OASPL, PNL, and PNLT) for an aircraft flying a specified set of speeds, orientations, and space coordinates. For each individual source, the levels are free field with no correction for propagation losses other than spherical divergence. The total spectra can be corrected for the usual effects of atmospheric attenuation, extra ground attenuation, ground reflection, and aircraft shielding; and the corresponding values for overall sound pressure level (OASPL), perceived noise level (PNL), and tone-weighted perceived noise level (PNLT) are then calculated. From the time history at each point, true effective perceived noise levels (EPNL) are calculated. Values of EPNL, maximum PNL, or maximum PNLT are thus found as desired for a grid of specified points on the ground. The user has the option of centering the time history on the closest point of approach of the aircraft to each observer or of starting the history at the first aircraft position given.

The noise program RADIUS was devised to predict engine noise source levels at a fixed radius and at various angles, such as would simulate the ground acoustic testing of an engine. This program interpolates in the specific engine variables needed for each noise source and corrects these for actual-day, ambient conditions. It replaces programs FOOTPR and NOIS in calling the noise source subroutines.

The computer program is simple enough so that the user can make any modifications that might better suit the application. RADIUS constructs a table of SPL values at each angle and frequency; calculates the acoustic power, OASPL, PNL, and PNLT; and prints a page of output for each source and for the total noise from all the sources.

All data read in for program variables are in namelisted form, except for the first line, so that order within each set is arbitrary and omissions can be made. Each main and subroutine program for noise sources (and for shielding and ground reflection) has one or more namelist blocks under which input variable values for that program can be read.

The program is written in FORTRAN IV for an IBM 360 machine, but it can be run on any FORTRAN language computer with at least 120,000 bytes (30,000 words on IBM 360) of program storage available.

This program was written by Bruce J. Clark of **Lewis Research Center.** *For further information, Circle F on the COSMIC Request Card.*
LEW-13778

Minimum Induced Drag of Nonplanar Wings

Numerical optimization techniques calculate the required bound-circulation distribution.

Increased interest in fuel-efficient unconventional aircraft concepts for future transport aircraft has created the need for accurate estimation of the induced

drag of nonplanar configurations. Examples of these novel configurations include wings fitted with end plates or winglets, the tandem wing, and the joined wing. The DRG program incorporates numerical optimization techniques for calculating the bound-circulation distribution required for minimum induced drag of nonplanar wings.

DRG employs a two-dimensional advanced panel far-field potential flow model of the undistorted interacting wakes of multiple lifting surfaces. Wake-vortex sheet strengths are assumed to vary in a piecewise linear fashion. Analytical expressions for induced normal velocity, bound circulation, induced drag, and lift are in terms of the assumed wake model. These expressions are used to obtain minimum-drag wake-vortex sheet strengths, bound-circulation distributions, and induced drag coefficient values for minimum drag at a given lift — for nonplanar multiple interacting lifting surfaces — using both Munk's criterion and a direct optimization technique. Accuracy of the method is approximately five times better, for a fixed number of wake panels, than for a discrete vortex filament wake model.

DRG is written in FORTRAN IV for batch execution and has been implemented on a CDC 6000 series computer with a central memory requirement of approximately 120K (octal) of 60-bit words. The DRG program was documented in 1981.

This program was written by Tzuchun Jeffrey Ku and John M. Kuhlman of Old Dominion University Research Foundation for **Langley Research Center.** *For further information, Circle G on the COSMIC Request Card.*
LAR-12925

Wing Subsonic Aerodynamic Performance Estimates

Solution by iteration estimates performance of twisted and cambered wings of arbitrary planform.

The SUBAER computer program estimates the subsonic aerodynamic performance of twisted and cambered wings of arbitrary planform with attainable thrust and vortex lift considerations taken into account. SUBAER is based on a linearized-theory lifting-surface solution that provides a spanwise distribution of theoretical leading-edge thrust, in addition to the surface distribution of perturbation velocities.

The program approach relies on a solution by iteration rather than on the common practice of obtaining linearized theory results by simultaneous solution of a large set of equations. SUBAER also features a superposition of independent solutions for a cambered and twisted wing and a flat wing of the same planform. This feature readily provides results for a large number of angles of attack or lift coefficients. The program employs a semiempirical method to assess the portion of the theoretical thrust actually obtained and the portion that is felt as a vortex normal force.

This program is written in FORTRAN IV for batch execution and has been implemented on a CDC CYBER 170 series computer with a central memory requirement of approximately 66K (octal) of 60-bit words. SUBAER was developed in 1982.

This program was written by Harry W. Carlson and Kenneth B. Walkley of Kentron International for **Langley Research Center.** *For further information, Circle H on the COSMIC Request Card.*
LAR-12987

Boundary-Layer Equations for Two-Dimensional and Axisymmetric Flow

Finite-difference procedure solves for laminar, transitional, or turbulent flows.

A numerical algorithm, incorporated into the VGBLP computer program, solves the laminar, transitional, or turbulent two-dimensional or axisymmetric compressible boundary-layer equations for perfect-gas flows. In the program, a coupled, iterative implicit finite-difference procedure solves the system of equations for laminar, transitional, or turbulent boundary-layer flows. The program includes several features that enhance computation efficiency and flexibility, including the Blottner variable-grid scheme, an iteration scheme allowing convergence of the coupled systems of equations to a specified accuracy level, and an iteration scheme for variable-entropy calculations.

Turbulence-closure options in VGBLP include either two-layer eddy-viscosity or mixing-length models. Eddy conductivity is modeled as a function of eddy viscosity through a static turbulent Prandtl number formulation. The transitional boundary layer is treated through a streamwise intermittency function that modifies the turbulence-closure model. This model is based on the probability distribution of turbulent spots and ranges from zero to unity for laminar and turbulent flow, respectively.

This program is written in FORTRAN IV for batch execution and has been implemented on a CDC CYBER 170 series computer and has a problem dependent central memory requirement. The VGBLP program was developed in 1982.

This program was written by Julius E. Harris and Doris K. Blanchard of **Langley Research Center.** *For further information, Circle J on the COSMIC Request Card.*
LAR-13015

Fast Generation of Boundary-Conforming O-Type Grids

Algorithm generates grids for arbitrary wing-body and axial turbomachinery geometries.

A fast algorithm accurately generates boundary-conforming three-dimensional consecutively refined computational grids for arbitrary wing-body and axial turbomachinery geometries. This algorithm has been incorporated into the GRID30 computer program.

The method employed in GRID30 is based on using an analytic function to generate two-dimensional grids on a number of coaxial axisymmetric surfaces positioned between the centerbody and the outer radial boundary. These grids are of the O-type and are characterized by quasi-orthogonality, geometric periodicity, and an adequate resolution throughout the flow field. Because the built-in nonorthogonal coordinates stretching and shearing

(continued on next page)

cause the grid lines leaving the blade or wing trailing edge to end at downstream infinity, use of the generated grid simplifies the numerical treatment of three-dimensional trailing vortex sheets.

The GRID30 program is written in FORTRAN IV for batch execution and has been implemented on an IBM 370 series computer with a central memory requirement of approximately 450K of 8-bit bytes. The GRID30 program was developed in 1981.

This program was written by Djorjie S. Dulikravich of **Lewis Research Center.** *For further information, Circle K on the COSMIC Request Card.*
LEW-13818

Calculating the Vortex-Lift Effect of Cambered Wings

Program computes the vortex-lift effect by using an improved supersonic suction analogy.

The computer program VORCAM calculates the vortex-lift effect of cambered wings by the suction analogy. VORCAM is based on an improved version of Woodward's chord plane aerodynamic panel method for subsonic and supersonic flow. This method was developed specifically for cambered wings exhibiting edge-separated vortex flow, including those with leading-edge vortex flaps.

An exact relation between leading-edge thrust and suction force in potential flow is employed in the suction analogy. Instead of assuming that the rotated suction force is normal to the wing surface at the leading edge, a new orientation for the rotated suction force is determined through consideration of the momentum principle. The supersonic suction analogy is improved by using an effective angle-of-attack defined through a semiempirical method.

VORCAM is written in FORTRAN IV for batch execution and has been implemented on a CDC CYBER 170-series computer with a central memory requirement of approximately 161K (octal) of 60-bit words. The program was developed in 1981.

This program was written by C. Edward Lan and Jen-Fu Chang of the University of Kansas Center for Research, Inc., for **Langley Research Center.** *For further information, Circle L on the COSMIC Request Card.*
LAR-12985

Machinery

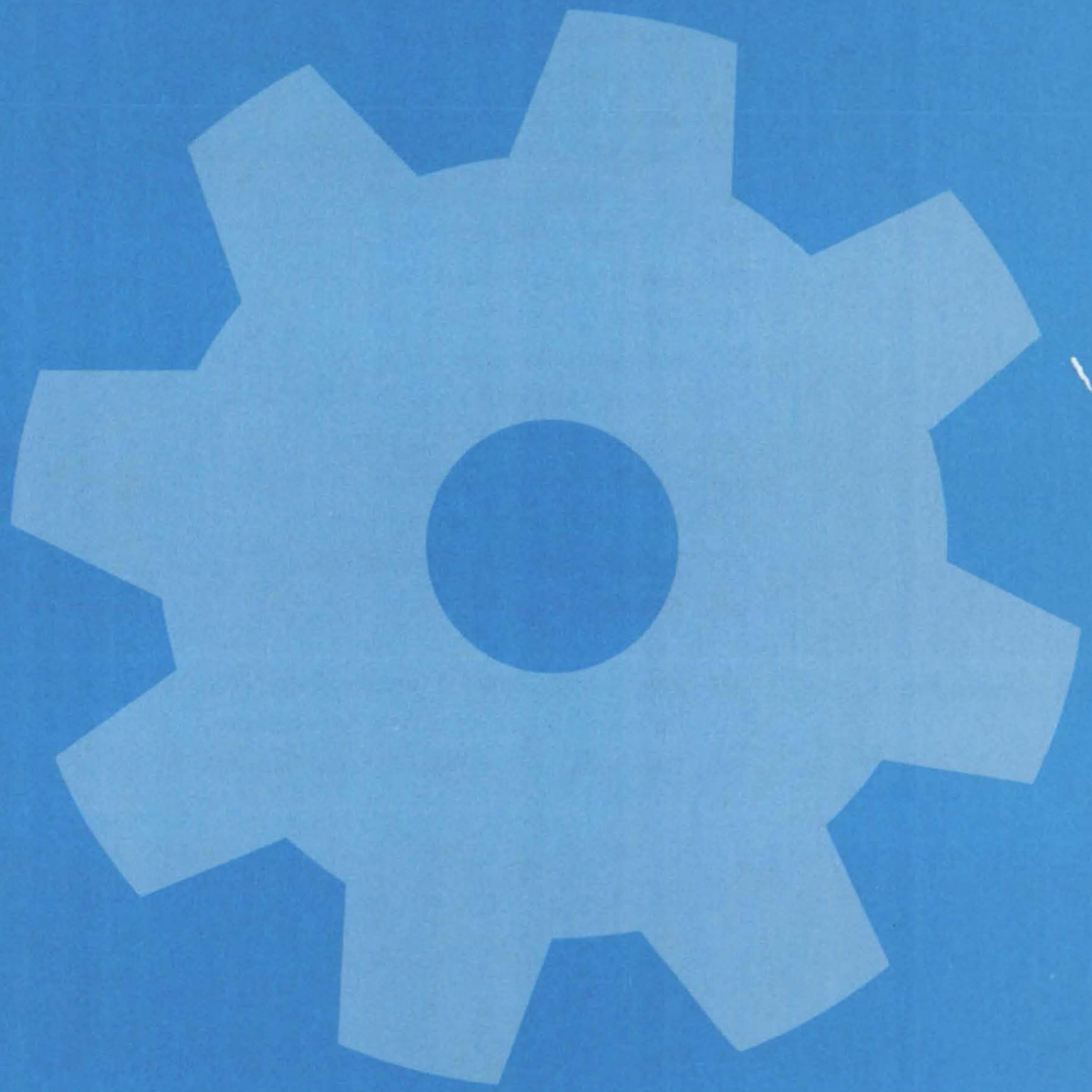

Hardware, Techniques, and Processes

Computer Programs

Remote Manipulator Has Realistic "Feel"

The operator feels the load but not the manipulator inertia or friction.

NASA's Jet Propulsion Laboratory, Pasadena, California

A new computer-aided remote manipulator does not transmit the weight and inertia of its own joints and segments. Instead, the operator feels only the load, an important advantage over conventional manipulators when carrying out delicate tasks.

The new system achieves its unique load sensitivity by processing the signals that move the manipulator (in response to the operator's movements of the hand controller) separately from those that apply reflective forces and torques on the hand controller. These reflective forces and torques are images of those felt by sensors mounted directly on the manipulator arm. Thus, they give the operator a true feel of the work the manipulator is doing.

In the system shown in Figure 1, the manipulator is used to handle a wrench. The hand controller generates five angular command signals and one radial command signal. These signals are compared in the computer with signals from position sensors on the joints, and the resulting error signals are sent to the manipulator to move its joints. The computer applies the required linear or nonlinear scale factors and transforms the geometry of the hand controller to the different geometry of the arm.

The signals for the reflective forces and torques are generated by sensors on the manipulator. They are a synthesis of the effector loads, not a proportion of effector and linkage loads as in conventional systems. The computer processes the two signal sets — command and reflective — independently (see Figure 2), permitting an immense range of scale factors, functional and geometric transformations, and response shaping to be applied to either or both signal sets.

In the reflective signal loop, the sensors on the effector generate signals that are processed and applied to the hand controller actuators, three of the signals generating forces and three generating torques against the operator's hand. These signals may also be scaled, transformed, and shaped. Some of the position sensor signals may also be involved in the reflective loop as parts of the geometric transformations.

(continued on next page)

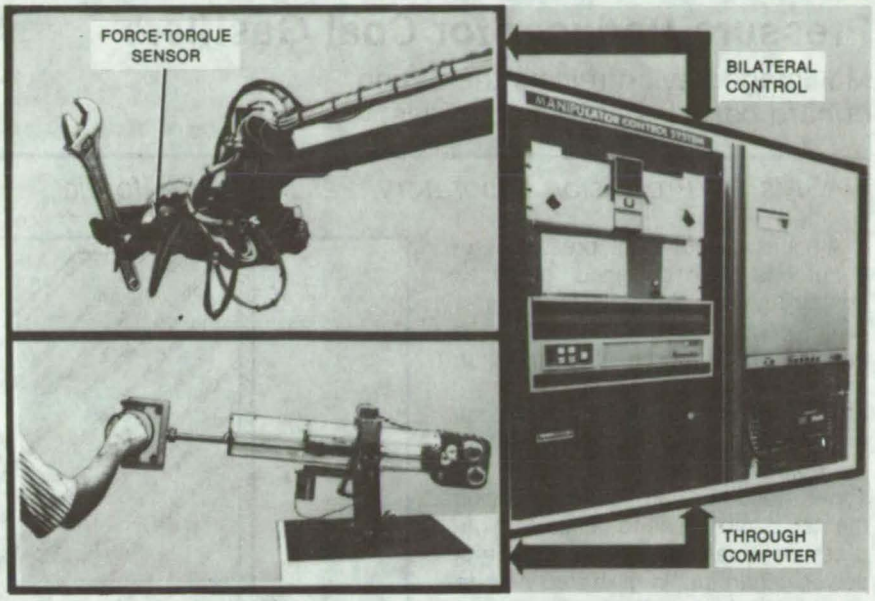

Figure 1. The **Remote Manipulator** consists of an end effector with force/torque sensors, a hand controller, and a computer.

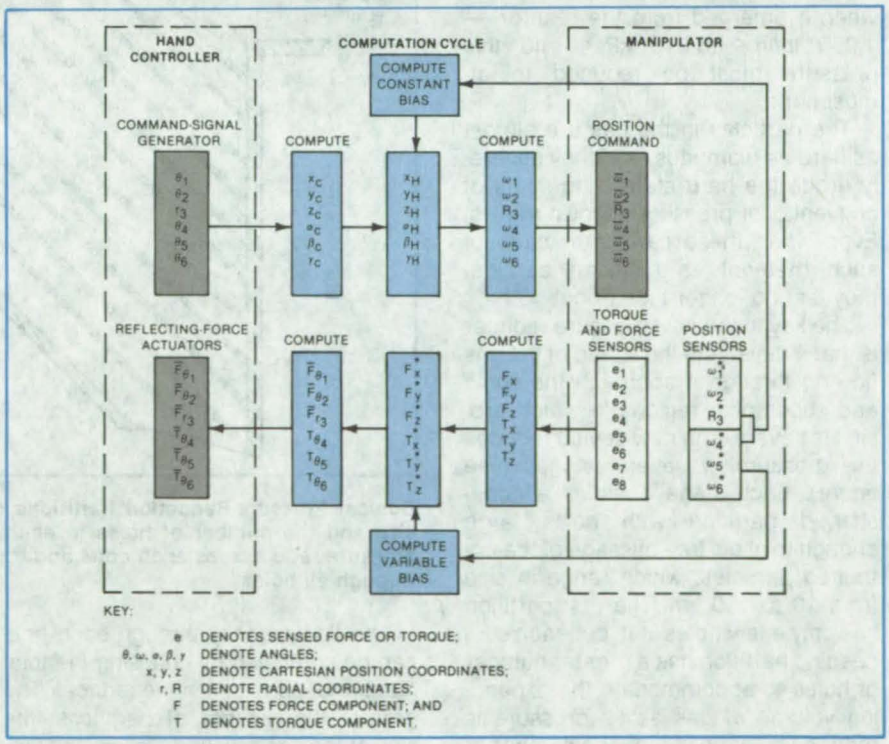

Figure 2. **Load-Force, and Command Signals** are processed separately so as to suppress the effects of inertia and friction. The operator feels a processed version of the load sensed at the grasping end of the manipulator. The motion of the manipulator is governed by error signals that result from the difference between the commanded and sensed positions.

The operator experiences force and torque resistances closely resembling those felt in operating the wrench. If the wrench needs an operating torque in excess of human capabilities, the scaling can be adjusted to give the operator the feel of a load within human capability. If the scaling is highly nonlinear, the operator would feel forces for light and delicate tasks fairly strongly, yet the forces for heavier tasks would be greatly reduced.

This work was done by Antal K. Bejczy of Caltech for **NASA's Jet Propulsion Laboratory.** *For further information, Circle 53 on the TSP Request Card.*
NPO-15065

Pressure Reducer for Coal Gasifiers

Multistage device resists the action of hard particles entrained in gas.

NASA's Jet Propulsion Laboratory, Pasadena, California

A quasi-porous-plug pressure reducer has been designed for gases containing abrasive particles. The new device reduces the pressure of such gases with a lower rate of erosion than in conventional letdown valves.

The device was developed for coal-gasification plants. Gas emerges from the reactor at a high temperature — about 1,000° F (538° C). The heat in the gas can be used to generate high-pressure steam to drive an electric-power generator. In giving up heat to the steam, the gas drops in temperature to about 150° F (66° C). The gas pressure, however, is still as high as when it emerged from the reactor — 1,250 lb/in.^{2} (8,618 kPa), and this pressure must be reduced to atmospheric.

The particles in the gas are almost as hard as diamonds, and they severely erode the hard stems and seats of conventional pressure-letdown valves. Even when these parts are made of such material as tungsten carbide, they last no longer than about 10 h.

The key to the new pressure reducer is that it never lets the speed of the gas flowing through it approach the sonic and supersonic regions in which erosion is severe. The new device reduces the pressure in several stages (see figure). Each stage contains a cone-shaped partition with holes large enough to allow free passage of the entrained particles, which range in size from 10 to 100 μm. The first partition has only a few holes in it, but each succeeding partition has a greater number of holes to accommodate the expanding volume of gas as its pressure is reduced by each stage. The number of holes is selected to give equal pressure ratios across all the partitions.

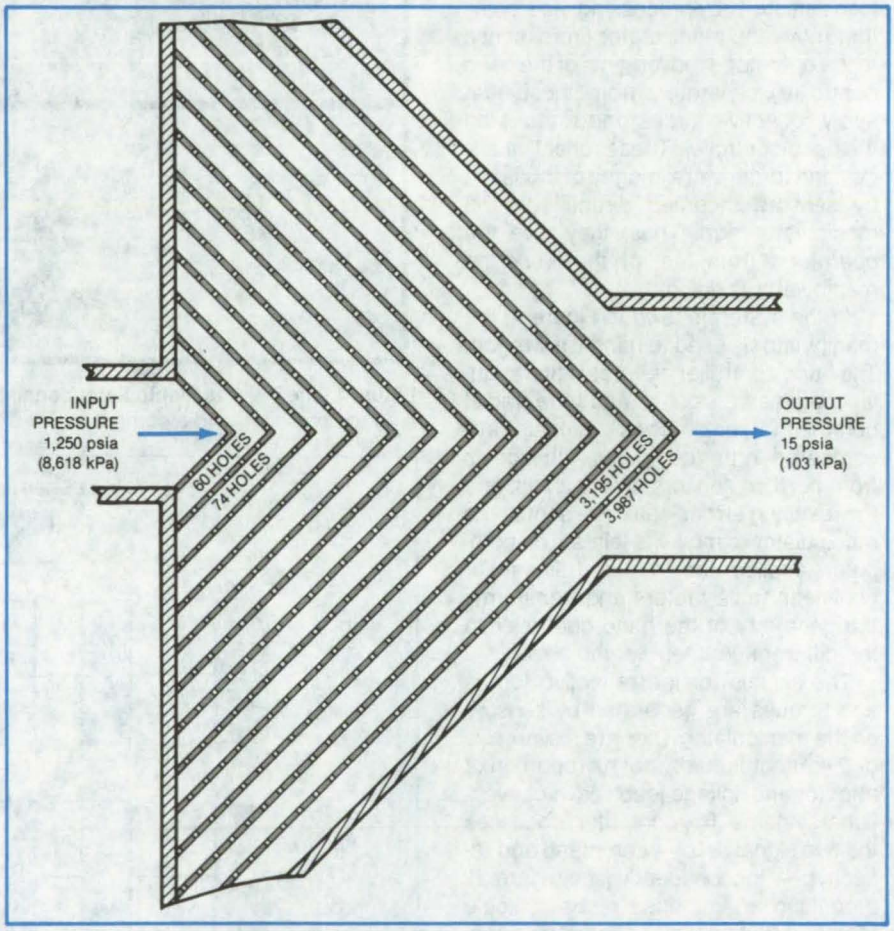

Conical Pressure-Reduction Partitions contain progressively more holes. The hole size and the number of holes in each cone are chosen to maintain the required pressure ratio across each cone and to keep the gas velocity at the same low value through all holes.

The flow velocity through each hole can be controlled by choosing the total number of partitions in the reducer. The greater the number of partitions, the slower the gas flow and the less the erosion. For a coal gasifier with a pressure drop from 1,250 to 15 lb/in.^{2} (8,618 to 103 kPa), a gas flow of 0.583 kg/s, ¼-in. (0.635-cm) hole diameter, and 20 partitions, the gas velocity would be 482.6 ft/s (147.1 m/s) for a mach number of 0.475.

This work was done by James M. Kendall, Sr., of Caltech for **NASA's Jet Propulsion Laboratory.** *For further information, Circle 54 on the TSP Request Card.*
NPO-15100

Passive Magnetic Bearing

A torsion wire assists permanent-magnet elements in maintaining shaft centering.

Goddard Space Flight Center, Greenbelt, Maryland

A new magnetic bearing for limited-rotation devices requires no feedback-control system to sense and correct the shaft position. The weight and bulk of position-control electromagnets, electronics, and power supply are therefore eliminated. The configuration easily lends itself to the incorporation of an integral torque motor, with only a modest increase in weight. Since no parts rub, no wear particles are generated and no lubricant is required. Thus, long life is assured, even in vacuum and other environments in which debris accumulation, lubricant evaporation, or cold welding impair bearing operation.

As shown in the figure, a cylindrical, axially-polarized permanent magnet is rigidly joined to a soft ferromagnetic cylinder by a nonmagnetic rod. The parts are clamped to two brackets attached to one of the two machine parts that are to move relatively to each other. Soft ferromagnetic endbells are clamped to another pair of brackets attached to the other machine part.

A torsion wire is stretched tightly between the endbells along the axis and is attached to the connecting rod to maintain the axial position of the cylinder pair: If there were no wire, the unstable equilibrium of the magnetic attraction would draw the cylinder pair into contact with one or the other endbell. Of course, rotation is limited by the strength of the torsion wire or by mechanical interference of the flanges or brackets.

When the cylinder pair becomes radially misalined with one or both endbells, the magnetic attraction between an endbell and the adjacent cylinder end exerts a restoring force. To insure against instability in the magnetic force, the cylindrical parts must have a sufficiently large ratio of length to diameter, while the cylinder ends and endbell faces must have congruent shapes. Stability is enhanced by making the endbell faces and cylinder ends spherical, concentric with the centroid of the cylinder pair.

With little modification, a torque motor can be incorporated into the bearing to provide small angular displacements (as for a scanning mirror or galvanometer). In this configuration, the cylindrical magnet is replaced by a soft ferromagnetic cylinder, and two radially-polarized cylindrical magnets are mounted on the outside of this cylinder. Shaped coils in the gap between the magnets and the outer cylinder are clamped to the endbells. When energized, the coils exert a small torque on the cylinder pair, causing it to rotate with respect to the endbells.

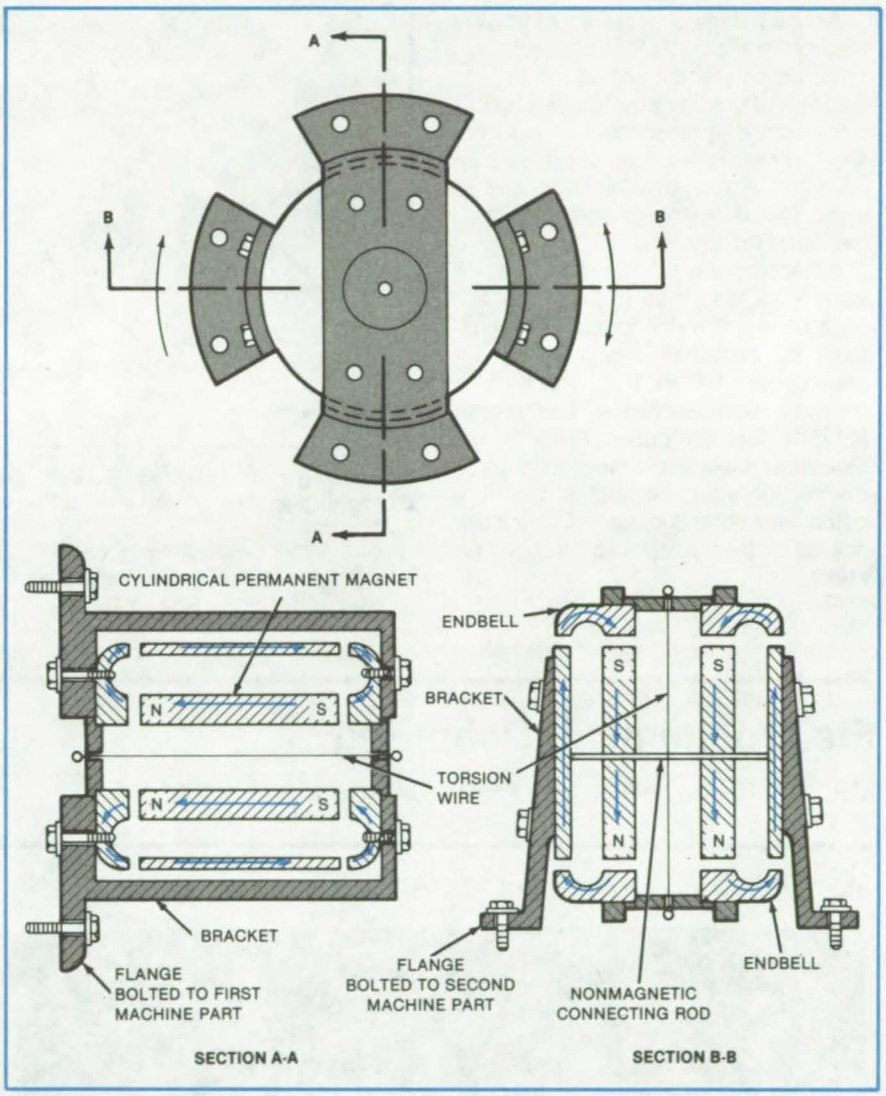

The **Passive Magnetic Torsion Bearing** requires no power supply and has no rubbing parts. The torsion wire restrains against axial instability. The magnetic-flux geometry is chosen to assure lateral stability with a radial restoring force that maintains alinement.

This work was done by Philip A. Studer of **Goddard Space Flight Center.** *For further information, Circle 55 on the TSP Request Card.*

This invention is owned by NASA, and a patent application has been filed. Inquiries concerning nonexclusive or exclusive license for its commercial development should be addressed to the Patent Counsel, Goddard Space Flight Center [see page A5]. Refer to GSC-12726.

Wind Turbine With Concentric Ducts

Proposed device would be relatively compact and efficient.

John F. Kennedy Space Center, Florida

A wind turbine concept would employ two concentric ducts to increase the air-pressure differential across the turbine blades and thereby to extract additional work from a given amount of wind energy. It is expected to be suitable for installation on such existing structures as water towers, barns, houses, and commercial buildings.

Air enters the turbine duct, and its velocity increases as it flows over the nose cone in the interior duct, in which the cross-sectional area gradually decreases (see figure). The air velocity in the inner duct reaches a maximum as the air enters the turbine. Passing over the blades, the air does work on them. In the section after the turbine, the truncated-cone outer duct augments the discharge of the spent air by the venturi effect.

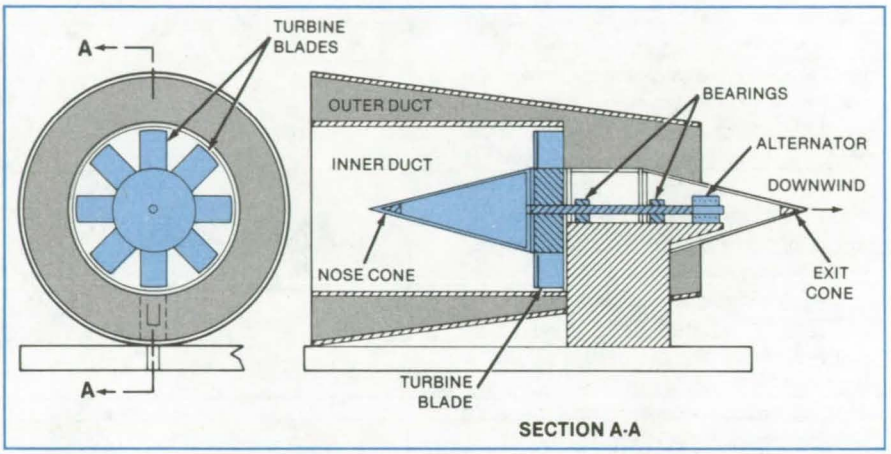

Converging Inner and Outer Ducts increase the pressure difference across the blades of a wind turbine. The turbine shaft drives an alternator housed inside the exit cone.

This work was done by Alvin J. Muhonen of Boeing Services International for **Kennedy Space Center.** *For further information, Circle 56 on the TSP Request Card.*
KSC-11191

Electrochemical Deburring

Machining burrs are removed from inaccessible areas.

Marshall Space Flight Center, Alabama

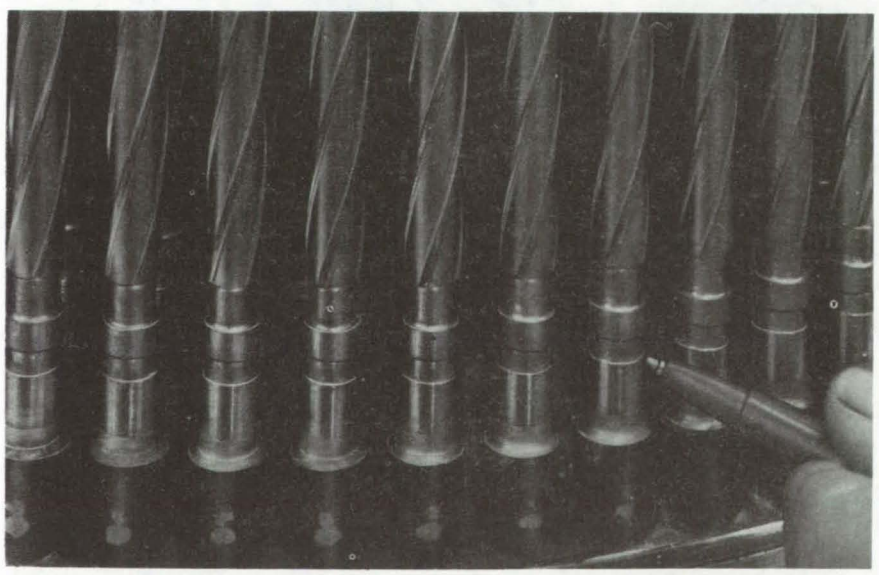

Figure 1. **Electrochemical Deburring** removes burrs from the assembled injector tubes. Because the process uses a liquid anodic dissolution in a liquid electrolyte to provide the deburring action, it can smooth surfaces and edges in otherwise inaccessible areas.

A special electrochemical deburring tool is used to remove machining burrs from assembled injector tubes, shown in Figure 1. Conventional deburring methods could not be used because of the close proximity of the tubes.

The apparatus, shown in Figure 2, involves a direct-current power supply, an electrolyte, the deburring tool, and electrical connections between the tube to be deburred and one side of the power supply. The electrolyte is forced to flow between the tool and the tube to conduct electricity. The electrolyte flow also drags away the byproducts of the chemical reaction.

Electrochemical deburring removes burrs quickly. Because of electric-field concentration at sharp edges, electrochemical deburring works mainly at

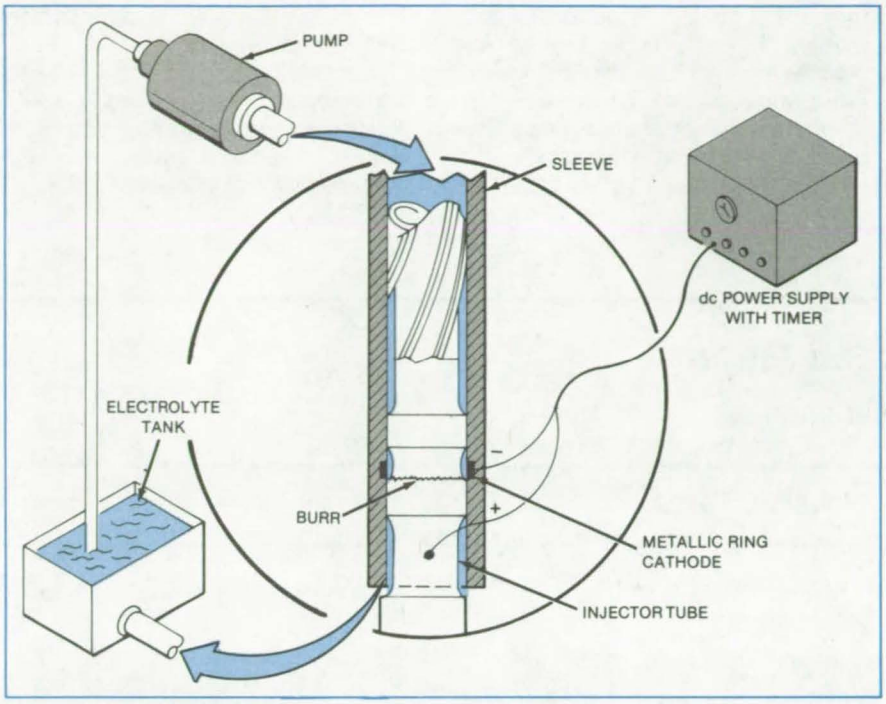

Figure 2. The **Deburring Tool** consists of a sleeve that contains a metallic ring cathode. The sleeve is placed over the tube, and an electrolytic solution is forced to flow between the tube and the sleeve. The workpiece serves as the anode.

the rough edges of a workpiece and does not significiantly affect the nominal dimensions of the workpiece.

This work was done by R. K. Burley of Rockwell International Corp. for **Marshall Space Flight Center.** *No further documentation is available.*

Inquiries concerning rights for the commercial use of this invention should be addressed to the Patent Counsel, Marshall Space Flight Center [see page A5]. Refer to MFS-19693.

Coil-Welding Aid

A positioner holds a coil inside a cylinder during tack welding.

Lyndon B. Johnson Space Center, Houston, Texas

A welding aid spaces the turns of a coil inside a cylinder and applies contact pressure while the coil is being tack-welded to the cylinder. The device facilitates the fabrication of heat exchangers and other structures by eliminating hand-positioning and clamping of the individual coil turns.

The positioner (see figure) includes a shaft with an aluminum mandrel at one end and a crank at the other. Two grooves around the circumference of the mandrel are separated by the required coil pitch. Additional components include rollers, a shaft pivot point, and a screw jack.

A preformed coil is placed inside the cylinder to which it is to be welded. The cylinder is mounted on the roller assembly, and the mandrel is placed in the cylinder over the first two windings of the coil. After the first winding has been positioned, the location of the second winding is automatically established by the mandrel. The screw

(continued on next page)

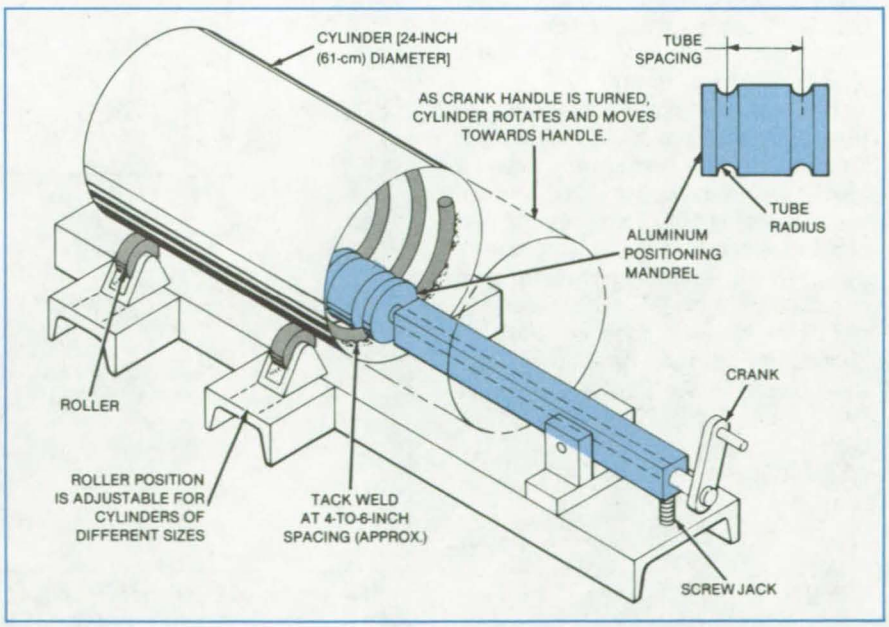

This **Coil Positioner** and clamp could be used wherever coiled materials need to be positioned in or on a cylinder during welding. It could be used with arc, heliarc, gas or spot welders. Fabrication of the device is straightforward and can be done in machine shops without specialized equipment.

jack forces the mandrel down so that it presses the first two turns of the coil against the cylinder wall. The first two turns of the coil are then tack welded to the cylinder.

After welding, the crank is rotated to advance the mandrel along the coil (in the case of the figure, the rotation is to the left). This rotating action turns the cylinder and also moves the cylinder axially toward the crank. When the cylinder is rotated the desired distance, the clamped turns of the coil are again welded to the cylinder. These steps are repeated until the entire coil has been tack-welded to the cylinder.

This work was done by William T. Wiesenbach and Melvin C. Clark of Rockwell International Corp. for **Johnson Space Center.** *No further documentation is available.*
MSC-20470

Gage Measures Recessed Gaps

Tool permits fast and easy measurements.

Lyndon B. Johnson Space Center, Houston, Texas

A new tool measures the separation between recessed parallel surfaces. The tool was developed for measuring the gap between adjacent tiles on the Space Shuttle. Because the tiles have overhanging edges, the tool is designed to slip into the gap from the end so that it extends through a 0.040-inch (1-millimeter) crack (see figure). It measures gaps between 0.200 and 0.400 inch (5.1 and 10.2 millimeters) so that gap fillers of the proper thickness can be selected.

The tool consists of two arms 0.030 inch (0.76 millimeter) thick having a three-finger gaging mechanism at the bottom and a dial indicator at the top. A pin attached to the moving arm passes through a slot in each finger (see figure). The pin-arm motion causes the fingers to fan out until they touch the sides of the gap. The moving arm causes movement of the plunger on the dial indicator that is attached to the other arm.

The new tool makes it unnecessary to use feeler gages to measure the gap. The feeler gages had to be used with great care to avoid damaging the tile; the new tool is both faster and gentler and should prove useful in numerous industrial situations involving gap measurements in inaccessible places.

This work was done by Jose L. Zepeda of Rockwell International Corp. for **Johnson Space Center.** *For further information, Circle 57 on the TSP Request Card.*
MSC-20230

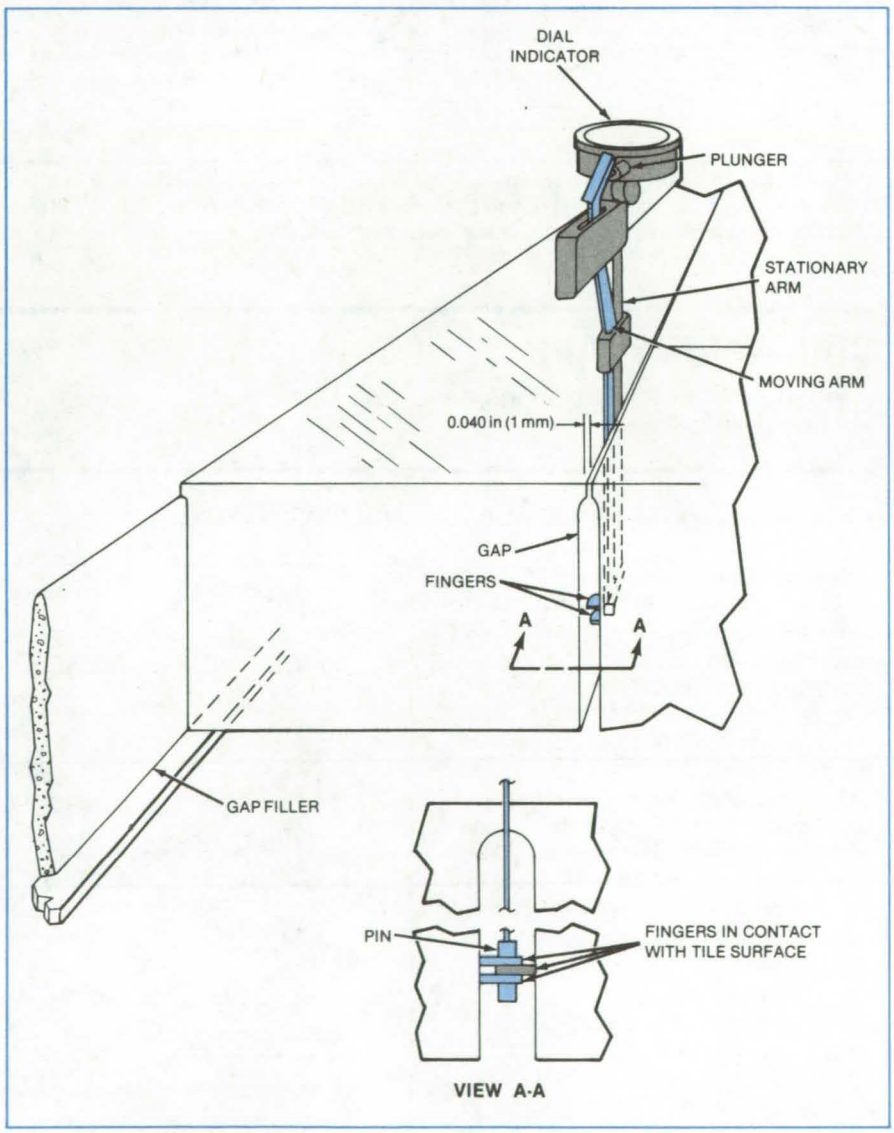

The **Fingers Spread,** the scissors arms open, the fingers rock, the dial plunger slides, and the gap at the base of adjacent tiles is measured.

Tooling Converts Stock Bearings to Custom Bearings

Grinding process uses a special bearing holder.

Langley Research Center, Hampton, Virginia

A technique for reworking stock bearings saves time and produces helicopter-rotor bearings that are ground more precisely than new bearings purchased from the manufacturer. The grinding setup meets strict machining requirements, including: unobstructed upper surfaces of the bearing, 100-lb (440 - N) preload on the inner race, and a tool block with surface flushness equal to or better than the table of the grinding machine.

Special ground bearings used in several helicopter rotor research models throughout the Government and industry were manufactured about 8 years ago. However, the low bearing life on some of the models depleted the spares supply. Moreover, increased costs, a 12-month-plus waiting period, and other problems related to obtaining a new supply from the original manufacturer made it necessary to develop an alternative solution.

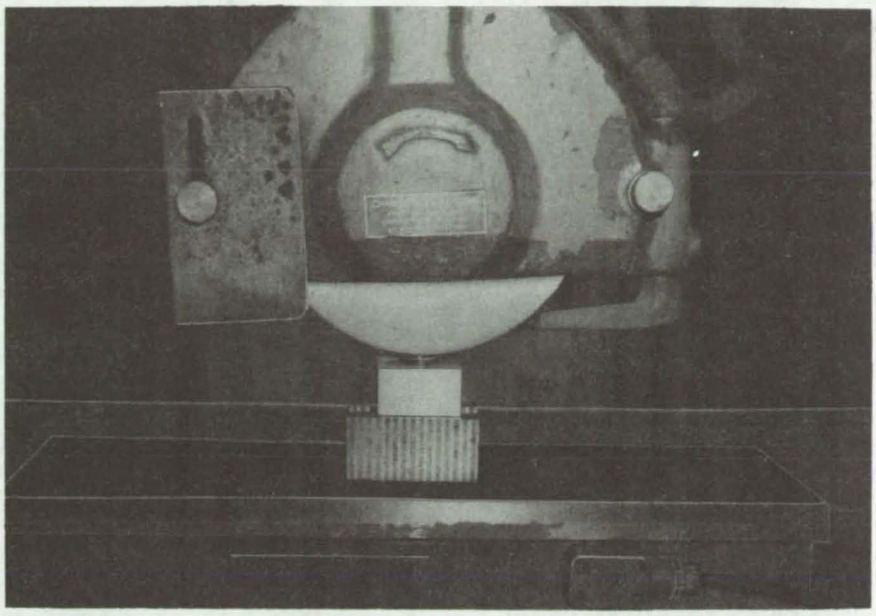

Figure 1. A **Grinding Operation** produces bearings of higher quality than commercially available bearings.

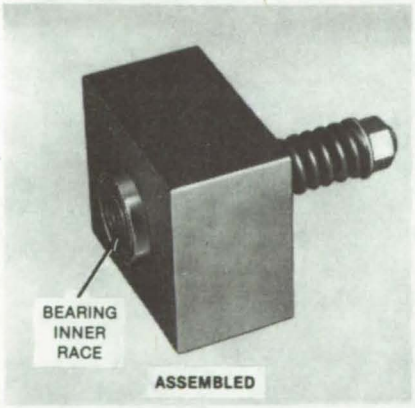

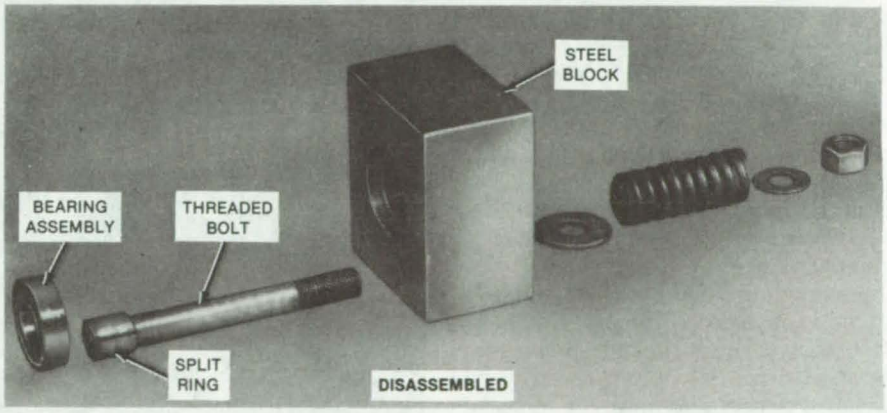

Figure 2. A **Split, Tapered Ring,** at one end of the threaded bolt, expands to hold the inside of the inner race of the bearing assembly; the nut, at the other end of the bolt, adjusts the amount of spring tension. The new piece of hardware grasps the bearing firmly without interfering with the grinding operation.

A substitute bearing found in Government supply meets all the rotor-bearing specifications except one. The bearings are used in a model rotor hub cuff and are stacked in groups of five to share the thrust loads, as well as to permit rotor-blade pitching motion. The requirement lacking in the stock bearing was that, with the inner race under a 100-lb preload in the thrust direction, the inner and outer faces on both sides must be within ± 0.0002 inch (± 0.0005 cm) of the same thickness and ± 0.0002 inch of being parallel.

The main problem in grinding the stock bearing is devising a piece of hardware to put the 100-lb preload on the inner race and to grasp the bearing firmly without interfering with the grinding operation. Figure 1 shows the new piece of hardware used in the grinding operation. As shown in Figure 2, a linear coil spring with a threaded bolt through the center is used. On one end of the bolt is a split, tapered ring that expands to hold the inside of the inner race. On the other end of the bolt, a nut is turned to adjust

(continued on next page)

the amount of spring tension and to expand the split ring to hold the inner race.

The attachment, bolt, nut, and spring are anchored to a steel block with a hole in the middle. The bearing rests in a recess on top of the block over the hole, with the spring coming up under the bottom of the block. The top recess and bottom of the block are smooth and precisely flat and parallel. The spring is calibrated to determine the deflection required for the 100-lb load. This arrangement fulfills the requirements for precise grinding.

The stock bearings include shields on both sides; but to minimize the chance of material getting into the bearings, a jelly lubricant is added to the cracks and then wiped off after the grinding operation. A quality check of 25 bearings following this grinding operation showed the precision of flushness between inner and outer races to be about 25 percent better than that from a sampling of the manufacturer's precise experimental bearings.

This work was done by Edward N. Fleenor, Jr., of **Langley Research Center.** *No further documentation is available.*
LAR-12922

Drilling Precise Orifices and Slots

A combination of mechanical drilling and EDM is used.

Lyndon B. Johnson Space Center, Houston, Texas

Machinists working on the Space Shuttle reaction-control system have used numerical control and electric-discharge machining in a tooling combination that could save time and labor in other applications as well. Whereas an experienced machinist was previously tied up full time drilling a complex set of orifices, the new tooling system is operated by one person without special machining skills. Moreover, it automates the production of identical parts so that several are completed in less time than it previously took to fabricate one part.

Figure 1 is a view of one side of the reaction-control-thrustor injector. This critical element controls the precise mix of fuel and oxidizer that enters the thrustor. Near the center of the injector is a circular array of orifices that feed the oxidizer to the reaction chamber. The orifice sizes must be precisely controlled, as must their pitch with respect to the surface of the injector. The fuel-feed slots radiate out near the perimeter of the injector. These slots are of varying width and depth to give the proper spatial distribution of fuel as it enters the reaction chamber.

The tooling setup consists of a rotary table, a numerical-control system, and a torque-sensitive drill press. These components are used to drill the oxidizer orifices. An electric-discharge machine drills the fuel-feed orifices.

The complete tooling system integrates the drilling system and the rotary table for the 12 angular locations required for the drill heads. Also included

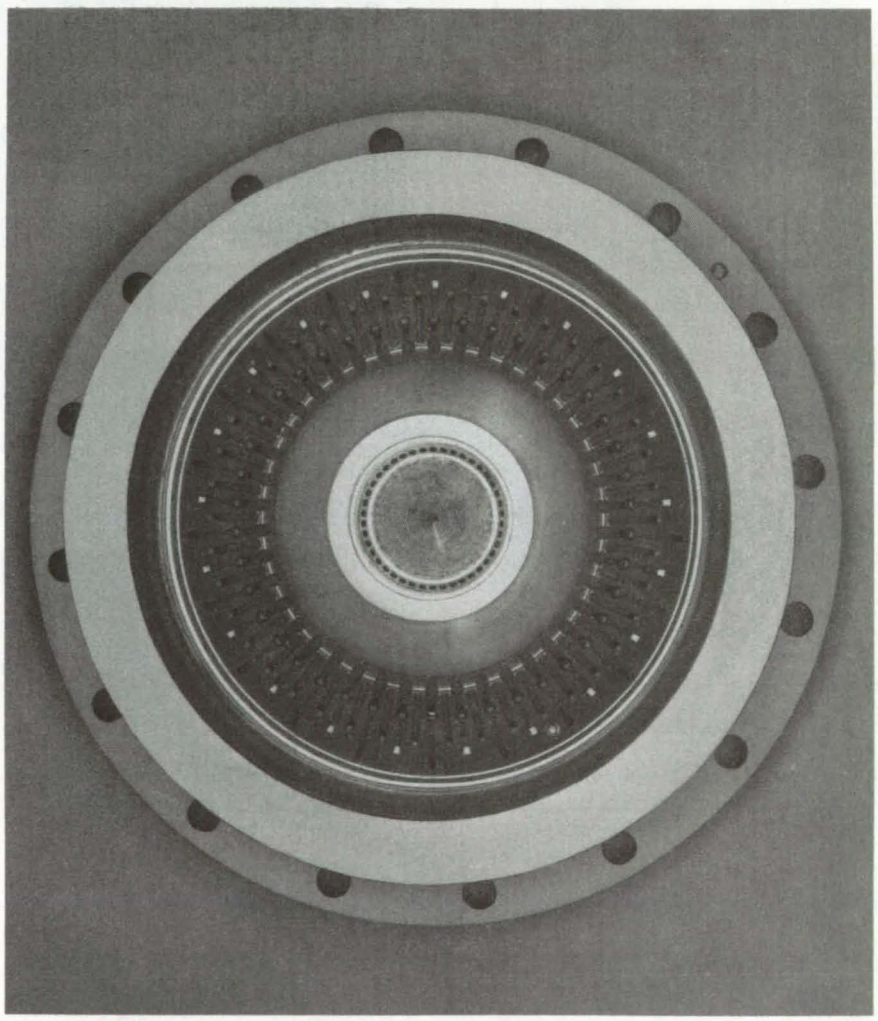

Figure 1. The **Space Shuttle Reaction-Control-Thrustor Injector** requires precisely machined orifices and slots. The Columbia has 38 thrustors.

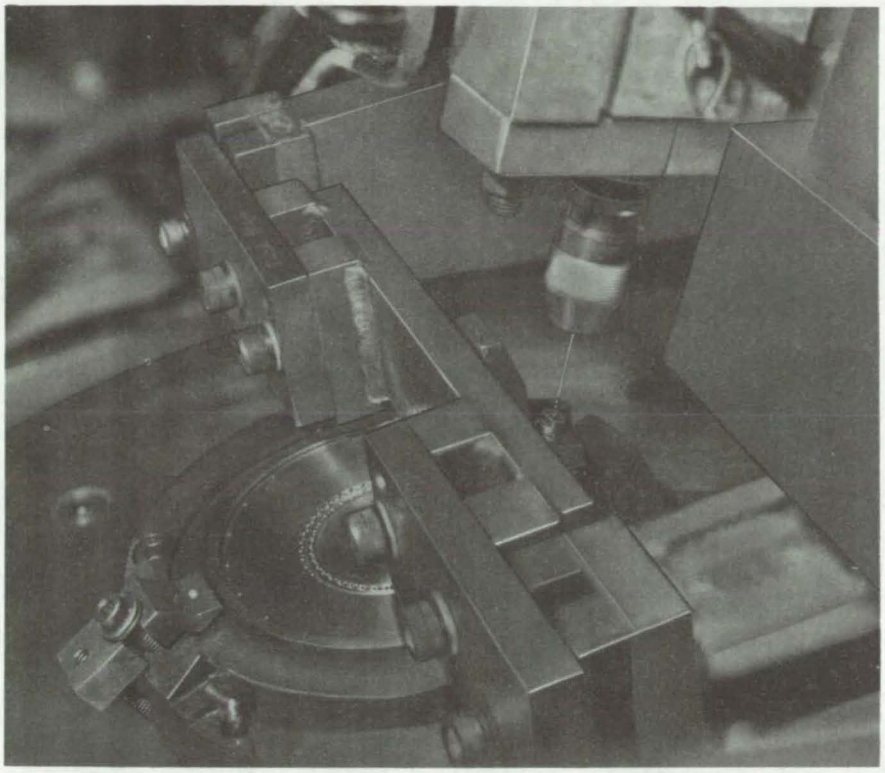

Figure 2. **Orifices Are Drilled by Cobalt Bits** under numerical control in this setup, which gives the correct orifice diameters [0.0154 to 0.050 in. (0.39 to 1.27 mm)] and entry angles. Tolerances on hole size and location are very tight.

is the fixturing, bushings for each of the angles, and spot-face bushing fixtures for each hole size and angle (see Figure 2).

Special cobalt drills with 135° points are purchased and inspected before use. Drills not within established standards are reground. Drill breakage with the smallest orifices [0.0154 in. (0.39 mm) in diameter] was reduced as the operators gained experience. The maximum number of holes that could be drilled safely with a single drill was determined after a few trial runs. A small electrical-discharge machine was set up in the drillroom and used to remove broken drills.

The manifold slots are produced by electrical-discharge machining. The balance of the injector, including the fuel closure system, the fuel and oxidizer inlet tubes, and the remaining support structure, is electron-beam welded. The assembly receives a final acceptance test before delivery.

This work was done by Charles W. Richards and James E. Seidler of The Marquardt Co. for **Johnson Space Center.** *No further documentation is available.*
MSC-20053

Robotic Water-Blast Cleaner

Automated system will be fast, safe, and efficient.

Marshall Space Flight Center, Alabama

A water-blasting system under development will remove hard, dense, extraneous material from surfaces. A high-pressure pump [up to 20,000-lb/in.^{2} (138-MPa)] forces water at supersonic speed through a nozzle manipulated by a robot (see figure). The impact of the water blasts away unwanted material from the workpiece, which is rotated on an air-bearing turntable. Designed for removing thermal-protection material from the Space Shuttle during post-flight refurbishment, the system is adaptable to such industrial processes as cleaning iron or steel castings.

Two 200-hp (149-kW) electric motors drive two five-plunger positive-displacement pumps. Pump speed is continuously variable between 50 and 400 r/min. The robot is a 25-hp (18.6-kW) waterproof industrial machine that can withstand 225 lb (1,000 N) of reaction force and still maintain position with an accuracy of 50 mils (1.3 mm). The robot manipulator can rotate on six axes. The turntable provides a seventh axis of rotation. A computer subsystem monitors and controls such parameters as turntable location, position, and speed; pump speed, pressure, and flow rate; robot program; and anticollision signals.

The robot can manipulate the blast nozzle in any of four distinct modes:

1. The workpiece is rotated continuously on the turntable while the robot moves the nozzle vertically, removing material in a spiral pattern. This mode ordinarily allows the fastest removal.
2. The workpiece is rotated back and forth on the turntable while the robot moves the nozzle vertically, removing material completely from a section. This mode allows the removal of material in horizontal strips without using excessive amounts of robot memory.
3. The workpiece is held stationary at a predetermined point while the robot moves the nozzle over a section of the surface. This mode removes material in difficult areas, such as around posts.
4. The workpiece is rotated incrementally in fractions of a degree while the robot sweeps the nozzle vertically. This mode is effective in open areas between protrusions.

Air bearings support the turntable during rotation and raise it above the floor when it is moved into or away from the

(continued on next page)

blast area. Powered by a 9-hp (6.7-kW) electric motor, the turntable can be positioned with an angular accuracy of one-fourth degree.

The automatic removal system is intended to replace manual water-blast equipment in which an operator must make split-second decisions in manipulating a blast nozzle under adverse conditions of noise, poor visibility, and wet, restrictive clothing. The new system removes the operator from the hazardous blast area and greatly improves the safety of personnel and equipment.

This work was done by Max H. Sharpe, Marion L. Roberts, William E. Hill, and Charles H. Jackson of **Marshall Space Flight Center.** *For further information, Circle 58 on the TSP Request Card.*

Inquiries concerning rights for the commercial use of this invention should be addressed to the Patent Counsel, Marshall Space Flight Center [see page A5]. Refer to MFS-25519.

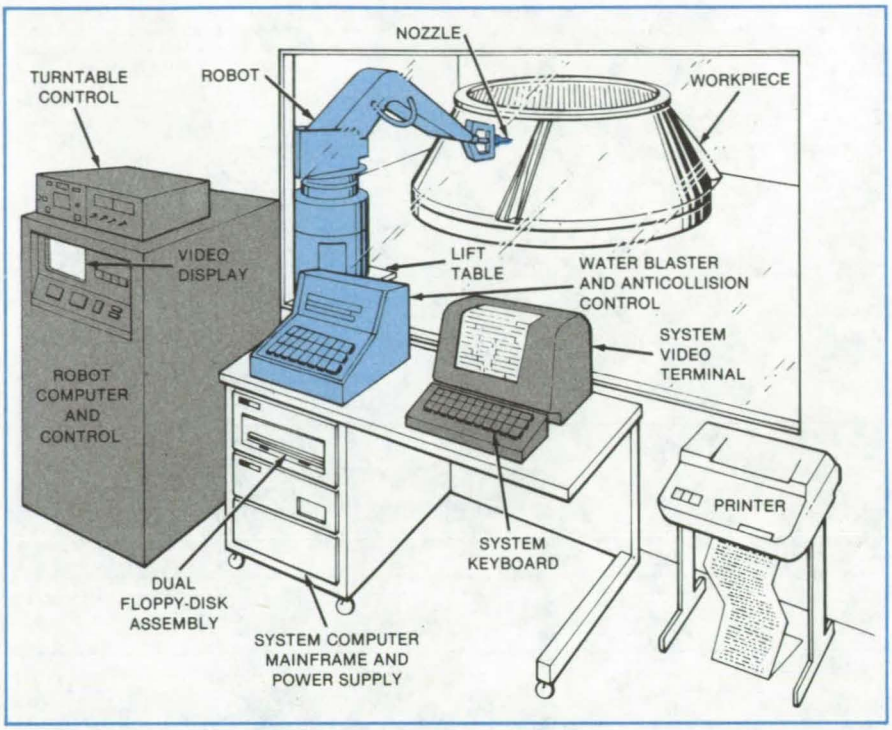

Safely Away From the Hazards of the water-blast cleaning area, a variety of control equipment operates the robot and turntable with great precision, despite the great forces involved in the cleaning process.

Staked-Bearing Removal Tool

A portable air-powered tool enables rapid bearing replacement with minimum effort.

Lyndon B. Johnson Space Center, Houston, Texas

An air-powered device cuts away retaining lips on one side of a bearing in preparation for removal of the bearing from an assembled structure. The tool makes it possible to replace the bearings without having to disassemble the structure.

As shown in the figure, the device includes a shouldered post that is inserted into the bearing bore to position the tool and a set of Belleville springs and a nut to hold the tooling post tight against the bearing. The cutting blade is held in a standard air drill. A second set of Belleville springs and nut control the cutting pressure.

The tooling post remains in place and does not rotate during the cutting operation. The springs apply a steady cutting pressure and also provide pressure

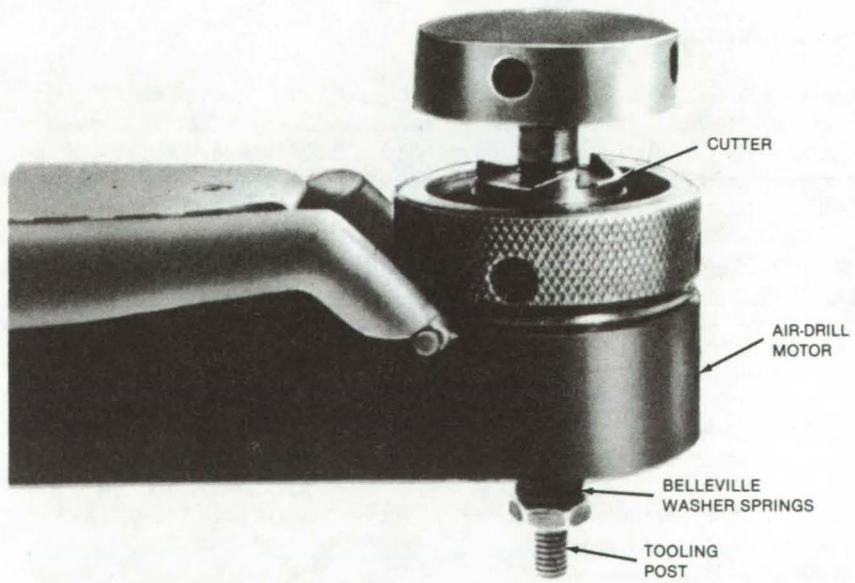

The **Bearing-Removal Tool,** shown with assembled components, can expedite bearing replacement in aircraft, ground vehicles, and other applications. The new tool cuts the lip on one side to facilitate bearing replacement. After the bearing retaining lip has been cut away, the bearing can be pressed out.

relief to the cutter if it is impeded by a burr or other obstacle.

The tool removes the bearing lip with minimal damage to the surrounding structure. It eliminates costly and time-consuming disassembly prior to conventional machining and pressing out of spherical bearings.

This work was done by Leo A. Berson and Richard G. Bird of Rockwell International Corp. for **Johnson Space Center.** *For further information, including detailed engineering drawings of the tool, Circle 59 on the TSP Request Card.*
MSC-20337

Self-Alining Quick-Connect Joint

Tapered joint is compact and lightweight.

Langley Research Center, Hampton, Virginia

A quick-connect tapered joint is used with a minimum of manipulation and force. Originally developed to assemble large space structures, the joint is simple, compact, strong, lightweight, self-alining, and has no loose parts.

The joint consists of matching male and female thin-walled metallic or molded plastic cones, split metallic locking rings of graduated sizes, and several metallic split-ring retainers. Split locking rings in concentric grooves in the outside surface of the male cone mate with concentric grooves in the inside surface of the female cone to provide a positive lock (see Figure 1). No rotation is required to assemble the joint, yet it retains most of the features of a threaded joint through the use of the multiple split locking rings in the concentric grooves.

One side of each groove in the female part is tapered, and there is a corresponding taper on the locking rings. Only minimal force is needed to position the male part in the female part, at which time the split-ring retainers are triggered to release the split locking rings and the energy stored in them. The combination of stored radial energy and the tapered mating surfaces on the split locking rings and in the grooves in the female part results in a net force that pulls the male piece into the female piece.

The split retainers are fully confined within the male part before and after release; there are no loose parts. The male piece has a retaining device that holds the split locking rings, with their stored potential energy, compressed. When the male and female members are properly brought together, the split-ring retainer is released so that its ears slide off the locking rings, freeing the rings to move radially outward into the female grooves.

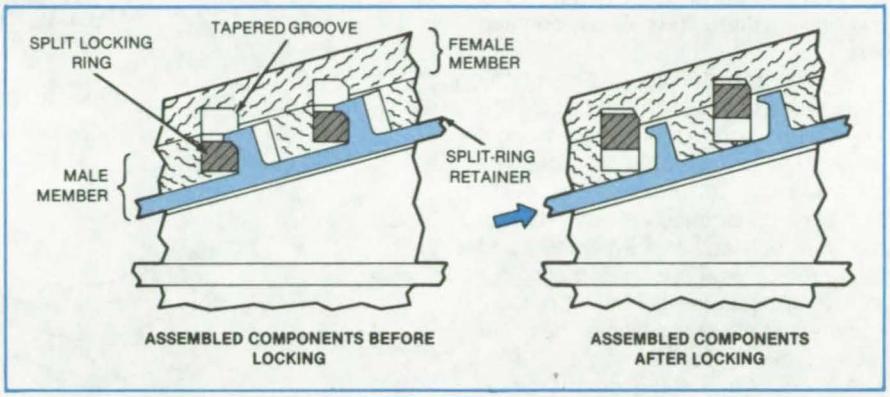

Figure 1. The **Split-Ring Retainer** holds the locking ring in place. Only minimal force is required to position the male in the female joint, at which time the split-ring retainers are triggered to release the split locking rings.

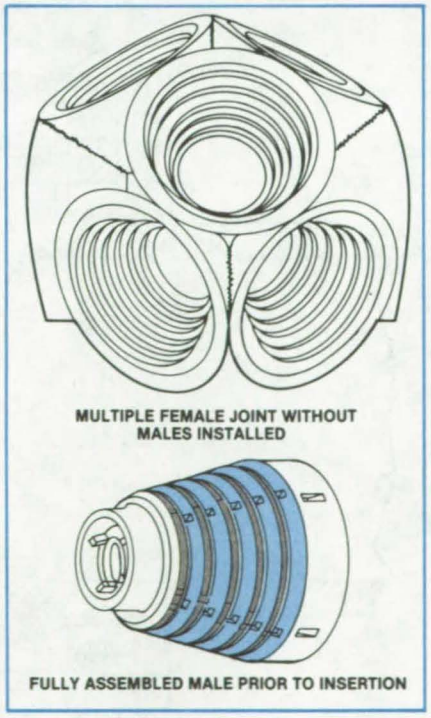

Figure 2. In a **Multiple-Joint Assembly,** maximum use is made of the intersection of walls of the conical female parts to stiffen the entire assembly.

Special provisions in the male prevent the retainer from falling free once it has released the split locking rings. A special device is used to push on the retainer causing it to slide when release of the locking rings is desired, thereby protecting the retainer from premature release. Once assembled, the joint cannot be disassembled. The joint connection can also be designed for multiple connections (see Figure 2).

The joint may be fabricated of machined or investment-cast metals or of plastic molding material. It may be hollow, allowing for the routing or passage of wires, tubes, fluids, or gases. If plastic molding material is used, it can be compounded with graphite fibers, carbon black and other additives, or coated to achieve certain design requirements, such as electrical conductivity, UV protection, or proper surface emissivity.

This work was done by Melvin H. Lucy of **Langley Research Center.** *No further documentation is available.*
LAR-12711

Self-Locking Connector

Mechanism is spring-loaded into a normally locked position.

Marshall Space Flight Center, Alabama

A connector lock resists vibration, automatically compensates for wear, and exhibits no backlash when the parts are seated. The mechanism is built into the coupling nut on the outer connector body (see figure). An outer collar is turned clockwise to tighten the threaded coupling nut, transmitting torque to the coupling nut through six radially oriented pins.

As shown in the upper part of the figure, three rollers are forced clockwise by compression springs into wedge-shaped spaces between the coupling-nut and connector bodies. The rollers thus become jammed between the nut and the connector body, preventing counterclockwise (loosening) motion but permitting clockwise (tightening) motion. An outer set of springs biases the collar in the clockwise position.

The collar is rotated counterclockwise to unlock: The six pins (two for each roller) push the rollers out of the wedge spaces. The nut is then free to turn counterclockwise for uncoupling in the normal manner.

Vibrations will not loosen the connector even if the installer fails to tighten the nut. On the contrary, once the nut has been started onto the thread, vibrations will gradually tighten it since the locking mechanism permits only tightening motions.

This work was done by K. C. Gaspar of Rockwell International Corp. for **Marshall Space Flight Center.** *For further information, Circle 60 on the TSP Request Card.*

Inquiries concerning rights for the commercial use of this invention should be addressed to the Patent Counsel, Marshall Space Flight Center [see page A5]. Refer to MFS-19716.

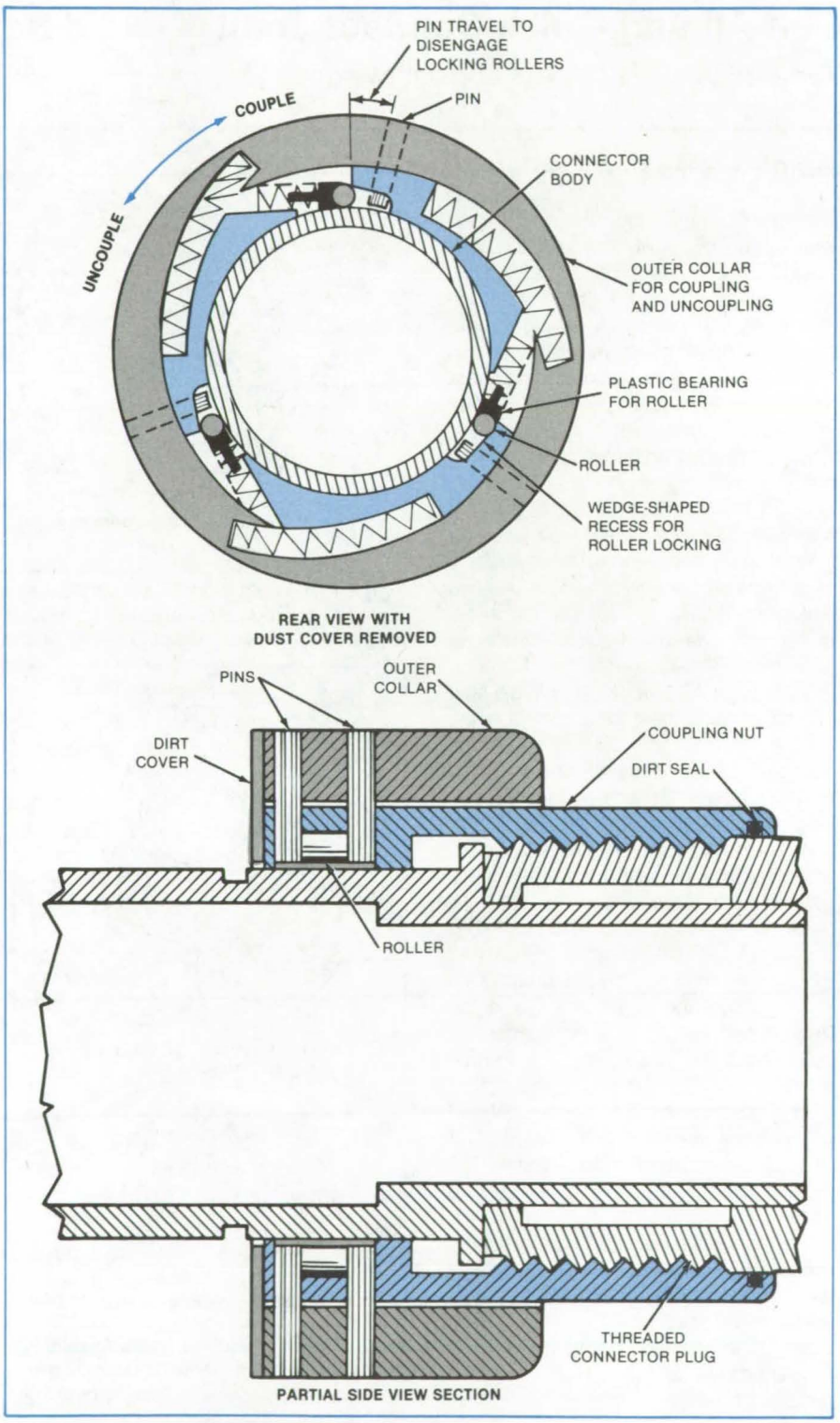

Spring-Loaded Rollers are jammed into wedge-shaped recesses between the nut and the connector body, thus preventing counterclockwise (loosening) motion of the nut.

Latching Mechanism for Umbilical Connectors

Connectors for power, data, and coolant are automatically mated.

Lyndon B. Johnson Space Center, Houston, Texas

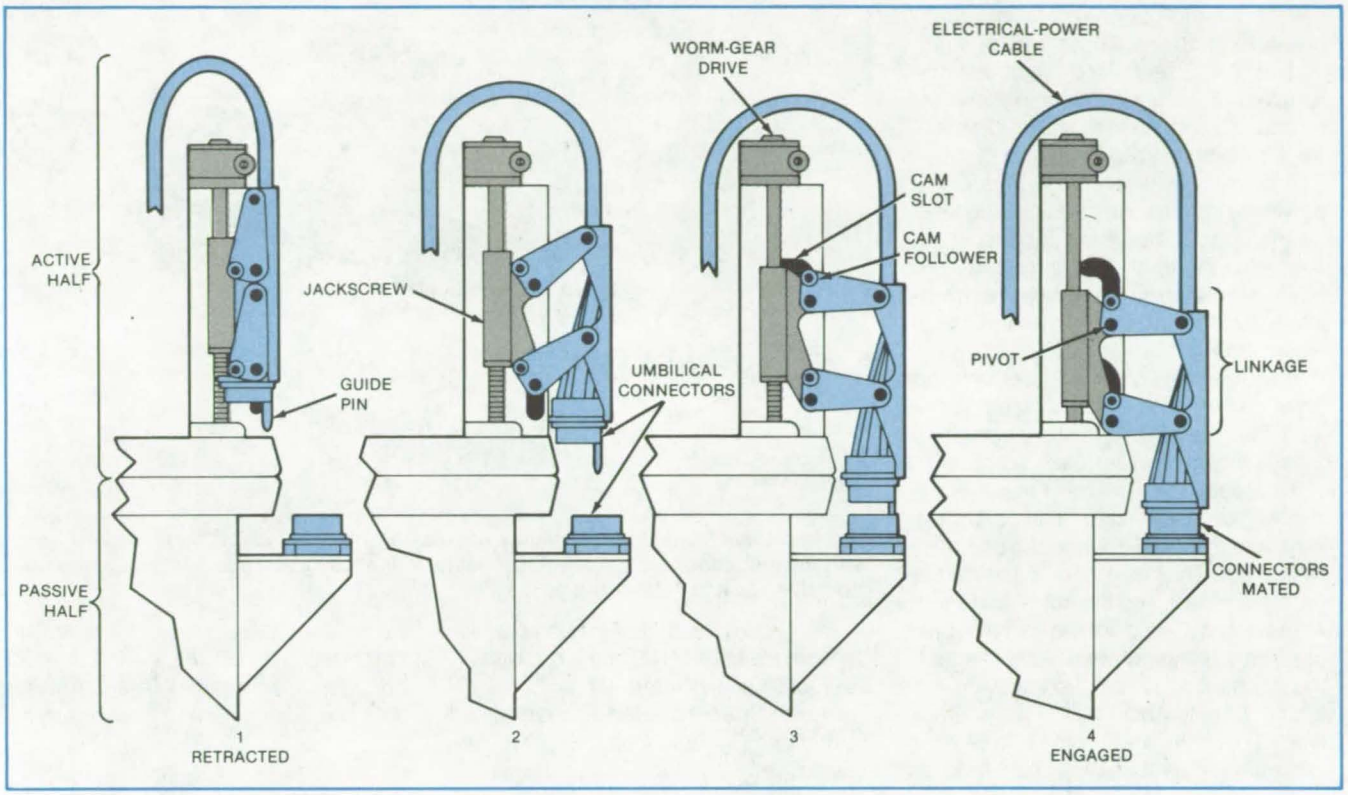

A Motor-Actuated Jackscrew moves a connector on the active half of an interface to a mating connector on the passive half.

A proposed electromechanical interface would transfer electric power, data, and coolant from one system to another. Originally suggested for spacecraft, the concept may also be adaptable to underwater connections.

In the design for spacecraft, a latching mechanism and an umbilical connector are mounted on each of the three clear sides of the hexagonal berthing frame on one of the vehicles — the active half of the berthing setup. The mating halves of the umbilical connectors are fixed to the corresponding sides of the other vehicle — the passive half. An umbilical mechanism on the active half is stowed behind the face of the berthing frame.

The umbilical connector is attached to a linkage (see figure). As the linkage pivot points are moved down by a jackscrew, the connector is rotated out and down by cam followers that follow stationary slots, so that it engages the mating connector on the passive half. Dual motors turn the worm gear driving the jackscrew. A clutch on the motor-drive shaft allows the worm gear to be manually operated in case both motors fail.

The electric-power wiring in the proposed interface would have a capacity of 8 kW at 28 to 33 Vdc. The data-transfer connections would handle scientific data at rates to 5 megabits per second, control and display (20 circuits), caution and warning (2 circuits), a bi-directional data bus (1.024 MHz), hardware commands at 1 megabit per second, and telemetry at 4 kilobits per second. Each of two coolant circuits (four lines) will carry 2,175 lb (987 kg) of Freon-21 coolant per hour with a pressure drop of no more than 5 lb/in.^{2} (34.5 kPa).

Since power, data, and coolant carriers will be distributed around a connector in a pattern unique to each umbilical mechanism, some way of orienting one berthing frame with respect to the other will be needed. Each carrier pair — whether for power, data, or coolant — will need fine adjustment so that mismatches introduced in manufacture or assembly can be corrected. In addition, a fluorocarbon-coolant connection in vacuum may need special design provisions.

This work was done by Gene C. Burns of McDonnell Douglas Corp. for **Johnson Space Center.** *No further documentation is available.*

MSC-20242

Reusable High-Pressure Connector

Connector for tests at 9,000 psi requires only minimal modification to the free end of the fluid line.

Lyndon B. Johnson Space Center, Houston, Texas

A fluid-line connector for high-pressure tests has a split ferrule, a nut, and an O-ring seal. Following a test, the ferrule nut, and O-ring fitting are removed, leaving the line unaltered except for a bushing brazed to its free end.

Previously, a tapered polytetrafluoroethylene ring was used for fluid-line tests on the Space Shuttle orbiter. However, the seal frequently deformed at the 9,000-psi (62-MPa) test pressure, causing a sudden pressure loss and occasional "blowoff" of fittings.

In the new design (see figure), only the male part of the joint is brazed to the fluid line. The brazed bushing serves as a base for the split ferrule.

To prepare the line for a test a nut is slipped over the brazed male part of the joint, and the ferrule halves are captured by the nut. The male part is inserted in the female part, and the nut is tightened. A recessed O-ring in the female part assures a leakproof seal. After the test, the connection is removed, leaving the tubing free for connection to another line. The nut and split ferrule are reusable for tests on other fluid lines.

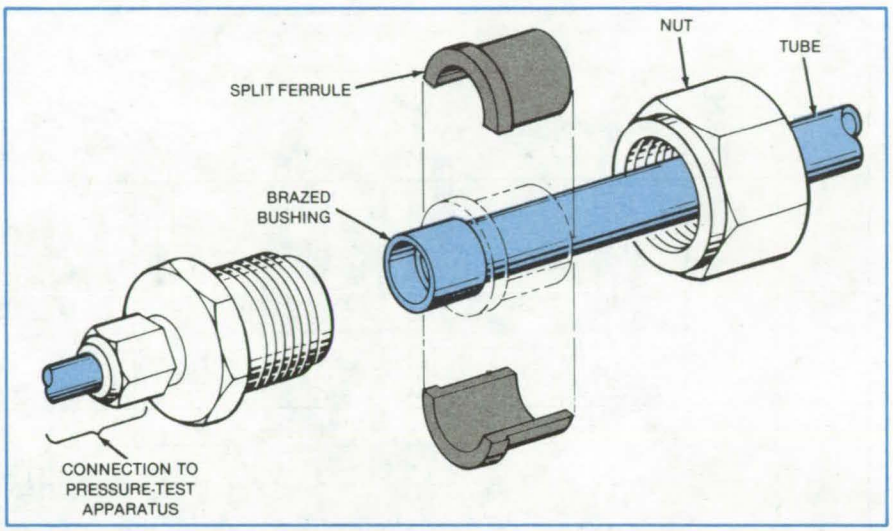

The **Improved Fluid-Line Connector** assures a strong joint for high-pressure testing without redundant parts requiring post-test debrazing. Its use has resulted in considerable savings in time and cost.

This work was done by Hans-Ove C. Jensen, Howard M. Maltby, and John A. Stein of Rockwell International Corp. for **Johnson Space Center.** *For further information, Circle 61 on the TSP Request Card.*

Inquiries concerning rights for the commercial use of this invention should be addressed to the Patent Counsel, Johnson Space Center [see page A5]. Refer to MSC-20339.

Retaining-Ring Installation Tool

Simple piston device speeds up assembly.

Marshall Space Flight Center, Alabama

A tool installs spiral-wound retaining rings quickly, reliably, and safely. The tool inserts rings in splined or irregularly shaped bores, bores at the bottom of deep holes, and other limited-access installations.

The tool consists of a piston in a tube (see figure). A user inserts a retaining ring into the tube through a slot and places the tube over the bore into which the ring is to be inserted. The user pushes the piston handle, which squares the ring in the bore and pushes it along the bore until it engages the ring groove in the bore.

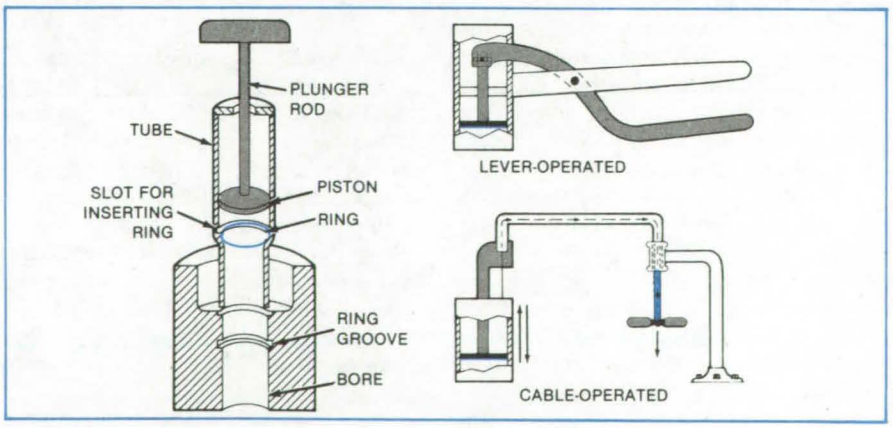

A **Piston in a Tube** squares the spiral ring and slides it along the bore until it nests in its groove (left). The piston can be moved by a variety of linkages (right).

The tube inside diameter should be 0.127 millimeter (0.005 inch) smaller than the bore diameter. The piston diameter should be 0.051 millimeter (0.002 inch) smaller than the tube inside diameter.

Previously, a pair of pliers or a screwdriver was used to install spiral rings. The new tool eliminates damage to the ring through improper tool use. It provides a better-quality installation since there is less elastic deformation of the ring. Installation with the new tool is also less hazardous, since the ring cannot pinch, cut, or stab the user.

The piston-actuating mechanism can be varied to suit special installation conditions. For example, a lever or a cable mechanism can be used instead of a plunger to move the piston in close quarters.

This work was done by S. B. Christian of Rockwell International, for **Marshall Space Flight Center.** *No further documentation is available.*
MFS-19725

Machining Three Prongs on a Shaft

A simple tool reduces set-up and machining time.

Marshall Space Flight Center, Alabama

A slightly unorthodox tooling arrangement is used to machine three prongs on the end of a special-purpose wrench. The arrangement reduces the setup and machining time by more than 70 percent below that required to perform the same task on a milling machine using conventional methods.

A modified carbide-tipped spot-facing tool (see figure) is rotated at 1,400 to 1,600 revolutions per minute in a small milling machine and applied to the workpiece, which is held with its corners in the spaces of a three-cornered collet.

After one pass, the workpiece is loosened in the collet, rotated 120°, and retightened in the collet at the new position. The machining operation is repeated at the second position, followed by indexing to the third position for the final machining operation.

This work was done by Charles Hewitt of Rockwell International for **Marshall Space Flight Center.** *No further documentation is available.*
MFS-19729

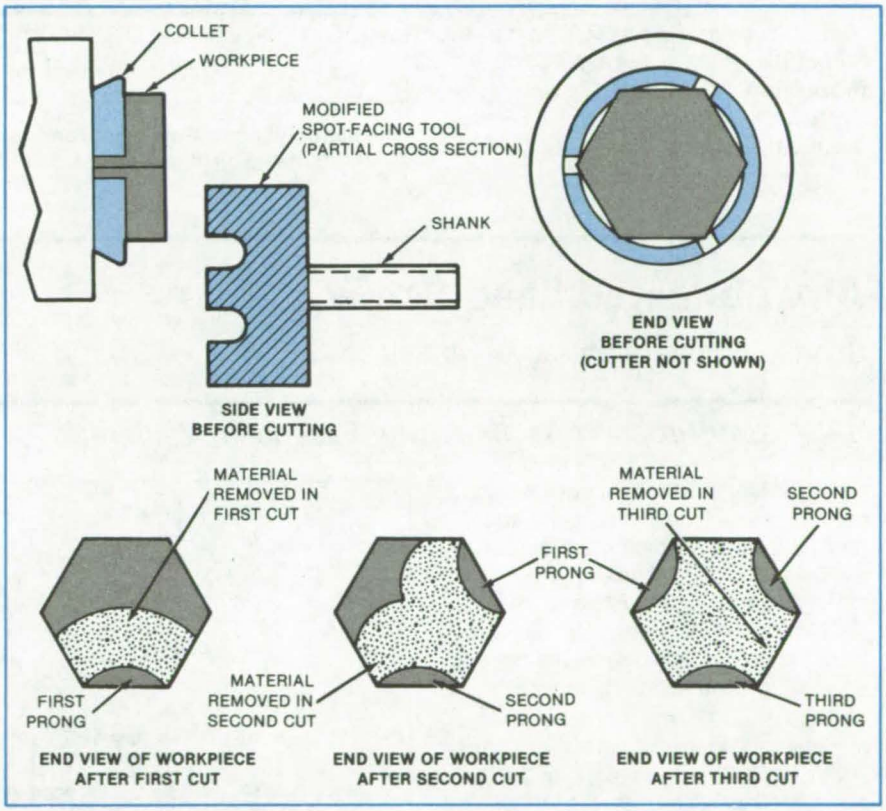

Time is Reduced for set-up and machining three prongs by this tooling arrangement.

Self-Cleaning Tubular-Membrane Module

Cleaning proceeds continuously, without hindering processing.

NASA's Jet Propulsion Laboratory, Pasadena, California

Tubular membranes of the type used to concentrate milk, sugar solutions, and soup — and in many other food- and drug-processing applications — may be made self-cleaning with the aid of a flow-reversing valve. The proposed scheme is expected to reduce the frequency and duration of shutdowns for cleaning.

The method has been suggested as a solution to some nagging problems in membrane processing: the clogging of

(continued on next page)

membrane pores, the formation of a hard gel layer on the membrane surface and, changes in the structure of the membrane material. To prevent irreversible fouling, a membrane processor must be stopped at least once a day and flushed — a time-consuming procedure that cuts production.

In the new method, sponge balls scrub the membrane surfaces as they travel inside the membrane tubes. A four-way flow-reversal valve automatically reverses the flow in the tubes at preset intervals so that the sponge balls reciprocate along the tubes (see figure). Baskets at the ends of the tubes prevent the sponges from escaping. The automatic cleaning feature can be added to existing membrane processing equipment with minimal modifications.

This work was done by Muhammad N. Sarbolouki of Caltech for **NASA's Jet Propulsion Laboratory.** *For further information, Circle 62 on the TSP Request Card.*
NPO-15245

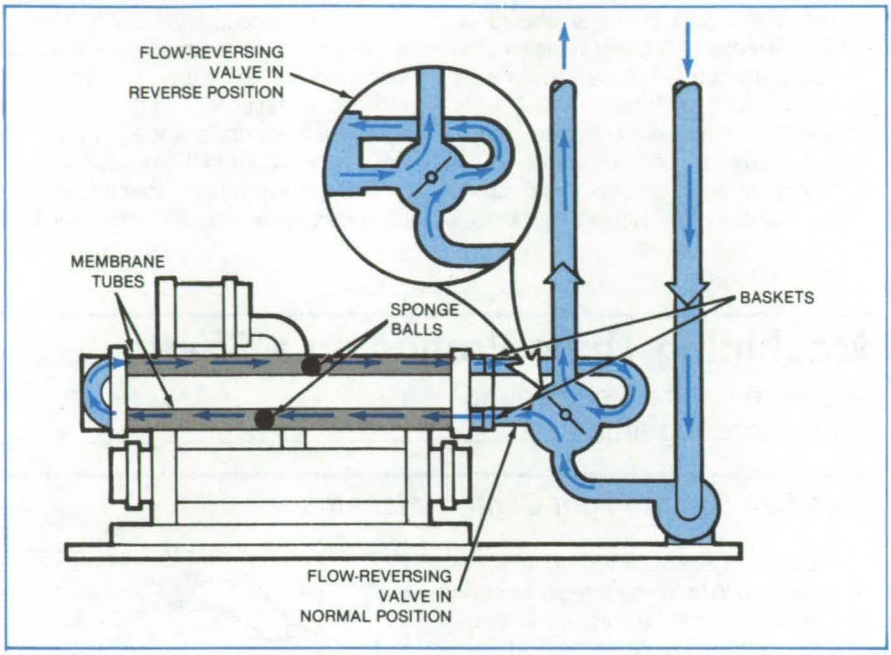

The **Back-and-Forth Motion** of sponge balls scrubs the membrane tubes. A flow-reversal valve alternates the direction of flow of the solution and sponges.

Air-Lubricated Lead Screw

Submicrometer accuracy is anticipated.

NASA's Jet Propulsion Laboratory, Pasadena, California

A translation stage under development at NASA's Jet Propulsion Laboratory rides on a cushion of compressed air. Originally developed to position precisely an interferometer retroreflector for airborne measurement of solar infrared radiation, the device will have a positioning accuracy of 0.25 micron.

The translation mechanism includes a metallic lead screw with 40 threads per inch (16 threads per centimeter) and a matched plastic nut that is fabricated in two half sections (see figure). Compressed air is injected into plenums in the two halves of the nut and from there is channeled into the passageway between the mating threads through 12 orifices (6 in each half of the nut) of 0.005-in. (0.127-mm) diameter. The plenums are formed by machining peripheral recesses and capping them with a cylindrical cover after boring the orifices.

The mating threads are finished to smoother than 5 μin. (0.127 μm). Because the clearance is minimal, com-

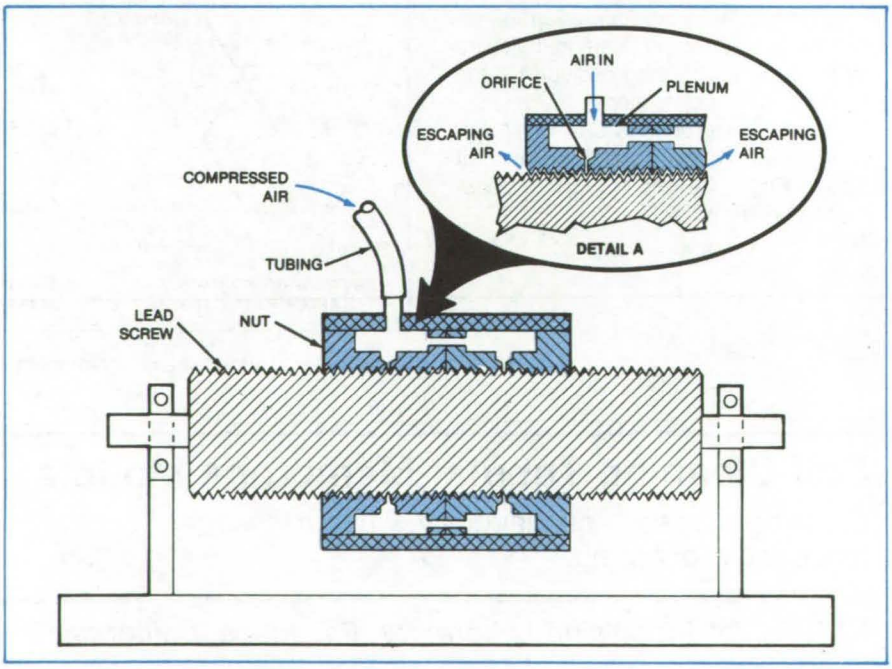

An **Air-Lubricated Lead Screw and Nut** are carefully machined to have closely matched, closely fitting threads. Compressed air is injected into the two plenums that encircle the nut and flows through orifices to lubricate the mating threads.

pressed air escapes very slowly. The fit between the mating threads provides a positive-clearance path for the compressed air to escape, and the air pressure on the threads provides a load-carrying capability.

This work was done by Gerald S. Perkins of Caltech for **NASA's Jet Propulsion Laboratory.** *For further information, Circle 63 on the TSP Request Card.*
NPO-15617

Computer Programs

These programs may be obtained at very reasonable cost from COSMIC, a facility sponsored by NASA to make new programs available to the public. For information on program price, size, and availability, circle the reference letter on the COSMIC Request Card in this issue.

Flow Through a Rotating Turbomachinery Blade Row

Full potential, transonic quasi-three-dimensional flow is calculated.

A computer program, QSONIC, has been developed for calculating the full potential transonic quasi-three-dimensional flow through a rotating turbomachinery blade row. The need for lighter, more efficient turbomachinery components has led to the consideration of machines with fewer stages, each with blades capable of higher speeds and higher loading. As speeds increase, the numerical problems inherent in the transonic regime have to be resolved. These problems include the calculation of imbedded shock discontinuities and the dual nature of the governing equations, which are elliptic in the subcritical flow regions but become hyperbolic for supersonic zones. QSONIC provides the flow analyst with a fast and reliable means of obtaining the transonic potential flow distribution on a blade-to-blade stream surface of a stationary or rotating turbomachine blade row.

QSONIC combines several promising transonic analysis techniques. The full potential equation in conservative form is discretized at each point on a body-fitted period mesh. A mass balance is calculated through the finite volume surrounding each point. Each local volume is corrected in the third dimension for any change in stream-tube thickness along the stream tube. The nonlinear equations for all volumes are of mixed type (elliptic or hyperbolic), depending on the local mach number. The final result is a block-tridiagonal matrix formulation involving potential corrections at each grid point as the unknowns. The residual of each system of equations is solved along each grid line. At points where the mach number exceeds unity, the density at the forward (sweeping) edge of the volume is replaced by an artificial density. This method calculates the flow field about a cascade of arbitrary two-dimensional airfoils. Three-dimensional flow is approximated in a turbomachinery blade row by correcting for stream-tube convergence and radius change in the through-flow direction.

Several significant assumptions were made in developing the QSONIC program, including: (1) the flow is inviscid and adiabatic, (2) the flow relative to the blade is steady, (3) the fluid is a perfect gas with constant specific heat, (4) the flow is isentropic and any discontinuities (shocks) are weak enough to be approximated as isentropic jumps, (5) there is no velocity component normal to the stream surface, and (6) the flow relative to a fixed frame in space (absolute velocity) is completely irrotational.

These assumptions place some limitations on the application of QSONIC. Sharp leading edges at high incidence and high-mach-number turbine-blade trailing edges with substantial deviation will both cause large velocity peaks on the blade. In addition, the program may have difficulty converging if the passage is nearly choked.

Input to QSONIC consists of case control parameters, a geometry description, upstream boundary conditions, and a rotor description. Output includes solution-scheme parameters and flow-field parameters. A data file is also output; it contains data on the solution mesh, surface mach numbers, surface static pressures, isomachs, and the velocity vector, field. These data may be used for further processing or for plotting.

The QSONIC is written in FORTRAN IV for batch execution and has been implemented on an IBM 370 series computer with a central memory requirement of approximately 500K of 8-bit bytes. QSONIC was developed in 1982.

This program was written by Charles A. Farrell, Jr., of **Lewis Research Center.** *For further information Circle M on the COSMIC Request Card.*
LEW-13832

Compressible Flow About Wind Turbine Blades

Program solves the three-dimensional potential equation for flow through an arbitrary rotor.

WIND numerically solves the exact, full-potential equation for three-dimensional, steady, inviscid flow through an isolated wind-turbine rotor. The program automatically generates a three-dimensional, boundary-conforming grid and iteratively solves the full-potential equation while fully accounting for the rotating and Coriolis effects. WIND is capable of numerically analyzing the flow field about a given blade shape of the horizontal-axis wind turbine.

The rotor hub is assumed representable by a doubly infinite circular cylinder. An arbitrary number of blades may be attached to the hub and these blades may have arbitrary spanwise distributions of taper and of the twist, sweep, and dihedral angles. An abritrary number of different airfoil section shapes may be used along the span as long as the spanwise variation of all the geometeric parameters is reasonably smooth.

The numerical techniques employed in WIND involve rotated, type-dependent finite differencing, a finite volume method, artificial viscosity in conservative form, and a successive overrelaxation combined with the sequential grid refinement procedure to accelerate the iterative convergence rate. Consequently, WIND is capable of accurately

(continued on next page)

analyzing incompressible and compressible flows, including those that are locally transonic and terminated by weak shocks. Along with the three-dimensional results, WIND provides the results of the two-dimensional calculations to aid the user in locating areas of posssible improvement in the aerodynamic design of the blade.

Output from WIND includes the chordwise distribution of the coefficient of pressure, the mach number, the density, and the relative velocity components at spanwise stations along the blade. In addition, the results specify local values of the lift coefficient and the tangent and axial aerodynamic force components. These are also given in integrated form expressing the total torque and the total axial force acting on the shaft. WIND can also analyze the flow around isolated aircraft propellers and helicopter rotors in hover, as long as the relative oncoming flow is subsonic.

WIND is written in FORTRAN IV for batch execution and has been implemented on an IBM 370 series computer with a central memory requirement of approximately 253K of 8-bit bytes. WIND was developed in 1980.

This program was written by Djorje S. Dulikravich of **Lewis Research Center.** *For further information, Circle N on the COSMIC Request Card.*
LEW-13740

Calculating the Flow Field in a Radial Turbine Scroll

Finite-difference and finite-element methods give flow solutions.

In many applications, radial turbines offer benefits over axial turbines. With advantages such as high efficiency over a range of speeds, less sensitivity to tip clearance, simplicity, and ruggedness, radial gas turbines are being used or considered for helicopter engines, automotive engines, small power systems, and a number of other applications.

A set of two computer programs calculates the flow field in a radial turbine scroll. These new programs represent an improvement in analyzing flow in radial turbine scrolls and provide the designer with tools for designing better scrolls.

One of the programs provides flow solutions in cross-sectional planes (perpendicular to the throughflow direction) of the scroll. The cross-sectional-plane solution employs a finite-difference method to determine the two-dimensional velocity-potential distributions on the selected planes. This program requires a throughflow velocity profile to be specified. The other program solves for the flow on a mid-channel plane (blade-to-blade direction) through the entire scroll-nozzle assembly. A finite-element method is employed to obtain the two-dimensional imcompressible midchannel plane solution.

Input for both programs consists primarily of the inlet flow conditions and overall geometric conditions. Output from both programs includes the flow velocity and direction at the specified mesh points or nodes. Results of the cross-sectional-plane computations may also be output in the form of plots of constant-potential contours, with arrows indicating the velocity directions.

These programs are written in FORTRAN IV for batch execution and have been implemented on an IBM 370 series computer with the largest program having a central-memory requirement of approximately 590K of 8-bit bytes. Plotted output is generated for a CALCOMP plotter. These programs were developed in 1977 and 1979.

These programs were written by E. Baskharone, S. Abdallah, A. Hamed, and W. Tabaoff of the University of Cincinnati for **Lewis Research Center.** *For further information, Circle P on the COSMIC Request Card.*
LEW-13437

Fabrication Technology

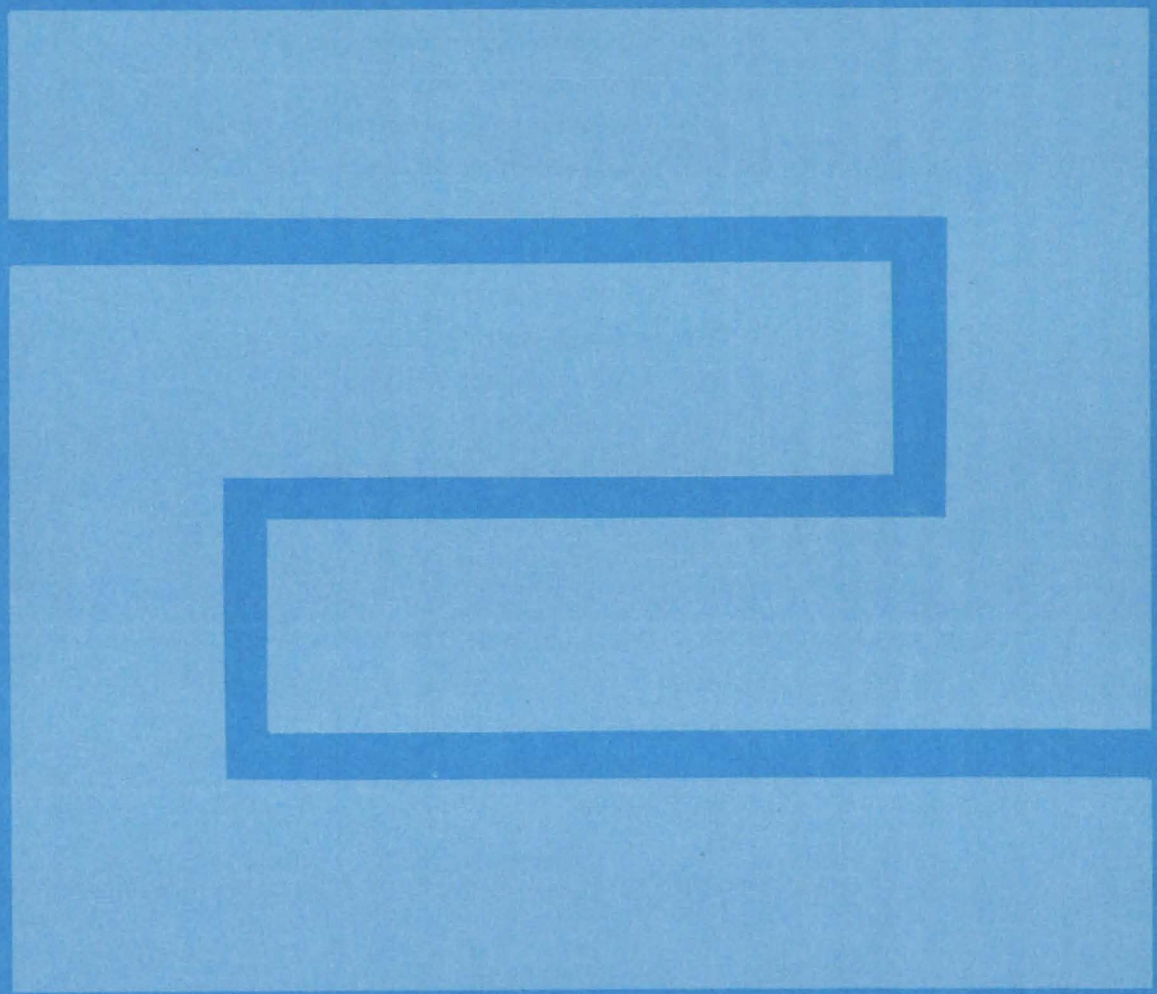

Hardware, Techniques, and Processes

Curved Caps Raise Corrugation Strength

Construction concept would increase the strength-to-weight ratio of corrugated panels.

Langley Research Center, Hampton, Virginia

Flat caps are replaced by curved caps in a new concept for constructing corrugated panels. The curvature would significantly increase the buckling strength over that of previous panels. Also changed is the beaded web of the conventional panel, which was previously reduced to a single thickness at the point of attachment to the cap. In the new design, the web is moved under the cap strip edge to spread the attachment over more of the cap. The wider joint restrains the cap, enabling it to carry its design load without edge rotation or premature buckling.

Figure 1 illustrates conventional corrugated-panel construction. A thin metal sheet is formed to make the beaded web and to form flat edges for bonding the cap strips. The caps are separate strips bonded to the corrugated segment. The beaded web is reduced to a single sheet thickness at the edge of the cap strips.

The new design is seen in Figure 2. A curved cap replaces the flat cap, and the web edge is no longer reduced to a straight line at the attachment point. The resulting cap is more resistant to buckling, and the edge joint at the web/cap intersecton is less susceptible to rotation. The beaded-web corrugation makes use of superplastically formed and diffusion-bonded technology for its construction. Corrugated panels fabricated this way would have high strength-to-weight ratios and would be attractive as primary construction materials for aircraft and other structures.

As with conventional panels, structures of any width can be made by repeating any number of corrugation segments. Alternate configurations include the cap strips being curved inward to improve the damage resistance of the curved-cap beaded-web corrugation. Also, the edges of the cap strips can be extended and crimped over the beaded webs, improving the damage resistance of the caps and further stabilizing them against buckling.

This work was done by Randall C. Davis, Thomas T. Bales, Dick M. Royster, and L. Robert Jackson of **Langely Research Center.** *For further information, Circle 64 on the TSP Request Card.*

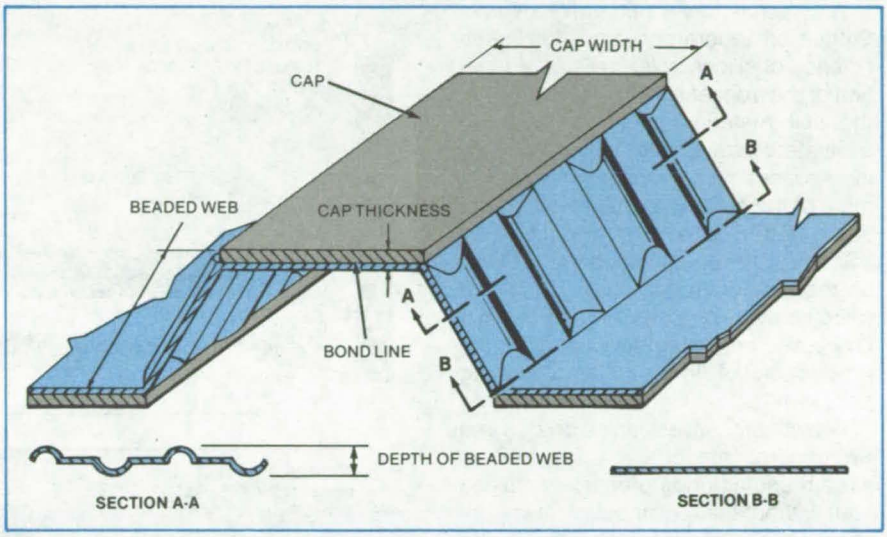

Figure 1. **Conventional Corrugated-Panel Geometry** shows beaded-web corrugation core with flat cap strips, to carry the compressive load. The thickness-to-width ratio of the cap determines its ability to resist local buckling.

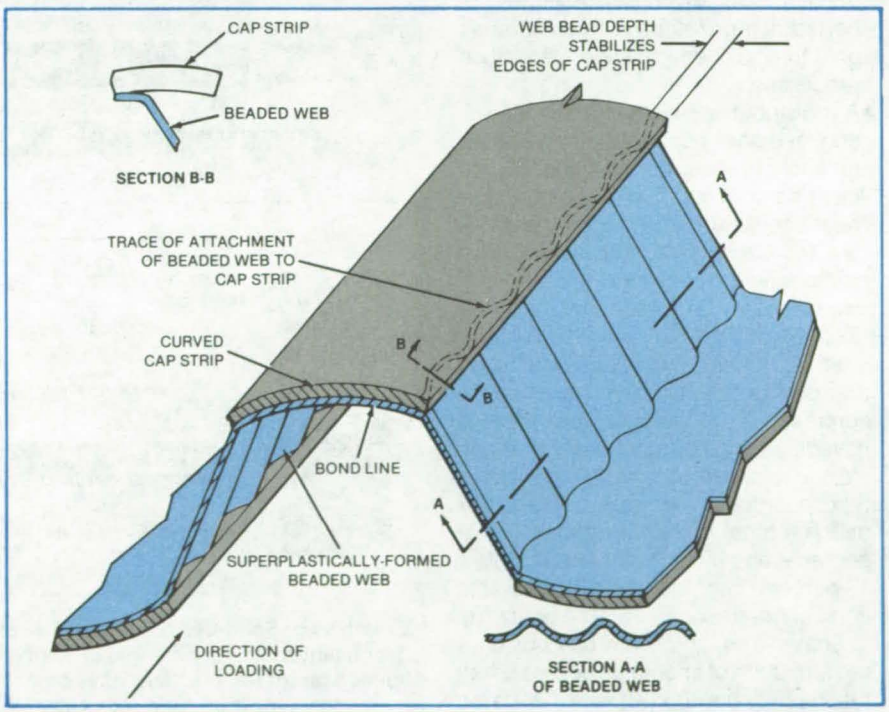

Figure 2. The **New Geometry** utilizes a curved cap for a wider cap/web attachment. Beading the web prevents local buckling in the web while allowing maximum separation between the cap strips. This geometry offers a significant weight saving over the conventional geometry for a wide range of loading.

This invention is owned by NASA, and a patent application has been filed. Inquiries concerning nonexclusive or exclusive license for its commercial development should be addressed to the Patent Counsel, Langley Research Center [see page A5]. Refer to LAR-12884.

Solar-Cell Slide Rule

Slide rule relates efficiency, impurity types, impurity concentrations, and process types.

NASA's Jet Propulsion Laboratory, Pasadena, California

A slide rule developed at NASA's Jet Propulsion Laboratory calculates the efficiency of silicon solar cells as a function of the concentration of impurities in the cell material. It can be used to evaluate crystal-growth methods involving sequential or continuous replenishment of the melt. The slide rule is useful because the effects of impurities on solar-cell performance depend not only on the type of impurity but also on the silicon-growth process — and various processes are being developed for the production of low-cost photovoltaic cells.

Growth processes can be divided into two general categories:

- The manufacturing process is carried out without the redistribution of impurities in the silicon feedstock; that is, the impurity distribution in the finished solar cell is essentially the same as that in the feedstock. Examples are edge-supported film growth, silicon-on-ceramic growth, and chemical-vapor-deposition processes.
- A redistribution of impurities in the silicon feedstock occurs in the cell-manufacturing process during unidirectional freezing of silicon from the melt under near-equilibrium conditions. Examples are the Czochralski process with and without replenishment of the melt, the web dendrite process, and the heat-exchanger process.

Scales 1 and 2 on the rule (see figure) are used to calculate the tolerable concentration of an impurity when there is no redistribution of impurities. For example, the rule is set for iron (A). The impurity concentration in atomic parts per million (ppma) is read for the allowable degradation in cell efficiency. For a 10-percent degradation, the allowable iron concentration is 7×10^{-3} ppma (B).

Scales 3, 4, and 5 are used when a redistribution of impurities occurs First, the impurity-buildup (IB) factor is determined. For five sequential replenishments (C), the IB factor is 46 if 90 percent of the melt is grown between replenishments (D). If iron is set at this IB factor (E), the tolerable iron concentration in the silicon feedstock is then 23 ppma for a 10-percent degradation in cell performance (F).

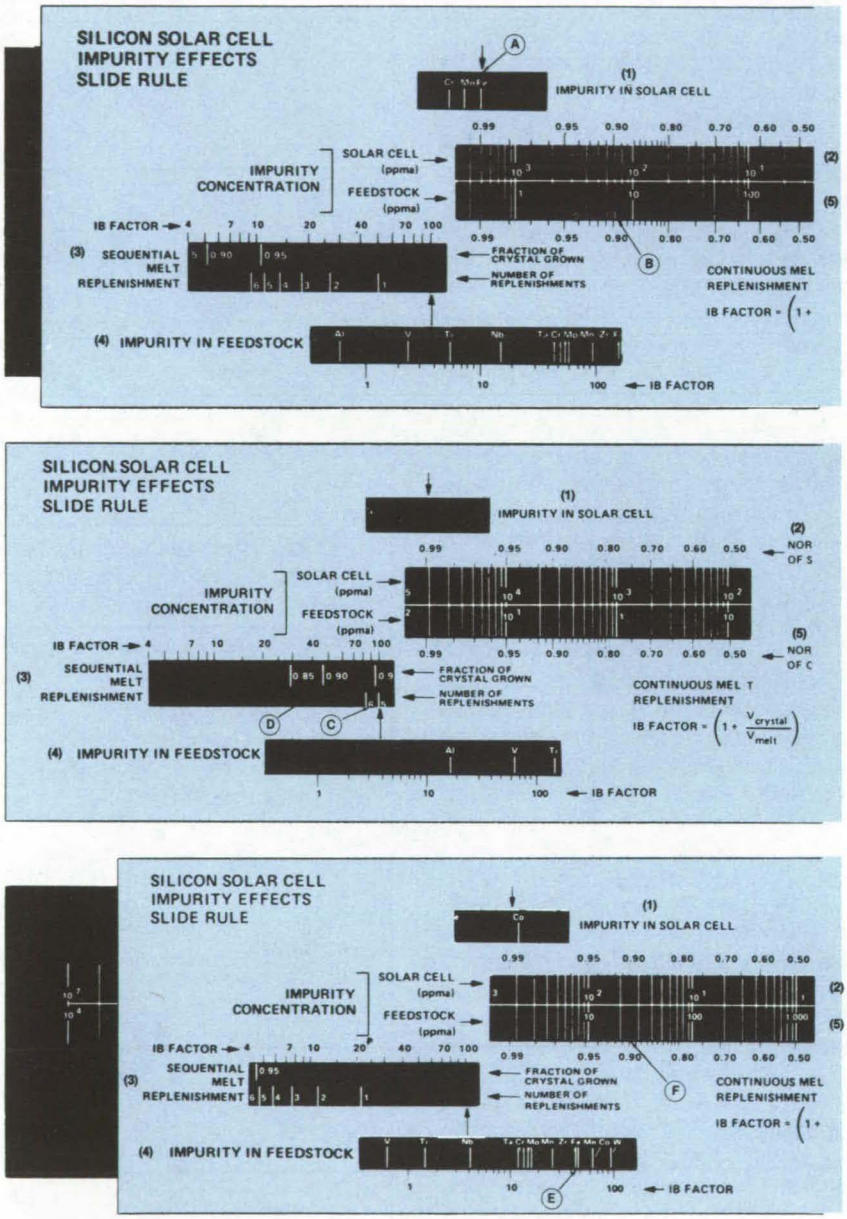

Examples of Solar-Cell Slide-Rule Calculations are determination of allowable impurity concentration for a nonredistributive process (top), determination of the impurity-buildup factor for a redistributive process (middle), and determination of allowable impurity concentration for a redistributive process (bottom).

This work was done by Kazuo A. Yamakawa of Caltech for **NASA's Jet Propulsion Laboratory.** *For further information, Circle 65 on the TSP Request Card.*

NPO-15646

Ultrasonics and Optics Would Control Shot Size

Uniformly-sized silicon shot would be produced by a proposed feedback system.

NASA's Jet Propulsion Laboratory, Pasadena, California

A proposed feedback system would assure the production of silicon shot of uniform size. The new control method is particularly advantageous in that constant size could be maintained even while other process variables are changed deliberately or inadvertently (for example, the increase in nozzle diameter with erosion).

As shown in the figure, a piezoelectric ultrasonic transducer is placed on the nozzle to vibrate the silicon stream. The shot size is determined, in part, by the wavelength of vibrations in the liquid stream as it breaks up into drops. Thus, the vibration frequency can be varied to control the shot size.

The drops fall through a light beam/photodetector apparatus that measures their size. The photodetector output is used to control the vibrator frequency and thus to maintain shot size at the desired value.

While the new control system was proposed for silicon-shot production, it is applicable to other materials as well. Some experimentation will be necessary to determine nozzle diameters, drop sizes, vibration frequencies, and other process variables for each material.

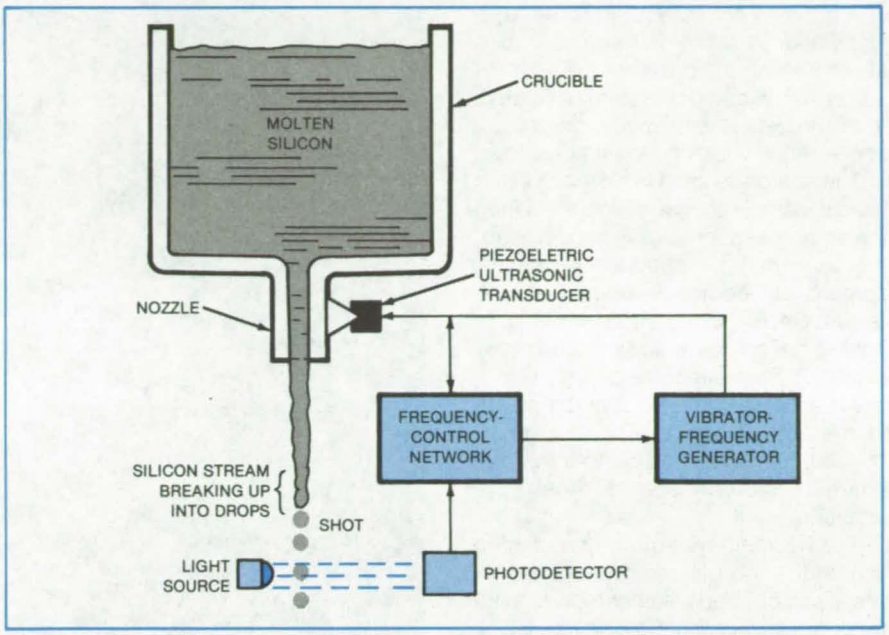

The Breakup of a Silicon Stream Into Drops is controlled, in part, by varying the frequency of vibrations imparted to the stream by an ultrasonic transducer. Drop size is monitored by the photodetector.

This work was done by Andrew D. Morrison of Caltech for **NASA's Jet Propulsion Laboratory.** *For further information, Circle 66 on the TSP Request Card.*
NPO-15608

Reinforcement for Stretch Formed Sheet Metal

Metal reinforcement is flame-sprayed on the edges gripped in the stretch-forming setup.

Lyndon B. Johnson Space Center, Houston, Texas

The tearing of aluminum sheet metal during stretch forming is prevented by flame spraying a layer of aluminum on the edges held in the stretch-forming machine. The technique improves the grip of the machine on the metal, and the reinforced sheet is better able to withstand the concentration of force in the vicinity of the grips.

In fabricating manifold covers for radiators on the Space Shuttle orbiter, the thickness of 0.016-inch (0.41-mm) sheet was increased by 0.005 to 0.016 inch (0.13 to 0.41 mm) by flame spraying. In this application, conventional commercially-available flame-spray equipment was used.

The flame-spray reinforcement technique should be applicable to other metals besides aluminum. It should be particularly helpful in custom, limited-run applications.

This work was done by John B. Lea and Charles R. Baxter of Vought Corp. for **Johnson Space Center.** *No further documentation is available.*

Inquiries concerning rights for the commercial use of this invention should be addressed to the Patent Counsel, Johnson Space Center [see page A5]. *Refer to MSC-20228.*

Hot-Melt Adhesive Attachment System

An adhesive "system" is effective on Earth and in space.

Langley Research Center, Hampton, Virginia

A hot-melt adhesive attachment system works as well in vacuum as it does at atmospheric pressure. The new adhesive attachment system uses electronic heaters to warm a fiberglass cloth impregnated with a hot-melt adhesive.

The fiberglass cloth is mounted in the head assembly shown in Figure 1. When the adhesive reaches melt temperature, the head may be attached to metals, composites, ceramics, and other materials. Once it is attached, the head is cooled rapidly for a quick "stick" (see Figure 2). For normal release, current is again applied to the electronic heaters to melt the adhesive. For emergency release, current is applied to a thermoelectric cooler/heater to melt the adhesive.

The hot-melt system can be used in space or at normal atmospheric pressure. It can be used to tether tools or to attach temporary scaffolding to walls, buildings, or beams.

Electronic temperature-control boxes set the hot melt to any desired temperature from room temperature to above 250° C with ±2° C variation. Each head contains one foil heater, a fiberglass cloth, the hot-melt adhesive, a thermocouple, a heat sink, and a retainer ring.

The foil heater melts the hot-melt adhesive in preparation for an attachment or a detachment. Current is applied in either direction to the thermoelectric cooler/heater, depending on whether heating for emergency release or cooling for attachment is desired. In normal use, the cooler quickly cools the hot melt.

This work was done by Robert L. Fox, Alan W. Frizzell, Bruce D. Little, Donald J. Progar, Robert H. Coultrip, Richard H. Couch, Bland A. Stein, John D. Buckley, and Terry L. St. Clair of **Langley Research Center** *and John R. Gleason of AVRADCOM. No further documentation is available.*

This invention is owned by NASA, and a patent application has been filed. Inquiries concerning nonexclusive or exclusive license for its commercial development should be addressed to the Patent Counsel, Langley Research Center [see page A5]. Refer to LAR-12894.

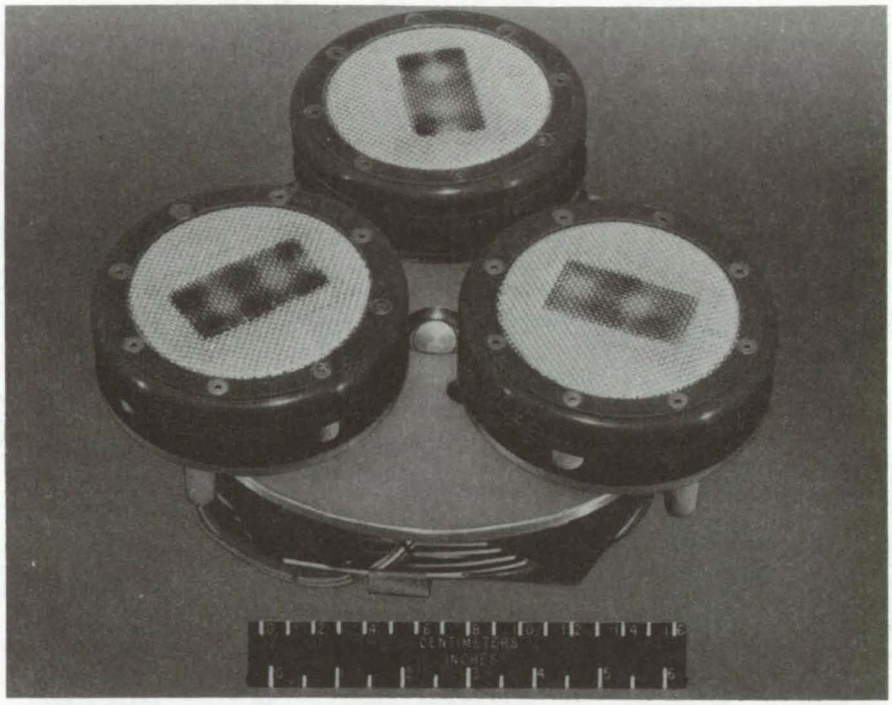

Figure 1. A **Three-Head Assembly** with fiberglass cloth impregnated with hot-melt adhesive

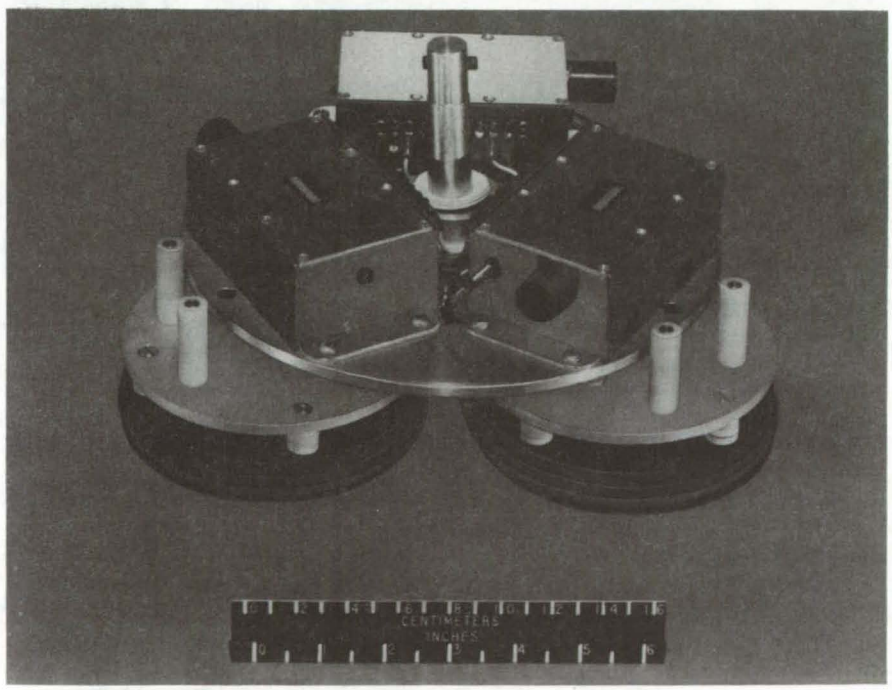

Figure 2. A **Thermoelectric Cooler/Heater and Heat Sink** quickly cool the hot-melt adhesive.

High-Absorptance Radiative Heat Sink

A change in geometry improves the absorptance of a black honeycomb surface.

Goddard Space Flight Center, Greenbelt, Maryland

The absorptance of black-painted open-cell aluminum honeycomb is improved by cutting the honeycomb at an angle or bias rather than straight across (see figure). This ensures that at least two specular reflections occur before energy entering the honeycomb cavities escapes. At each reflection the radiation is attenuated by absorption.

Bias-cut honeycomb enhances the absorptive or emissive properties of surfaces relatively inexpensively. Its applications may include space-background simulators, space radiators, solar absorbers, and passive coolers for terrestrial use.

In constructing a radiative cooler, honeycomb is cut on a bias prior to expanding it to form the open cells. After expansion, the honeycomb is dipped in high-gloss black paint, cured, and then bonded to the aluminum plate, using a thin layer of cryogenic adhesive. After adhesive curing, the bottoms of the honeycomb cells are sprayed with the glossy black paint, using an airless sprayer to minimize paint buildup on the outer edges of the honeycomb. (The edges should be knifelike to minimize single-bounce specular reflections from them. Glossy paint (rather than mat) is used to avoid single-bounce backscattering of the incident radiation.

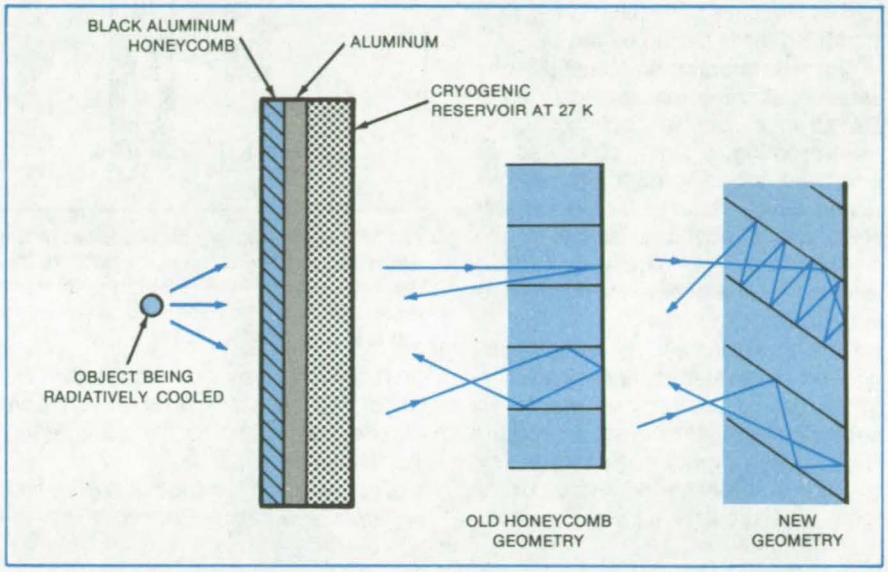

A **Honeycomb-Surface Radiation Sink** is used in a space-background simulator. The new bias-cut honeycomb cell geometry guarantees that at least two specular reflections occur before the incident radiation escapes. With straight-cut honeycomb geometry, incident radiation from some directions escapes after just one reflection. The bias-cut geometry yields an overall absorptance closer to unity. Sample radiation paths are shown in color.

This work was done by T. Cafferty of Hughes Aircraft Co. for **Goddard Space Flight Center.** *No further documentation is available.*

This invention is owned by NASA, and a patent application has been filed. Inquiries concerning nonexclusive or exclusive license for its commercial development should be addressed to the Patent Counsel, Goddard Space Flight Center [see page A5]. Refer to GSC-12739.

Rewaterproofing Silica Tiles

A waterproofing agent is deposited deep into pores.

Lyndon B. Johnson Space Center, Houston, Texas

A new technique applies waterproofing agents to silica tiles. Originally developed to rewaterproof surface-insulation tiles of the Space Shuttle orbiter, the technique might also be used to waterproof concrete brick walls, and other porous articles.

A portion of the initial waterproofing agent burns out after each Space Shuttle flight. If the hard exterior coating is damaged, then water can be absorbed in nonwaterproofed zones. The absorbed water may then cause a tile failure because of freezing and subsequent cracking.

The rewaterproofing system includes a gas supply of any nonreactive gas, such as N_2, that can be operated at about 80° F (27° C) and at pressures ranging from 0 to 5 psi (0 to 34.5 kN/m^2), a bubbler that allows the gas to bubble through a solution of the waterproofing agent, and a cover plate that can be temporarily sealed over the tile surface (see figure). The N_2 gas flows through a flowmeter to the bubbler where it entrains some of the waterproofing agent and carries the agent to the tile surface. The entrained waterproofing agent then flows into the tile through a small hole in the tile coating.

(continued on next page)

Flow rates of 10 to 20 ft^3/h (0.3 to 0.6 m^3/h) with exposure times of 0.25 to 2 minutes provide adequate rewaterproofing in the Space Shuttle application. A vapor pressure of 20 torr (2.7 kN/m^2) at room temperature is sufficient to provide the necessary amount of waterproofing material. Under these conditions, generally less than 1 g of fluid is vaporized, resulting in a less-than-0.1-g mass pickup by the tile.

The waterproofing agent used is hexamethlydisilazane maintained at 80° F (27° C) in a suitable container. Other waterproofing agents can also be employed, including methyl-trimethoxysilane, which requires activation with acids, such as acetic acids. In that case, the activating agent is first introduced, followed by the similar introduction of the waterproofing agent.

Flow conditions can be varied to provide proper waterproofing deposition. By increasing the temperature of the waterproofing agent, the vapor pressure is increased, producing shorter exposures at the same flow rates or the same exposure time at lower flow rates.

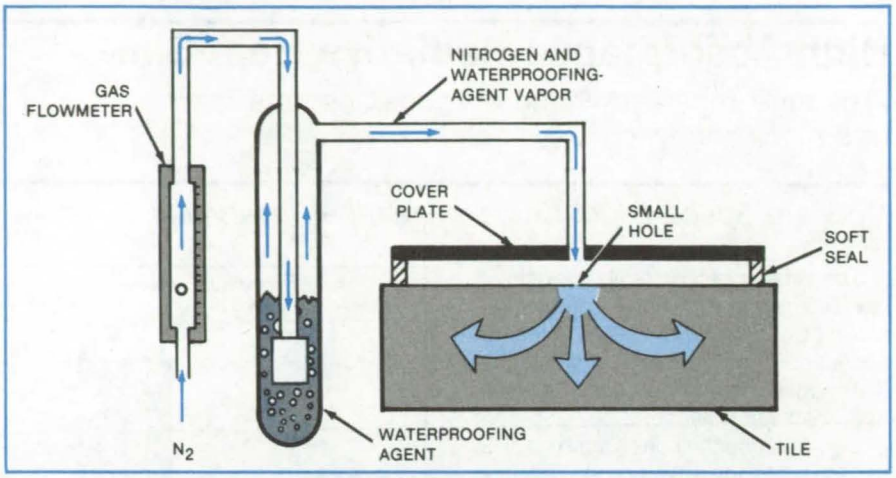

The **Waterproofing Agent,** vaporized in the bubbler, is transported by the gas flowing in the system and deposits in the pores of the tiles. The vapor is carried through a hole of approximately 1/16-inch (1.6-mm) diameter that has been made in the tile coating. The technique could be used also to waterproof buildups (concrete and brick) and possibly fabrics.

This work was done by Lubert J. Leger and Donald C. Wade of **Johnson Space Center.** *No further documentation is available.*

This invention is owned by NASA, and a patent application has been filed. Inquiries concerning nonexclusive or exclusive license for its commercial development should be addressed to the Patent Counsel, Johnson Space Center [see page A5]. Refer to MSC-20340.

Gas-Jet Meniscus Control in Ribbon Growth

Analysis finds jet parameters to control thickness of ribbon pulled vertically from melt.

NASA's Jet Propulsion Laboratory, Pasadena, California

The use of a gas jet has been proposed to control the shape of the meniscus and thus to regulate ribbon thickness in vertical silicon-ribbon growth. The gas jet would also cool the ribbon, increasing the maximum possible pull speed. The meniscus shape and stability has been analyzed for various jet geometries.

The gas-jet method is meant to replace the method in which the thickness is controlled by pulling the ribbon between two flat plates. A major deficiency of that approach is that the plates do not directly control the shape of the liquid meniscus. Fluctuations in the meniscus height can occur due to variations in melt temperature and pull speed. A change in meniscus height causes a change in the contact angle at the vapor/liquid/solid junction, resulting in nonuniform ribbon thickness.

The meniscus analysis problem was treated as two-dimensional; that is, the meniscus shape was assumed to be the

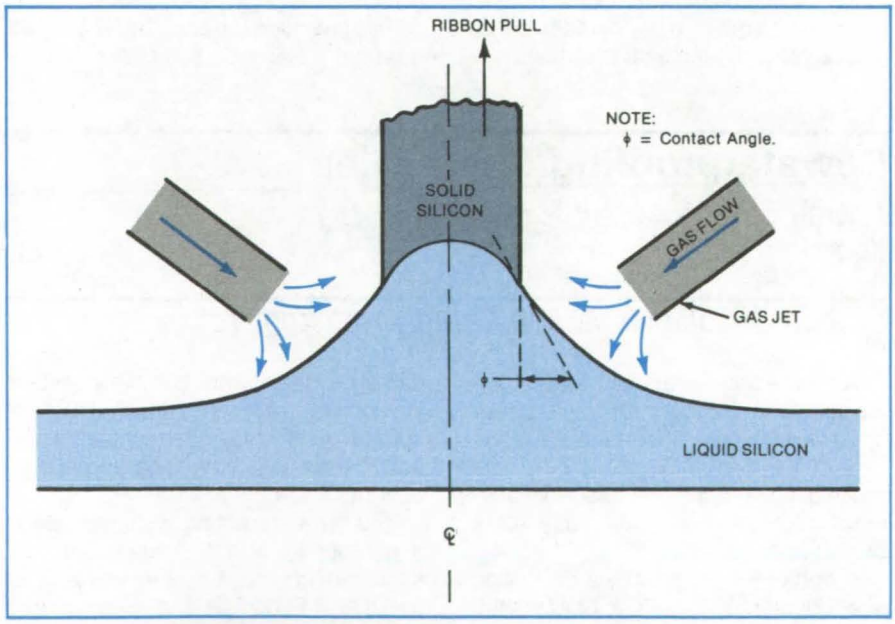

A **Gas Jet Controls the Meniscus Contact Angle** at the solid/liquid interface. For silicon, a contact angle of 11° ± 1° is required for constant-thickness ribbon growth. The cooling effect of the gas jet increases the maximum possible pull speed.

same at all points across the ribbon. End effects due to finite ribbon width were not studied. The analysis starts with a differential equation describing the equilibrium meniscus in terms of the surface tension, material density, and applied gas-jet pressure. That equation together with appropriate boundary conditions determine the theoretical meniscus shape. Since the integration of the differential equation involves elliptic integrals of the first kind and second kind, numerical integration is required to obtain the solution.

The contact angle for equilibrium silicon-ribbon growth has previously been determined to be 11° ± 1°. According to the theoretical numerical results, this contact angle occurs at a meniscus height of 7.0 mm with no gas flow. Effective control of the contact angle should allow for both positive and negative changes in meniscus height. To allow a reasonable swing in meniscus height while maintaining constant contact angle, the meniscus-control arc length (nozzle height) should be kept to a minimum. Small gas-jet height also helps to maintain nonturbulent (laminar) gas flow.

An argon gas jet with a 0.5-mm nozzle height placed at the solid/liquid/atmosphere contact point will allow a total swing of 3 mm in meniscus height while maintaining an 11° contact angle if the mean meniscus height is 5.5 mm. At that height, the gas flow required is 8 liters/minute per centimeter of ribbon width. A swing up to 7 mm meniscus height would reduce the required gas flow to zero; a drop to 4 mm would require 11 l/min, which corresponds to a gas velocity of 30 m/s and a Reynolds number of about 1,500, which is within the laminar-flow region. This high flow rate would require gas recirculation to be economical.

This work was done by John A. Zoutendyk and Oldwig vonRoos of Caltech for **NASA's Jet Propulsion Laboratory.** *For further information, Circle 67 on the TSP Request Card.*
NPO-14978

Attitude Control by Localized Outgassing

Reaction forces and torques would be generated by vaporizing material with a laser.

NASA's Jet Propulsion Laboratory, Pasadena, California

The orientation of a freely floating object can be controlled by vaporizing material from its surface. In a test, the orientation of a levitated sample in an acoustic chamber was controlled by directing a laser beam or an intense focused light beam at points on the surface of the object (see figure). Another test was run under simulated zero-gravity conditions in an airplane.

The laser heats the material (such as a glass, metal, or any compound) that will sublime or outgas. To obtain a torque the reaction force vector from the subliming material must not pass through the center-of-mass of the object. This can be achieved either by heating a rough surface with a nearly tangential beam.

A laser would provide a beam suitable for controlling objects in noncontact manufacturing processes in acoustic-levitation chambers. Precise control should be possible since the energy transferred by the laser beam can be accurately controlled both in amount and direction.

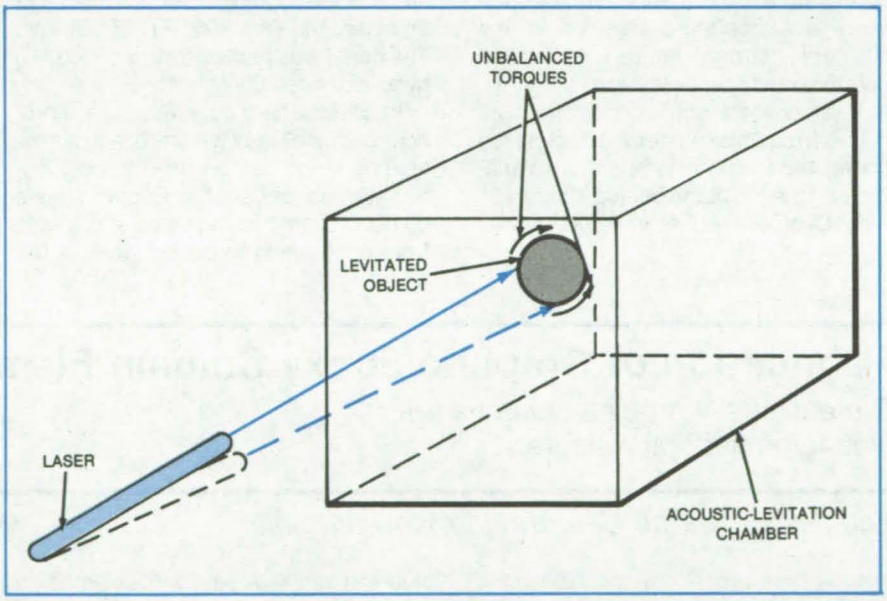

Attitude Control of a levitated object was achieved by using a laser to vaporize selectively a sublimate coating.

This work was done by Daniel D. Elleman, Taylor G. Wang, and Arvid Croonquist of Caltech for **NASA's Jet Propulsion Laboratory.** *For further information, Circle 68 on the TSP Request Card.*
NPO-15575

More-Uniform Heat Curing for Structural Repairs

A copper lining helps to distribute the heat under a heating blanket.

Lyndon B. Johnson Space Center, Houston, Texas

Repairs and the construction of large structures made of graphite/epoxy composites or other materials are aided by a technique that ensures more uniform heating during curing. A layer of copper sheet is placed between the heating blanket and the structure. Since the copper has a much higher heat conductivity than do typical composite structural materials, the copper smooths the uneven temperature distribution that would otherwise result from hotspots in the heating blanket.

In one application, for example, "beefup" straps are bonded to the original structural surface. The adhesive is cured by heat applied by electric strip heaters 6 in. (15.2 cm) wide. In some hotspots, temperatures are as much as 90° F (50° C) above the average temperature. Thus, even though the average temperature may be in the allowable curing range, local temperatures may be excessive.

Insertion of a soft copper sheet 20 mils (0.5 mm thick) under the heater (see figure) reduced the temperature variations on the top of the beefup strap to 5° F (3° C) or less. Adhesive temperatures were maintained between 232° and 258° F (111° to 126° C) — within the limits prescribed by the process specifications. The temperature of the facesheet of the bonding strap was maintained at less than the 350° F (177° C) limit. The panel was heated to 145° F (63° C) by a separate 200-W heater.

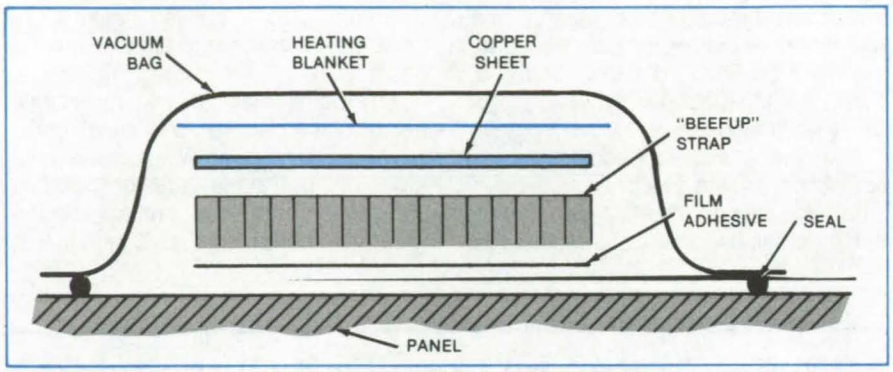

Bond-Curing Setup employs a heating blanket over a copper sheet within a vacuum bag. The copper sheet smooths out the temperature distribution under hotspots in the heater.

In cases where edge effects are pronounced, individually-controlled narrow heating strips can be used in conjunction with copper sheets. Copper sheets do not prevent heating strips or blankets from conforming to the surfaces of the parts or interfere with vacuum bagging. Copper sheets, used with flexible heat blankets, can also help to dry surfaces while preventing heat damage to them. Moreover, the method is applicable to uniformly heating such low-thermal-conductivity metals as titanium or stainless steel.

This work was done by Paul E. Bauer and Michael A. Walker of McDonnell Douglas Corp. for **Johnson Space Center.** *No further documentation is available.*
MSC-20101

Fabrication of Graphite/Epoxy Column Elements

Dimensionally precise columns are wound on vertical mandrels.

Langley Research Center, Hampton, Virginia

In a new procedure for fabricating graphite/epoxy column elements, the dry fiber is wound on a tapered aluminum mandrel in a vertical winding machine, and resin is injected between the mandrel and an outer sleeve. The winding and injection are done at elevated temperature to minimize the thermal-expansion problems that arise during curing of the resin.

Tapered columns proposed for the construction of large space platforms are comprised of two half columns snapped together at a center joint (see figure). Graphite/epoxy was selected for the fabrication of these columns because of its high modulus-to-density ratio and near-zero coefficient of thermal expansion.

To demonstrate the new process, graphite half columns 102 inches (2.59 m) long, representative of longer columns, were fabricated. The columns tapered from a diameter of 4 inches (10.16 cm) at one end to 2 inches (5.08 cm) at the other end. This taper permits the columns to be stacked like paper cups to make maximum use of the weight capability of the Space Shuttle. Tight tolerances are required on both the inside and outside diameters to ensure efficient stacking. For future space applications, half columns in excess of 33 feet (10 m) in length may be needed; and the fabrication process can be expanded to meet this requirement.

A hot process was selected to avoid separating the integrally-wound aluminum fittings from the column during cure. The aluminum mandrel length increases about 0.25 inch (63.5 mm) during heatup for cure and drives the end

fittings with it. The use of a heated mandrel during fiber placement precludes the presence of resin during fiber placement. Therefore a resin injection process was developed. Hard tooling, both inside and out, is used to control the column wall thickness.

The vertical process produces the precise straight columns required to make stacking, handling, and assembly easy. A horizontal steel mandrel 32.8 feet (10 m) long having a 0.5-inch (1.27-cm) wall thickness will sag 0.41 inch (1.04 cm) at its center. A steady rest at the midpoint or at other points of the mandrel would be impractical; rolling contact could possibly damage uncured material. A major portion of the manufacturing development effort required for horizontal fabrication is eliminated by using winding machines with stationary mandrels vertically suspended.

The 90/0/90 fiber-winding technique and longitudinal fiber laydown, used in the textile industry, result in columns having a fiber volume in excess of 60 percent. The columns are compact and have slightly-resin-rich external surfaces.

Two Tapered Graphite/Epoxy Half Columns snap together at a center joint. Tight tolerances on the inside and outside diameters of the half columns allow them to be stacked within each other like paper cups.

This work was done by Ray M. Bluck, Gerald H. Grotbeck, and William M. Reighard of Lockheed Missiles & Space Co., Inc., for **Langley Research Center.** *For further information, Circle 69 on the TSP Request Card.*
LAR-12915

Low-Weight Inserts for Aluminum Honeycomb Panels

Fiber/epoxy composites would be used in place of solid aluminum.

Lyndon B. Johnson Space Center, Houston, Texas

The aluminum honeycomb sandwich panels that reduce weight in aerospace applications often include strengthening inserts at high-stress points, such as attachment points. Current practice is to fashion the inserts out of solid aluminum; however, a new proposal suggests that it may be possible to make the inserts out of such lightweight, high-strength materials as fiber/epoxy composites or high-density aluminum honeycomb.

The composite insert could be fabricated in either of two ways:

- The insert could be prepared and cured separately in a mold and then placed in the honeycomb panel assembly the same way a solid aluminum insert would be used, or
- The insert could be laid up directly in the panel with the other components and cured at the same time as the adhesive used to bond the honeycomb to the aluminum skins. One composite preparation compatible with the autoclave-curing conditions used to bond the panels is Narmco® 5208 resin with either style 133 graphite cloth or style 285 Kevlar® cloth; however, other equivalent materials could be substituted.

The composite insert could be the same size and shape as the aluminum insert it replaces. However, in some applications, weight could be reduced further by redesigning the insert to take full advantage of the properties of the composite.

No dissimilar-metal corrosion problem arises when the composite inserts are encapsulated in the aluminum sandwich panel. With high-density aluminum honeycomb inserts, it would be advisable to use a core-fill material (e.g., syntactic foam) in hardware-attachment holes to keep moisture out.

Narmo® is a registered trademark of Celanese Plastics Co., and Kevlar® is a registered trademark of E. I. Du Pont de Nemours & Co., Inc.

This work was done by George S. Bumgarner and Madison W. Reed of Vought Corp. for **Johnson Space Center.** *No further documentation is available.*

Inquiries concerning rights for the commercial use of this invention should be addressed to the Patent Counsel, Johnson Space Center [see page A5]. *Refer to MSC-20227.*

Acoustical-Levitation Chamber for Metallurgy

The sample can be moved to different positions for heating and quenching.

NASA's Jet Propulsion Laboratory, Pasadena, California

An acoustical-levitation chamber accommodates large temperature gradients and manipulates metallurgical samples or fusion pellets without permitting solid material to contact them. A sample can be moved back and forth between stable levitation positions for heating and quenching simply by changing the signals to the acoustic drivers (see figure).

The acoustical-levitation chamber has four drivers that operate at one, two, or more frequencies simultaneously. A radial/azimuthal resonance mode constrains the sample along the axis of the chamber. The fundamental longitudinal mode constrains the sample at the middle of its length, while the second longitudinal harmonic has two stable sample positions: A and B as shown in the figure.

With the drivers operating at the second harmonic, the sample will levitate either at position A or at position B. By shifting briefly to the fundamental, the sample is shifted toward and through the central position C and thus transferred to and from the heater at B.

The sample is placed in the cylinder through the port at A: It is supported on a screen until the levitation drive is turned on. The drivers are coupled to the chamber through ports located near the periphery of the end cap to maximize coupling to the modes being excited. Any of several heat sources could be used, including an induction furnace, a conventional furnace, or a laser beam.

The simplest chamber design consists of a horizontal circular cylinder, but cylinders of elliptical or rectangular cross section would also work. The chamber could also be oriented vertically. In that case, the sample could be quenched quickly by turning off the acoustic drivers and letting the sample fall out of the furnace region into a quenching liquid. The bottom end of the cylinder would be opened at the moment when the drivers are turned off.

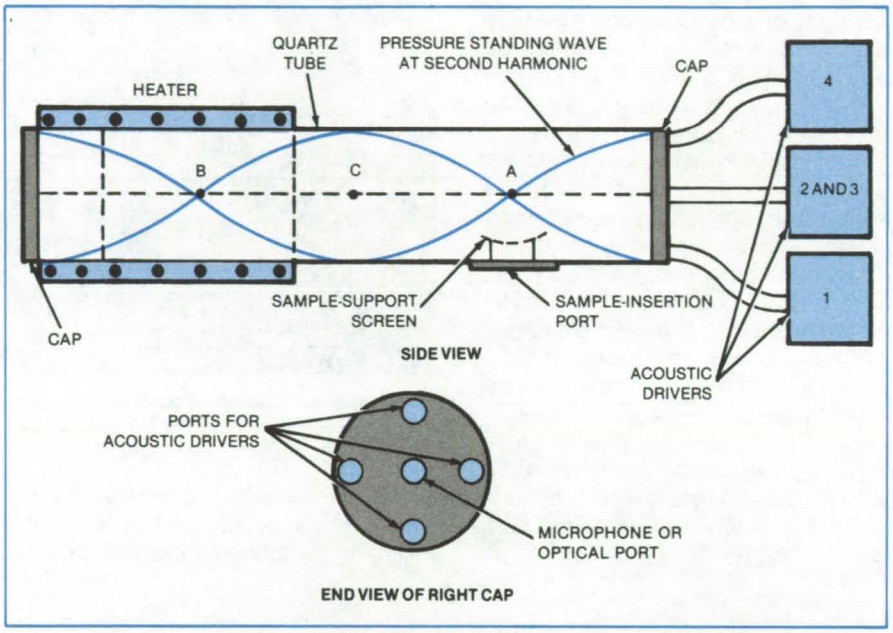

This **Acoustical-Levitation Chamber** is selectively excited in the fundamental and second-harmonic longitudinal modes to hold the sample at one of three stable positions: A, B, or C. The levitated object is quickly moved from one of these positions to another by changing modes. Thus, for example, the object can be rapidly quenched at A or C after heating in the furnace region at B.

This work was done by Martin B. Barmatz, Eugene Trinh, Taylor G. Wang, Daniel D. Elleman, and Nathan Jacobi, of Caltech for **NASA's Jet Propulsion Laboratory.** *For further information, Circle 70 on the TSP Request Card.*

This invention is owned by NASA, and a patent application has been filed. Inquiries concerning nonexclusive or exclusive license for its commercial development should be addressed to the Patent Counsel, NASA's Jet Propulsion Laboratory. *[see page A5].* *Refer to NPO-15453.*

Acoustic Levitation With Less Equipment

Certain chamber shapes require fewer than three acoustic drivers.

NASA's Jet Propulsion Laboratory, Pasadena, California

Most previous work on acoustic levitation has dealt with rectangular chambers. Three drivers excite the chamber along three orthogonal axes — x, y, and z. The three drivers must be used simultaneously to position an object at the center of the chamber, where they create a point of minimum acoustic potential.

Now, however, calculations and experiments have demonstrated that three-orthogonal-plane levitation is really a special case. More generally, positions of stable acoustic levitation are

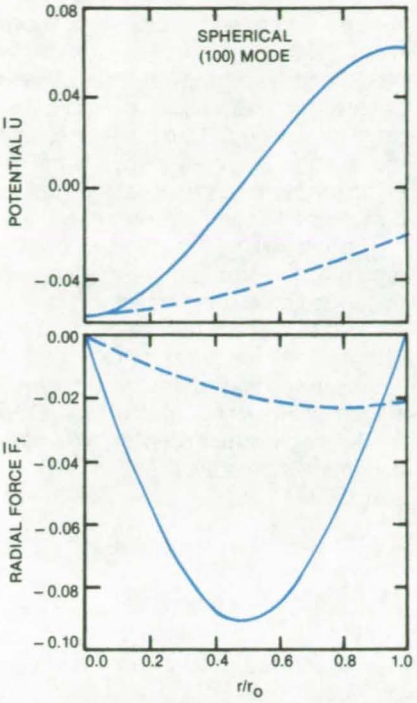

Levitation at the Center of a Spherical Chamber can be attained using only one acoustic driver. The excitation of the lowest spherical mode produces an asymmetric acoustic potential well. The dimensionless potential (top) and corresponding radial force (bottom) are shown for the azimuthal angles $\theta = 0°$ (solid line) and $\theta = 90°$ (dashed line).

possible for various simple and complex chamber geometries, such as spherical and cylindrical, and for higher-order multidimensional excitation modes. For example, such stable positions for a small rigid sphere of radius R are found where the time averages of gas-particle velocity and oscillating acoustic pressure combine to yield a minimum acoustic force potential $\overline{U}$ as follows:

$$\overline{U} = 2\pi R^3 [(\overline{p^2}/3\varrho c^2) - (\varrho\overline{v^2}/2)]$$

where ϱ = gas density, c = the speed of sound, $\overline{v^2}$ = time-averaged square of gas-particle velocity, and $\overline{p^2}$ = time-averaged square of oscillating acoustic pressure. The acoustic force components are obtained from the expression $\mathbf{F} = -\text{grad}\,\overline{U}$.

For example, in a spherical chamber of radius r_o, just one acoustical driver can levitate an object at the center by exciting the lowest-order spherical normal mode. For this mode, $\overline{U}$ is an asymmetric potential well with a unique minimum at the center (see figure). An object located anywhere in the chamber can be thought of as rolling down the slope of the well to the minimum. The radial inward force is proportional to the slope of the potential well at the object position.

In a cylindrical chamber, an object may also be levitated using fewer than three acoustic drivers. In one method, two drivers are used. The first driver excites the lowest-order cylindrical mode that forces the object to the cylindrical axis. The other driver excites various plane-wave z-axis modes that can move and position the object along the axis. A second method requires only one driver to excite a higher-order multidimensional cylindrical mode that can uniquely levitate the object at the center of the chamber.

This work was done by Martin B. Barmatz and Nathan Jacobi of Caltech for **NASA's Jet Propulsion Laboratory.** *For further information, Circle 71 on the TSP Request Card.*
NPO-15562

Pull Test Verifies Gap Loading

The force necessary to initiate movement of a thin plastic strip is a measure of the gap tightness.

Lyndon B. Johnson Space Center, Houston, Texas

A "pull" test determines whether the gap between tiles or other parts is properly filled. A strip of polyester film is embedded in the gap along with the filler material, and the force necessary to withdraw the film is measured. The force is a measure of the pressure applied to the gap filler; that is, the tightness of the filled gap.

Fillers for the gaps between Space Shuttle thermal-protection tiles, are trimmed to fit and inserted, but not bonded, in their designated locations. A polyester strip (Mylar, or equivalent) is inserted along with the filler, as shown in Figure 1.

(continued on next page)

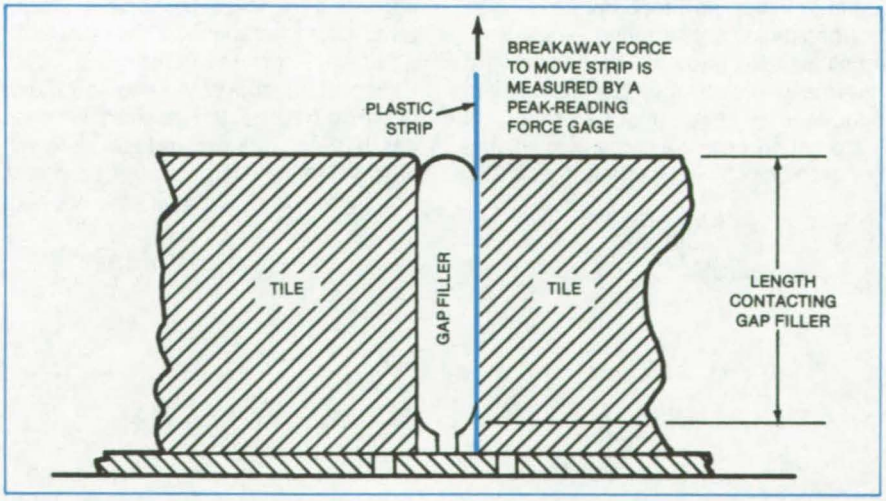

Figure 1. A **Thin Plastic Strip** is pulled away from the gap by a force gage to measure the pressure applied on the gap filler.

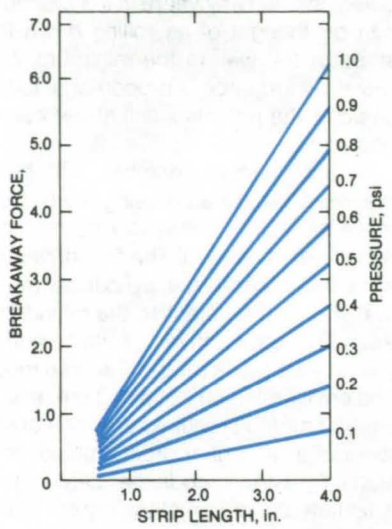

Figure 2. The **Breakaway Force** determines the adequacy of the gap filler. Each combination of gap and gap-filler material has a set of experimentally determined graphs such as these.

A peak-reading force gage measures the breakaway force. If the force reading falls within the required limits, the gap filler is ready for bonding. The acceptable breakaway force is experimentally determined for different dimensions and combinations of gap material and gap filler.

The breakaway force needed to initiate movement of the strip is a function of the pressure applied on the strip, by the gap filler and tiles, and the coefficient of friction between the gap filler, the polyester strip, and the gap material. A typical set of curves relating the breakaway force to pressure for different strip lengths are shown in Figure 2. The curves are drawn from data points gotten by applying a known pressure to a length of strip and then measuring the breakaway force. A set of curves, such as shown in Figure 2, is then derived by varing the pressure, measuring the breakaway force for each pressure, and repeating the procedure for different strip lengths.

The procedure can determine interface pressures or loads where conventional load-measuring equipment cannot be used. It can be used to check refrigerator-door seals, for example.

This work was done by George R. Hagen of Rockwell International Corp. for **Johnson Space Center.** *No further documentation is available.*
MSC-20231

Annealing Solar Cells With Lasers

Large-area process removes ion damage.

NASA's Jet Propulsion Laboratory, Pasadena, California

A laser can anneal silicon solar cells rapidly enough for use in production, according to a recent study. The laser is a frequency-doubled neodymium: yttrium-aluminum-garnet (Nd:YAG) device. The 30-m-diameter spot formed by the laser covers enough area to process silicon wafers rapidly.

The laser is intended for use on solar cells in which pn junctions have been formed by ion implantation — a technique that is likely to replace the standard thermal-diffusion method of forming junctions in cells because of its high automation potential. However, a major problem with ion implantation is that a thin layer at the surface of the silicon is damaged, often losing its crystal structure and becoming completely amorphous.

Annealing can restore the crystallinity. A conventional annealing method is to place an ion-implanted wafer in a furnace at 900° to 1,000° C for 20 to 30 minutes. However, although furnace annealing restores the crystal structure, it also introduces dislocations. In addition, certain combinations of temperature and time tend to diffuse dopants beyond the desired junction depth. Such effects reduce minority-carrier lifetime and spectral response and hence decrease cell efficiency.

Under proper conditions, a Q-switched Nd:YAG laser completely recrystallizes the surface layer, restores its electrical activity, and changes the implanted-dopant profile to a broader, nearly-flat-top distribution. Laser-annealed cells have efficiencies greater than 15 percent and with processing improvements can probably be made routinely with efficiencies higher than 16 percent.

This work was done by Jerry S. Katzeff and Mike Lopez of Lockheed Missiles & Space Co., Inc., for **NASA's Jet Propulsion Laboratory.** *For further information, Circle 72 on the TSP Request Card.*
NPO-15694

Mathematics and Information Sciences

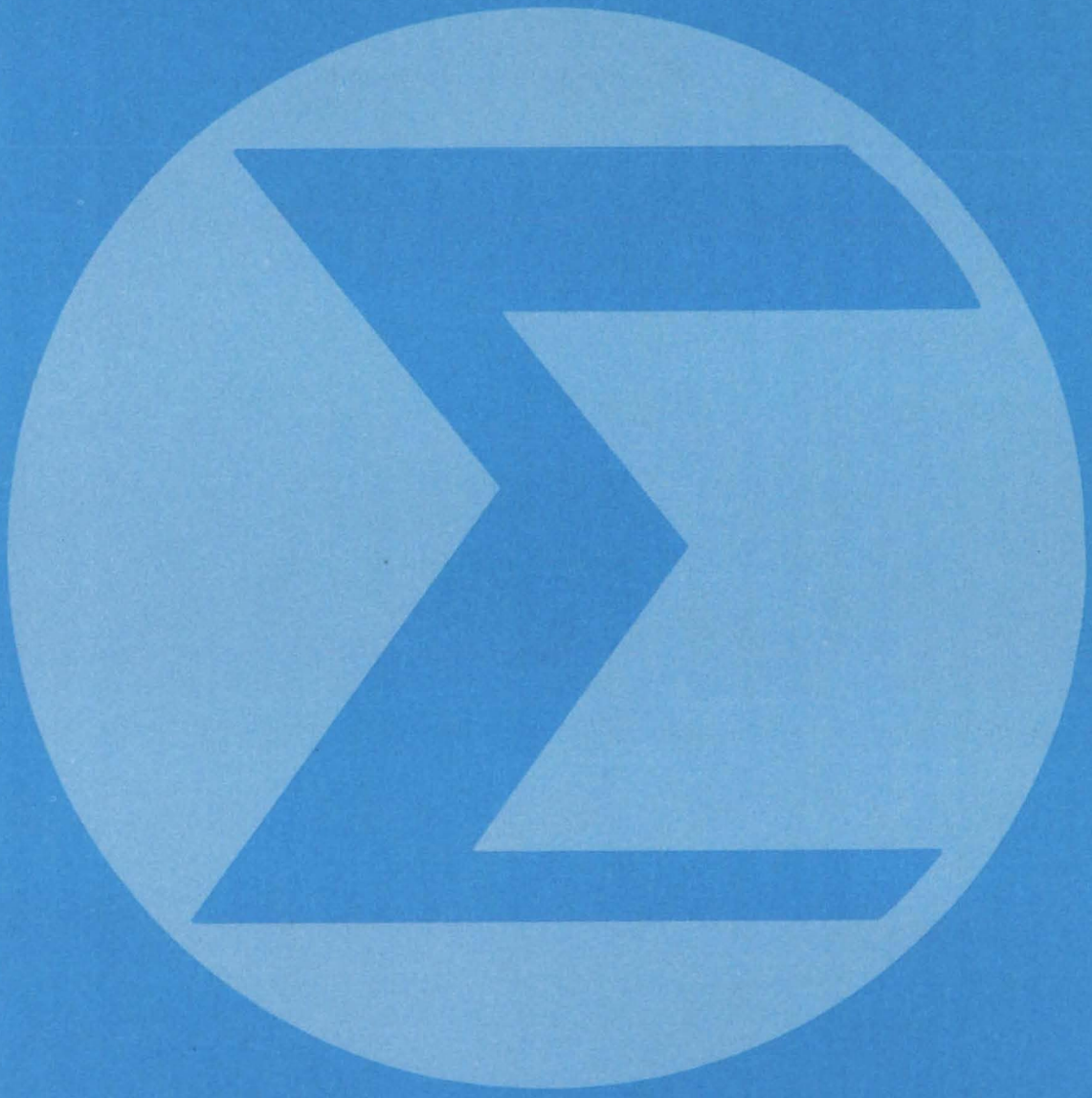

Information-Systems Data-Flow Diagram

A single form presents a clear picture of an entire system.

NASA's Jet Propulsion Laboratory, Pasadena, California

Any information system is described by inputs, outputs, and associated processes. The interface between these parameters is depicted graphically in an easy-to-use form that is independent of the specific data-base structure and applications. The form, which gives a relational review of data flow, is well suited to information-system planning, analysis, engineering, and management. It can be used to review the data flow for a developing system or one already in use.

The form is organized as a "three-dimensional" matrix that describes the data flow. The data flow through the matrix clockwise and include the source of every input to the data base, everything that is stored in the data base, every access to the data base to form each output, every output that is processed, all the processors that are employed in generating the various outputs, as well as the output generation and output destination.

The diagram is explained by using the example shown in the figure and temporarily ignoring the clockwise data-flow direction. Consider the Payroll Report output to be processed. This output is the last within the outputs and is generated (G) by Data Processing. The users (destination, D) of the Payroll Report output are Finance and Personnel. The data types or files needed to produce the Payroll Report product are marked with an I (input from the Data Base); in this case, it is only Employee File. The processors needed to produce the Payroll Report output are General Accounting, Budget and Tax, and Compensation. Finally, the sources (S) of the data files used for the Payroll Report output are the sources of Employee File: Finance and Personnel.

Since data flow is clockwise, some of the users (destination) can become sources again. In this way, repetitive or higher-order data processing can be described.

This work was done by Julian O. Bloşiu of Caltech for **NASA's Jet Propulsion Laboratory.** *For further information, Circle 73 on the TSP Request Card.*
NPO-15492

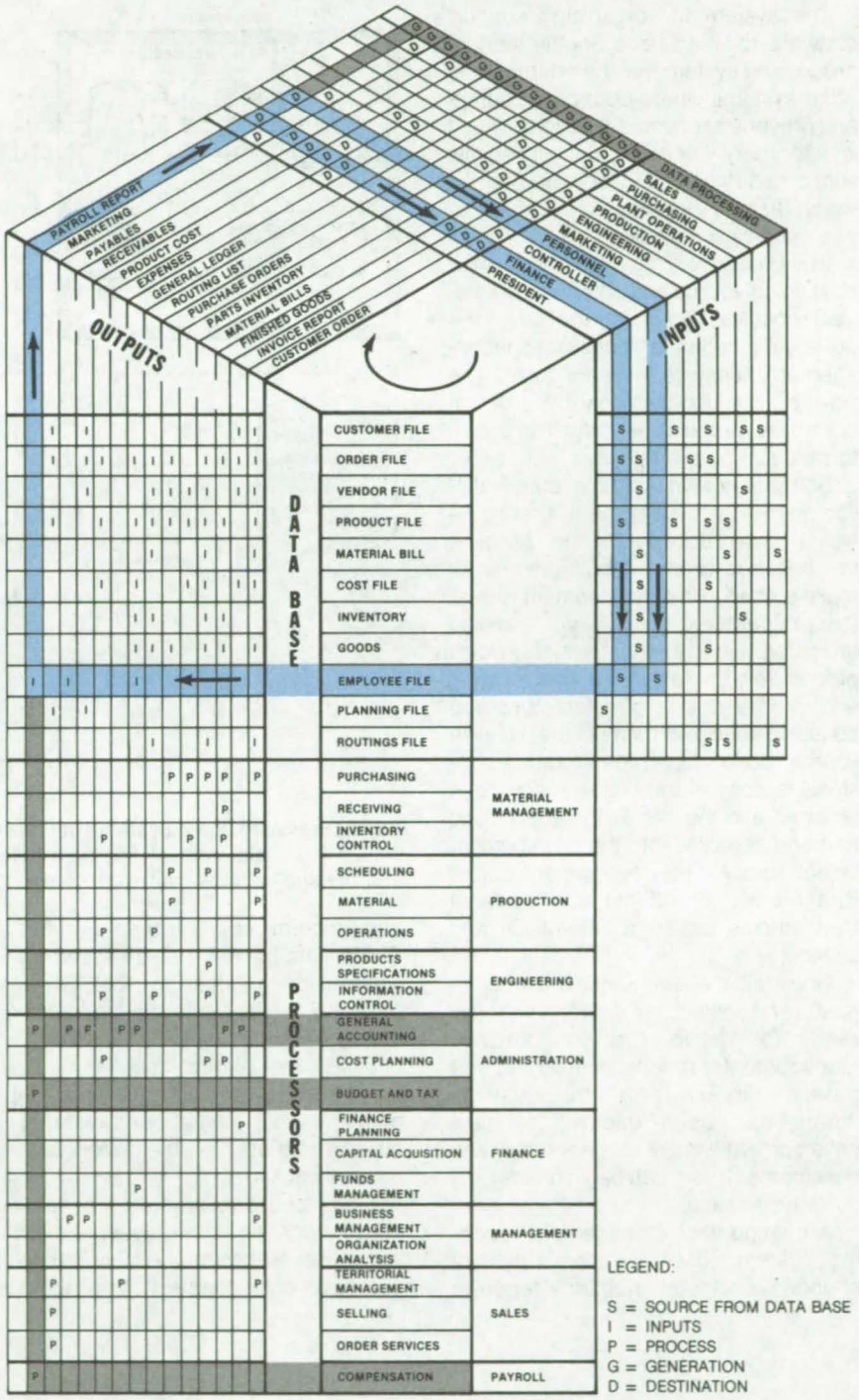

The **Relationship of the Payroll Report** to other components of the information system is traced on the three-dimensional (x,y,z) matrix diagram. Through its parameters, the diagram provides on a single page an understanding of the information network with all the interrelationships and data flow between subsystems.

Large-Scale Software Management System

Changes are organized and controlled according to consistent procedures.

John F. Kennedy Space Center, Florida

The system for organizing support software for the Space Shuttle launch-processing system may be adaptable to other systems where control of change and prevention of unauthorized changes is a primary concern. It is especially suited to a "multi-flow" environment, in which there is more than one version of each software module.

In the new system, baseline libraries containing source and object programs, load modules, and job-control language are maintained by a configuration-management subsystem (see figure). The libraries are updated only by a set of controlled procedures, which are performed just before release.

Software is developed in another set of libraries — the development libraries — which have access to the baseline libraries but cannot modify them. To make a change in a development library, the programer creates what is called an "alter" file. Through a set of uniform procedures, an "alter" file can replace, add, or delete lines of selected source code. No change is made in the baseline source code during development. Instead, a copy of the baseline source is obtained and the alterations are applied to it and compiled into the development object library. The development object library is then linked into an executable load module (called a RUNMOD) and tested.

Once all the alterations have been made and tested, the "alter" files are ready for delivery to configuration management for incorporation in the baseline library. After the baseline library has been updated, a new development library is generated and development work can begin on the next software release.

A configuration-management reporting system (CMRS) keeps track of changes. Engineering change requests and problem reports are entered in the CMRS data base. When an assembly is scheduled for change, CMRS automatically schedules for release all components affected by the change.

CMRS can extract detailed information from the data. This feature keeps managers informed about the status of support requests, problem reports, and release packages.

Since updating procedures, naming conventions, and other aspects of software development are consistent across all components, it is possible for someone experienced in one area of support software to move to another area without having to learn a new set of procedures. With a set of source listings from the new component, the new developer can begin productive work in a short time.

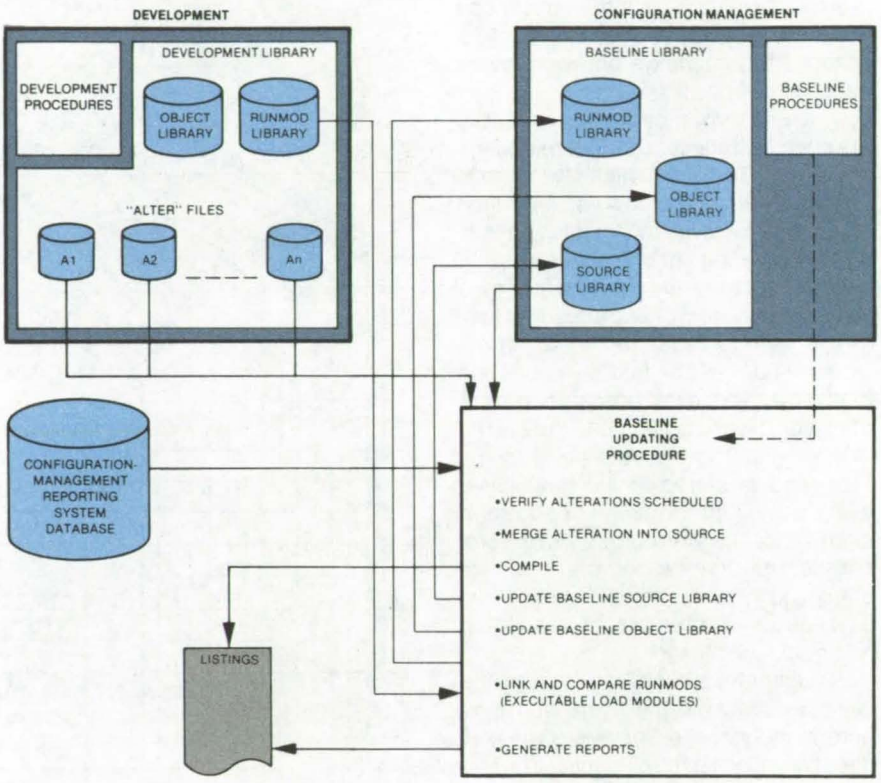

Software Management System contains two sets of libraries: baseline and development. A library is a hierarchical catalog and file structure in which catalog levels and entries identify and delineate software components and functions within components.

This work was done by G. L. Kirkland of International Business Machines Corp. **Kennedy Space Center.** *For further information, Circle 74 on the TSP Request Card.*
KSC-11230

Planning Transport and Manufacturing for Lowest Cost

A method originally developed for spacecraft path-planning is also applicable to transportation and manufacturing.

NASA's Jet Propulsion Laboratory, Pasadena, California

A new algorithm alleviates some of the mathematical difficulties of planning segmented trajectories for lowest cost. Although originally developed to plan spacecraft trajectories, the method has terrestrial applications as well. For example, with modifications, it can be used to minimize freight costs and energy costs, which often change in steps, and mass production costs, which depend on the number of machines used. The algorithm involves a modified Newtonian iterative method in which the periapse times, the closest approach distances, and the orientations of the approach hyperbolas serve as the independent variables.

A tour of many planets or moons involves a complex trajectory with ballistic segments between maneuver points at which rockets are fired (see figure). The cost is directly related to the sum of the magnitudes of the separate velocity changes at these points. Earlier optimization schemes used the sum of magnitudes: This introduced computational difficulties due to discontinuities in the gradient of the cost function that occur whenever any of the individual velocity changes approaches zero.

In the new algorithm, the cost function is defined as the weighted sum of the squares of the magnitudes of the velocity changes (instead of the sum of the magnitudes). The sum-of-squares cost function has important advantages:

- It eliminates discontinuities in the cost gradient when a velocity change approaches zero.
- A close approximation to the second-derivative matrix — a critical element in the calculations — can be developed from only the first derivatives of the velocity vectors. This feature allows the use of a Newton optimization algorithm, which yields a spectacular speedup in solution convergence and reduction in computer time.

To generate a sum-of-magnitudes solution while retaining the advantages of the sum-of-squares cost function, each velocity change in the cost function is weighted. The optimization method automatically computes new weights, which are inversely proportional to the magnitudes of the velocity changes, and restarts the optimization using the new weights. After several restarts of a few iterations each, the solution is found.

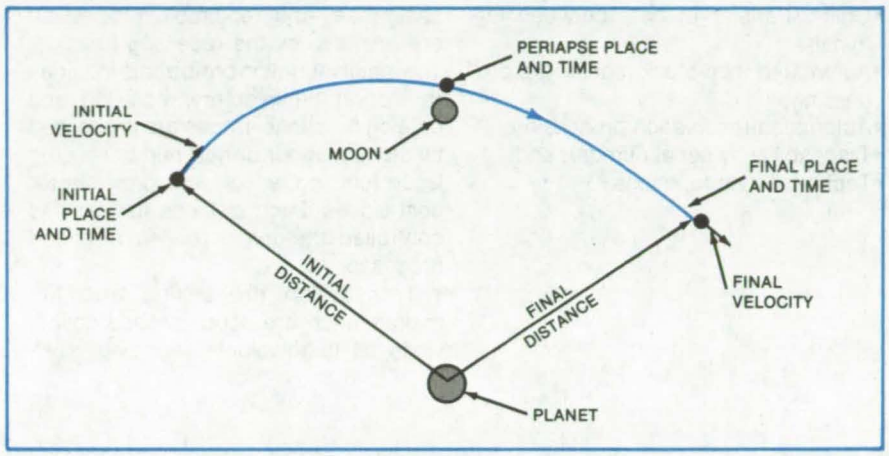

Each Segment of a Satellite Multiple Flyby trajectory is generated in two steps. First, the components of the initial velocity are varied to satisfy the conditions of the periapse (point of closest approach to the body in question). Second, the trajectory is propagated from the periapse to the point for the next maneuver. On the segment shown here, the spacecraft is being flown past one of the moons of a planet.

This work was done by Louis A. D'Amario, Dennis V. Byrnes, and Richard H. Stanford of Caltech for **NASA's Jet Propulsion Laboratory.** *For further information, Circle 75 on the TSP Request Card.*
NPO-15391

Computer Programs

These programs may be obtained at very reasonable cost from COSMIC, a facility sponsored by NASA to make new programs available to the public. For information on program price, size, and availability, circle the reference letter on the COSMIC Request Card in this issue.

Shuttle Inventory Management

All supply activities and requirements are controlled from a single point.

The Shuttle Inventory Management System (SIMS) consists of a series of integrated support programs providing supply support for both the Shuttle program and Kennedy Space Center base operations. SIMS controls all supply activities and requirements from a single point. It employs a system design concept with a large-scale data-base environment controlled by a transaction-driven, automated inventory-control system. A management-by-exception approach allows SIMS to handle the central inventory control of spare and repair parts, supplies requisitioning, and requisition statusing performed by an array of decentralized supply points.

(continued on next page)

SIMS provides the user with the following capabilities:

- Online part number to stock number cross-reference,
- Automated document control,
- Automated transaction suspense,
- Online status for documents in process,
- Online transaction audit trail,
- Online transfer of data between terminals,
- Automated non-stock-requisition processing,
- Automated reservation processing,
- Traceability by serial number, and
- Technical data functions.

To facilitate effective and efficient online processing, the SIMS functions are divided into five subfunctions. The inventory management function provides file management control with transaction suspense and release features. The catalog function manages the part number file and the technical data file. Receipt processing, suspense, quality assurance, and repairable processing are provided by the receiving function. The inquiry function preformats inquiries to support the inventory, receiving, and catalog functions. Issues are processed by stock number or part number by the issue function, which also provides for post issues. Each of these functions is controlled through a related front-end processor.

Transaction processing and file maintenance are accomplished online, while all large-volume reporting is effected in offline batch processing. The size and complexity of the SIMS requirements dictated the necessity of a highly modular design, which should be flexible to the growing needs of the users.

The SIMS programs are written in COBOL for integrated batch and interactive execution and have been implemented on a Honeywell 66/60 computer with the largest program having a central memory requirement of approximately 65K of 36-bit words. SIMS was last updated in 1980.

This program was written for the Computer Services Division of **Kennedy Space Center.** *For further information, Circle Q on the COSMIC Request Card.*

KSC-11219

SUBJECT INDEX

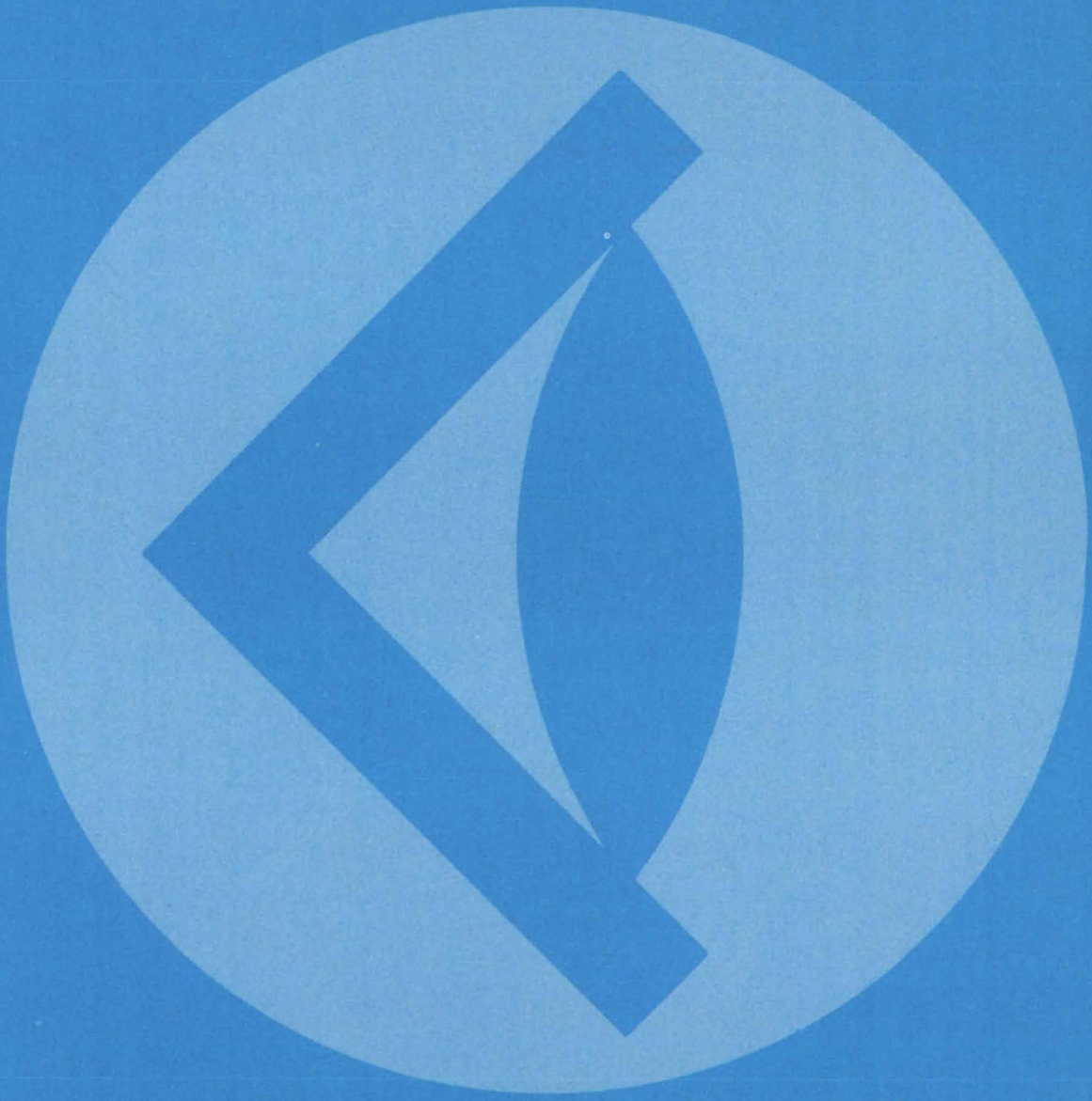

☆ U.S. GOVERNMENT PRINTING OFFICE: 1983-412-084

National Aeronautics and
Space Administration

Washington, D.C.
20546

25th Anniversary
1958-1983

NASA

Protected by gloves, hat, and facemask, this researcher is studying the atmosphere in the volcanic crater at Mount St. Helens. The portable aerosol analyzer at his side, originally developed by NASA, is now marketed as a commercial product by a California company. [*See the bottom of page A1.*]